

Seismic Behaviour and Design of Mixed RC-URM Wall Structures

THÈSE N° 6419 (2015)

PRÉSENTÉE LE 27 MARS 2015

À LA FACULTÉ DE L'ENVIRONNEMENT NATUREL, ARCHITECTURAL ET CONSTRUIT
LABORATOIRE DU GÉNIE PARASISMIQUE ET DYNAMIQUE DES STRUCTURES
PROGRAMME DOCTORAL EN GÉNIE CIVIL ET ENVIRONNEMENT

ÉCOLE POLYTECHNIQUE FÉDÉRALE DE LAUSANNE

POUR L'OBTENTION DU GRADE DE DOCTEUR ÈS SCIENCES

PAR

Alessandro PAPARO

acceptée sur proposition du jury:

Prof. M. Bierlaire, président du jury
Prof. K. Beyer, directrice de thèse
Prof. S. Cattari, rapporteuse
Dr P. Lestuzzi, rapporteur
Prof. T. Sullivan, rapporteur



ÉCOLE POLYTECHNIQUE
FÉDÉRALE DE LAUSANNE

Suisse
2015

In loving memory of my Dad

Francesco Paparo

Preface

In recent years, new residential buildings in regions of moderate seismicity are often constructed as mixed structural system with unreinforced masonry (URM) walls and reinforced concrete (RC) walls which are coupled by RC slabs. Lack of knowledge on their seismic behaviour leads to rather rough and sometimes questionable assumptions when such buildings are designed for seismic action.

With his thesis Alessandro Paparo contributes to the understanding of the seismic response of such mixed structural systems. Alessandro conducted large-scale experimental tests on two wall systems, which consisted each of a URM wall and a RC wall coupled by two RC beams. The tests were particular since the test setup allowed measuring the reaction forces at the base of the URM walls—a true challenge considering the size of the forces and moments. The models, which he developed in the following, could therefore not only be validated with regard to the global response but also with regard to the force distribution between the walls and its evolution with increasing displacement demand. In the final chapter of his thesis, Alessandro proposes a displacement-based design approach for mixed RC-URM wall structures, which combines the established direct displacement-based design procedure with novel components derived from shear-flexure cantilever models and continuous beam element models to account for the particularities of the mixed structural system and the coupling by the RC slabs.

Lausanne, February 2015

Katrin Beyer

Acknowledgements

This research has been carried out at the Earthquake Engineering and Structural Dynamics Laboratory (EESD) at the Ecole Polytechnique Fédérale de Lausanne (EPFL) under the supervision of Prof. Katrin Beyer. It is first to her that I want to express my gratitude. Thank you for the commitment to this research, the guidance and the help during these years.

I sincerely thank the members of the jury, Prof. Serena Cattari, Dr. Pierino Lestuzzi and Prof. Timothy Sullivan, and the president of the jury, Prof. Michel Bierlaire. Thanks for your interest and all the comments that improved the quality of the work.

I would like to thank the technical staff from the structural laboratory of EPFL, with special thanks to Gilles, Gérald, Fréd, Armin and Sylvain.

I wish to thank all the members and friends of the EESD laboratory. First of all Raluca “the grandmother”, my almost five-year office mate. Thanks for your friendship and help! Thanks to Shenghan, it was really nice to know you and your “think-positive attitude”! Thanks to Georgia, Pia and Sarah, former colleagues of mine at the EESD. I would like to also thank Marco for his constant support and help. Thanks to Angelica, João, Danilo, Ovidiu, Panos, Boyan, Francesco, Bastian and Matteo. Finally I want to also thank Yvonne and Marie-Madeleine for helping me with all the administrative things.

I would like to also thank other friends I met at the EPFL. In particular Fra, Fabio, Ioannis, Francisco, Jaime, Carlos, Manu, Marina, Ben, Dan, James, Alexis and Hadi. Thanks for the support and the friendship! A special thank goes to Hadi who really helped and supported me during difficult moments over these years. Thank to my previous flatmates, Karim and Stéphanie (“the first coloc”) and Georgios (“the second coloc”). It is nice that you are my friends!

I wish to also thank my friends from Ravenna, my hometown. Thanks to Misi, Bacca, Vito, Cico, Candy and Bertaz. Thanks also go to the “cavemen”: Juri, Barge, Maio, Ale, Orto, Gigi, Blorgio, Genna, Pigna and Fabius. Thanks to my friends from Bologna Simo, Matte, Chiara, Mirko, Dani, Jack, Amaduz and Enea. Another special thank goes to Chris for the unconditional support and help!

Finally I want to thank my mother and my sister. These years have been difficult for all of us, thanks for the support and the strength you gave me. This thesis is dedicated to my father, who did not manage to see this achievement. Papà, mi manchi.

Abstract

In several countries of central Europe, many modern residential buildings are braced by reinforced concrete (RC) and unreinforced masonry (URM) walls coupled with RC slabs. Such mixed constructions, in fact, behave better under seismic loading than buildings with URM walls alone. Similarly, the insertion of RC walls is a technique used to retrofit existing modern URM constructions that feature RC slabs, since both strength and displacement capacities of the repaired structure increase with respect to the un-retrofitted configuration.

Although modern mixed RC-URM wall buildings are rather common, very little is known about their seismic behaviour and codes do not provide adequate design and assessment guidelines. Hence, the thesis focuses on four objectives: (1) to provide experimental data on the seismic behaviour of mixed RC-URM wall structures; (2) to formulate recommendations for setting up numerical models for structures with both RC and URM walls; (3) to develop a mechanical model that represents the interaction between RC and URM walls; (4) to propose a displacement-based seismic approach for the design of new mixed RC-URM wall structures and the retrofitting of URM wall buildings by adding RC walls or replacing URM walls with RC ones.

An experimental investigation of two mixed RC-URM wall substructures leads to new findings with respect to the actual distribution of the reaction forces between RC and URM walls and gives insight into the displacement profile of mixed RC-URM wall structures. The results are used to validate two numerical strategies and recommendations for setting up models for structures with both RC and URM walls are formulated. A simple mechanical model, which takes into account the most important parameters influencing the seismic behaviour of mixed RC-URM wall structures, is proposed and validated. The model is based on the shear-flexure interaction as URM and RC walls display dominant shear and flexural deformations, respectively. In the last part of the thesis a displacement-based design approach for mixed RC-URM wall structures is developed. The design method is verified through inelastic time-history analyses (ITHA) of three-to-five-storey case study buildings. Comparison between the design values and the results from ITHA suggests that the design methodology controls the horizontal deflection of the structures, being almost linear over their height, and avoids concentrations of deformations in the bottom storey, a typical feature of URM wall structures. On the other hand, for the three-storey configurations, it was observed that the approach overestimates the maximum horizontal displacement.

Keywords: Modern mixed reinforced concrete-unreinforced masonry wall buildings; Large-scale testing; Seismic behaviour; Non-linear analyses; Displacement-based design.

Riassunto

In molti stati dell'Europa centrale, diversi moderni edifici residenziali con solai in cemento armato vengono costruiti usando muri sia in cemento armato che muratura non armata. Tale sistema strutturale, infatti, presenta migliori caratteristiche sismiche rispetto a tradizionali edifici in muratura non armata. Analogamente, l'aggiunta di muri in cemento armato in moderne strutture in muratura con solai in cemento armato è una comune tecnica di riabilitazione strutturale.

Sebbene tali strutture miste in cemento armato e muratura siano abbastanza utilizzate, poche ricerche sul loro comportamento sismico sono state fatte e, di conseguenza, i regolamenti edilizi non forniscono supporto nè per la progettazione nè per la riabilitazione strutturale. La tesi dunque si focalizza su quattro aspetti: (1) fornire risultati sperimentali sul comportamento sismico di strutture miste in cemento armato e muratura; (2) proporre linee guida per costruire modelli numerici rappresentanti strutture con muri sia in cemento armato che in muratura; (3) sviluppare un modello meccanico capace di rappresentare l'interazione tra muri in cemento armato e muratura; (4) proporre una procedura basata sugli spostamenti per il progetto di nuove strutture miste in cemento armato e muratura e per la riabilitazione strutturale di edifici in muratura grazie all'aggiunta di muri in cemento armato.

Un'indagine sperimentale su due strutture miste in cemento armato e muratura porta nuovi risultati sulla distribuzione delle reazioni vincolari tra i vari muri e sul profilo degli spostamenti di tali edifici. I risultati sperimentali vengono anche utilizzati per validare due approcci numerici. Vengono altresì proposte raccomandazioni su come costruire modelli numerici. Viene poi presentato e validato un semplice modello meccanico che considera la tipica interazione taglio-flessione che si sviluppa quando muri in mattoni vengono accoppiati a muri in cemento armato. Nell'ultima parte della tesi viene sviluppata una metodologia progettuale basata sugli spostamenti. Tale metodologia viene poi validata attraverso analisi dinamiche non lineari di diversi casi studio di tre-cinque piani. Comparazione tra i valori di progetto e i risultati ottenuti con le analisi dinamiche suggerisce che la metodologia controlla bene la deformata della struttura ed evita concentrazioni di deformazioni nel piano terra, caratteristica tipica per strutture in muratura. D'altro canto, per le configurazioni di tre piani, è stato riscontrato che la metodologia progettuale sovrastima il massimo spostamento orizzontale.

Parole chiave: Moderne strutture miste in cemento armato e muratura non armata; Prove sperimentali su prototipi in grande scala; Comportamento sismico; Analisi non lineari; Progettazione basata sugli spostamenti.

Résumé

Dans plusieurs pays d'Europe centrale, de nombreux bâtiments résidentiels modernes sont réalisés avec des refends en béton armé ainsi qu'en maçonnerie non-armée et des dalles en béton armé. En effet, ces constructions mixtes ont l'avantage de se comporter mieux lorsqu'elles sont soumises à un chargement sismique par rapport à des bâtiments en maçonnerie uniquement. De la même façon, l'ajout de refends en béton armé dans une structure existante en maçonnerie permet de la renforcer efficacement en améliorant sa capacité de résistance et de déplacement.

Bien que ces structures mixtes en béton armé et maçonnerie soient passablement utilisées en pratique, leur comportement sismique n'est pas encore complètement compris et les normes actuelles ne fournissent pas de directives précises pour leur dimensionnement et leur évaluation. Par conséquent, le travail de la thèse se concentre sur quatre objectifs principaux: (1) fournir des données expérimentales sur le comportement sismique des structures mixtes en maçonnerie et béton armé ; (2) formuler des recommandations pour développer des modèles numériques de telles structures ; (3) développer un modèle mécanique qui représente l'interaction entre les refends en béton armé et en maçonnerie ; (4) proposer une approche basée sur les déplacements pour le dimensionnement de ce type de structures mixtes ainsi que pour le renforcement de bâtiments existant en maçonnerie avec refends en béton armé.

Une investigation expérimentale de deux structures mixtes, composées d'un refend en béton armé et d'un en maçonnerie, apporte de nouveaux résultats sur la distribution des forces de réaction entre les refends ainsi que sur le profil des déplacements. Les résultats expérimentaux sont utilisés pour valider deux modèles numériques. Des recommandations pour le développement de modèles numériques de structures avec des refends en béton armé et en maçonnerie sont aussi proposées. Un modèle mécanique, basé sur l'interaction effort tranchant-flexion qui se produit entre les refends en béton armée et en maçonnerie, est proposé et validé. Dans la dernière partie de la thèse, une méthodologie basée sur les déplacements pour dimensionner ce type de structures mixtes a été développée. Elle a été vérifiée par des analyses dynamiques non-linéaires de bâtiments de trois à cinq étages. Il a été démontré que cette méthodologie permet d'évaluer efficacement le profil des déplacements de ces structures et d'éviter les concentrations de déformations à l'étage inférieur propres aux structures en maçonnerie. Il a également été montré que, pour les configurations de bâtiments à trois étages, la méthodologie de dimensionnement proposée surestime les déplacements horizontaux.

Mots clés : Structures mixtes modernes en béton armé et maçonnerie non-armée ; Essais à grande échelle ; Comportement sismique ; Analyses non-linéaires ; Dimensionnement basé sur les déplacements.

Table of Contents

Preface.....	i
Acknowledgements	iii
Abstract.....	v
Riassunto	vii
Résumé	ix
Table of Contents.....	xi
Introduction	1
1 Motivations and description of the analysed buildings	3
2 Problem statement	9
3 Objectives.....	12
4 Methodology and main contributions.....	13
5 Outline of the report	14
6 References	15
State of the art	19
1 Seismic behaviour of mixed RC-URM wall buildings: numerical and experimental studies	21
1.1 Numerical studies	21
1.2 Experimental campaigns.....	23
2 Seismic behaviour and analyses tools for dual RC frame-wall buildings.....	25

2.1 Seismic behaviour of dual RC frame-wall buildings.....	25
2.2 Analysis technique for dual RC frame-wall buildings.....	28
2.3 Direct displacement-based design for dual RC frame-wall buildings	30
3 References	35
Paper I: Quasi-static cyclic tests of two mixed reinforced concrete-unreinforced masonry wall structures	39
Abstract	41
1 Introduction.....	42
2 Experimental investigation	44
2.1 Test units and reference structure.....	44
2.2 Material properties of the test units	46
2.3 Test set-up and instrumentation	48
2.4 Loading history	53
3 Test results.....	54
3.1 Global behaviour of the test units and their failure mechanisms	54
3.2 Hysteretic behaviour.....	60
4 Conclusions and outlook	64
5 Acknowledgments	65
6 References	65
Paper II: Modelling the seismic response of modern URM buildings retrofitted by adding RC walls	69
Abstract	71
1 Introduction.....	72
2 Seismic behaviour of interacting URM and RC walls	73
2.1 Deformation pattern of mixed RC-URM wall structures subjected to lateral loading.....	74
2.2 Advantages and drawbacks of adding RC walls to URM wall buildings	76
3 Numerical analyses of modern RC-URM wall buildings with RC slabs	78

3.1 EPFL tests	78
3.2 Shell-element model.....	79
3.3 Macro-element model.....	81
3.4 Comparison of the numerical and experimental results	88
4 Application to four buildings.....	92
4.1 Capacity curves.....	94
4.2 N2 method.....	97
5 Conclusions and outlook.....	100
6 Acknowledgments.....	101
7 References	101

Paper III: Development of a displacement-based design approach for modern mixed RC-URM wall structures 105

Abstract.....	107
1 Introduction	108
2 Features of mixed RC-URM wall structures	110
3 Shear-flexure cantilever model.....	111
3.1 Differential equations of the shear-flexure cantilever model.....	112
3.2 Comparison of the results of the shear-flexure cantilever model against numerical simulations.....	115
3.3 Application of the shear-flexure cantilever model.....	121
4 General direct displacement-based design procedure	125
5 Evaluation of the equivalent viscous damping	127
5.1 Remarks with regard to the use of the equivalent viscous damping approach in DDBD.....	128
5.2 Evaluation of the equivalent viscous damping	129
6 Proposed methodology for mixed RC-URM wall structures	132
7 Case studies	143
7.1 Description of the case studies	144
7.2 Modelling and analyses	146

7.3 Results of time-history analyses.....	147
8 Conclusions.....	150
9 Acknowledgments	151
10 References.....	152
10 Appendix: Design example.....	154
Conclusions.....	165
1 Outline.....	167
2 Contributions derived from the experimental campaign	168
3 Contributions derived from the numerical simulations	170
4 Contributions derived from the elaboration of the mechanical model.....	172
5 Contributions derived from the development of the design approach	173
6 Outlook.....	175
7 References	177
Appendix.....	181
1 Introduction.....	183
2 Test objectives.....	183
3 Organisation of the test data	185
3.1 Instrumentation	185
3.2 Test data	190
4 Additional photos describing the progressive damage in the test units	196
4.1 TU1.....	196
4.2 TU2.....	201
5 References	206
Curriculum vitae.....	207

Introduction

Introduction

1 Motivations and description of the analysed buildings

The re-evaluation of the seismic hazard in Europe [Share project, 2013] has generally led to higher seismic design spectra and, as a result, many unreinforced masonry (URM) buildings have failed to satisfy the new design safety check. In Switzerland, a country of low to moderate seismicity, several of these existing URM buildings, provided they feature reinforced concrete (RC) slabs which allowed a redistribution of forces, have been seismically retrofitted by adding RC walls or by replacing critical URM walls with RC ones (Figure 1). Moreover, in recent years, several newly constructed buildings of two to six storeys have been designed directly as mixed structural systems with RC and URM walls (Figure 2).

Mixed RC-URM construction varies significantly from region to region [Magenes, 2006; Cattari and Lagomarsino, 2013]. In this thesis, the examination is limited to typical building configurations of modern mixed RC-URM systems built in Switzerland. These systems are characterised by the following features:

- i)* The RC-URM edifices are modern buildings of three to five storeys with masses evenly distributed over the height.
- ii)* The RC and URM walls are continuous over the height and connected at each floor by 20 to 30 cm thick RC slabs that provide an efficient rigid diaphragm action.
- iii)* The length of the RC walls varies between 2 and 5 m and their aspect ratio is within 1.5 and 3. The RC walls are 20 to 30 cm thick and designed according to modern codes to develop a flexural behaviour with displacement capacities larger than those of URM walls. The

mean concrete cylinder compressive strength at 28 days is between 20 and 50 MPa and the reinforcement bars have mean yield strengths between 500 and 600 MPa. The total longitudinal reinforcement ratio of the RC walls varies between 0.2% and 4.0% [EN 1992-1, 2004]. In the RC slabs the longitudinal reinforcement ratio varies between 0.13% and 4.0% [EN 1992-1, 2004].

iv) The URM walls have lengths up to 7 m and aspect ratio in the range of 0.5 and 3. The URM walls, which always outnumber the RC ones, are built with hollow clay 20 to 30 cm thick bricks in combination with standard cement mortar. URM walls are characterised by mean masonry compressive strengths (f_{cm}) between 4 and 8 MPa and axial stress ratios (σ_0/f_{cm}) between 0.05 and 0.25. Since in such structures the URM walls are connected by RC slabs that introduce an important framing effect [Lang, 2002], the URM walls generally exhibit a dominant shear behaviour.

Despite the rather widespread use of such structures, very little research has been carried out on this topic (see research needs identified by Magenes [2006]) and several open issues should be addressed:

i) Effect of the interaction between RC and URM walls on the global structural behaviour of mixed systems. As vertical and horizontal forces are resisted by the combined action of RC and URM walls, such mixed structures will behave differently from buildings with URM or RC walls only. Both URM and RC walls must be taken into account when realistic estimates of the structural strength and displacement capacities are sought.

ii) Lack of experimental data. Experimental data on such mixed structures [Magenes, 2006] is lacking and, to the knowledge of the writer, only two experimental tests on mixed RC-URM wall buildings are reported in literature. (i) Tomažević et al. [1990] carried out a shake table test campaign on a URM wall structure with one internal RC column. Since the URM walls were considerably stiffer than the RC column, the latter had almost no influence on the global seismic behaviour. (ii) Jurukovsky et al. [1992] conducted shake table tests on 1/3-scale models composed of several URM walls and one RC frame replacing at the bottom floor three URM walls. They investigated several retrofitting techniques, one of which consisted in the addition of a central RC wall pinned to the foundation. Despite the relevance of these tests, they addressed different problems from those herein investigated and cannot be used as benchmark for the seismic validation of such mixed systems.



Figure 1: Examples of existing modern URM wall buildings with RC slabs retrofitted with RC walls. Photos: T. Wenk.



Figure 2: Examples of typical modern Swiss buildings with RC and URM walls and RC slabs. Photos: T. Wenk.

iii) Scarce numerical investigations. Also very little non-linear numerical investigations were carried out. Casoli [2007] examined an existing URM masonry structure and its retrofitting through the insertion of RC walls. Recently, non-linear investigations have been carried out by Cattari and Lagomarsino [2013] to simulate the interaction between URM and RC walls. Nonetheless, the latter were designed for vertical loads only and the displacement capacity of such RC elements was smaller than that of the URM walls. This thesis instead targets modern mixed structures composed of RC walls and slabs designed to have larger displacement capacities than those of URM walls.

iv) Numerical results sensitive to modelling assumptions. Mixed RC-URM structures can be modelled by shell-element models or macro-modelling approaches. The latter are commonly used in engineering practice because of the reasonable compromise between accuracy of results

and computational effort [Penna et al., 2013]. It is known that, regardless of the adopted modelling approach (shell-element or macro-model) and the analysed structural system (RC, URM or RC-URM buildings), numerical results are sensitive to modelling assumptions and material properties.

For mixed RC-URM buildings, the parameters which most influence the distribution of the reaction forces among the walls are those defining the strength and stiffness of the elements [Casoli, 2007; Paparo and Beyer, 2012]. As an example, the sensitivity of the base shear distribution among the walls to some of the aforementioned parameters is outlined with respect to the structure of Figure 3a. Pushover analyses are carried out with a macro-modelling approach (TREMURI, [Lagomarsino et al., 2013]). However, similar considerations can be outlined for analyses performed with shell-element programs.

Figure 3b shows the influence of the URM wall shear strength (V_{sh}) on the base shear distribution between the two walls. Two modelling options are analysed. In modelling option 1, V_{sh} is around 120 kN, whereas, in modelling option 2, V_{sh} is equal to 85 kN. Results show that the assumed V_{sh} does influence not only the base shear carried by the URM wall, but also the base shear carried by the RC wall. In fact, the reduction of V_{sh} decreases the framing effect provided by the RC beams and, as a consequence, the base shear carried by the RC wall.

Figure 3c illustrates the sensitivity of the system to the assumed stiffness of the RC wall when the RC members are implemented as bilinear. Also here two models are discussed. In the first one the RC wall stiffness EI_e is assigned as defined by Priestley et al. [2007], whereas in the second model, the RC wall stiffness is assigned as one half of the gross section stiffness, $0.5 EI_g$. Since $0.5 EI_g$ is around three times EI_e , the RC wall of modelling option 2 is stiffer than the RC wall of modelling option 1, carries more base shear in the elastic branch (grey dashed lines) and yields at a lower drift.

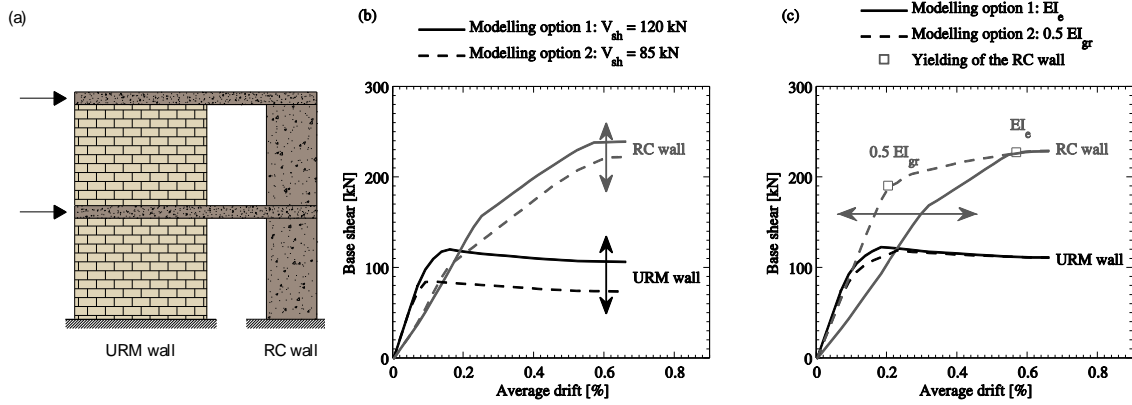


Figure 3: Macro-model: influence of assumed strength and stiffness on the distribution of the base shear between the walls. (a) Reference structure. (b) Average drift-base shear: influence of assumed strength of the URM wall. (c) Average drift-base shear: influence of assumed stiffness of the RC wall.

In mixed RC-URM buildings, when the RC members are modelled as bilinear, also the global drift profile is influenced by the assumed value of the RC wall stiffness. Figure 4a represents a mixed structure in which the RC walls are assigned either (i) one half of the gross section stiffness, $0.5 EI_{gr}$, or (ii) the effective stiffness EI_e as defined by Priestley et al. [2007]. Under lateral loading, shear dominated URM constructions concentrate the inter-storey drift in the lowest storey (Figure 4b, grey dashed line). On the other hand, flexural RC walls exhibit the largest inter-storey drift in the top storey (black dashed line). Due to the RC slabs connecting the walls, the inter-storey drift profile of a mixed system (i) lies in between that of buildings with URM or RC walls alone and (ii) depends on the relative stiffness between the RC and the URM walls. The stiffer the RC walls become, the larger is their influence on the global drift profile. As $0.5 EI_{gr}$ (modelling option 1) is around 5 times EI_e (modelling option 2), in the first modelling option the RC walls enforce larger inter-storey drifts in the top storeys, if compared to modelling option 2.

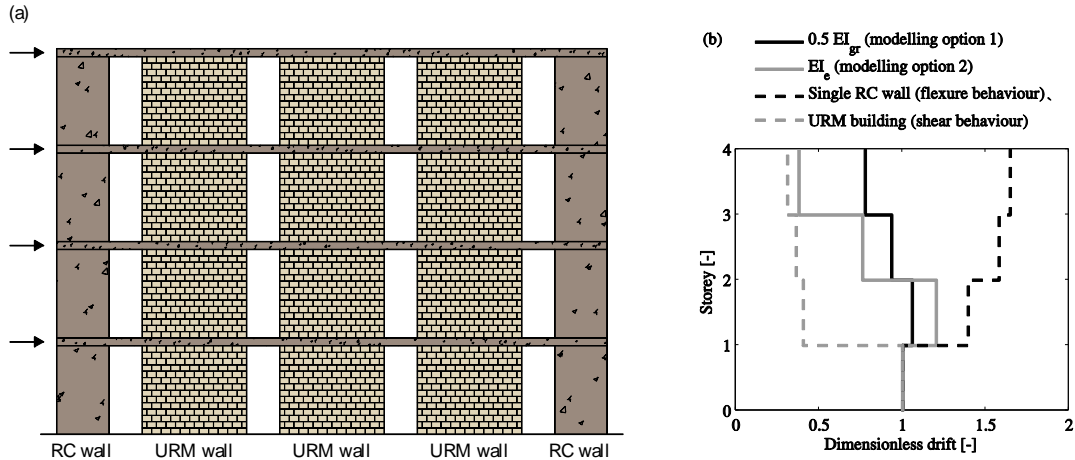


Figure 4: Macro-model: influence of assumed RC wall stiffness on the inter-storey drift profile. (a): reference structure; (b): global inter-storey drift profiles for the two modelling options (solid lines) and inter-storey drift profiles of one single RC wall and of the URM building (dashed lines).

v) Insufficient code provisions. Codes provide little support for the seismic design and retrofitting of mixed structures in general and RC-URM wall structures in particular. As a consequence, engineers generally design these mixed systems with oversimplified assumptions. In Switzerland, for instance, these mixed constructions are typically designed considering only the lateral stiffness and strength of the RC walls, while URM walls are designed to resist only vertical forces.

In order to evaluate all the aforementioned issues, a research programme was initiated at the EPFL to gain more insight into the seismic response of modern RC-URM structures [Paparo and Beyer, 2014; Beyer et al., 2014; Tondelli et al., 2014]. Experimental, numerical and mechanical investigations have been carried out with the objective of providing guidelines for the design of mixed RC-URM constructions and the retrofit of URM structures by addition or replacement of URM walls with RC ones.

2 Problem statement

As outlined in the previous section, in Switzerland several buildings are constructed with RC and URM walls connected by RC slabs. However, there is a general lack of knowledge on

their behaviour and generally such buildings are designed without taking into account the interaction which arises between the masonry and the concrete walls.

URM walls exhibit in-plane shear or flexural behaviour depending on several parameters such as the vertical load ratio, the wall geometry and the coupling effect provided by slabs and spandrels. Since in such structures the URM walls are connected by RC slabs which introduce an important framing effect [Lang, 2002], the URM walls exhibit a dominant shear behaviour. On the other hand, the considered RC walls exhibit a dominant flexural behaviour, leading to displacement capacities that are larger than those of the URM walls (see Section 1).

Under lateral loading, shear dominated URM constructions concentrate the inter-storey drifts in the lowest storey (Figure 5a). On the contrary, structures composed of flexural RC walls exhibit the largest inter-storey drift in the top storey (Figure 5b). In mixed RC-URM buildings, at the height of the slabs, URM and RC walls need to display by the same amount. Hence, the deformed shape of such mixed structures tends to be linear (Figure 5c) and, as proved also by quasi-static and dynamic tests (Figure 6), the damage in the URM walls is not concentrated in the lowest storey, but it also spreads to the storeys above.

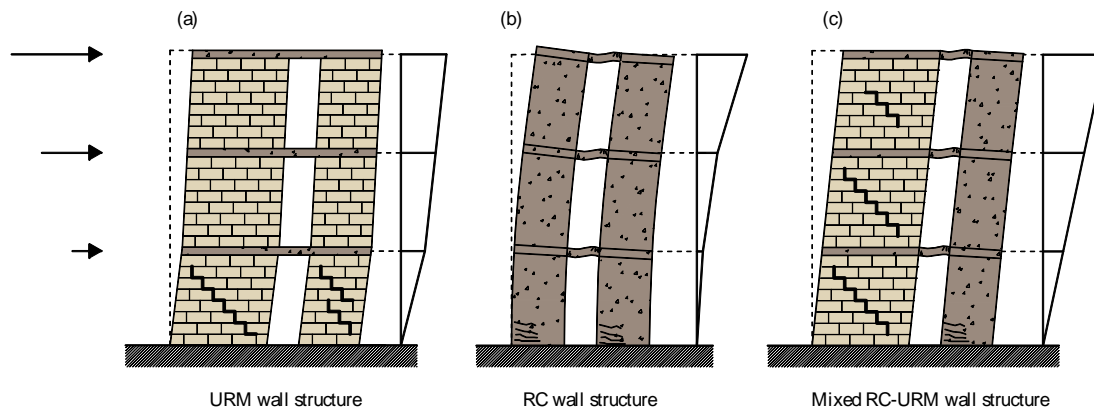


Figure 5: Deformed shape and inter-storey drift of a URM, RC and mixed RC-URM structure.



Figure 6: Crack pattern after failure for two mixed RC-URM wall structures [Paparo and Beyer, 2014; Beyer et al., 2014].

From the considerations of the previous paragraph, there appears to be possible to modify the global displacement profile of a shear dominated URM building by adding RC flexural walls. Indeed, Figure 7 compares the failure mechanisms of a mixed RC-URM structure versus that of a URM building with dominant shear behaviour. For the same amount of maximum inter-storey drift δ^* , the mixed configuration exhibits an increase in the displacement capacity, if compared to the URM construction: $\Delta_{mixed} > \Delta_{URM}$. From the aforementioned, it is clear that adding RC walls to shear dominated URM buildings might increase not only the strength but also the displacement capacity of the mixed system, if compared to the plain URM construction. The aim of the thesis is to propose a design approach which maximises this increase in displacement capacity by considering the in-plane shear-flexure interaction which develops between URM and RC walls.

On the other hand, if the URM walls present a dominant flexural response, their inter-storey drift profile is rather constant over the height. As a consequence, the modification of the deformed shape by coupling RC and URM walls with dominant rocking behaviour is less beneficial than the case where URM walls exhibit a dominant shear behaviour. However, as said before, in these structures the URM walls generally exhibit a shear behaviour because of the important framing effect introduced by the RC slabs.

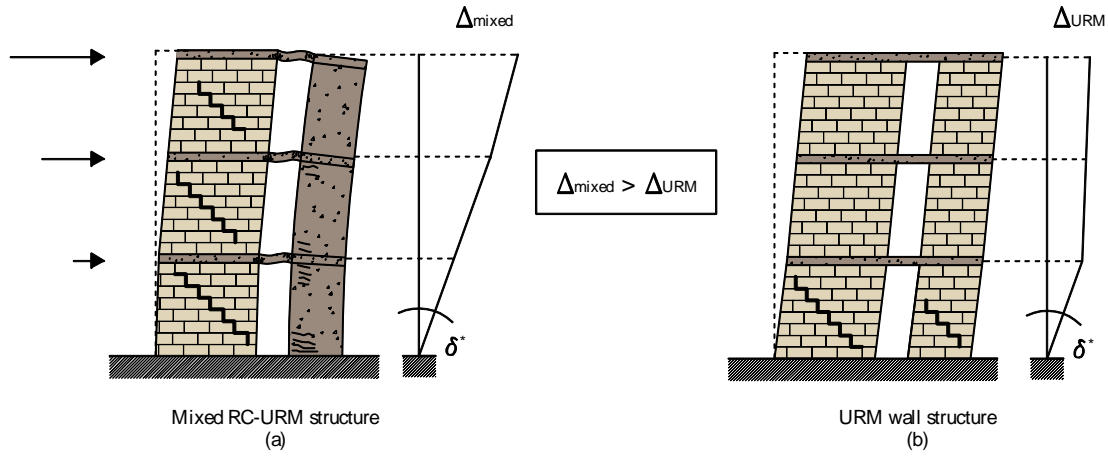


Figure 7: Failure mechanisms, for the same level of maximum inter-storey drift δ^* , of a mixed RC-URM structure (a) and a URM wall structure (b).

In structures with URM walls, in addition to the in-plane behaviour, the masonry walls might also experience local mechanisms, associated with their out-of-plane behaviour. Even though a complete seismic examination of structures with URM walls would require the evaluation of both failure modes, the thesis does not examine the out-of-plane failure of URM elements and focuses only on the in-plane interaction between RC and URM walls. Investigations on the out-of-plane behaviour of mixed RC-URM systems have been carried out by Tondelli and Beyer [2014].

3 Objectives

Since mixed RC-URM systems are rather common and, at the same time, there are several open issues to be addressed (Section 1), the thesis has the following objectives:

- i)* To understand better the seismic behaviour of modern buildings composed of both RC and URM walls and coupled together by RC slabs;
- ii)* To formulate practical recommendations for setting up numerical models, using as input the geometry of the structure and the results from material tests;

iii) To develop a mechanical model which represents the seismic behaviour of such mixed structures that attain moderate to extensive damage (i.e., significant damage, SD, limit state [EN1998-3, 2005]);

iv) To propose a displacement-based methodology for the design of new mixed RC-URM wall structures and the retrofit of URM buildings by adding RC walls or replacing URM walls with RC ones. The proposed displacement-based approach can be used for the design of systems expected to attain moderate to extensive damages (SD limit state). Design for operational limit states is not considered in this research.

4 Methodology and main contributions

Since there was lack of experimental data, the research programme started with an experimental campaign to examine the seismic response of such mixed systems. The campaign consisted of investigating two mixed RC-URM wall substructures which represent the most critical parts of an entire typical modern mixed RC-URM construction built in Switzerland (see Section 1). Two quasi-static cyclic tests on two-third scale models of a prototype structure were carried out. The specimens were composed of one RC wall coupled to one URM wall by two RC beams. The difference between the two tests was the axial load applied at the top of the walls: for the first test, it was chosen to achieve a dominant shear behaviour of the URM wall, while for the second one the axial load was reduced to obtain a dominant rocking mode. A particular test set-up was designed to allow calculating the distribution of the reaction forces (axial force, shear force and bending moment) between the two walls.

In order to evaluate the seismic behaviour of mixed RC-URM wall structures, two modelling approaches are chosen: a shell-element approach and a macro-element strategy. The numerical results are compared with each other and validated against the experimental evidence. The objective is to propose practical recommendations for setting up models using as input the geometry of the structure and results from standard material tests. Several mixed RC-URM wall structures, representing typical layouts resulting from this strengthening technique, are modelled and analysed. The improved behaviour of such mixed structures, compared to the un-retrofitted URM building, is evaluated in terms of global strength and displacement capacity.

A mechanical model capable of representing the behaviour of mixed RC-URM wall structures when subjected to horizontal loads is then developed. The model, originally developed for evaluating the shear-flexure interaction in dual frame-wall systems [e.g., Pozzati, 1980; Smith and Coull, 1991], consists of a pure bending cantilever that represents the entire RC walls and a pure shear beam that describes the entire URM walls. The two elements are continuously connected over the height by axial rigid links with zero moment capacity. As the mechanical model represents the mixed system close to failure (SD limit state), the RC walls are expected to yield. To account for the formation of the plastic hinge at the base of the RC walls, the standard boundary condition that assumes the flexure beam as fixed at the base is modified and the flexural cantilever is modelled with a pinned-base connection to which an external moment, corresponding to the total flexural capacity of the RC walls, is applied.

Finally, a displacement-based procedure for designing and retrofitting such mixed RC-URM wall structures is proposed. The methodology follows the direct displacement-based design (DDBD) approach by Priestley et al. [2007]. The proposed procedure can be used to design structures reaching the SD limit state, whereas design for operational limit states is not considered within this research. A displacement-based rather than a force-based methodology is chosen as design approach since it provides a better representation of the real seismic behaviour of the investigated structure and allows the designer to select the best structural alternative to satisfy the target standard for the given performance level.

5 Outline of the report

In addition to this introduction, the thesis is a collection of three journal papers integrated by an initial and a final chapter and an appendix. The list of the papers is:

- I. Quasi-static cyclic tests of two mixed reinforced concrete – unreinforced masonry wall structures (published in *Engineering Structures*, **71**, 201-211, 2014)
- II. Modelling the seismic response of modern URM buildings retrofitted by adding RC walls (submitted to *Journal of Earthquake Engineering*)
- III. Development of a displacement-based design approach for modern mixed RC-URM wall structures (submitted to *Earthquake and Structures*)

The initial chapter summarises the state of the art on the seismic behaviour and analysis of mixed RC-URM buildings. Additional considerations on the seismic behaviour and design of dual frame-wall systems are outlined since also in this type of buildings an interaction between shear and flexure dominated elements occurs. Afterwards, Paper I summarises the experimental campaign. The purpose of the test series is to obtain experimental evidence and insight into the seismic behaviour of mixed RC-URM wall buildings. The numerical modelling is presented in Paper II. Two modelling strategies are used: a shell-element approach and a macro-element one. The objective is to assess the two modelling strategies against the experimental results and propose practical recommendations that can be used by design engineers. Paper III presents the mechanical model for the representation of such mixed structures when subjected to lateral loading and formulates an extension of the direct displacement-based design [Priestley et al., 2007] for mixed RC-URM wall buildings. The concluding chapter summarises the main contributions of the thesis to the seismic behaviour and design of mixed RC-URM structures. Furthermore, topics for which further research is deemed necessary are outlined. The appendix provides additional information on the quasi-static cyclic tests, including a description of the data of the test series, which are available to the public.

6 References

- Beyer, K., Tondelli, M., Petry, S. and Peloso, S. [2014] “Dynamic testing of a 4-storey building with reinforced concrete and unreinforced masonry walls”, to be submitted to *Bulletin of Earthquake Engineering*.
- Casoli, D. [2007] “Assessment of existing mixed RC-Masonry structures and strengthening by RC shear walls”, Pavia, Italy.
- Cattari, S. and Lagomarsino, S. [2013] “Seismic design of mixed masonry-reinforced concrete buildings by non-linear static analyses”, *Earthquakes and Structures*, 4, N°3.
- EN 1992-1-1 [2004] *Eurocode 2: Design of concrete structures – Part 1-1: General rules and rules for buildings*, CEN, Brussels.
- EN 1998-1 [2004] *Eurocode 8: Design of structures for earthquake resistance – Part 1: General rules, seismic actions and rules for buildings*, CEN, Brussels.
- Hannenwald, P. [2013] “Seismic behaviour of poorly detailed RC bridge piers” Ph.D. thesis, EPFL, Lausanne, Switzerland.

- Jurukovski, D., Krstevska, L., Alessi, R., Diotallevi, P.P., Merli, M. and Zarri, F. [1992] “Shaking table tests of three four-storey brick masonry models: original and strengthened by RC core and by RC jackets”, *Proc. of 10th World Conference on Earthquake Engineering*, Madrid, Spain.
- Lagomarsino, S., Penna, A., Galasco, A. and Cattari S. [2013] “TREMURI program: an equivalent frame model for the non-linear seismic analysis of masonry buildings”, *Engineering Structures*, 6, 1787–1799.
- Lang, K. [2002] “Seismic vulnerability of existing buildings”, Ph.D. thesis, ETH Zurich, Zurich, Switzerland.
- Magenes G. [2006] “Masonry building design in seismic areas: recent experiences and prospects from a European standpoint” Keynote address, *Proc of 1st European Conference on Earthquake Engineering and Seismology*, Geneva, Switzerland.
- Paparo, A. and Beyer, K. [2012] “Pushover analyses of mixed RC-URM wall structures”, *Proc. of 15th World Conference on Earthquake Engineering*, Lisbon, Portugal.
- Paparo, A. and Beyer, K. [2014] “Quasi-static tests of two mixed reinforced concrete – unreinforced masonry wall structures”, *Engineering Structures*, 71, 201-211.
- Penna, A., Lagomarsino, S. and Galasco, A. [2013] “A nonlinear macro-element model for the seismic analyses of masonry buildings”, *Earthquake Engineering and Structural Dynamics*, 10.1002/eqe.2335.
- Pozzati, P. [1980] *Teoria e tecnica delle strutture*, UTET, Torino.
- Priestley, M.J.N., Calvi, G.M. and Kowalsky, M.J. [2007] *Displacement-Based Seismic Design of Structures*, IUSS Press, Pavia, Italy.
- Share Project [2013] <http://www.share-project.org/>.
- SIA 262 [2004] *Building code, Swiss Society of Engineers and Architects (SIA): Concrete Structures*, SIA, Zurich.
- Smith, B.S. and Coull, A. [1991] *Tall building structures: analysis and design*, John Wiley & Sons, Inc., New York.
- Tomažević, M., Modena, C., Velechovsky, T and Weiss, P. [1990] “The effect of reinforcement on the seismic behaviour of masonry buildings with mixed structural systems: an experimental study”, *Proc. of 9th European Conference on Earthquake Engineering*, Moscow, Russia.

- Tondelli, M., Beyer, K., M., Petry, S. and Peloso, S. [2014] “Data set of a shake-table test on a four-storey structure with reinforced concrete and unreinforced masonry walls”, to be submitted to *Bulletin of Earthquake Engineering*.
- Tondelli, M. and Beyer, K. [2014] “Observations on out-of-plane behaviour of URM walls in buildings with RC slabs”, *Proc. of 9th International Masonry Conference*, Guimaraes, Portugal.

State of the art

State of the art

The chapter briefly introduces topics relevant for the study of the seismic behaviour of mixed RC-URM wall structures. Section 1 outlines the existing numerical and experimental studies carried out on the seismic behaviour of mixed RC-URM structures. Section 2 resumes considerations on the seismic behaviour of dual frame-wall buildings as they present similar features to RC-URM wall constructions. An analysis technique and a design procedure developed for such dual systems are also outlined.

1 Seismic behaviour of mixed RC-URM wall buildings: numerical and experimental studies

From the beginning of the 20th century, the development of the RC technology gave rise to mixed solutions, in which masonry walls are coupled to concrete members [Magenes, 2006; Cattari and Lagomarsino, 2013]. Despite the popularity of such constructions, very little research has been carried out on the seismic behaviour of mixed RC-URM buildings [Magenes, 2006]. In this section, the existing numerical and experimental studies on structures constructed with both RC and URM walls are presented.

1.1 Numerical studies

The assessment of one existing masonry structure and its retrofitting with the addition of two RC walls have been carried out by Casoli [2007]. In his research it is outlined that (i) the addition of the RC walls affects the global response of the structure and, as a consequence, (ii)

in numerical simulations the assumption of the stiffness of the RC walls influences the global response of the retrofitted building (the RC members were modelled as bilinear elements). Furthermore, it is stated that (iii) the addition of RC walls allowed larger top displacement in the retrofitted configuration, if compared to the original URM structure.

Cattari and Lagomarsino [2013] carried out non-linear analyses on mixed RC-URM constructions to simulate several interventions on a URM building (Figure 1). One of the investigated configurations consisted of the demolition of the internal masonry walls and their replacement with RC frames and walls. However, the RC members were non capacity-designed and, differently from the buildings examined in this thesis, they exhibited smaller displacement capacities than the URM walls and decreased the displacement capacity of the mixed system, when compared to the original URM structure. In spite of such a difference, important considerations can be extended for the evaluation of the buildings analysed in this thesis:

- i) The addition of RC members changes the global behaviour of the system and their presence has to be taken into account for correct evaluations of strength and displacement capacity;
- ii) The addition of RC elements improves the seismic behaviour of URM buildings only if the RC members exhibit larger displacement capacities than those of the URM walls.

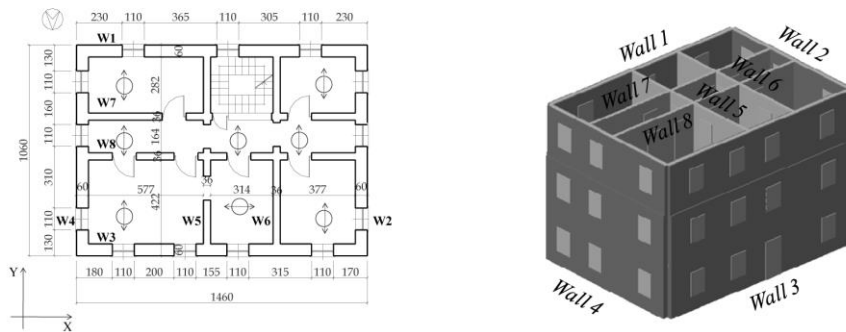


Figure 1: Ground floor plan (dimensions in cm) and 3D model of the URM structure before interventions, from Cattari and Lagomarsino [2013].

Augenti and Parisi [2008; 2009] studied the problem of predicting the seismic behaviour and the distribution of horizontal forces among the elements of torsionally and non-torsionally

eccentric buildings composed of URM walls and RC elements. They also studied the distribution of the internal forces among the members over the height, pointing out the importance of taking into account the interaction between the various structural elements. However, the procedures were developed only for linear elastic analyses and the application in the plastic range has not yet been carried out.

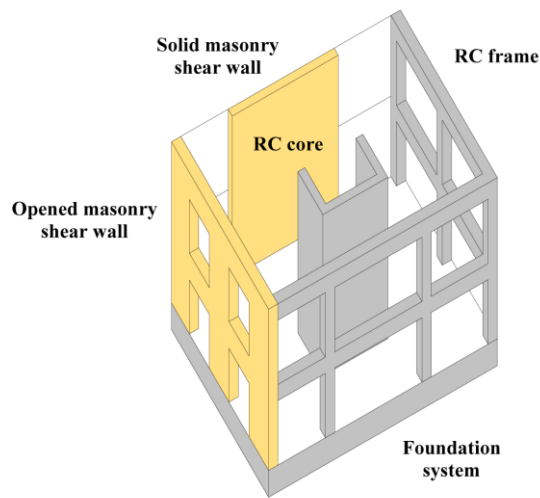


Figure 2: Isometric view of a mixed RC-URM building [Augenti and Parisi, 2009].

1.2 Experimental campaigns

Concerning experimental campaigns, apart from RC walls with URM infills, only few tests on mixed RC-URM structures were conducted in the past. (i) Tomažević and co-workers [Tomažević et al., 1990] carried out a shake table test campaign on URM wall buildings. One of the tested models consisted of a URM wall structure with an internal RC column and two RC beams (Figure 3). Nevertheless the RC column exhibited almost negligible contribution on the overall seismic behaviour of the system as the masonry walls were much stiffer than the RC column.

0.51g for the URM model and 1.07g for the retrofitted configuration. (iii) Also Alessi et al. [1994] dealt with experimental studies on the seismic behaviour of mixed RC-URM buildings. However, the high plan and elevation irregularity of the system addressed their research interests towards different topics from those studied in this thesis.

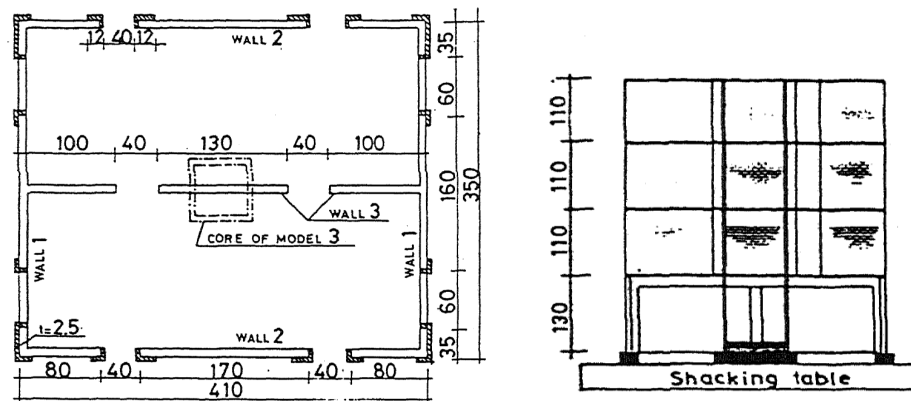


Figure 4: Plan of the second floor and elevation of the models tested by Jurukovsky et al. [1992], dimensions in cm.

2 Seismic behaviour and analyses tools for dual RC frame-wall buildings

The behaviour of mixed RC-URM buildings presents a similarity to that of dual RC frame-wall structures. In dual frame-wall systems, the walls which display mainly flexure deformations are coupled to the frames which - similarly to URM walls - exhibit primarily shear deformations. Due to this similarity, the following sections summarise considerations on the seismic behaviour of dual systems. An analysis technique and a design procedure developed for such dual buildings are also outlined.

2.1 Seismic behaviour of dual RC frame-wall buildings

The existence of phenomena of interaction between frame and walls constrained to work together because of the rigid diaphragm action provided by RC beams or slabs is well known

[e.g., Goodsir, 1985; Smith and Coull, 1991; Paulay and Priestley, 1992]. This interaction arises from the different deformed shapes of the two structural systems. Under lateral loading, frame elements deform primarily in a shear mode (Figure 5a), whereas isolated cantilever walls exhibit a dominant flexure behaviour (Figure 5b). When walls and frames are connected together, the global deflected shape of the structure exhibits a flexural profile in the lowest storeys and, if the RC frames are sufficiently stiff, a shear profile in the upper floors (Figure 5c) [Smith and Coull, 1991]. As a consequence, at the bottom storeys the inter-storey drift is controlled by the walls and at the top storeys by the frames. Such a shear-flexure interaction can be also observed in mixed RC-URM wall structures where the URM walls, somewhat analogous to RC frames, exhibit primarily a shear mode and are coupled to the RC walls which exhibit dominant flexure deformations.

Coupling frames and walls also causes a different distribution over the height of the internal forces among the elements, in comparison to the uncoupled systems. In fact, differently from single wall elements, the RC walls in dual systems exhibit a point of contra-flexure and reverse bending above it.

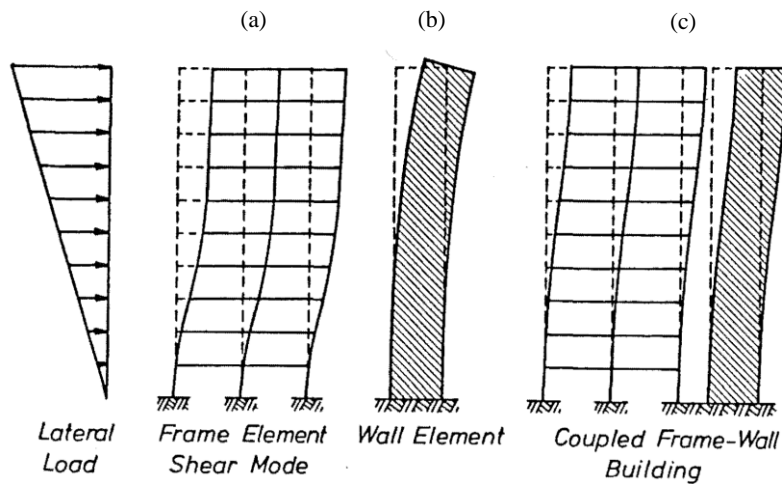


Figure 5: Deformation pattern of frames, walls and dual frame-wall structures, from Goodsir [1985].

Considering the plastic behaviour of dual frame-wall structures, Paulay [2002] identified several advantages of the use of such systems, in comparison to the ductile response of systems with only frames or walls. In the following, some of these advantages are reported:

i) If the strength requirements are satisfied, the displacement profile of the dual system will be mainly controlled by the first mode shape of the RC walls. This provides good control of the storey drifts and avoids the occurrence of soft storey mechanisms in the frames.

ii) Since the RC walls control the horizontal deformations and avoid soft storey mechanism, the development of strong-beam/weak-column mechanisms in the frames also acceptable.

iii) Cantilever RC walls cannot restrict the drift in the top storeys and, in order to avoid drifts which are larger than the design value, the ductility demand of the walls needs to be restricted. The addition of RC frames in dual systems reduces the rotations of the RC walls in the top storeys and, consequently, the ductility demand of the system is not limited any more by the top storey drifts of the RC walls and can be increased.

iv) In dual systems in which both frames and walls have yielded, the designer can arbitrary assign the lateral forces to frames and walls. Paulay [2002] proposed designing the beams of the RC frames to have the same strength demand over the height (except for the roof level). This implies that the frames are loaded by a concentrated force at the roof (Figure 6) and the strength repartition among walls and frames is a design choice, function of the moment capacity assigned to the beams.

In addition, in dual frame-wall structures, the ductile frames offer large amount of energy dissipation and significantly reduce the maximum displacements experienced by the building [Paulay and Priestley, 1992].

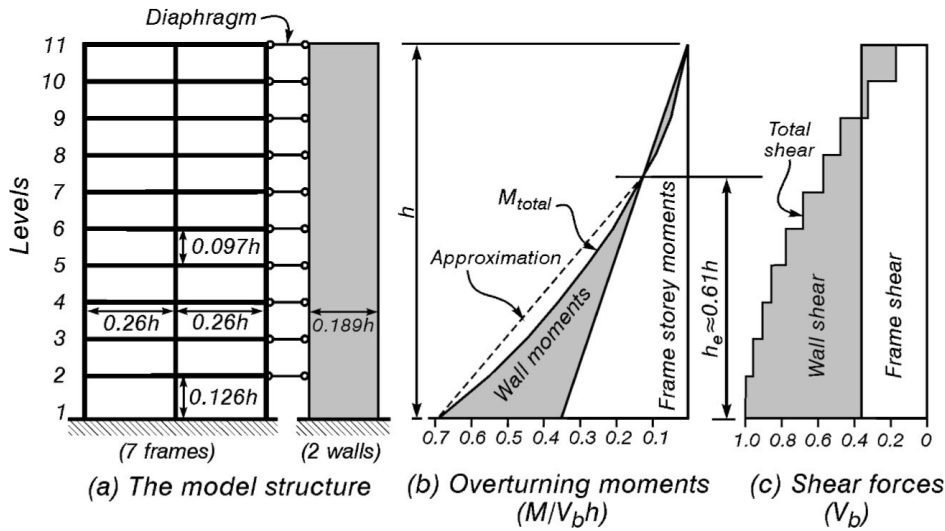


Figure 6: (a): frame-wall structure; (b, c): design choice for the strength repartition among walls and frames, from Paulay [2002].

2.2 Analysis technique for dual RC frame-wall buildings

There are several analysis techniques which aim to represent the shear-flexure interaction which arises between frame and walls. One of these is the so called “shear-flexure cantilever model” and it treats all the flexural walls as one flexural cantilever and all the frames as one shear cantilever [e.g., Chiarugi, 1970; Rosman, 1974; Pozzati, 1980; Smith and Coull, 1991]. The following assumptions are assumed to achieve the analytical solution:

- i) The properties of the walls and the frames are constant over the height;
- ii) The walls are represented by a single pure flexural cantilever characterised by flexure stiffness EI only;
- iii) The frames are represented by a single pure shear cantilever characterised by shear stiffness GA only;
- iv) The RC slabs or beams coupling the walls are modelled as axially rigid links with zero moment capacity. These rigid links connect continuously over the height the two cantilevers which deflect identically;
- v) The structure does not twist and the behaviour is totally plane.

From the aforementioned assumptions, rather simple equations describing the shear-flexure interaction can be formulated. The advantage of this analysis technique is that it gives rapid estimations of the global behaviour of the system and a good qualitative understanding of the influence of walls and frames on the overall behaviour (e.g., the global deformed shape and the distribution of the external forces among the shear and the flexure elements).

The “shear-flexure cantilever model” is described with a differential equation in which the only mechanical parameter is the stiffness ratio α , dimensionless value which represents the ratio between the shear stiffness of the shear cantilever (GA) and the flexure stiffness of the flexure cantilever (EI). Given H the total height of the system, the stiffness ratio α results as [Pozzati, 1980]:

$$\alpha = H \sqrt{\frac{GA}{EI}} \quad (1)$$

The solution of the differential equation can be written as:

$$\text{Shear cantilever:} \quad M_1(x) = A \cosh\left(\alpha \frac{x}{H}\right) + B \sinh\left(\alpha \frac{x}{H}\right) + M_p(x) \quad (2a)$$

$$\text{Flexure cantilever:} \quad M_2(x) = OTM(x) - M_1(x) \quad (2b)$$

Where $M_1(x)$ and $M_2(x)$ are the moments carried by the shear and the flexure cantilevers, respectively. $OTM(x)$ is the overturning moment introduced by the external forces and $M_p(x)$ is the particular solution, depending on the external applied load.

A and B are two constants which are found by assigning two boundary conditions. To the knowledge of the writer, in literature such boundary conditions are always that (i) the moment at the top of the shear cantilever is zero and that (ii) the rotation at the base of the flexure cantilever is zero, which implies that the flexure cantilever is fixed at the bottom. As a consequence, the model cannot represent the yielding at the base of the RC walls.

2.3 Direct displacement-based design for dual RC frame-wall buildings

2.3.1 Basic formulation of the method

Direct displacement-based design (DDBD) is a technique developed over the last 20 years [e.g., Priestley, 1993; Priestley, 1998; Priestley et al., 2007; Pennucci et al., 2009; Sullivan et al., 2012] aimed at designing structures to achieve the selected performance level. The technique is based on the substitute structure approach developed by Gulkan and Sozen [1974] and Shibata and Sozen [1976]. The substitute structure is an elastic single degree of freedom (SDOF) system which represents the performance of the real building at the peak displacement response [Priestley et al., 2007]. Thus, in order to achieve this, the SDOF system is characterised by an effective period (T_e) and an equivalent damping value (ξ_e).

The basic formulation of the DDBD is illustrated here with reference to Figure 7. The multi degree of freedom (MDOF) structure is converted into a SDOF system characterised by effective height (h_e) and effective mass (m_e), Figure 7a. From the knowledge of the yield and design displacements (Δ_y and Δ_d) of the SDOF system, the displacement ductility of the structure μ can be computed (Figure 7b). To account for the energy absorbed during the inelastic response, an equivalent viscous damping ξ_e , function of the design ductility μ and the structural typology, is defined (Figure 7c). From the over-damped spectra and the design displacement profile Δ_d , the effective period (T_e), the effective stiffness (K_e) and the design base shear (V_b) are derived, Figure 7d.

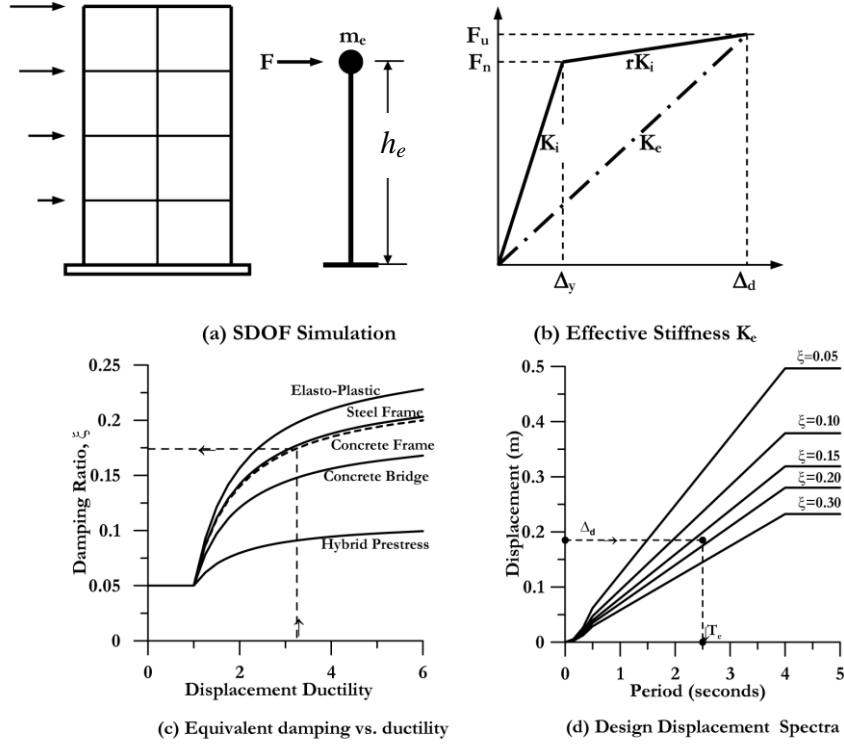


Figure 7: Fundamentals of displacement-based design [Priestley 1998].

In Priestley et al. [2007] the equivalent viscous damping is given by:

$$\xi_e = 0.05 + C \frac{\mu - 1}{\mu \pi} \quad (3)$$

where C is a factor calibrated over a large number of inelastic time history analyses (ITHA) and depends on the structural typology. From the equivalent viscous damping ξ_e the over-damped spectra are then derived by using the damping reduction factor η_ξ :

$$\eta_\xi = \left(\frac{0.07}{0.02 + \xi_e} \right)^{0.5} \quad (4)$$

Recently Pennucci et al. [2011] argued that the expressions of the equivalent viscous damping ξ_e are sensitive to the ground motion characteristics and proposed an alternative method based on the displacement reduction factor η_{in} , defined as the ratio of the maximum inelastic displacement (Δ_{in}) to the elastic displacement at effective period (Δ_{el, T_e}):

$$\eta_{in} = \frac{\Delta_{in}}{\Delta_{el,Te}} \quad (5)$$

This method does not require the definition of an equivalent viscous damping and does not appear to be significantly affected by ground motions characteristics. Figure 8 shows that, for the same ground motion set, the scatter of the results in the evaluation of η_{in} is lower than the scatter of the results in the evaluation of ξ_e .

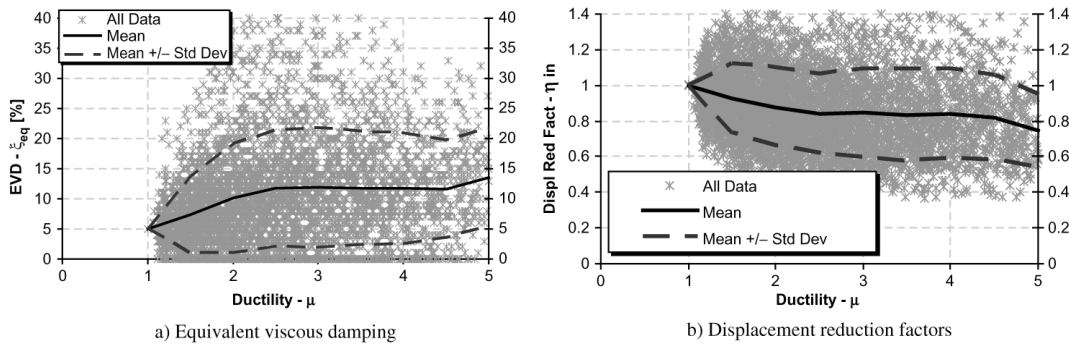


Figure 8: Equivalent viscous damping versus ductility and displacement reduction factor versus ductility for a ground motion set (Takeda Thin hysteresis loop), from Pennucci et al. [2011].

Additionally, Pennucci et al. [2011] observed a strong influence of the displacement spectral shape on the inelastic response and they showed that the maximum inelastic displacement should be related to the variation of the spectral displacement demand over the initial (T_i) and effective (T_e) periods.

Displacement reduction factors η_{in} for URM structures have been proposed by Graziotti [2013]. Figure 9 presents the displacement reduction factors η_{in} versus ductility μ for masonry structures with two Jacobsen hysteretic dampings. In addition, simplified formulations which account for the possible rocking or shear failure mechanism of the URM wall are proposed [Graziotti, 2013]:

$$\text{For flexure:} \quad \eta_{in} = 1 - 0.2 \log_{10}(\mu) \quad (6a)$$

$$\text{For shear:} \quad \eta_{in} = 1 - 0.15 \log_{10}(\mu) \quad (6b)$$

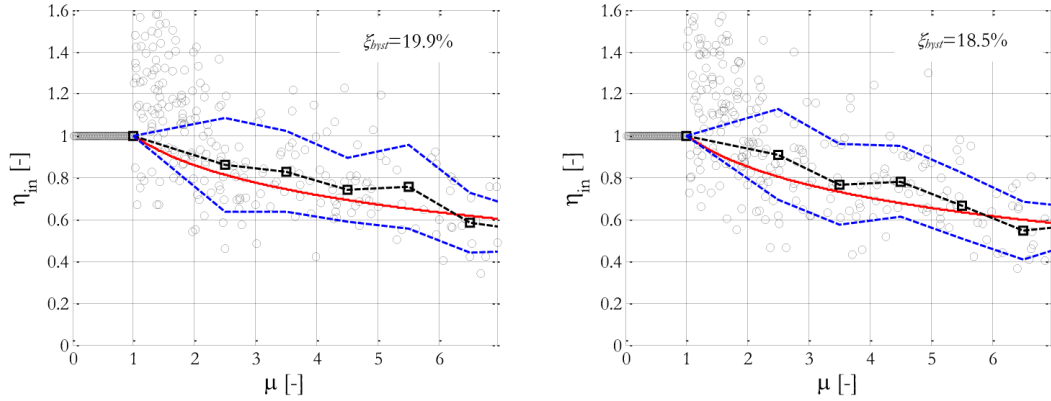


Figure 9: Displacement reduction factor versus ductility for URM structures with Jacobsen hysteretic dampings 19.9% and 18.5%, from Graziotti [2013].

2.3.2 Direct displacement-based design of dual frame-wall structures

The DDBD procedure for dual frame-wall structures has been developed by Sullivan et al. [2005, 2006] and is also presented in Priestley et al. [2007]. In the following, the main steps of the procedure are summarised.

The procedure starts with preliminary design choices, in which the designer defines (i) the repartition of the total shear carried by frames and walls and (ii) the vertical distribution of the beam strength, which is generally chosen to result in a constant frame shear at all levels. From the aforementioned design choices and since the global moment profile resulting from the external forces is known, the height of the contra-flexure point (H_{CF}), an important parameter in the definition of the design displacement, is calculated. Note that these considerations are applicable only if, as currently happens, the RC frames have yielded.

Since the RC walls generally govern the deformed shape, the yield displacement profile Δ_{yi} is calculated by assuming a linear curvature profile from the base to the height of contra-

flexure point. Above the contra-flexure point the curvature is assumed to be zero. On the basis of these assumptions, the displacement Δ_{yi} at height h_i results:

$$\text{For } h_i < H_{CF} \quad \Delta_{yi} = \phi_{yW} \left(\frac{h_i^2}{2} - \frac{h_i^3}{6H_{CF}} \right) \quad (7a)$$

$$\text{For } h_i > H_{CF} \quad \Delta_{yi} = \phi_{yW} \left(\frac{H_{CF}h_i}{2} - \frac{H_{CF}^2}{6} \right) \quad (7b)$$

Where ϕ_{yW} is the curvature at the wall base. Since the frames are much more flexible than the walls, the design displacement is limited by the material strain in the wall plastic hinge or by the (non-structural) drift limitation at H_{CF} . For instance, given ϕ_{ls} the limit strain curvature and L_P the plastic hinge length, for limit strain the design displacement profile results as follows:

$$\Delta_{Di} = \Delta_{yi} + (\phi_{ls} - \phi_{yW})L_P H_i \quad (8)$$

The design displacement (Δ_d), the effective mass (m_e) and the effective height (h_e) of the SDOF system are then given in the usual fashion [Priestley et al., 2007]:

$$\Delta_d = \frac{\sum m_i \Delta_i^2}{\sum m_i \Delta_i} \quad (9)$$

$$m_e = \frac{\sum m_i \Delta_i}{\Delta_d} \quad (10)$$

$$h_e = \frac{\sum m_i \Delta_i H_i}{\sum m_i \Delta_i} \quad (11)$$

The equivalent viscous damping of the system (ζ_{sys}) is then obtained from a weighted average, proportionally to the base resisting moment, of the damping provided by walls (ζ_W) and frames (ζ_F):

$$\xi_{sys} = \frac{\xi_W M_{OTM,W} + \xi_F M_{OTM,F}}{M_{OTM}} \quad (13)$$

M_{OTM} , $M_{OTM,W}$ and $M_{OTM,F}$ are the total overturning moment and the contributions of the walls and the frames to the total overturning moment. The ratios $M_{OTM,W}/M_{OTM}$ and $M_{OTM,F}/M_{OTM}$ are known from the design choice of the repartition of the total shear carried by walls and frames respectively. The ductility demand of the walls is given by:

$$\mu_W = \Delta_d / \Delta_{yW} \quad (14)$$

Where Δ_{yW} is found by substituting h_e into Eq. (7). The ductility demand of the frames can instead be estimated by dividing the design displacement by the yield displacement at h_e :

$$\mu_F = \Delta_d / (\theta_{yF} h_e) \quad (15)$$

Where θ_{yF} is the frame yield drift. The subsequent part of the procedure is standard and involves the calculation of the effective period (T_e), effective stiffness (K_e) and base shear (V_b). The latter is then distributed among walls and frames in accordance with the initial choice of the shear repartition.

3 References

- Alessi, A., Diotallevi, P.P., Merli, M., Zarri, F., Jurukovski, D., Tashkov, L. and Bojadziev, M. [1994] “Comparison of dynamic properties of a mixed reinforced concrete masonry building before and after strengthening”, *Proc. of 10th European Conference on Earthquake Engineering*, Vienna, Austria.
- Augenti, N. and Parisi, F. [2008] “Three-dimensional seismic analysis of masonry combined systems”. *Proc. of 14th World Conference on Earthquake Engineering*, Beijing, China.
- Augenti, N. and Parisi, F. [2009] “Numerical analyses of masonry-RC combined systems”. *Prohitech 2009*, Rome, Italy.
- Casoli, D. [2007] “Assessment of existing mixed RC-Masonry structures and strengthening by RC shear walls”, Pavia, Italy.

- Cattari, S. and Lagomarsino, S. [2013] “Seismic design of mixed masonry-reinforced concrete buildings by non-linear static analyses”, *Earthquakes and Structures*, 4, N°3.
- Chiarugi, A. [1970] “Indagine sulla ripartizione delle azioni orrizzontali in telai irrigiditi da pareti”, *Giornale del Genio Civile*, 2, 187-203.
- Goodsir, W.J. [1985] “The design of coupled frame-wall structures for seismic actions”, Christchurch, New Zeland.
- Graziotti, F. [2013] “Contribution towards a displacement-based seismic assessment of masonry structures”, Pavia, Italy.
- Gulkan, P. And Sozen, M. [1974] “Inelastic response of reinforced concrete structures to earthquake motions”, *ACI Journal*, 74(12), 604-610.
- Jurukovski, D., Taskov, L., Petkovski, M. and Kretevska, L. [1989a] “Basic and applied research study for seismic modelling of mixed reinforced concrete – masonry buildings. Shaking table test of reduced scale model”. IZIIS Test Report n° 89/66, Skopje, Macedonia.
- Jurukovski, D., Taskov, L., Petkovski, M. and Kretevska, L. [1989b] “Basic and applied research study for seismic modelling of mixed reinforced concrete – masonry buildings. Shaking table test of reduced scale repaired model”. IZIIS Test Report n° 89/75, Skopje, Macedonia.
- Jurukovski, D., Taskov, L., Petkovski, M. and Kretevska, L. [1991a] “Basic and applied research study for seismic modelling of mixed reinforced concrete – masonry buildings. Shaking table test of reduced scale model strengthened by external reinforced concrete walls”. IZIIS Test Report n° 91/01, Skopje, Macedonia.
- Jurukovski, D., Taskov, L., Petkovski, M. and Kretevska, L. [1991b] “Basic and applied research study for seismic modelling of mixed reinforced concrete – masonry buildings. Shaking table test of reduced scale model strengthened by concrete central core”. IZIIS Test Report n° 91/92, Skopje, Macedonia.
- Jurukovski, D., Kretevska, L., Alessi, A., Diotallevi, P.P., Merli, M. and Zarri, F. [1992] “Shaking table tests of three four-storey brick masonry models: original and strengthened by RC core and by RC jackets”, *Proc. of 10th World Conference on Earthquake Engineering*, Madrid, Spain.

- Magenes G. [2006] “Masonry building design in seismic areas: recent experiences and prospects from a European standpoint” Keynote address, *Proc of 1st European Conference on Earthquake Engineering and Seismology*, Geneva, Switzerland.
- Paulay, T. [2002] “A displacement-focused seismic design of mixed building systems”, *Earthquake Spectra*, 18(4), 689-718.
- Paulay, T. and Priestley, M.N.J. [1992] *Seismic design of reinforced concrete and masonry buildings*, John Wiley & Sons, Inc., New York.
- Pennucci, D., Calvi, G.M. and Sullivan, T.J. [2009] “Displacement-based design of pre-cast walls with additional dampers”, *Journal of Earthquake Engineering*, 13 (S1), 40-65.
- Pennucci, D., Sullivan, T.J. and Calvi, G.M. [2011] “Displacement reduction factors for the design of medium and long period structures”, *Journal of Earthquake Engineering*, 13(S1), 1-29.
- Pozzati, P. [1980] *Teoria e tecnica delle strutture*, UTET, Torino.
- Priestley, M.J.N. [1993] “Myths and fallacies in earthquake engineering – conflict between design and reality”, *Bulletin, NZ National Society for Earthquake Engineering*, 26(3), 329-341.
- Priestley, M.J.N. [1998] “Direct displacement-based design of buildings”, *Proc. of 11th European Conference on Earthquake Engineering*, Paris, France.
- Priestley, M.J.N., Calvi, G.M. and Kowalsky, M.J. [2007] *Displacement-Based Seismic Design of Structures*, IUSS Press, Pavia, Italy.
- Rosman, R. [1974] “Stability and dynamics of shear-wall frame structures”, *Building Science*, 9, 55-63.
- Shibata, A. and Sozen M. [1976] “Substitute structure method for seismic design in reinforced concrete”, *ASCE Journal of Structural Engineering*, 102(1), 1-18.
- Smith, B.S. and Coull, A. [1991] *Tall building structures: analysis and design*, John Wiley & Sons, Inc., New York.
- Sullivan, T.J., Priestley M.J.N. and Calvi, G.M. [2005] “Development of an innovative seismic design procedure for frame-wall structures”, *Journal of Earthquake Engineering*, 10 (Special Issue 1), 91-124.
- Sullivan, T.J., Priestley M.J.N. and Calvi, G.M. [2006] “Direct displacement-based design of frame-wall structures”, *Journal of Earthquake Engineering*, 9 (Special Issue 2), 279-307.

- Sullivan, T.J., Priestley M.J.N. and Calvi, G.M. [2012] *A Model Code for the Displacement-Based Seismic Design of Structures*, IUSS Press, Pavia, Italy.
- Tomaževič, M., Modena, C., Velechovsky, T and Weiss, P. [1990] “The effect of reinforcement on the seismic behaviour of masonry buildings with mixed structural systems: an experimental study”, *Proc. of 9th European Conference on Earthquake Engineering*, Moscow, Russia.

Paper I: Quasi-static cyclic tests of two mixed reinforced concrete-unreinforced masonry wall structures

Published in *Engineering Structures*, **71**, 201-211, 2014

Quasi-static cyclic tests of two mixed reinforced concrete-unreinforced masonry wall structures

Abstract

In several seismic countries, residential buildings are constructed using both reinforced concrete (RC) and unreinforced masonry (URM) walls. Despite their popularity, there is a general lack of knowledge concerning the seismic behaviour of such mixed systems and they are often designed using oversimplifying assumptions. For this reason, a research programme was initiated at EPFL with the objective of contributing to the understanding of the seismic behaviour of such structures. This paper presents two quasi-static cyclic tests on two-third scale models of a prototype structure. The two specimens are composed of a two-storey RC wall coupled to a two-storey URM wall by means of RC beams. The horizontal forces were applied at the two floor levels. The main difference between the two test units was the axial load applied at the top of the walls. A particular test set-up allowed measuring the reaction forces (axial force, shear force and bending moment) at the base of the URM wall. From the applied horizontal and vertical loads the reaction forces at the base of the RC wall were computed. It was hence possible to back-calculate the distribution of the reaction forces between the two walls. The article describes the design of the test units, the test set-up and the damage evolution during testing. The main results are summarised and behaviour patterns of mixed RC-URM wall structures identified.

Keywords: Seismic behaviour; Mixed wall structures; Reinforced concrete; Unreinforced masonry; Large scale tests.

1 Introduction

Existing unreinforced masonry (URM) buildings, which do not pass the seismic design check, are often strengthened by adding RC walls to the existing structure or by replacing selected URM walls with RC ones. The RC walls herein considered are designed for developing a stable flexural response and failing for larger displacement demands than the URM walls. In Switzerland, such mixed construction technique is also adopted for new residential buildings up to five-six storeys. Despite the popularity of these mixed constructions, very little is known about their seismic behaviour, as only few studies were carried out in the past [Magenes, 2006]. As a consequence, codes do not provide guidelines for mixed RC-URM wall structures and design engineers, when conceiving such structures, often adopt oversimplified assumptions. As an example, in Switzerland typically only the lateral stiffness and strength of the RC walls is taken into account for the seismic design of mixed RC-URM wall buildings. In most building configurations the URM walls outnumber, however, the RC walls and, as the paper will show, influence therefore significantly the lateral stiffness and strength of the building.

Numerical studies on mixed RC-URM wall structures [Paparo and Beyer, 2012; Casoli, 2006; Cattari and Lagomarsino, 2013; Cattari, 2007; Liberatore et al, 2007] confirmed that URM walls have to be considered when realistic estimates of the structure's stiffness and strength are sought. For example, since the global response of mixed RC-URM wall structures is influenced by both types of walls, the displacement profiles of mixed RC-URM wall structures differ from those of buildings with RC or URM walls only. At the same time, numerical results are very sensitive to the modelling assumptions [Paparo and Beyer, 2012; Casoli, 2006;] but the models could not be validated since experimental evidence on the seismic behaviour of mixed RC-URM wall structures was lacking [Magenes, 2006]. Non-linear static analyses on mixed RC-URM structures were carried out by Cattari and Lagomarsino [Cattari and Lagomarsino, 2013]. However, their analyses focused on mixed structures with RC walls designed for vertical loads only. As a consequence, the RC walls failed before the URM ones and decreased the displacement ductility capacity of the mixed structure when compared to a regular URM building.

Only two experimental campaigns on mixed RC-URM structures were conducted in the past (apart from RC frames with URM infills). The first study consisted of shake table tests on a URM wall building with one RC column [Tomažević et al., 1990]. Nevertheless, the latter had no influence on the behaviour of the structure under lateral loads since the URM walls were considerably stiffer than the RC column. Therefore this test cannot be used as benchmark for the seismic evaluation of mixed RC-URM wall structures. An additional study dealt with the behaviour of a mixed structure composed of URM walls and one RC frame on the ground floor [Alessi et al., 1990; Alessi et al., 1994; Jurukowski et al., 1989a; Jurukowski et al., 1989b; Jurukowski et al., 1991a; Jurukowski et al., 1991b; Jurukowski et al., 1992]. Coupling the two systems vertically addresses, however, very different issues than the horizontal coupling. The authors of this study also investigated different strengthening solutions including one which consisted in adding a RC central core wall connected to the foundation by means of a rubber plate [Jurukowski et al., 1991b; Jurukowski et al., 1992]. Hence, none of the experimental studies addressed the seismic behaviour of mixed RC-URM wall structures where RC and URM walls are continuous over the height and the RC walls fixed to the foundation. Moreover, existing studies only addressed the global behaviour and not the contribution of the individual components. For this reason, an experimental campaign was initiated at the École Polytechnique Fédérale de Lausanne (EPFL) in which both dynamic and quasi-static cyclic tests on mixed RC-URM wall structures were performed.

This paper describes the results of the quasi-static cyclic tests on two units representing two-third scale models of a prototype structure. The two-storey test units are composed of a RC wall and a URM wall which are coupled by means of RC beams. The test setup is particular as it allows measuring the reaction forces at the base of the URM wall. The objective of the test is to provide high quality experimental data for (i) calibrating and evaluating numerical and analytical models and (ii) investigating the contribution of the URM and RC walls to the system's strength, stiffness, deformed shape and displacement capacity. Following this introduction, Section 2 describes the design of the test units and the test set-up. Section 3 continues with the presentation of the test results and their discussion. A summary of the most important features of the behaviour of mixed RC-URM wall structures when subjected to lateral loading is presented in Section 4, which concludes with an outlook on future research activities.

2 Experimental investigation

Two large scale specimens were constructed and tested at the structural engineering laboratory of EPFL. In the following, the geometry of the test units, their relationship with a fictitious four storey mixed reference structure, the material properties, the test set-up and the loading history are described.

2.1 Test units and reference structure

Each of the two test units comprised a two-storey URM wall coupled to a two-storey RC wall by two RC beams. The main difference between the two systems was the axial load applied at the top of the walls. For the first system (TU1), an axial load of 400 kN was applied at the top of the URM wall leading to a behaviour of the latter controlled by shear deformations; for the second test (TU2) the axial load was reduced to 200 kN in order to achieve a prevalent rocking behaviour of the URM wall. The RC walls of TU1 and TU2 were subjected to axial loads of 125 kN and 0 kN, respectively.

Each test unit aimed at representing the most critical elements of a mixed RC-URM wall structure. The reference structure is a four storey building (Figure 1) with three URM walls and one RC wall. The walls are coupled at the floor levels by means of RC slabs. Due to the shear forces transferred by the RC slabs, the axial forces in the external walls vary when the building is subjected to lateral loading, whereas it is almost constant in the internal walls since RC slabs of equal strength and length frame into these walls from both sides.

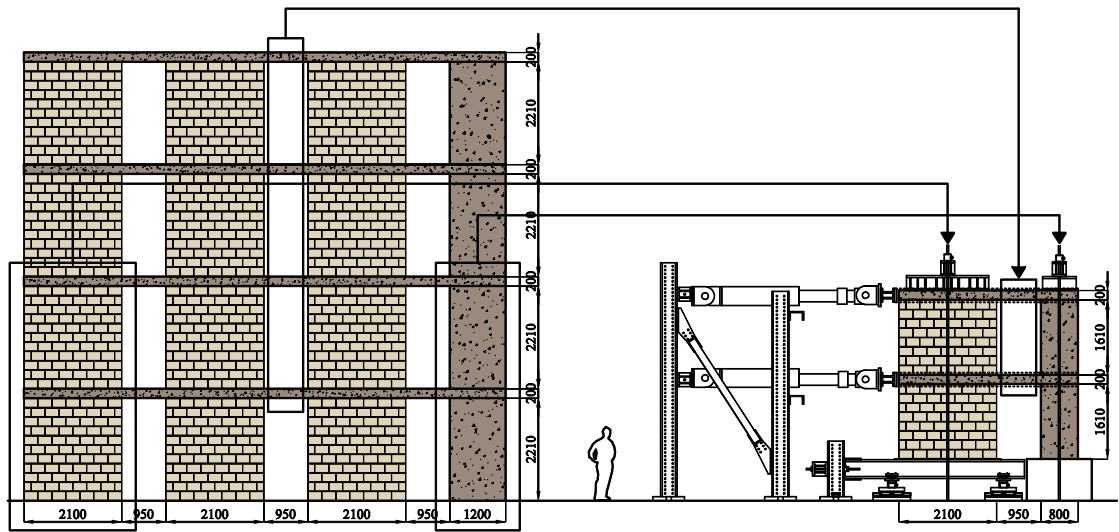


Figure 1: Reference structure and test unit: the elements of the reference structure represented in the test unit are encircled (all dimensions in mm).

The most interesting part of the reference structure comprises the two lower storeys of the two external walls: the walls are expected to fail in the lower storeys and, since the behaviour of URM and RC walls is sensitive to the variation of axial force, the outer walls are of particular concern. The test units represented therefore the two lower storeys of the outer walls of the reference structure. The storey height of the specimens was 1.61 m, which corresponds approximately to two thirds of the storey height of a full-scale structure (Figure 2c). The length of the URM and RC wall were 2.1 m and 0.8 m, respectively; the width of both walls was 0.15 m.

The length of the URM walls was not scaled by a factor of $2/3$ in order to increase their influence on the overall behaviour of the test units, as the number of URM walls from the reference structure to the specimens was reduced from three to one. The RC beams, connecting the two walls, had a cross section of 0.45×0.20 m (width x height) and represented the effective width of the slabs in the reference structure. According to Priestley et al. [2007], the effective width of slabs coupling internal walls can be estimated as three times the wall thickness. The two RC beams were designed to provide approximately the same variation of axial force at the wall base as in the reference structure. Pushover analyses of the reference structure and the test unit showed that the behaviour of the test unit is representative of the behaviour of the reference

structure with regard to the failure mechanism of the URM wall and the redistribution of axial force between the two walls.

The URM walls were constructed using hollow clay bricks which, according to EN 1996-1 [2005], belong to “Group 2”. Furthermore, the selected brick type has continuous longitudinal webs (Figure 3), which are necessary for carrying the in-plane shear forces of the masonry walls. The thickness of the bed joints was 10 mm with dry vertical joints. The RC walls are “model” capacity-designed ductile walls and the RC beams are designed to develop a stable flexural mechanism. The reinforcement layouts of RC walls and RC beams are shown in Figures 2a and 2b, respectively.

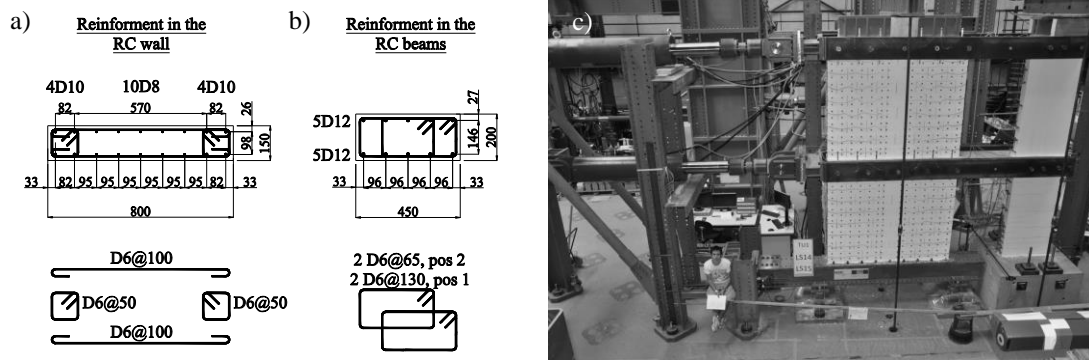


Figure 2: Reinforcement layouts of TU1 and TU2: (a) reinforcement layout of RC walls, (b) reinforcement layout of RC beams, (c) Test set-up showing TU1.

2.2 Material properties of the test units

In addition to the two quasi-static experiments, material tests on bricks, mortar, masonry wallets, concrete and reinforcing bars were carried out. In the following, the most important material properties are summarised. The masonry walls were constructed using hollow-core tongue-and-groove clay bricks with standard dimensions of 300x190x150 mm (length x height x thickness, Figure 3). E-modulus and strength of the bricks were determined according to EN 772-1 [2000] and the results are summarised in Table 1. The mortar was a standard cement mortar (Weber Mur 720). The bed joints had an average thickness of 10 mm; the head joints were not filled. The E-modulus, compressive strength and Poisson’s ratio of the masonry were determined according to EN 1052-1 [1998] and are summarised in Table 2. Triplet tests

according to EN 1052-3 [2002] were used to determine the interface strength between mortar and bricks. Table 3 summarises the Mohr-Coulomb relationships characterising the peak and residual shear strength of the bed joints.

The mechanical properties of the concrete are given in Table 4. Each test unit was cast with two batches of concrete: the first batch was used to construct the foundation and the first storey wall, the second one to build the second storey wall and the two beams. Table 5 summarises the mechanical properties (yield and tensile strength) of the reinforcing steel in beams and walls.

Table 1: Mechanical properties of the bricks (median values and standard deviations)

Test unit	E_{bx} [GPa]	E_{by} [GPa]	f_{cbx} [MPa]	f_{cby} [MPa]
TU1 and TU2	9.8±2.7	4.7±2.0	23.5±1.9	8.4±0.1

E_{bx} and E_{by} : E-modulus for loading along the brick's height and length, respectively;
 f_{cbx} and f_{cby} : Compressive strength for loading along the brick's height and length.

Table 2: Mechanical properties of the mortar (f_{tm} , f_{cm}) and masonry wallets (E_{cM} , f_{cM} and ν_M)

Test unit	f_{tm} [MPa]	f_{cm} [MPa]	E_{cM} [GPa]	f_{cM} [MPa]	ν_M [-]
TU1	5.2±0.6	29.2±3.8	5.2±0.8	4.8±0.8	0.21±0.12
TU2	4.8±0.5	29.5±3.1	5.0±0.7	7.8±0.6	0.14±0.01

f_{tm} and f_{cm} : Tensile and compressive strength of mortar [Beyer et al., 2010];
 E_{cM} , f_{cM} and ν_M : E-modulus, compressive strength and Poisson's ratio of masonry panels subjected to compression orthogonal to bed-joints [EN 1052-1, 1998].

Table 3: Triplet tests: friction coefficient μ , cohesion c and correlation coefficient R^2 for peak and residual strength of mortar-brick interfaces of bed joints (median values)

Mohr-Coulomb relationship	TU1			TU2		
	μ [-]	c [MPa]	R^2 [-]	μ [-]	c [MPa]	R^2 [-]
Peak stress: $\tau_{\max} = \mu_{\text{peak}} \sigma + c_{\text{peak}}$	0.60	0.41	0.90	0.67	0.35	0.94
Residual stress: $\tau_{\text{res}} = \mu_{\text{res1}} \sigma + c_{\text{res1}}$	0.67	0.13	0.90	0.68	0.09	0.98
Residual stress: $\tau_{\text{res}} = \mu_{\text{res2}} \sigma$	0.99	0.00	0.68	0.89	0.00	0.88

Table 4: Mechanical properties of the concrete (median values and standard deviations)

Test unit	f'_c [MPa]	E_c [GPa]	f_{tc} [MPa]	f'_{28c} [MPa]
TU1, Batch 1	57.8±0.9	36.2±0.5	4.6±0.3	50.2±2.2
TU1, Batch 2	45.4±1.5	32.9±1.3	3.6±0.2	38.1±1.7
TU2, Batch 1	60.3±0.5	35.6±0.4	4.4±0.3	52.6±0.9
TU2, Batch 2	47.9±1.8	35.4±1.9	3.7±0.3	43.6

f'_c, E_c, f_{tc} : Cylinder compression strength, E-modulus and tensile strength obtained from double punch tests on half cylinders [SIA262/1, 2003; Chen, 1970] at the day of testing of TU1 and TU2, respectively.

f'_{28c} : Cylinder compression strength after 28 days

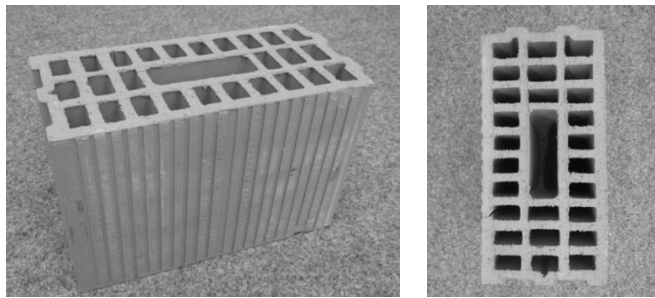


Figure 3: Brick type used for the construction of TU1 and TU2.

Table 5: Properties of reinforcing steel (median values and standard deviations)

Test unit and bar diameter	f_y [MPa]	f_t [MPa]	f_t/f_y [-]
TU1 and TU2: D12 mm bars	527.0±7.5	608.5±8.4	1.155
TU1: D10 mm bars	526.8±1.4	618.9±5.1	1.175
TU2: D10 mm bars	549.9±0.4	617.5±6.1	1.123
TU1 and TU2: D8 mm bars	544.2±10.2	661.2±5.4	1.215
TU1 and TU2: D6 mm bars	471.3	613.9±4.5	1.303

f_y, f_t : Yield strength and tensile strength of the reinforcing steel.

2.3 Test set-up and instrumentation

The behaviour of a mixed RC-URM wall structure depends largely on the relative contribution of URM and RC walls to the system's stiffness and strength. To determine the forces carried by the URM wall of the test unit, a particular test set-up that allowed measuring the reaction forces (axial force, bending moment, shear force) at the base of the URM wall (Figures 2c and 4a) was developed. The URM wall was constructed on one stiff steel beam supported by two systems of sliders and load cells measuring the variation of axial force and

bending moment during the test. In addition, the variation of shear force at the base of the URM wall was measured by a system of load cells and rotational hinges at the left end of the steel beam. Figure 5a shows a close-up of the steel beam with the systems measuring the horizontal and vertical reaction forces at the base of the URM wall. The functionality of the system was verified before the construction of the first test unit by applying different configurations of horizontal and vertical forces of known magnitude to the steel beam. The RC wall was connected to the strong floor through a RC foundation. According to Figure 5b, the reaction forces (variation in axial force ΔN_{URM} due to the applied horizontal forces, shear force V_{URM} and bending moment M_{URM}) at the base of the URM wall can be calculated as follows:

$$\Delta N_{URM} = N_1 + N_2 - N_3 \quad (1)$$

$$V_{URM} = H \quad (2)$$

$$M_{URM} = (-N_1 + N_2) \cdot a + N_3 \cdot b + V_{URM} \cdot c \quad (3)$$

where N_1 and N_2 are the vertical reaction forces and H the horizontal force in the steel beam corresponding to the base shear in the URM wall. The parameters a , b and c are the lever arms of the reaction forces with respect to the centre of the URM wall (Point A, Figure 5b) and are equal to 1.200 m, 2.445 m and 0.220 m, respectively. N_3 is a parasitic force caused by the friction in the two rotational hinges which are part of the system measuring the horizontal reaction force. This force N_3 is considered when computing the axial force ΔN_{URM} and the bending moment M_{URM} at the base of the URM wall; N_3 can account for up to 2% of the variation in axial force ΔN_{URM} and 4% of the moment M_{URM} .

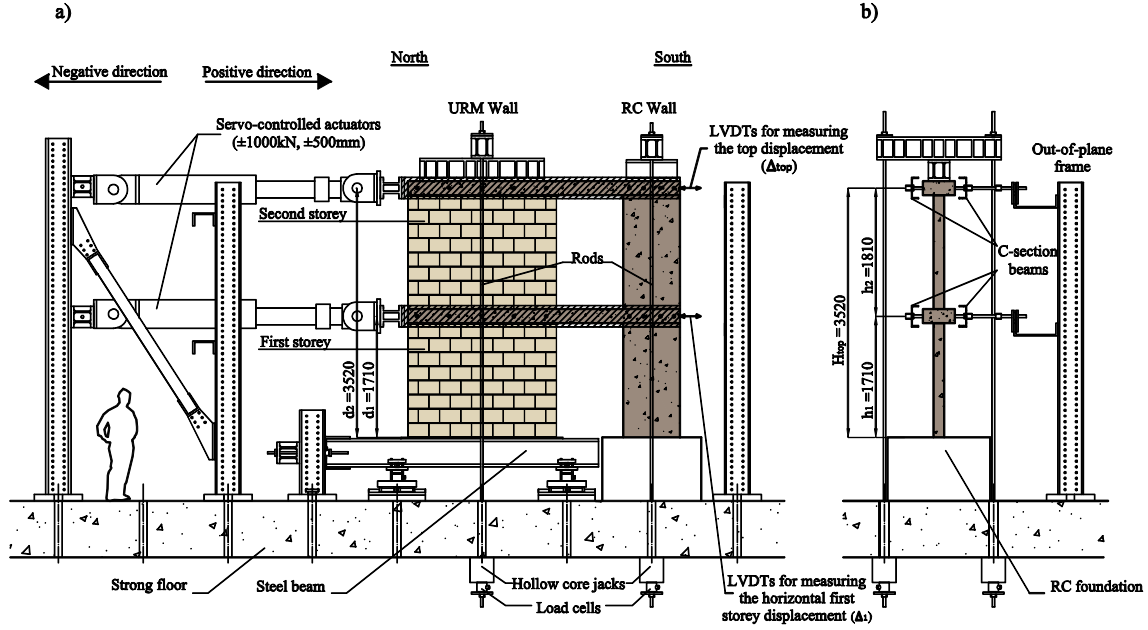


Figure 4: Test set-up: (a) front view, (b) side view; all dimensions in mm.

The external forces acting on the system are: (i) the two horizontal forces (F_{act}) that are applied by the two horizontal actuators, (ii) the vertical forces applied by the system of hollow core jacks and rods, (iii) the self-weight of the test unit and (iv) the weight of the parts of the test set-up that were supported by the test unit. From the external forces and the measured reaction forces at the base of the URM wall, the reaction forces at the base of the RC wall can be back-calculated (variation in axial force ΔN_{RC} due to applied horizontal forces, shear force V_{RC} and bending moment M_{RC}):

$$\Delta N_{RC} = -\Delta N_{URM} \quad (4)$$

$$V_{RC} = V_{tot} - V_{URM} \quad (5)$$

$$M_{RC} = OTM - M_{URM} - \Delta N_{URM} \cdot L_{base} \quad (6)$$

where L_{base} is equal to 2.400 m and corresponds to the distance between the wall axes. The total overturning moment OTM at the base of the walls equates to:

$$OTM = F_{act} \cdot d_1 + F_{act} \cdot d_2 \quad (7)$$

where d_1 is equal to 1.710 m and d_2 is equal to 3.520 m; they correspond to the height of the two horizontal actuators above the base of the walls (Figure 4a). The shear forces V_{URM} and V_{RC} as well as the bending moments M_{URM} and M_{RC} were considered positive for the positive loading direction (see arrows in Figure 4a).

The axial load was applied at the top of the walls by means of vertical rods and hollow core jacks (Figure 4a) and kept constant during the test. A frame behind the test unit prevented out-of-plane deformations during testing (Figure 4b). The axial force at the base of the two walls N_{URM} and N_{RC} was calculated by adding to the variation of the axial force (ΔN_{URM} , ΔN_{RC}) the vertical forces applied by the hollow core jacks and rods (W_1 and W_2 , Figure 6) plus the self-weight of the test unit and the parts of the test set-up that were supported by the URM wall (~60 kN) and the RC wall (~25 kN):

$$N_{URM} = \Delta N_{URM} + W_1 + 60kN \quad (8)$$

$$N_{RC} = \Delta N_{RC} + W_2 + 25kN \quad (9)$$

In Eqs. 8 and 9 a compression axial force at the base of the walls was considered as positive. For the positive loading direction the axial force at the base of the RC wall increases while the axial force at the base of the URM wall decreases (see arrows in Figure 4a). During the quasi-static cyclic test, the servo-controlled actuator at the second storey applied a sequence of cyclic lateral displacements (Figure 4a). The actuator of the first storey was slaved to the one of the second storey to apply the same horizontal force. A fixed load rather than a fixed displacement pattern was applied since the drift profile of the mixed system was one of the sought output quantities (for further information on quasi-static tests on systems with several storeys see Calvi and Kingsley [1996]). The actuator forces F_{act} were transferred to the two walls through two C-section beams attached to the outer edges of the RC beam by means of nine bars per storey. The nine bars allowed distributing the horizontal load along the length of the RC beam. A rather similar system for distributing the horizontal loads in coupled wall systems is documented in Lequesne et al. [2009]. Applying a concentrated force at the end of the RC beam, which is often done in quasi-static cyclic tests, would have introduced an

additional axial force in the coupling beams, which would have modified their moment capacity. The final bar configuration is shown in Figure 6. The bars did not all transmit the same force, since the deformation of the C-section beams between two bars was not negligible. With the chosen bar configuration, approximately 70% of the lateral load was applied to the URM wall and 30% to the RC one; this distribution corresponds approximately to the ratio of the wall lengths, which are taken as indicator for the size of the tributary areas of the walls.

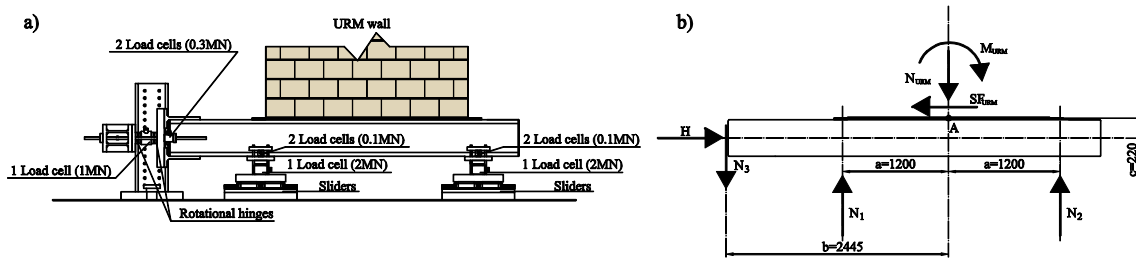


Figure 5: Steel beam with systems to measure the horizontal and vertical forces at the base of the URM wall (a); free body diagram of the steel beam with reaction forces (b). All dimensions in mm.

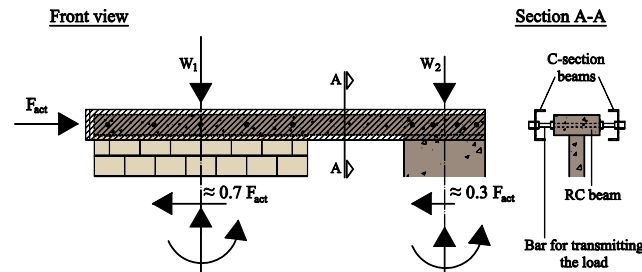


Figure 6: System of C-section beams and bars to distribute the applied horizontal forces along the length of the RC beams: front view and section.

During the tests, in addition to the forces, a significant number of global and local deformation quantities were measured. The horizontal top displacement (Δ_{top}), the horizontal first storey displacement (Δ_1) and the displacements of the foundations were measured by means of linear variable differential transformers (LVDTs). Strain-gauges were placed along the central longitudinal bars of the RC beams. The elongation of the edges of the RC wall was measured by chains of LVDTs; the shear displacement of the RC wall was measured by diagonal string pots. The deformation pattern of the URM wall was recorded using the LED

based optical measurement “Optotrak” from NDI [NDI, 2009]. Additional LEDs were placed on the RC beams, the steel foundation and the C-section beams. At peak displacements and when the horizontal load was zero, the width of selected cracks was measured manually. In the following, “peak crack width” is referred to the crack width measured at the peak displacement, while “residual crack width” to the measurements when the horizontal load was zero.

2.4 Loading history

The loading history comprised two fully reversed cycles with increasing amplitudes up to a drift δ_c for which the strength dropped for one loading direction by more than 10%. For both test units, this drop in strength was first attained in the negative loading direction (TU1: $\delta_c = -0.3\%$; TU2: $\delta_c = -0.4\%$). After the drift δ_c , to avoid a premature axial load failure of the URM wall, the test was continued with half cycles in the positive direction only. The drift of the structure δ (average drift) was defined as the ratio of horizontal top displacement (A_{top}) and height of the structure (H_{top}). The amplitudes of each half-cycle are shown in Figure 7. The definition of the positive and negative directions is indicated in Figure 4a. After each load step the loading was stopped, photos were taken and cracks were marked. The drift controlled load steps commence with LS2. LS0 refers to the state before any displacements or forces were applied (zero measurements). LS1 refers to the load state when the axial loads at the top of the walls were applied and the servo-hydraulic actuators for the horizontal loads were connected.

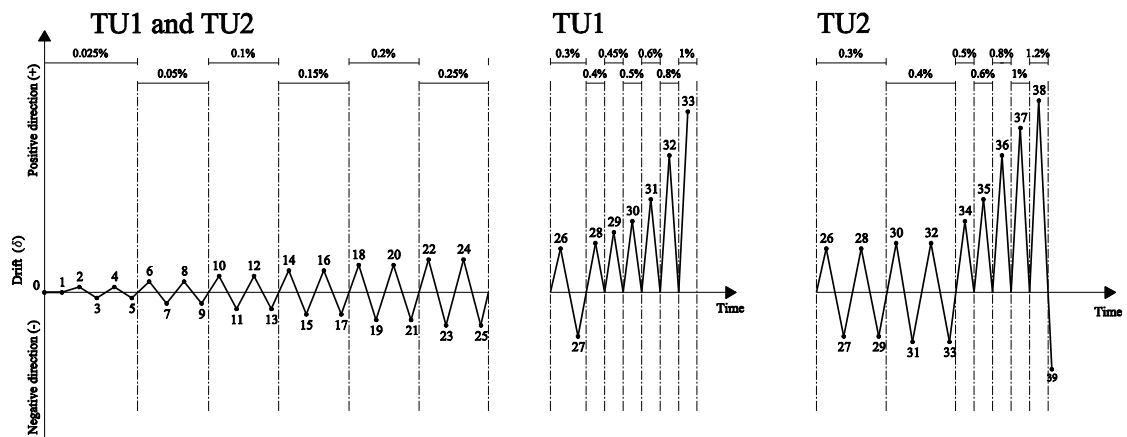


Figure 7: Loading history for TU1 and TU2.

3 Test results

This section presents selected test results of TU1 and TU2 which illustrate the global behaviour of the specimens and their failure mechanisms (Section 3.1) as well as the distribution of the reaction forces between the two walls (Section 3.2). The objective is to provide experimental evidence required for validating numerical or analytical models of mixed RC-URM wall structures and to yield insights into the seismic behaviour of such structures. In the following, the term horizontal load failure describes the shear strength degradation of one wall by 20% of its maximum strength. Axial load failure describes the loss of axial load bearing capacity in one of the URM walls.

3.1 Global behaviour of the test units and their failure mechanisms

3.1.1 Distribution of the inter-storey shear drifts

The distribution of inter-storey shear drifts over the height of the structure yields insights into the interaction of URM and RC walls. For the first and second storey, the inter-storey shear drift δ_s was calculated as follows:

$$\delta_s = \frac{\Delta_i - \Delta_j}{h} - \theta_i - (\theta_j - \theta_i) \quad (10)$$

where Δ_i , Δ_j , θ_i and θ_j are the horizontal displacements and rotations of the beams underneath and above the selected storey and were calculated from the optical measurements [NDI, 2009]. The horizontal displacements (Δ_i , Δ_j) were considered positive for the positive loading direction (see arrows in Figure 4a); the beam rotations (θ_i , θ_j) were considered positive when clockwise.

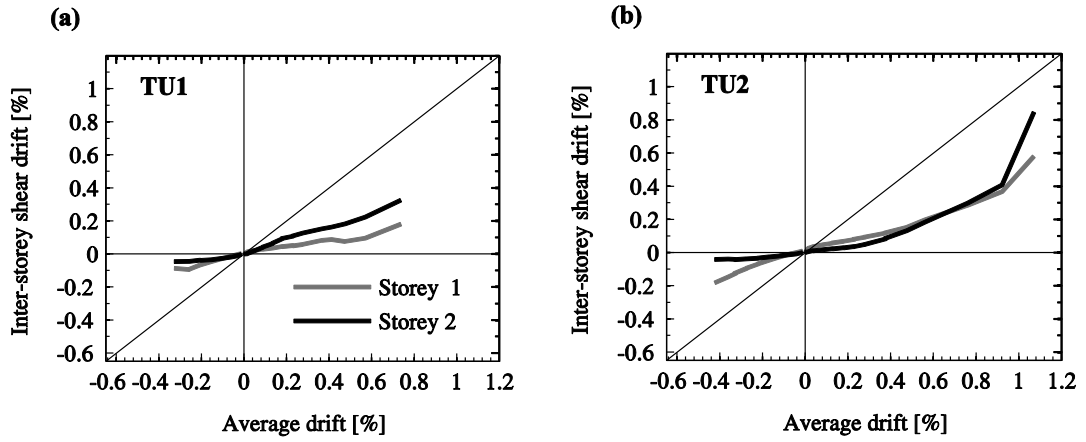


Figure 8: URM inter-storey shear drift for TU1 (a) and TU2 (b).

Figure 8 shows that for the positive loading direction of TU1, the shear deformations of the second storey of TU1 are larger than that of the first storey, while for TU2 the shear deformations of the two storeys are comparable. Indeed, TU1 coupled a RC flexural wall to a URM wall where shear deformations prevailed, leading to large shear forces in the second storey of the URM wall. On the contrary, in TU2 the URM wall displayed a rocking behaviour. Since its deformation mode was more similar to the RC wall, it led to smaller shear forces and hence smaller shear deformations of the second storey of the URM wall.

3.1.2 TU1

The first crack of TU1 developed at the base of the RC wall. It was a horizontal crack which appeared during the very first cycle ($\delta = 0.025\%$). Unlike the RC wall, which second storey remained during the entire test uncracked, the URM wall developed simultaneously cracks in the first and second storey: for the positive and negative loading direction inclined shear cracks formed in both storeys during the cycles with $\delta = 0.1\%$. They followed initially the joints ($\delta = 0.1\%$) but passed soon also through some of the bricks ($\delta = 0.15\%$). The distribution of damage over the entire height of the URM wall differs from buildings with URM walls only, where damage tends to be concentrated in the first storey.

Similar to the behaviour of RC wall-frame structures, the even damage distribution over the height of the structure results from the mixed structural system including flexure-dominated slender RC walls and shear-dominated URM walls. In mixed RC-URM wall structures, these two systems are coupled at the storey levels by RC beams or slabs, which impose equal horizontal displacements on the two types of walls and cause damage to both storeys of the URM wall [Paparo and Beyer, 2012].

For the negative loading direction, the cracks through the bricks of the first storey soon increased in number and width. At $\delta = -0.3\%$ the test unit's horizontal strength reduced (LS27, Figure 9a) and the URM wall featured a horizontal load failure. The URM wall would have also reached axial load failure had the horizontal load not been quickly reduced to zero. The failure mechanism that developed included toe-crushing of the north bottom corner of the first storey of the URM wall and steeply inclined shear cracks with maximum residual crack widths of ~ 3 mm in the first storey whereas only thin inclined shear cracks appeared in the second storey. At the same drift demand for loading in the positive direction (LS26, $\delta = +0.3\%$), the crack pattern of the URM wall comprised shear cracks distributed over the two storeys. Nevertheless, the cracks were larger in terms of number and width in the second storey since δ_s of the second storey was larger than that of the first storey (Figure 8a).

Horizontal load failure initiated for loading in the negative rather than the positive direction as a consequence of the coupling by the two RC beams. For the negative loading direction the axial force in the URM wall increased and, as a result, the deformation capacity of the URM wall was reduced. Petry and Beyer [2014] showed that even if the failure mechanism remains the same, an increase in axial stress reduces the deformation capacity of URM walls. This was confirmed by the tests on the mixed structure, where for the negative loading direction, the URM toe crushing started at smaller displacement demands, leading to a smaller displacement capacity than for loading in the positive direction. Since the axial and shear forces were larger in the first than in the second storey of the URM wall, it was the first storey that failed. Hence the most critical loading direction was the negative one, i.e. when the axial force in the URM wall increased.

After LS27, the test was continued with half cycles in the positive loading direction only. Horizontal load failure of TU1 occurred during the half cycle with $\delta = +0.95\%$ (LS33, Figure 9c), i.e. at a drift demand around three times the drift capacity for loading in the negative

direction. This underscores again the large influence of the axial load ratio on the deformation capacity of URM walls. Axial load failure of the first storey of the URM wall, due to subsequent crushing of the compression struts of the fan pointing towards the compressed toe, followed immediately afterwards and the second storey failed simultaneously along an inclined shear crack. Due to the larger base moment at the first storey, the length of the compressed toe of the URM wall was smaller at the first storey than at the second storey. As a consequence, the compressive strength of the masonry was reached first at the bottom storey, causing the axial load failure of the URM wall. In the previous cycle (LS32, $\delta = +0.8\%$, Figure 9b) the URM wall was already heavily damaged but still capable of bearing the gravity loads.

The cracks in the RC wall, which started developing from the very beginning of the test, were horizontal flexural cracks. At the end of the test, they extended over the entire first storey. The first inclined shear-flexure crack formed at $\delta = +0.8\%$, indicating that the shear force carried by the RC wall had increased significantly since the stiffness of the RC wall was still increasing. At the end of the test (LS33, $\delta = +0.95\%$), other two inclined shear-flexural cracks appeared and some of the longitudinal reinforcing bars at the north edge of the RC wall had yielded but the RC wall was far from failure.

The RC beams connecting the two walls deformed primarily in flexure and at a drift of $\pm 0.05\%$ the first flexural cracks at the ends of the beams appeared. During the test, the length over which the beams were cracked increased and at the north end of the beam the cracked length of the beam penetrated more and more into the URM wall. At $\delta = +0.3\%$, the cracked beam length penetrating the URM wall was 20 cm long and at $\delta = +0.8\%$ it had increased up to 70 cm. At the end of the test, the longitudinal top reinforcement bars at the south end of the beams had yielded.

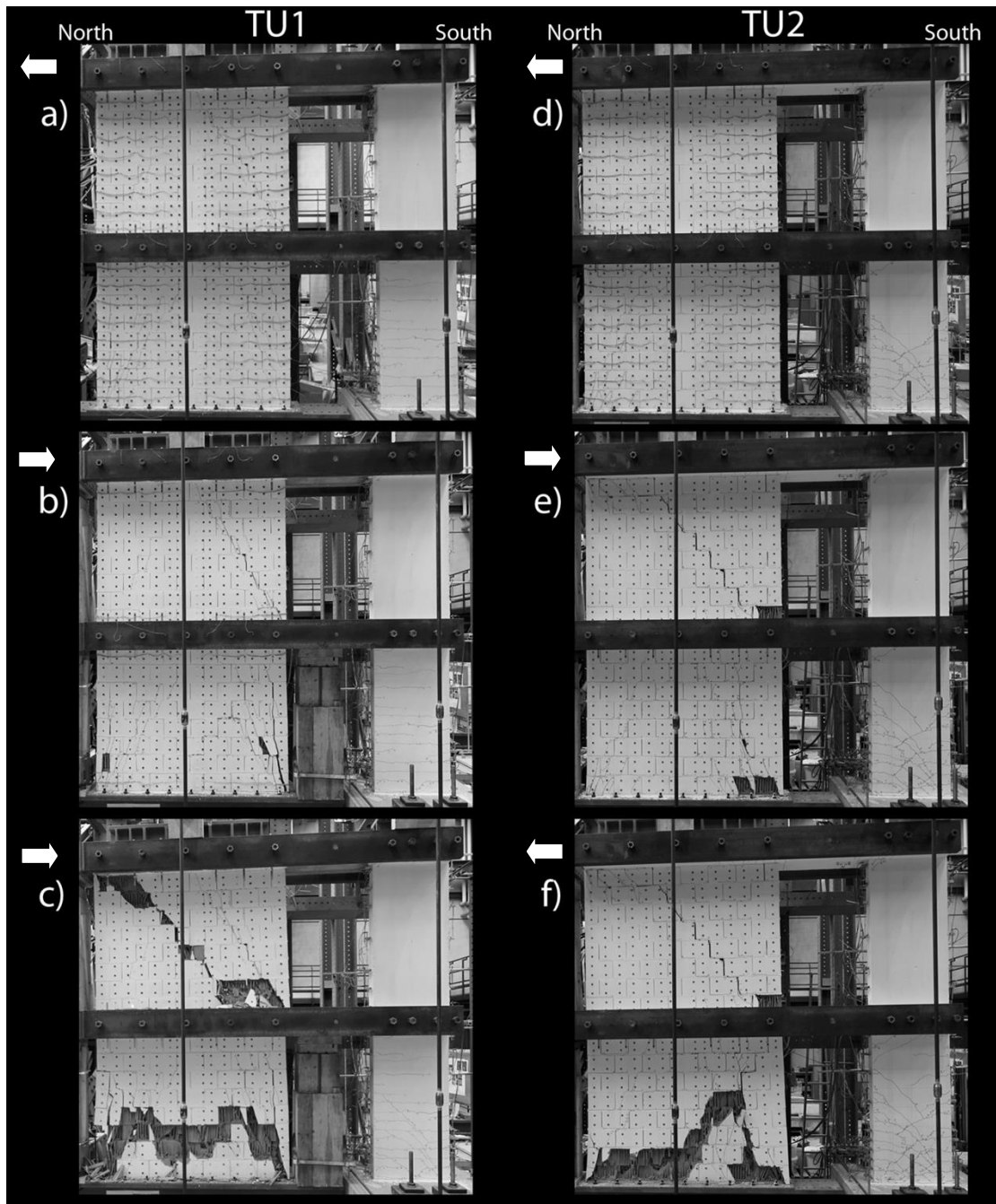


Figure 9: LEFT: crack pattern of TU1 at $\delta = -0.3\%$, LS27 (a), $\delta = +0.8\%$, LS32 (b) and $\delta = +0.95\%$, LS33 (c). RIGHT: crack pattern of TU2 at $\delta = -0.4\%$, LS33 (d), $\delta = +1.12\%$, LS38 (e) and $\delta = -0.6\%$, LS39 (f).

3.1.3 TU2

The axial loads applied at the top of the RC and URM walls of TU2 were reduced when compared to TU1 (Section 2.1). As a consequence, the URM wall of TU2 exhibited, in particular for the positive direction of loading, a rocking behaviour, while the behaviour of the URM wall of TU1 was governed by shear deformations.

During the first cycles ($\delta = 0.025\%$), horizontal cracks formed at the base of the RC and the URM walls of TU2. With increasing drift demand, the cracks became longer and additional horizontal cracks formed further up the walls. Both storeys of the URM wall displayed a clear rocking behaviour until at $\delta = 0.15\%$ inclined shear cracks formed in the first storey. The shear cracks followed initially the joints but from cycles with $\delta = 0.2\%$ onwards they passed also through the bricks. At this stage, inclined shear-flexure cracks developed in the first storey of the RC wall. In the second storey of the URM wall inclined shear cracks appeared at $\delta = 0.25\%$.

Until $\delta = 0.25\%$, the crack pattern developing for the positive and negative loading direction were rather similar. At larger cycles, for the negative direction of loading, the behaviour of the first storey of the URM wall changed from rocking to a prevalent shear mode, which was associated with the formation of large inclined shear cracks, mainly in the first storey, until $\delta = -0.4\%$ (LS33 Figure 9d). At this drift demand the horizontal resistance of the test unit dropped by 10%. The horizontal force was immediately reduced to zero to avoid axial load failure of the URM wall. The crack pattern in the URM wall comprised in the first storey a fan pointing towards the compressed toe with residual crack widths up to ~ 2 mm. At the north bottom corner toe crushing was observed. The second storey was crossed by one thin shear crack. The horizontal cracks at the base of the second storey of the URM still opened up significantly, indicating that at the second storey the prevalent mode was flexural. As for TU1, due to the coupling by the RC beams and the resulting axial force variation for the two directions of loading, the deformation capacity was smaller in the negative than in the positive loading direction.

After LS33, the test was continued with half cycles in the positive loading direction only. With each cycle, the inclined shear cracks in the two storeys of the URM wall and the vertical splitting cracks at the toe of the walls, which were caused by the rocking motion, increased in width and number. At LS38 ($\delta = +1.12\%$, Figure 9e), the residual width of the shear cracks in the first and second storey were ~ 6 mm and ~ 10 mm, respectively. It was found in fact that, for

this drift demand ($\delta = +1.12\%$), the inter-storey shear drift δ_s of the second storey was larger than that of the first storey (Figure 8b). At this stage, the maximum residual crack width in the RC wall was around 1 mm and several longitudinal bars had yielded. However, the RC wall was still in an excellent state and far from failure. At LS38 the horizontal load dropped by around 20% and therefore the damage state is comparable to TU1 at the final load step (LS33, $\delta = +0.95\%$). Due to the reduced axial force, the drift capacity of TU2 was about 20% larger than that of TU1.

As for TU1, the RC beams deformed primarily in flexure. The first flexure cracks appeared at the edges of the beams at $\pm 0.05\%$ and increased in number and width during the test. At the north end of the beams the cracked length penetrated deeper into the URM wall and, at the end of the test, the longitudinal top reinforcements at the south side of the beams had yielded. Since the negative loading direction is the more critical one, it was decided to finish the test by applying one last half cycle in this direction. At a drift of approximately $\delta = -0.6\%$ (LS39, Figure 9f) the horizontal load failure of the first storey of the URM wall was followed almost immediately by its axial load failure. The latter was triggered by the toe-crushing of the north bottom corner of the first storey of the URM wall and produced, from the north side towards the south side, the crushing of the bricks along the base of the URM wall.

3.2 Hysteretic behaviour

Figure 10 shows the envelope of the axial forces and Figure 11 the hysteresis of the base shears as a function of the average drift δ of the test unit. Due to the coupling by the RC beams, the two units behaved differently when loaded in the positive and the negative direction (for the sign convention concerning the loading directions see Figure 4a): in the positive one, the axial force in the URM wall decreased whereas in the negative direction the axial force in the URM wall increased (Figure 10). Though the vertical forces applied to the walls differed between TU1 and TU2, the trends observed for the variation of axial and shear forces at the wall bases were rather similar. The following observations hold therefore for both specimens.

The vertical forces that were applied by means of jacks and bars at the top of the walls were controlled to remain approximately constant throughout the test. The total axial force at the test unit's base was therefore also constant. The variation in axial load at the base of the RC and the URM walls yields from the shear forces transmitted by the RC beams. For very small

drifts ($\delta = 0.025\%$) the beams were uncracked and the axial forces at the base of the walls varied strongly with δ . For drifts larger than $\delta = 0.025\%$ flexural cracks formed at the beam ends and, as a consequence, the variation in axial force with δ decreased. A further decrease in slope was observed for drifts larger than 0.8% , when the top longitudinal reinforcements of the first storey RC beam started to yield and the effective length of the beams increased due to uplift of the RC beam from the URM wall.

Due to the increase in axial force, the URM wall was stronger when the load was applied in the negative direction. However, an increase in axial force results also in a reduction of deformation capacity (see Section 3.1.2 and Petry and Beyer [2014]). For this reason, in both test units, the URM walls lost their horizontal strength first in the negative loading direction leading to a drop in the test unit's lateral strength of 20% and 10% for TU1 and TU2, respectively (Figures 11a and 11b).

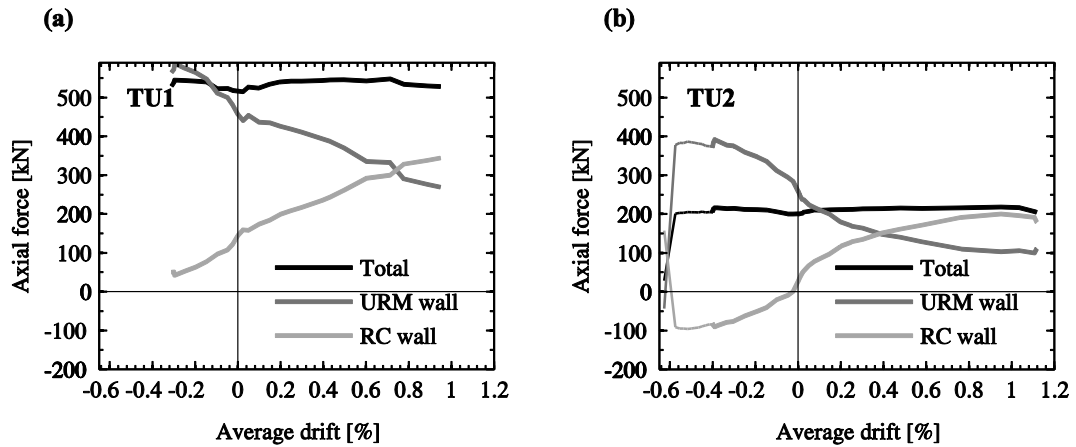


Figure 10: Axial forces at the wall bases as a function of the imposed drift: (a) TU1, (b) TU2.

For loading in the positive direction the axial force in the URM wall decreased with increasing drift demand. For drift demands larger than $+0.3\%$ (TU1) and $+0.2\%$ (TU2), the horizontal strength of the URM wall decreased. This strength deterioration was very pronounced for the URM wall of TU1, the behaviour of which was dominated by shear failure with a rapid strength and stiffness degradation. On the other hand, TU2's URM wall displayed a rocking behaviour for loading in the positive direction, which was not accompanied by a fast

strength degradation. The loss in strength of TU2's URM wall is therefore chiefly caused by the decrease in axial force in the URM wall. At the same time, due to the presence of the RC wall, the total base shear of both test units for loading in the positive and negative direction did not deteriorate until the end of the test because the relatively slender RC walls remained over a large range of drifts elastic. They could therefore somewhat compensate the gradual loss in strength due to the softening of the URM walls. The system's horizontal load failure was, for both test units, caused by the axial load failure of the URM wall. The RC walls underwent only relatively limited ductility demands and at the end of the tests were still far from failure. As a consequence, they could have been designed, according to EN 1998-1 [2004], for medium ductility ("DCM").

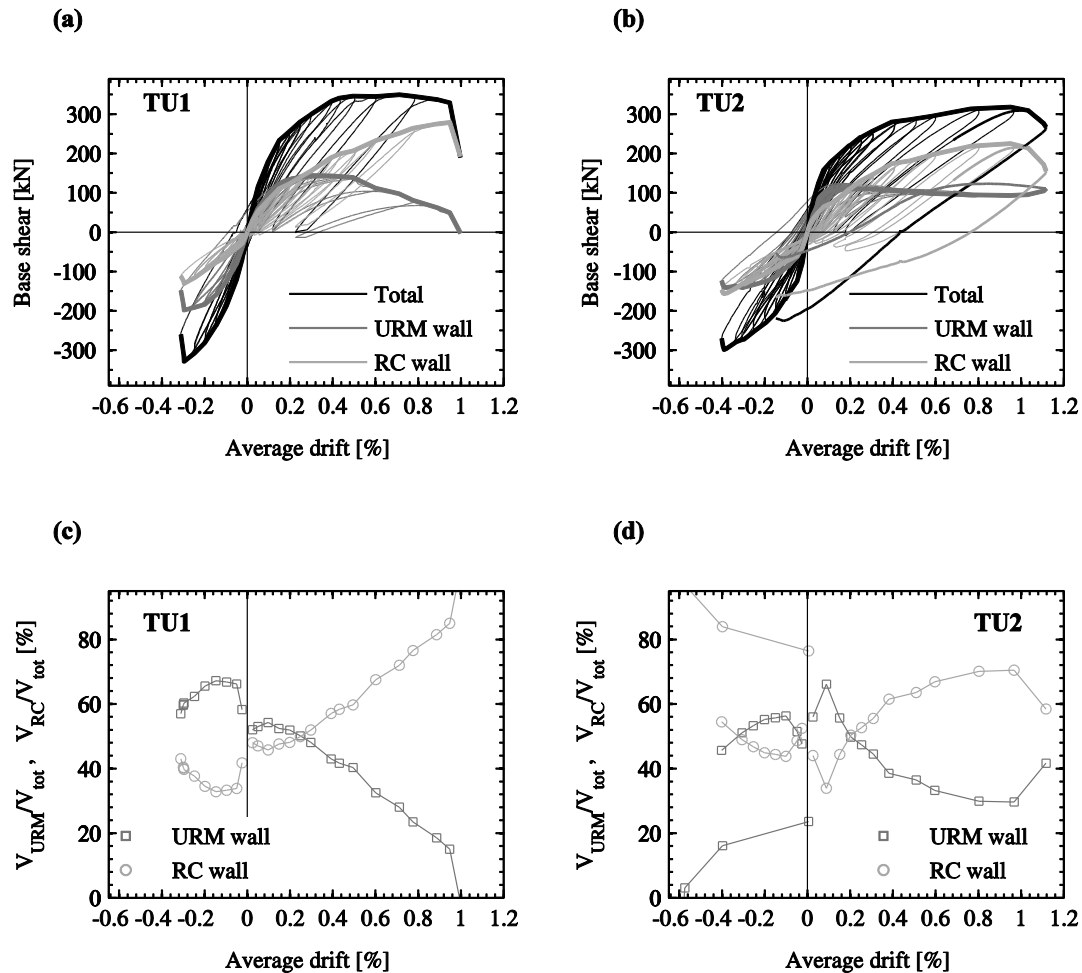


Figure 11: Hysteretic curves of the base shear in the URM and RC walls: (a) TU1, (b) TU2. Ratio of the base shear of the two walls to the total shear force: (c) TU1, (d) TU2.

The URM walls of TU1 and TU2 carried approximately 50% of the total base shear when responding elastically, that is for drifts lower than 0.025%. With drifts between 0.025% and 0.1%, the base shear absorbed by the URM wall increased; for larger drift demands, the URM wall carried a decreasing but still significant portion of the system's base shear regardless the direction of loading (Figures 11c and 11d). Table 6 summarises the base shear distribution between the walls for the following limit states:

i) $\delta = \pm 0.1\%$: no significant stiffness degradation of the URM wall;

ii) $\delta = \pm 0.3\%$ (TU1) and $\delta = \pm 0.4\%$ (TU2): horizontal load failure of the test units for the negative loading direction;

iii) $\delta = +0.6\%$: URM wall heavily damaged: strength of TU1's URM wall dropped by ~20%; crack pattern of TU2's URM wall mainly developed (both storeys displayed horizontal cracks due to the rocking behaviour and inclined cracks associated to the onset of the toe-crushing and the shear deformations);

iv) $\delta = +0.95\%$ and $\delta = +1.12\%$: onset of horizontal load failure of the test units for loading in the positive direction.

Table 6: Percentage of base shear taken by the URM wall in comparison to the total base shear for selected drift demands

Nominal drift [%]	TU1		TU2	
	$V_{\text{URM}}/V_{\text{tot}}$ [%]	Total [kN]	$V_{\text{URM}}/V_{\text{tot}}$ [%]	Total [kN]
+0.1%	54%	181	59%	179
-0.1%	67%	-186	55%	-165
+0.3%	48% (*)	300	43% (*)	257
-0.3%	60% (*)	-328	51%	-272
+0.4%	43%	333	38%	280
-0.4%	-	-	47% (*)	-299
+0.6%	32%	345	33%	295
+0.95%	15%	328	29%	319
+1.12%	-	-	41%	226

Values marked with an asterisk () indicate when the URM wall's strength was maximum.*

Table 6 shows that for both loading directions until $\delta = \pm 0.3\%$ the URM wall carried more than 40% of the total base shear. For larger drifts the URM wall's strength deteriorated

and the portion of base shear carried by the URM wall decreased. For TU2, during the last cycle ($\delta = +1.12\%$) the base shear carried by the URM wall increased with respect to the previous load step because the second storey of the URM wall changed its primary deformation from flexural to shear. Since the RC beams continued enforcing the same horizontal displacement at the floor levels, additional axial forces developed in the beams which increased the shear force taken by the URM wall and, on the other hand, decreased the base shear of the RC wall.

4 Conclusions and outlook

This paper presents the results of two quasi-static cyclic tests on mixed RC-URM wall structures. Although many multi-storey residential buildings in central Europe are constructed as mixed RC-URM wall buildings, experimental evidence on their seismic behaviour was missing. It is believed that this experimental campaign will contribute to the understanding of such mixed structures and will help to develop adequate seismic design guidelines, which allow for the interaction of the two different types of structural members and exploit the full deformation and force capacity of such mixed structures. This is necessary since in practice often oversimplified design assumptions are used, such as neglecting the lateral strength and stiffness of the masonry walls.

The tests have shown that, for mixed structures with slender RC walls, *(i)* the ultimate drift was always controlled by the URM walls which attained horizontal and axial load failure when the RC walls were far from failure. As a consequence, *(ii)* the RC walls can be generally designed, according to EN 1998-1 [2004], for medium ductility (“DCM”). Since the deformation capacity of the URM wall decreases with increasing axial load ratio [Petry and Beyer, 2014], *(iii)* the most critical loading direction in terms of ultimate average drift of the test units was the direction for which the axial force in the URM wall increased. The variation in axial force results from the shear forces transferred by the RC beams which represented the effective width of RC slabs. In addition, *(iv)* it was found that the loss of strength due to the softening of the URM wall was somewhat compensated by the slender RC wall which remained over a large range of drifts elastic. Furthermore, unlike for buildings with URM walls only, *(v)* inelastic deformations in the URM walls tend to distribute over the height of the structure and do not concentrate in the first storey.

The tests provided high quality experimental data which will be used to validate numerical models of mixed RC-URM wall structures. This is necessary since important design quantities such as the distribution of the base shear between RC and URM walls proved strongly sensitiveness to the modelling assumptions [Paparo and Beyer, 2012; Casoli, 2007]. Once such models have been validated, a large variety of mixed RC-URM wall systems will be studied. For example, (i) different wall length ratios of RC and URM walls or (ii) the effect of different masonry types can be evaluated. The results of such analyses will form the basis of force-based and displacement-based design guidelines for mixed RC-URM wall systems.

5 Acknowledgments

Professor D. Kuchma is gratefully acknowledged for his advice on the design of the test set-up. The authors would also like to thank the staff of the laboratory of the Institute of Civil Engineering (IIC) at the EPF Lausanne where the tests were performed, in particular S. Demierre, G. Guignet, and G. Rouge.

6 References

- Alessi, A., Diotallevi, P.P., Jurukovski, D., Petkovski, M., Tashkov, L. and Zarri, F. [1990] “Shaking table test of reduced scale model of brick masonry building”, *Proc. of 9th European Conference on Earthquake Engineering*, Moscow, Russia.
- Alessi, A., Diotallevi, P.P., Merli, M., Zarri, F., Jurukovski, D., Tashkov, L. and Bojadziev, M. [1994] “Comparison of dynamic properties of a mixed reinforced concrete masonry building before and after strengthening”, *Proc. of 10th European Conference on Earthquake Engineering*, Vienna, Austria.
- Beyer, K., Abo-El-Ezz, A. and Dazio, A. [2010] “Quasi-static cyclic tests on different types of masonry spandrels”, Test report, Institute of Structural Engineering, Swiss Federal Institute of Technology, Zürich, Switzerland.
- Calvi, G.M. and Kingsley G.R. [1996] “Problems and certainties in the experimental simulation of the seismic behaviour of the seismic response of MDOF structures”, *Engineering Structures*, 18(3), 213-226.

- Casoli, D. [2007] “Assessment of existing mixed RC-Masonry structures and strengthening by RC shear walls”, Pavia, Italy.
- Cattari, S. and Lagomarsino, S. [2006] “Non-linear analysis of mixed masonry and reinforced concrete buildings”, *Proc. of the first European Conference on Earthquake Engineering and Seismology* Geneva, Switzerland.
- Cattari, S. and Lagomarsino, S. [2013] “Seismic design of mixed masonry-reinforced concrete buildings by non-linear static analyses”, *Earthquakes and Structures*, 4, N°3.
- Chen, W. [1970] “Double punch test for tensile strength of concrete”, *ACI Journal*, 67, 993-995.
- EN 1052-1 [1998] *Eurocode 6: Methods of test for masonry – Part 1: Determination of the compressive strength*, CEN, Brussels.
- EN 1052-3 [2002] *Eurocode 6: Methods of test for masonry – Part 3: Determination of the initial shear strength*, CEN, Brussels.
- EN 1996-1 [2005] *Eurocode 6: Design of masonry structures – Part 1: General rules for reinforced and unreinforced masonry structures*, CEN, Brussels.
- EN 1998-1 [2004] *Eurocode 8: Design of structures for earthquake resistance – Part 1: General rules, seismic actions and rules for buildings*, CEN, Brussels.
- EN 772-1 [2000] *Eurocode 6: Methods of test for masonry units – Part 1: Determination of compressive strength*, CEN, Brussels.
- Jurukovski, D., Taskov, L., Petkovski, M. and Kretevska, L. [1989a] “Basic and applied research study for seismic modelling of mixed reinforced concrete – masonry buildings. Shaking table test of reduced scale model”. IZIIS Test Report n° 89/66, Skopje, Macedonia.
- Jurukovski, D., Taskov, L., Petkovski, M. and Kretevska, L. [1989b] “Basic and applied research study for seismic modelling of mixed reinforced concrete – masonry buildings. Shaking table test of reduced scale repaired model”. IZIIS Test Report n° 89/75, Skopje, Macedonia.
- Jurukovski, D., Taskov, L., Petkovski, M. and Kretevska, L. [1991a] “Basic and applied research study for seismic modelling of mixed reinforced concrete – masonry buildings. Shaking table test of reduced scale model strengthened by external reinforced concrete walls”. IZIIS Test Report n° 91/01, Skopje, Macedonia.

- Jurukovski, D., Taskov, L., Petkovski, M. and Kretevska, L. [1991b] “Basic and applied research study for seismic modelling of mixed reinforced concrete – masonry buildings. Shaking table test of reduced scale model strengthened by concrete central core”. IZiIS Test Report n° 91/92, Skopje, Macedonia.
- Jurukovski, D., Kretevska, L., Alessi, A., Diotallevi, P.P., Merli, M. and Zarri, F. [1992] “Shaking table tests of three four-storey brick masonry models: original and strengthened by RC core and by RC jackets”, *Proc. of 10th World Conference on Earthquake Engineering*, Madrid, Spain.
- Lequesne, R.C., Parra-Montesinos, G.J. and Wight, J.K. [2009] “Test of a coupled wall with high performance fiber-reinforced concrete coupling beams”, *ACI Journal*, 265, 1-18.
- Liberatore, L., Decanini, L.D. and Benedetti, S. [2007] “Le strutture miste muratura-cemento armato: uno stato dell’arte”, *12° Convegno Nazionale L’Ingegneria Sismica in Italia*, Pisa, Italy.
- Magenes G. [2006] “Masonry building design in seismic areas: recent experiences and prospects form and european standpoint” Keynote address, *Proc. of 1st European Conference on Earthquake Engineering and Seismology*, Geneva, Switzerland.
- NDI. [2009] “Optotrak Certus HD”, *Northern Digital Inc.*, Waterloo, Ontario, Canada, <http://www.ndigital.com/industrial/certushd.php>.
- Paparo, A. and Beyer, K. [2012] “Pushover analyses of mixed RC-URM wall structures”, *Proc. of 15th World Conference on Earthquake Engineering*, Lisbon, Portugal.
- Petry, S. and Beyer, K. [2014] “Influence of boundary conditions and size effect on the drift capacity of URM walls”, *Engineering Structures*, 65, 76-88.
- Priestley, M.J.N., Calvi, G.M. and Kowalsky, M.J. [2007] *Displacement-Based Seismic Design of Structures*, IUSS Press, Pavia, Italy.
- SIA 262/1 [2003] *Building code, Swiss Society of Engineers and Architects (SIA): Concrete structures – Supplementary specifications*, SIA, Zurich.
- Tomaževič, M., Modena, C., Velechovsky, T and Weiss, P. [1990] “The effect of reinforcement on the seismic behaviour of masonry buildings with mixed structural systems: an experimental study”, *Proc. of 9th European Conference on Earthquake Engineering*, Moscow, Russia.

Paper II: Modelling the seismic response of modern URM buildings retrofitted by adding RC walls

Submitted to *Journal of Earthquake Engineering*

Modelling the seismic response of modern URM buildings retrofitted by adding RC walls

Abstract

Modern unreinforced masonry buildings with reinforced concrete slabs are often retrofitted by inserting reinforced concrete walls. The main advantages of this retrofit technique are the increase in strength and displacement capacity with respect to the original structure. In engineering practice, such structures are best analysed by means of macro-element models. The objective of the paper is to formulate practical recommendations for setting up a macro-element model using as input the geometry of the structure and results from standard material tests. To validate the modelling recommendations, the results from macro-element model analyses are benchmarked against experimental results and numerical results from shell-element models. The paper concludes with the analyses of some structural configurations of modern masonry buildings that have been retrofitted by reinforced concrete walls. These configurations highlight the effect of inserting reinforced concrete walls on the force and displacement capacity of modern masonry buildings.

Keywords: Seismic behaviour; Modern mixed masonry and reinforced concrete wall structures; Non-linear analyses; Shell-element model; Macro-element model; Equivalent frame.

1 Introduction

In recent years, the seismic hazard in several countries of Europe was re-evaluated and, as a result, the seismic design spectra increased. Many modern residential unreinforced masonry (URM) buildings no longer fulfil the seismic design check for the new spectra and have to be retrofitted. Adding RC walls to the existing structure or replacing selected URM walls with RC ones can be an effective retrofit strategy if RC slabs allow a redistribution of the forces. This retrofit approach might not only increase the strength but also modify the global deformed shape of the structure, leading to an increase in the system's displacement capacity. For new constructions, it is pertinent to conceive similar structures directly as mixed RC-URM systems because they show an improved seismic behaviour, when compared to buildings with URM walls only. In addition, when compared to buildings with RC walls only, such mixed structures have better thermal and insulation properties at a lower construction cost.

Mixed RC-URM construction varies significantly from region to region [Magenes, 2006; Cattari and Lagomarsino, 2013]. In this paper, the examination is limited to a common configuration of modern mixed RC-URM systems built in Switzerland, a detailed description of which is provided in the introduction of the thesis.

Despite the popularity of this construction and retrofitting technique, very little research has been carried out [Magenes, 2006] and there are several open issues to be addressed:

i) Response of mixed RC-URM wall structures: Vertical and horizontal forces are resisted by the combined contribution of the existing URM walls and the new RC walls. Hence the retrofitted structure will behave differently from the uncoupled systems since each type of wall results in a different displaced shape when subjected to horizontal forces (Figure 1).

ii) Numerical modelling: Numerical results on RC-URM wall structures are sensitive to mechanical and geometrical assumptions [Casoli, 2007; Paparo and Beyer, 2012] but models could not be validated as experimental results of such mixed structures were missing. For these buildings, the parameters which most influence the distribution of reaction forces among the walls are those defining the strength and stiffness of the elements.

iii) Lack of experimental data: There are only few experimental tests on mixed RC-URM structural buildings. Tomažević et al. [1990] conducted a shake table test on a URM wall building with one RC column. However, the latter had no influence on the behaviour of the

structure under lateral loads since the URM walls were considerably stiffer. Jurukovsky et al. [1992] conducted shake table tests of 1/3-scale models. They investigated several strengthening techniques for a mixed structure composed of URM walls and one RC frame at the ground floor. In one case they added a central RC core wall to the URM building and they tested this retrofitted solution up to the near collapse limit state, but the presence of the RC frame at the ground floor added a vertical irregularity. Hence, none of the experimental studies addressed the seismic behaviour of mixed structures where RC and URM walls are regular and continuous over the height.

iv) Scarce numerical investigations: Recently non-linear numerical investigations [Cattari and Lagomarsino, 2013] studied the interaction of RC and URM walls. They simulated the response of buildings where the RC walls were not capacity-designed and failed before the URM walls. The study presented herein targets structures where the RC members are designed to fail for larger displacement demands than the URM walls.

In order to address the aforementioned issues, a research programme was initiated at EPFL with the objective to understand better the seismic behaviour of mixed RC-URM wall structures. Both experimental (Figures 2 and 3) and numerical investigations were carried out. The objective of this paper is to provide some indications for the modelling and analysis of structures with both RC and URM walls. Two modelling approaches will be investigated: a shell-element model and a macro-element approach; the latter is commonly used in engineering practice for analysing such structures. Section 2 will present the main characteristics of the seismic behaviour of mixed RC-URM wall structures and will outline advantages and drawbacks of coupling URM walls with RC walls. In Section 3 the two modelling approaches will be presented and validated against experimental results. The paper concludes with the discussion of four case studies (Section 4), outlining for which structural configurations of URM buildings adding RC walls can be an efficient retrofit measure.

2 Seismic behaviour of interacting URM and RC walls

Retrofitting a modern URM building by replacing some URM walls with RC ones does not only increase the strength of the structure, but can also improve the system's displacement capacity. The section describes qualitatively the interaction of URM and RC walls connected by

RC slabs when subjected to lateral forces (Section 2.1) and outlines the resulting advantages and disadvantages of this retrofit technique (Section 2.2).

2.1 Deformation pattern of mixed RC-URM wall structures subjected to lateral loading

URM walls have a dominant flexural or shear response depending on several parameters such as the axial load ratio, the pier geometry and the coupling moment introduced by RC slabs or masonry spandrels. RC walls are designed to have a dominant flexural behaviour and a displacement capacity larger than that of URM walls. The RC slabs are assumed to provide a rigid diaphragm action, allowing an effective force redistribution between walls of one plane.

Under lateral loading, uncoupled URM walls which deform primarily in shear lead to larger inter-storey drifts at the bottom storeys (Figure 1a). Single slender RC walls display instead primarily flexural deformations, with larger inter-storey drifts at top storeys (Figure 1b). At the height of the RC slabs, URM and RC walls need to displace by the same amount because of the rigid diaphragm action provided by the RC slabs. Hence, the deformed shape of mixed RC-URM wall structures lies in between that of buildings with RC and URM walls alone (Figure 1c). As a consequence, for such mixed structures the damage in the URM walls is not concentrated in the first storey—as for URM buildings—but it also spreads to the storeys above. This behaviour was noted in quasi-static and dynamic tests on mixed RC-URM wall structures (Figures 2 and 3) and also Jurukovsky et al. [1992] observed that the presence of the pin-based RC wall “distributed the failure mechanism all over the structure”.

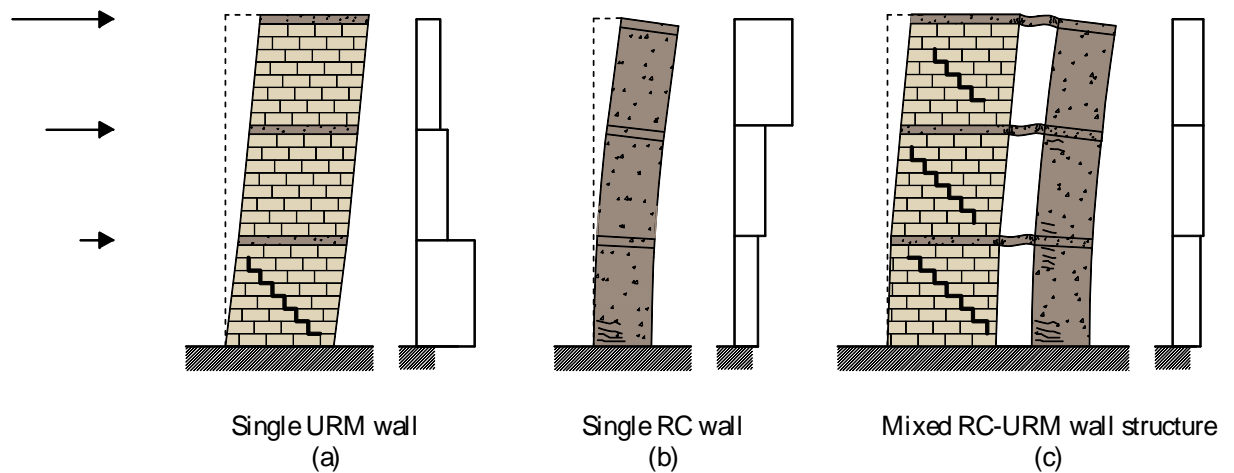


Figure 1: Deformation pattern and inter-storey drift profile due to lateral forces of a single URM wall with dominant shear behaviour (a), a single RC wall with dominant flexure behaviour (b) and a mixed RC-URM structure (c).

Mixed RC-URM wall structures present similarities to dual RC frame-wall buildings. Slender wall elements, which display mainly flexural deformations, are coupled to frames, which globally deform—as do most URM piers—in a predominant shear mode [Smith and Coull, 1991]. As a consequence, and similar to mixed RC-URM wall structures, the deformed shape of dual RC frame-wall buildings is modified and tends to be rather linear over the height of the structure [Paulay and Priestley, 1992].

If the masonry walls have a dominant flexural response, in the URM walls the inter-storey drift profile is rather constant over the height and the modification of the deformed shape is less accentuated. For modern URM buildings with RC slabs such a behaviour is, however, uncommon since the RC slabs connecting the walls feature a significant out-of-plane stiffness and strength and introduce therefore an important framing effect which leads to a more shear critical behaviour of the URM walls [Lang, 2002].

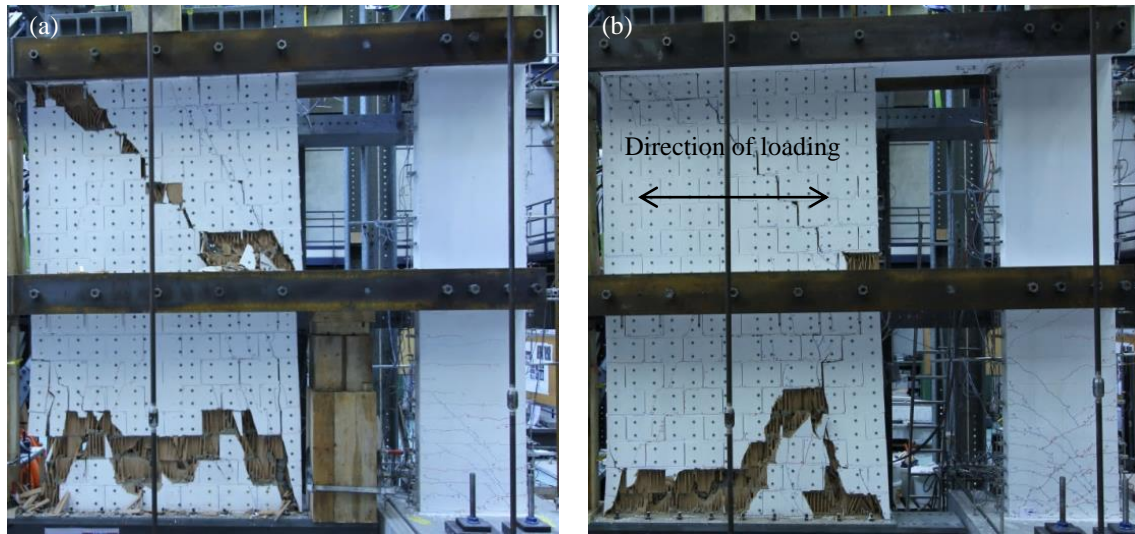


Figure 2: EPFL tests on two mixed RC-URM wall substructures: crack pattern after failure. (a): TU1. (b): TU2 [Paparo and Beyer, 2014].

2.2 Advantages and drawbacks of adding RC walls to URM wall buildings

Figure 4 compares failure mechanisms of a mixed RC-URM structure versus that of a URM building where shear deformations prevail. The presence of the RC wall in the retrofitted configuration leads, for the same level of inter-storey drift δ^* at the ground floor, to larger top displacements: $\Delta_{mixed} > \Delta_{URM}$. Consequently, the displacement capacity of mixed RC-URM wall structures is larger than that developed by shear dominated URM wall buildings. Furthermore, in retrofit design, the URM walls with the smallest displacement capacity can be replaced by RC walls.

In addition, in such mixed systems, the strength degradation of shear dominated URM walls generally starts at drifts of around 0.3%-0.5%. At these drift levels, RC walls that are designed to develop a stable flexural behaviour are still in the pre-peak response. As a consequence, in mixed RC-URM wall structures the strength degradation of the URM walls can be somewhat compensated by the presence of the RC walls.

A drawback of the procedure is the increase in seismic mass related to the addition of RC walls to the structure. However, since large parts of the dead loads result from the weight of the RC slabs and the added RC walls in the retrofitted systems are usually few, the increase in total weight is, generally, less than 5%.



Figure 3: Crack pattern in a four-storey mixed RC-URM wall structure, from Beyer et al. [2014].

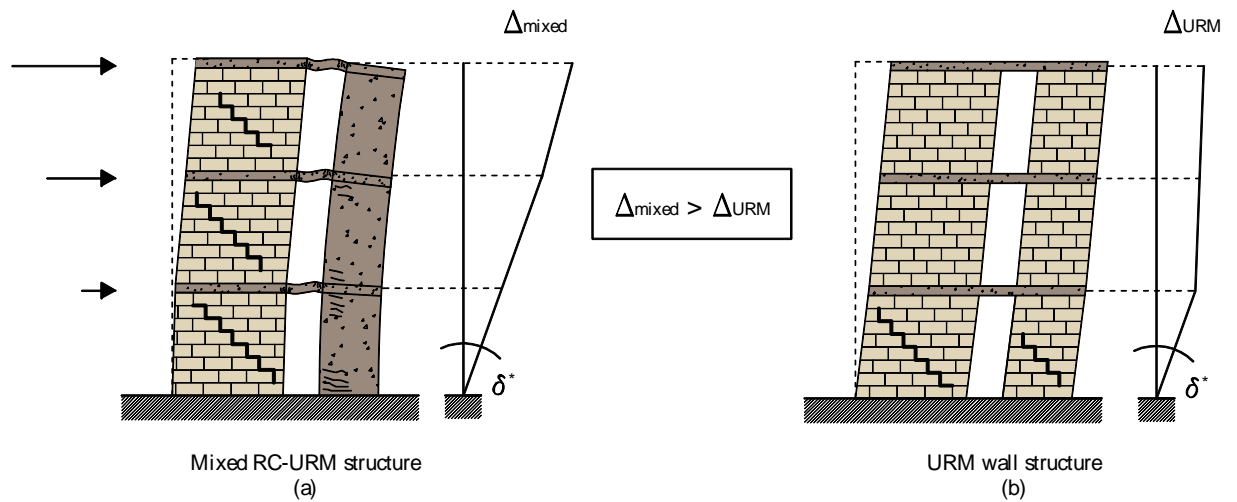


Figure 4: Deformation capacity, for the same level of inter-storey drift δ^* , of a mixed RC-URM structure (a) and a shear dominated URM building (b).

3 Numerical analyses of modern RC-URM wall buildings with RC slabs

Several modelling approaches are used for evaluating the seismic behaviour of mixed RC-URM wall structures, ranging from sophisticated strategies (shell-models) to more simplified approaches (macro-models). Although computer power increases continuously, it seems unlikely that shell-models will become a standard tool for the practically oriented analyses, as they require too much computational time.

Previous studies [Casoli, 2007; Paparo and Beyer, 2012] have also shown that numerical investigations using macro-models are sensitive to some modelling assumptions, such as the assumed effective stiffness of the members or the effective length of the coupling RC beams. In this paper, to validate two modelling approaches, a two-step validation procedure is used: (i) first, a detailed shell-model is assessed against the results from quasi-static cyclic tests. This model is then used to study additional parameters. (ii) The results of the macro-model are then compared and recommendations for the analysis of such mixed structures formulated. Before the presentation and comparison of the two modelling approaches, a brief overview of two quasi-static tests on two mixed RC-URM wall structures is outlined.

3.1 EPFL tests

Two mixed RC-URM substructures were tested under a quasi-static cyclic loading regime at the structural engineering laboratory at EPFL. Each of the two specimens comprised a two-storey RC wall coupled to a two-storey URM wall through two RC beams. The RC beams connecting the two walls represented the slabs in the reference structure.

The main difference between the two systems was the axial load applied at the top of the URM walls. For the first specimen (TU1), an axial load of 400 kN was applied and led to a shear dominant behaviour of the masonry. For the second test (TU2) the axial load was reduced to 200 kN in order to achieve a prevalent rocking behaviour. Figure 2 shows the crack pattern of the two specimens after failure. In Section 3.4, the global force-displacement characteristics, as well as the inter-storey drift profile, will be introduced and compared with the analysis results. For further details on the EPFL tests, the reader is referred to Paparo and Beyer [2014].

3.2 Shell-element model

In the shell-element model, (i) URM walls are simulated by using the simplified micro-modelling approach [Lourenço, 1996] and (ii) RC walls and beams are represented by shell elements for the concrete, shell elements for the transverse reinforcements and trusses for the longitudinal reinforcements. The simulations are carried out using the software ATENA [Červenka et al., 2010]. The mechanical properties, summarised in Table 1, were obtained from standard material tests, Paparo and Beyer [2014]. In the following, a description of the adopted mechanical properties is provided.

i) URM walls: Shell elements to which the SBETA constitutive model [Červenka et al., 2008] is assigned are used to simulate the bricks as elastic in compression. Their tensile strength f_{tb} instead is limited to 1.4 MPa and the fracture energy G_b^I is set equal to 0.08 N/mm [Lourenço, 1996]. The mortar joints are modelled by zero-thickness contact interfaces with a Mohr-Coulomb failure criterion. The interface friction μ and cohesion c between mortar and bricks were obtained from standard triplet tests [EN 1052-3, 2002]. The interface tensile strength f_{im} is calculated by considering a parabolic tension cut off:

$$f_{im} = \frac{c}{2\mu} \quad (1)$$

The constitutive law assigned to the interfaces does not account for compression failure. As a consequence, the crushing of the masonry is not represented by the shell element model and, therefore, the failure of the masonry cannot be fully captured. Thus, the shell element model is used to investigate the behaviour before failure, i.e. the shear-flexure interaction which develops between the RC and URM walls (Section 2.1) and the effective length of the RC beams.

As the software can only account for isotropic material behaviour, an equivalent E-modulus of the bricks, which lies in between the E-modulus of the bricks for loading parallel (E_{bx}) and orthogonal (E_{by}) to the perforations, is adopted (E_b). The different masonry E-modulus in the two directions of loading (E_{mv} and E_{mh}) can be matched by varying the normal and tangent interface stiffnesses (K_{nn} and K_{tt}). In the experimental program [Paparo and Beyer, 2014] the vertical masonry E-modulus E_{mv} was obtained from standard compression tests on masonry wallettes [EN 1052-1, 1998]. Compression tests in horizontal direction were not carried out.

Table 1: Mechanical properties adopted for shell-model

Materials	Material properties	Shell-model	Material test results
Bricks	E_{bx}	[GPa]	5.60
	E_{by}	[GPa]	5.60
	f_{tb}	[MPa]	1.4
	G_b^I	[N/mm]	0.08
Mortar joints	μ	[-]	0.63
	c	[MPa]	0.38
	f_{tm}	[MPa]	0.30
	K_{nn}	[MN/m ³]	3.00 x 10 ⁵
	K_{tt}	[MN/m ³]	1.00 x 10 ⁴
	G_f^I	[N/mm]	0.41
	G_f^{II}	[N/mm]	0.50
Masonry walls	E_{mv}	[GPa]	-
	E_{mh}	[GPa]	-
Concrete	E_c	[GPa]	34.5
		51.4 (unconfined)	
	f_c & f_{cc}	[MPa]	80.0 (confined – RC walls) 75.0 (confined – RC beams)
	f_{tc}	[MPa]	3.00
Reinforcing bars	f_y	[MPa]	540
	f_u	[MPa]	600

E_{bx} : brick E-modulus for loading along the brick's height;
 E_{by} : brick E-modulus for loading along the brick's length;
 f_{tb} : brick tensile strength;
 G_b^I : brick fracture energy;
 μ and c : interface friction and cohesion coefficient;
 f_{tm} : interface tensile strength;
 K_{nn} and K_{tt} : interface normal and tangent stiffness;
 G_f^I and G_f^{II} : interface Mode I and II fracture energy;
 E_{mv} and E_{mh} : vertical and horizontal masonry E-modulus;
 E_c : concrete E-modulus;
 f_c and f_{cc} : confined and unconfined concrete compressive strength;
 f_y and f_u : reinforcing bar yield and ultimate tensile strength, [SIA162/1, 1995].

According to Beyer and Dazio [2012], who tested similar masonry walls under horizontal and vertical loads, the ratio E_{mh} / E_{mv} is estimated as 0.25. Hence it was assumed that $E_{mh} = 0.25 E_{mv}$. As the investigated URM walls had dry head joints, the vertical masonry E-modulus (E_{mv}) can be related to the normal interface stiffness (K_{nn}) and the horizontal masonry E-modulus (E_{mh}) can be related to the tangent interface stiffness (K_{tt}). Simple compression tests with

loading orthogonal and parallel to bed joints are simulated, allowing the calibration of K_m and K_t to obtain the two desired masonry E-moduli E_{mh} and E_{mv} .

The fracture energies of the joint interfaces (G_f^I and G_f^{II}) were not determined within this project [Paparo and Beyer, 2014]. The interface Mode II fracture energy G_f^{II} is assumed to be equal to 0.50 N/mm, according to Beyer and Dazio [2012]. Since for the interface Mode I fracture energy G_f^I no experimental results for hollow clay bricks were found, it is assumed that the ratio G_f^I/G_f^{II} is equal to the ratio f_m/c [Reyes et al., 2008]. Since G_f^I and G_f^{II} were not determined directly from material tests, sensitivity analyses of their influence to the response of single URM walls were carried out. Also according to Lourenço [1996], it was found that the assumed values of G_f^I and G_f^{II} are parameters which do not strongly affect the results of the analyses.

ii) RC walls and beams: The concrete behaviour of RC walls and beams is modelled using shell elements in conjunction with the SBETA model [Červenka et al., 2008]. The concrete behaviour in compression is parabolic up to the cylinder compressive values f_c and f_{cc} . The cylinder compressive value f_c is used for modelling the unconfined concrete in the RC walls. In the boundary elements of the RC walls and in the RC beams, the concrete compressive strength adopted is f_{cc} . This value accounts for the effect of the confinement and is calculated according to Mander et al. [1988]. After the peak stresses f_c and f_{cc} , the softening law of the concrete would be linearly descending but this was not reached in any of the analyses. The concrete behaviour in tension is modelled using a linear-elastic relation until the tensile strength (f_{tc}). After the stress peak f_{tc} , the concrete is modelled with an exponential tension softening law. The concrete tensile strength f_{tc} was experimentally determined from double punch tests on half cylinders [Chen, 1970]. A bilinear stress-strain relation is adopted for the reinforcing bars in conjunction with (i) truss elements for representing longitudinal reinforcements and (ii) shells for representing transverse smeared reinforcements. Perfect bond between steel and concrete is always assumed.

3.3 Macro-element model

The macro-model strategy consists of modelling each structural member as single elements which are then assembled to an equivalent frame. The macro-element developed by Penna et al. [2013] is used to describe the behaviour of masonry walls. Timoshenko beams

characterised by an elasto-plastic law represent RC members [Cattari and Lagomarsino, 2013]. The simulations are carried out with the software TREMURI [Lagomarsino et al., 2009; Lagomarsino et al., 2013, Penna et al., 2013].

The adopted mechanical properties are summarised in Table 2. The equivalent friction and cohesion parameters for masonry piers (μ_{eq} and c_{eq}) are computed as follows:

Step1) Calculation of the shear strength: For single masonry walls, Penna et al. [2013] proposed to set the equivalent friction and cohesion (i) on the basis of the strength criterion which is representative of the expected failure and (ii) assuming the axial force N acting on the section. For multi-storey (mixed RC-URM and plain URM) wall buildings with RC slabs, Mandirola [2014] used the same approach and set μ_{eq} and c_{eq} (i) on the basis of the shear criterion which represents the expected shear failure and (ii) assuming the axial force N at the base of the URM walls considering the gravity loads only. The latter assumption means that the calibration is made without taking into account the variation of the axial force in the URM walls due to the floor level and the load transferred by the RC slabs.

As the objective of the paper is to provide practical guidelines for setting up models by using standard material tests only, the approach proposed by Mandirola [2014] is followed herein. Note that, in a multi-storey building, the approach would require different values of μ_{eq} and c_{eq} depending on the floor level to account for the variation of axial force over the height of the building. However, since in the top storeys the URM walls are dominated by rocking deformations because of the low axial force acting on the URM walls, a variation of μ_{eq} and c_{eq} is unlikely to affect the results significantly.

Step 2) Calculation of μ_{eq} and c_{eq} : In the macro-element developed by Penna et al. [2013], the shear strength of a masonry wall V_{sh} is the sum of the friction component V_{μ} and the cohesion component V_c :

$$V_{sh} = V_{\mu} + V_c \quad (2)$$

The equivalent friction and cohesion parameters μ_{eq} and c_{eq} can be found by assigning half of the shear strength to the friction component V_{μ} and half of the shear strength to the cohesion component V_c :

$$0.5 \cdot V_{sh} = V_{\mu} = \mu_{eq} \cdot N \quad (3a)$$

$$0.5 \cdot V_{sh} = V_c = c_{eq} \cdot A_{gross} \quad (3b)$$

Note that (i) the cohesion component V_c is determined considering the gross section area A_{gross} and that (ii), for URM walls with shear behaviour, plastic displacements occur when the shear force V is bigger than the friction component (V_{μ}). The assignment of 50% of the total shear (V_{sh}) to cohesive and friction components is chosen on the basis of the experimental results. In fact, in the hysteretic behaviour of TU1 and TU2, the stiffness degradation in the masonry walls starts for values of shear forces V equal to around 50% V_{sh} . The force-displacement results of two quasi-static cyclic tests [Petry and Beyer, 2014a] on URM walls exhibiting dominant shear behaviour are used to validate the approach for the calculation of μ_{eq} and c_{eq} . The comparison (Figure 5) shows that the TREMURI models with the proposed values of μ_{eq} and c_{eq} provide good estimates of the stiffness degradation in the pre-peak response and of the dissipated energy ($\beta = 0.25$).

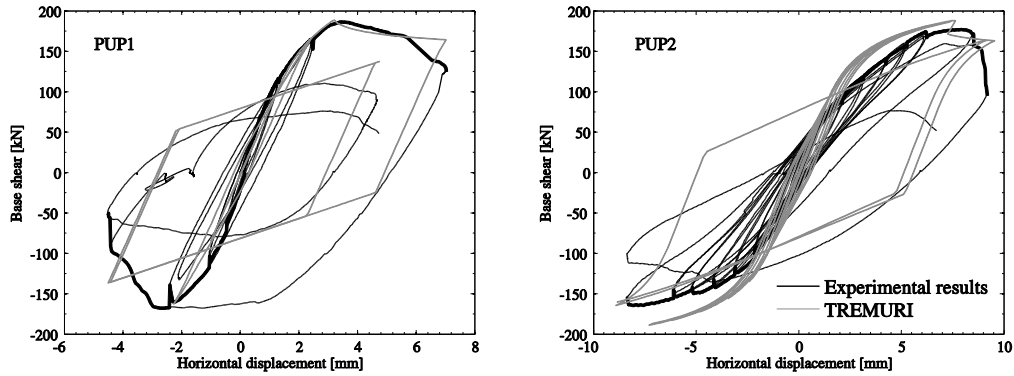


Figure 5: Comparison of the force-displacement curves obtained from in-plane cyclic tests [Petry and Beyer, 2014a] and numerical simulations.

Concerning the calculation of the shear strength of the masonry wall, Penna et al. [2013] propose to use the strength criterion which is representative of the expected failure. As in TU1 and TU2 the masonry stress ratio σ_0/f_{cM} is rather height (i.e., $\sigma_0/f_{cM} = 0.24$ for TU1 and $\sigma_0/f_{cM} =$

0.14 for TU2), the strength of the masonry panel is calculated by using the shear strength criterion which accounts for the brick tensile strength [Mann and Müller, 1982]:

$$V_{sh} = lt \frac{f_{tb}}{2.3(1 + \alpha_v)} \sqrt{1 + \frac{N}{ltf_{tb}}} \quad (4)$$

where l and t are the length and the thickness of the masonry wall, N the axial force acting on section and f_{tb} the brick tensile strength. $(1 + \alpha_v) = (1 + H_{CF}/l)$ is a correction coefficient proposed by Magenes and Calvi [1997] to account for the effect of complex stress distribution. H_{CF} is the height of the contra-flexure point of the masonry wall. According to such a calibration, for TU1 the shear strength V_{sh} is equal to 141 kN ($N = 460$ kN) and for TU2 the shear strength V_{sh} is equal to 123 kN ($N = 260$ kN). The experiments have shown that, for TU1 and TU2, H_{CF} can be assumed equal to the storey height. The tensile strength of the brick, f_{tb} , is set equal to 1.27 MPa according to Petry and Beyer [2014a] who tested masonry walls similar to those herein considered.

In Table 2, the adopted E-modulus corresponds to the vertical masonry E-modulus (E_{mv}) obtained from standard compression tests on masonry wallettes [EN 1052-1, 1998], see Section 3.2. The shear modulus (G_m) is calculated from the E-modulus E_{mh} (compression parallel to bed-joints, see Section 3.2):

$$G_m = \frac{E_{mh}}{2 \cdot (1 + \nu_M)} = \frac{(0.25 \cdot E_{mv})}{2 \cdot (1 + \nu_M)} \quad (5)$$

ν_M is the Poisson ratio of the masonry wall which was found to be equal to 0.18 according to EN 1052-1 [1998].

For the construction of the macro-model, additional assumptions on the stiffness and deformation capacity of the elements are required:

i) Stiffness of URM walls: The stiffness of URM walls corresponds to the uncracked stiffness of the section. For the shear damage model, non-linear plastic deformations in the pre-peak response are taken into account by the effect of the shear deformability parameter Gc_t [Penna et al., 2013]. The latter is set equal to one so that, at peak strength (V_{sh}), the total horizontal displacement u_{tot} is 1.5 times the elastic one u_{el} :

$$u_{tot} = 1.5u_{el} \quad (6)$$

with $u_{el} = V_{sh}h/(G_m lt)$. h , l , t are the height, length, thickness of the wall. For the flexural behaviour, non-linear elastic deformations are taken into account in terms of kinematic variables (rotation and vertical displacement of the section). A no tension model is attributed to the zero-length springs in which flexural and axial deformations are lumped [Penna et al., 2013].

Table 2: Adopted material properties for macro-model

Materials	Material properties		Macro-model	Material test results
URM members	μ_{eq} / μ	[-]	0.15 (TU1) 0.24 (TU2)	0.63
	c_{eq} / c	[MPa]	0.23 (TU1) 0.20 (TU2)	0.38
	f_{cM}	[MPa]	6.30	6.30
	E_{mv}	[GPa]	5.10	5.10
	G_m	[GPa]	0.54	-
	Gc_t	[-]	1.00	-
	β	[-]	0.00	-
RC members	E_c	[GPa]	E_{eff} (1 st storey & beams) 18.0 (above storeys)	36.0 36.0
	G_c	[GPa]	$E_{eff}/2.4$ (1 st storey & beams) 7.5 (above storeys)	7.50 7.50
	f_y	[MPa]	550	537

μ_{eq} and c_{eq} : equivalent friction and cohesion coefficients;
 μ and c : friction and cohesion coefficient from triplet tests;
 f_{cM} : masonry compressive strength;
 E_{mv} : E- modulus of masonry panels subjected to compression orthogonal to bed-joints;
 G_m : masonry shear modulus;
 Gc_t : shear deformability parameter;
 β : softening parameter;
 E_c and G_c : RC member's Young's and shear modulus;
 f_y : reinforcing bar yield tensile strength adopted in RC members.

ii) *Softening parameter β* : The parameter β , which describes the softening post-peak response of the URM walls, is here set equal to zero. This means that the macro-element does not display any strength degradation after the peak.

iii) *Failure criterion for URM walls*: The failure criterion follows the formulation proposed by EN 1998-3 [2005] in which the near collapse (NC) inter-storey drift δ_u of a masonry wall depends on its failure mechanism:

$$\text{For shear failure} \quad \delta_u = 0.53\% \quad (7a)$$

$$\text{For flexural failure} \quad \delta_u = 1.07\% \cdot (H_{CF} / L) \quad (7b)$$

For flexural failure, the near collapse drift is also dependant on the ratio H_{CF}/L (height of the contra-flexure point over length of the pier). Although the pier's displacement capacity is defined as horizontal load failure, tests have shown that URM walls lose their vertical load bearing capacity soon after the horizontal load failure [Petry and Beyer, 2014b]. Once the first URM pier fails, it is assumed that the system reaches its ultimate displacement capacity. The inter-storey drift δ is calculated as follows:

$$\delta = \frac{\Delta_i - \Delta_j}{h} \quad (8)$$

where Δ_i and Δ_j are the horizontal displacements of the beams below and above the considered wall and h the height of the wall.

iv) *Stiffness of RC members*: Experiments on mixed RC-URM wall structures [Paparo and Beyer, 2014; Beyer et al., 2014] have shown that the RC walls crack only in the first storey, while the above storeys feature just thin cracks, mainly in the construction joints connecting walls and slabs (or beams). As a consequence, the reduction of stiffness according to Priestley et al. [2007] is applied to the first storey of the RC walls and to the RC beams. This reduction is taken into account by considering the effective stiffness EI_e :

$$EI_e = \frac{M_N}{\phi_y} \quad (9)$$

where M_N is the nominal yield moment, calculated considering the axial force acting at the base of the wall before applying the horizontal load, and ϕ_y is the nominal yield curvature, which is equal to $C\varepsilon_y/l_w$. C is a constant depending on the geometrical properties of the section; ε_y is the yield strain of the longitudinal reinforcing bars and l_w is the length of the wall. To

account for the presence of thin cracks in construction joints between the RC walls above the first storey and the slabs (or beams), the concrete E-modulus of the RC walls above the first storey is reduced by 50%. The latter assumption is considered applicable if the mean longitudinal reinforcement ratio of the RC walls is larger than 0.2% (0.2% is the minimum longitudinal reinforcement ratio for RC walls according to EN 1992-1 [2004]).

v) *Axial stiffness of RC beams*: The RC beams are modelled with infinite axial stiffness to guarantee that the walls at each floor display horizontally by the same amount.

vi) *Failure criterion for RC members*: All RC elements are designed to form a ductile flexural mechanism. The ultimate chord rotation θ_u of RC members is estimated according to EN 1998-3 [2005]. However, the deformation capacity of RC members developing a stable flexural response is much larger than that of URM walls. In all the analyses presented in this paper, the RC elements do not reach their deformation capacity.

vii) *Effective length of the RC beams*: In the macro-model the user can control the effective length of the RC beams (L_{be}) by introducing rigid offsets. To account for the curvature penetration of RC beams into URM walls, the deformable part is increased by its section depth h_b on either side where the beam frames into an URM wall [Priestley et al., 2007]:

$$L_{be} = h_b + L_b + h_b \quad (10)$$

where L_b is the distance between the ends of the two walls. The effective length of the beams influences their stiffness and therefore their shear force, which lead to the variation of axial force at the base of the walls. Figure 6a compares the variation of the axial force at the base of the URM wall for macro-models with different effective lengths to the data obtained from TU2. Results indicate that the best match in terms of variation of axial force at the base of the URM wall is, indeed, obtained for L_{be} according to Eq. 10.

A parametric study comparing the response between the shell-model and the macro-model is carried out. The investigated parameters are (i) the axial load applied at the top of the two storeys of the URM wall and (ii) the strength of the RC beams (Figures 6b and 7). The objective is to ascertain if the estimation of L_{be} according to Eq. 10 in the macro-model can be used also for different configurations of masonry structures. The study is carried out by comparing the variation of axial stress at the base of the URM wall since such a variation is directly related to the assumed deformable length of the RC beams (L_{be}). The results confirm

that in the macro-model the effective length of the RC beams is accurately estimated by Eq. 10 also for different strengths of the RC beams ($\rho_b = 0.6\% - 1.2\%$) and different axial load ratios of the URM walls ($\sigma_0/f_{cM} = 0.2 - 0.6$).

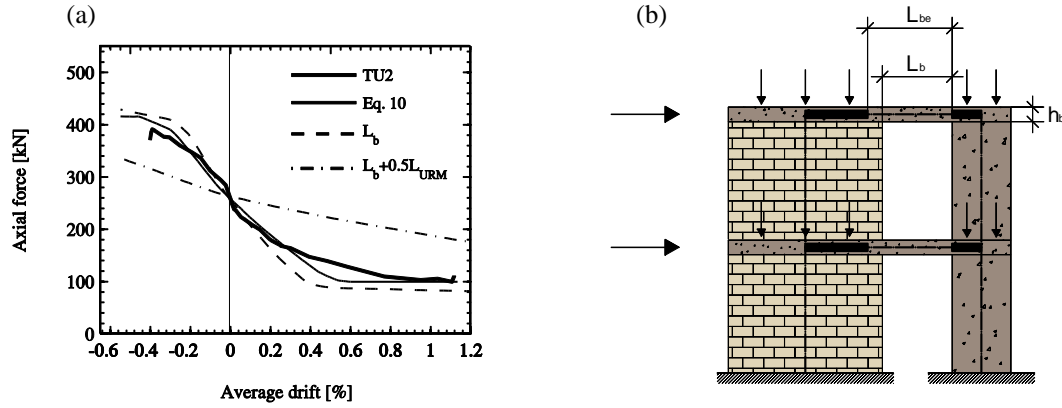


Figure 6: Effective length (L_{be}) of the RC beams in the macro-model. (a): comparison of the variation of the axial force at the base of the URM wall between TU2 (experiment) and macro-models with different effective lengths. (b): model for the parametric study.

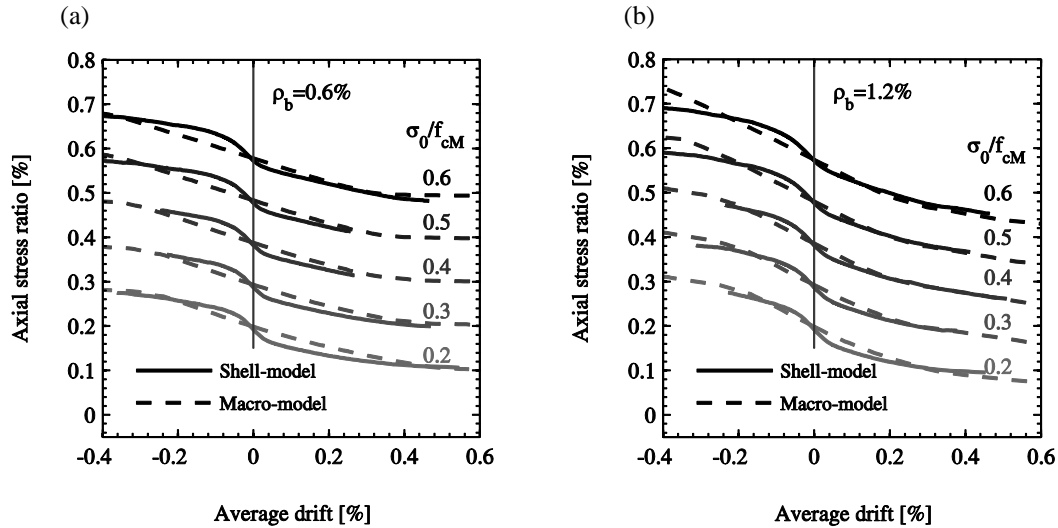


Figure 7: Effective length (L_{be}) to be adopted in the macro-model, parametric study. Variation of axial stress ratio for different axial loads applied to the URM wall (σ_0/f_{cM}) and different beam reinforcement ratios (ρ_b).

3.4 Comparison of the numerical and experimental results

Comparison between the two numerical models and the experiments is made by analysing:

- i) *The distribution of the base shear among the walls, to assess the influence of the relative stiffness of the members;*
- ii) *The distribution of the axial force between the walls, to check the assumptions of the effective length of the RC beams;*
- iii) *The inter-storey drift profile over the height of the structure, to ascertain the predicted deformed shapes.*

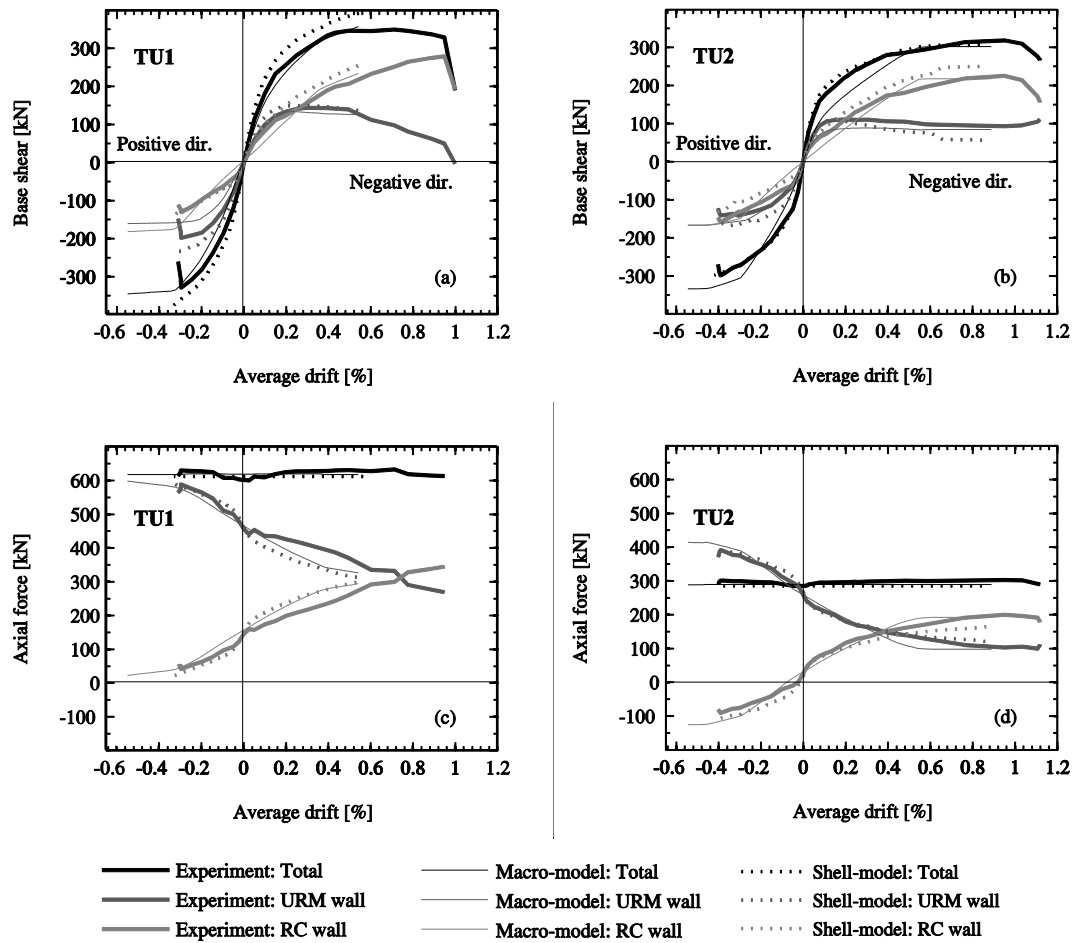


Figure 8: Distribution of the reaction forces between the two walls. (a), (b): base shear; (c), (d): axial force.

Figures 8a and 8b show that the shear carried by the URM walls is estimated rather accurately by both numerical approaches. With regard to the shear carried by the RC walls, on the other hand, the two models perform differently: before yielding of the RC walls, the macro-model underestimates the shear force carried by RC walls due to the bilinear relation adopted for the RC members and the assumed effective stiffness adopted for the first storey of the RC wall (EI_e), which is considerably smaller than the uncracked stiffness of the section. On the other hand, the shell-model is able to capture the stiffness degradation of the RC members.

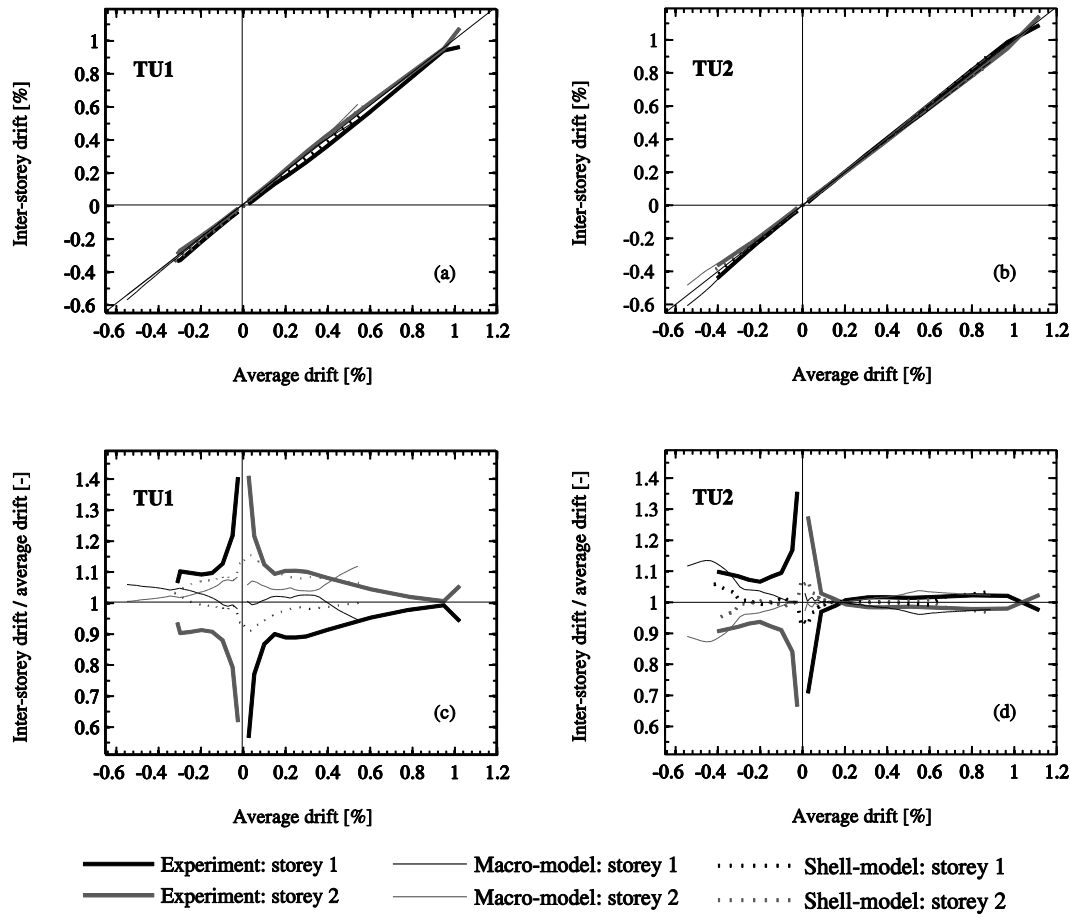


Figure 9: (a), (b): inter-storey drift profile over the height of the structure; (c), (d): ratio inter-storey drift average drift.

For TU1 there are some discrepancies in the distribution of the axial force between the models and the experimental results (Figure 8c). During testing of TU1, the total axial load applied at the top of the URM wall varied with around 30 kN while the simulations kept the axial load constant. As a consequence, both numerical models did not capture this variation in axial force due to the variation of the external vertical load. On the other hand, for TU2 (Figure 8d), the axial load applied at the top of the URM wall was constant throughout the testing procedure and the difference between experiments and numerical results is small.

During the testing of TU1 and TU2, the inter-storey drift δ of the first storey was almost equal to that of the second storey and the same trend is found from the simulations (Figures 9a and 9b). Figures 9c and 9d represent the ratio between the inter-storey drift and the average drift. Except for absolute average drifts smaller than 0.1%, the comparison between experiments and simulations is satisfactory and differences smaller than 15% are found. The evaluation of the displacement capacity, calculated only with the macro-model, gives good results although the displacement capacity of the structure is somewhat overestimated for the negative direction of loading. In Figures 8 and 9 the numerical simulations performed with the macro-model are stopped when the failure criterion is attained. In addition, the two numerical strategies are able to capture the prevailing shear and flexure damage modes that occurred over the height of the URM walls.

The macro-model can be used for practically oriented analyses of complete mixed RC-URM wall structures and, following the indications proposed in Section 3.3, relative accurate results with a limited computational effort can be obtained. The shell-element approach instead, can be adopted for detailed analyses of the mechanical behaviour of small substructures to give a better understanding about their local behaviour. Moreover, the shell-element approach can be used when an irregular arrangement of openings does not allow the definition of an equivalent frame in the macro-model approach or when the URM walls have not sufficiently large dimensions to be treated as macro-elements [Lourenço, 1996]. However, due to the regularity of the herein analysed mixed buildings, the macro-modelling technique can be generally used and is the most suitable tool for practically oriented analyses of such buildings.

4 Application to four buildings

One reference structure and three retrofit solutions (Figure 10) are compared to exemplify the benefits of retrofitting URM buildings by replacing or adding RC walls. The reference structure is a four-storey building composed of three URM walls. The adopted geometrical configuration leads to a shear failure mechanism at the bottom storey. In case study 1 one URM wall is replaced by one RC wall of the same length. Case study 2 represents the retrofit design made by the insertion of one RC wall which is parallel but not in the same plane of the other URM walls. As a consequence, in the numerical simulations the RC wall is connected to the URM structure with axially rigid links with zero moment capacity at each floor as represented in Figure 10c. In case study 3 two slender RC walls are added to the original URM building. Figure 10 shows the elevation of the four structures and the lateral load pattern applied. The thickness of the walls is always equal to 0.20 m. Two-dimensional simulations are carried out and RC beams 0.25x0.60 m represent the slabs. The thickness of the RC beams is three times that of the walls [Priestley et al., 2007] and the free span of the RC beams is 1.05 m. The axial stress ratio σ_0/f_{cm} at the base of the URM walls is around 0.14. All RC walls and slabs are designed such that the URM walls fail before any RC element. RC member's longitudinal reinforcement ratios are listed in Table 3; the shear reinforcement of RC walls and beams are designed to prevent shear failure. The total masses of the buildings are proportional to the sum of the length of the walls, that is 180 t for the reference structure and case study 1; 240 t for case studies 2 and 3.

Table 3: RC member's reinforcement ratios

RC walls	ρ_{mean} (case studies 1 & 2)	0.26 %
	ρ_{mean} (case study 3)	0.35 %
RC beams	$\rho_{b,top} = \rho_{b,bot} = \rho_b$	0.90 %

ρ_{mean} : mean longitudinal reinforcement ratio in RC walls;

$\rho_{b,top} = \rho_{b,bot} = \rho_b$: top and bottom longitudinal reinforcement ratios (RC beams).

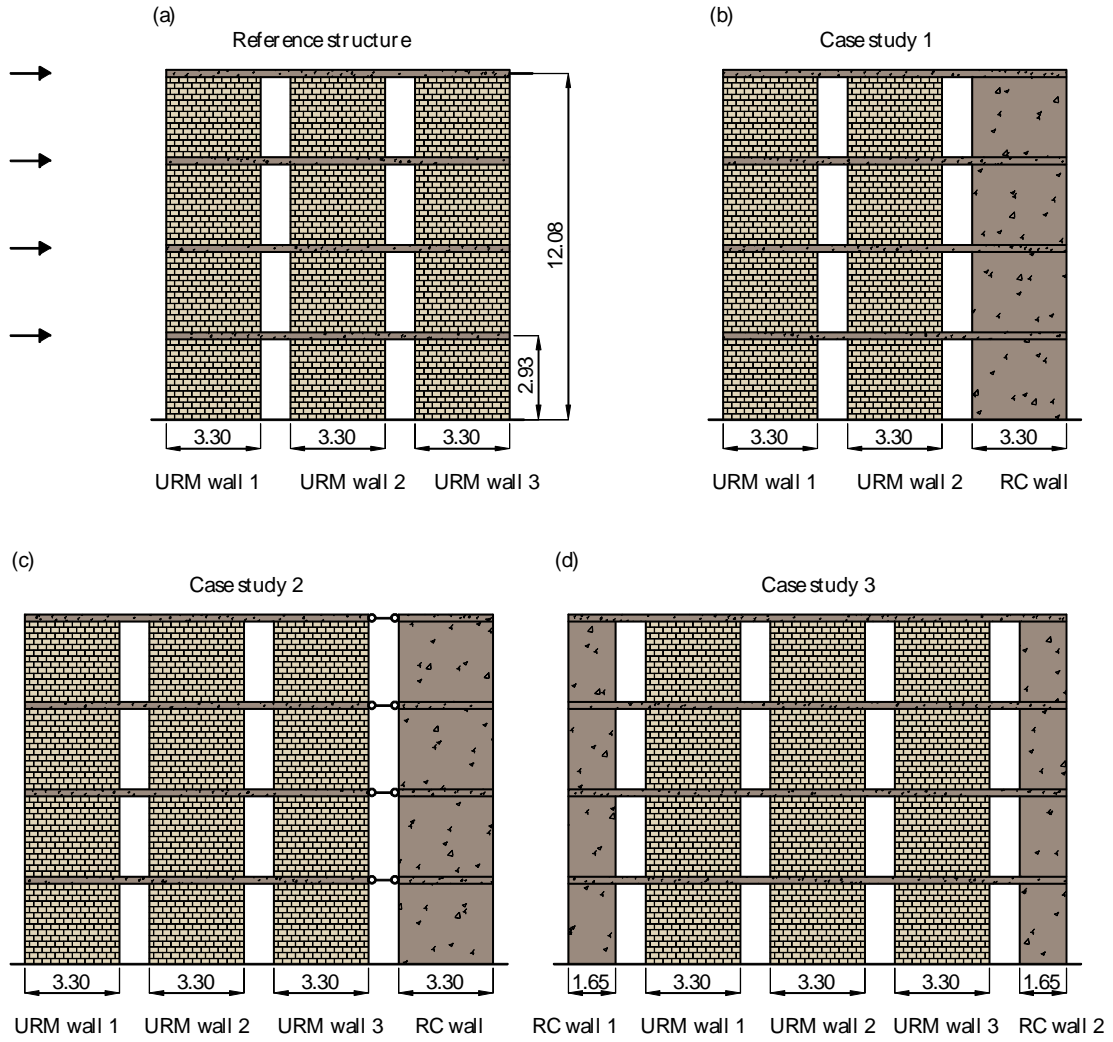


Figure 10: (a): reference URM structure; (b): case study 1; (c): case study 2; (d): case study 3. All dimensions in m.

The reference structure and case study 1 (Figures 10a and 10b) are also analysed considering a lower coupling provided by the RC beams (ρ_b equal to 0.20%). The objective is to decrease the coupling effect provided by the RC beams and achieve dominant rocking behaviour of the URM walls. This configuration will show that for buildings with rocking URM walls the increase in displacement capacity after the retrofitting is smaller than for buildings where the URM walls develop a dominant shear behaviour.

The analyses are carried out with the macro-model following the indications described in Section 3.3. μ_{eq} and c_{eq} , the equivalent friction and cohesion coefficients, are equal to 0.18 [-]

and 0.17 MPa respectively. The analyses are performed until the structures reach their Significant Damage (SD) limit state, which corresponds to the instant when the first URM wall reaches the target inter-storey drift capacity δ_{cap} . For walls failing in shear, the inter-storey drift capacity at the SD limit state is assumed as 0.4% [EN 1998-3, 2005]. For URM walls failing in flexure, their inter-storey drift capacity δ_{cap} is set equal to 0.8% H_{CF}/L [EN 1998-3, 2005]. The inter-storey drift demand of each wall (δ_D) is calculated as follows:

$$\delta_D = \frac{\Delta_i - \Delta_j}{h} - \theta_i \quad (11)$$

where Δ_i and Δ_j are the horizontal displacements of the beams below and above the considered wall, h the height of the wall and θ_i the rotation of beam below the wall. Comparisons will be carried out by analysing the capacity curves (Section 4.1) and the results from the N2 method (Section 4.2).

4.1 Capacity curves

Figure 11 represents the capacity curves of the four case studies for the two directions of loading. Besides the augmentation in strength, there is an increase in average drift capacity between approximately 50-60% (see also Table 4). As outlined in Section 2, the RC walls change the deformed shape and avoid a concentration of damage in the first storey.

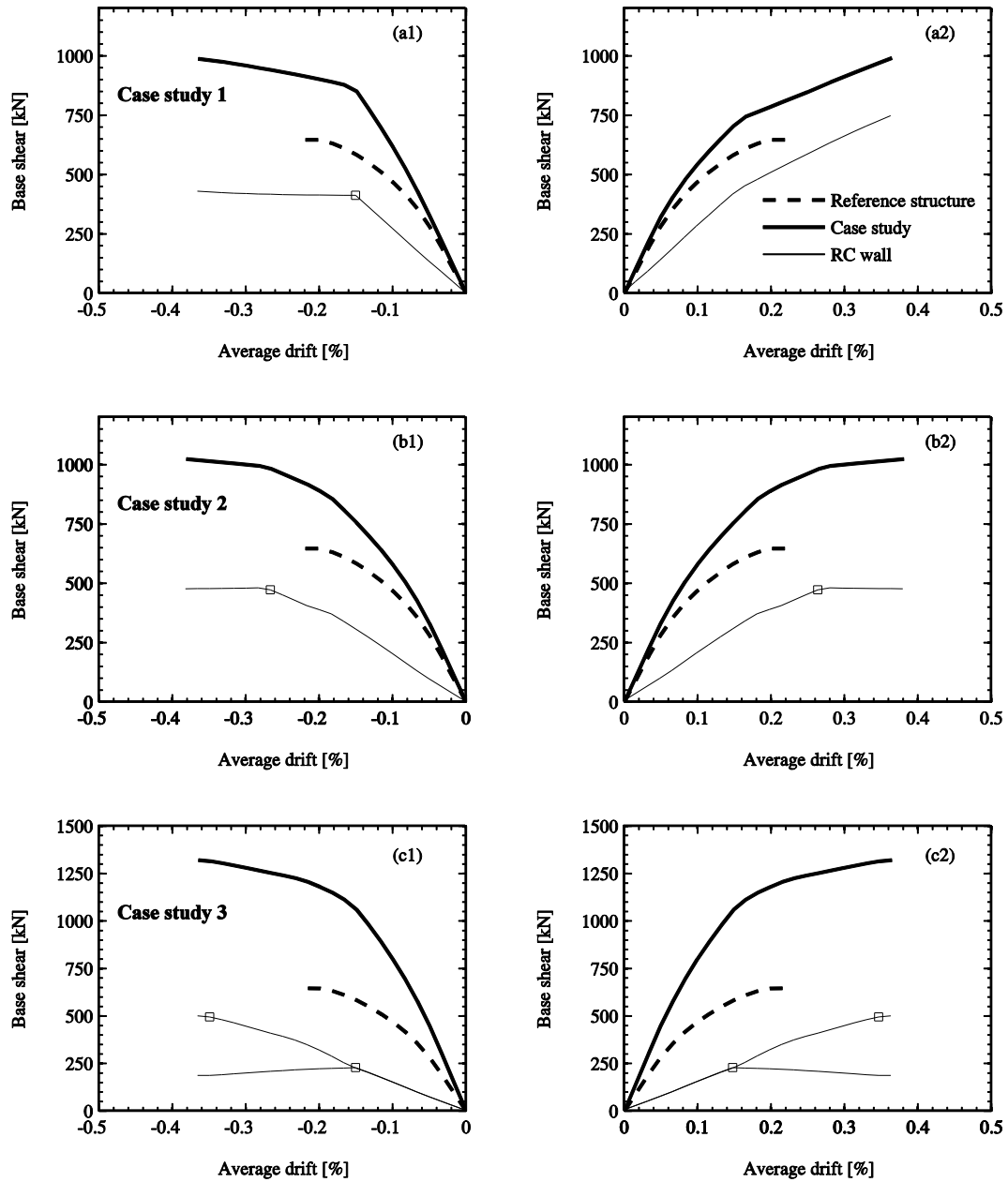


Figure 11: Force-displacement relations: reference URM structure and retrofitted configurations; squares indicate yielding of the RC walls.

Case study 1 is not plan-symmetric and its response changes whether the structure is pushed towards one direction or another (Figure 11a). URM walls are, in fact, much more sensitive to the variation of the axial force if compared to RC walls with respect to their stiffness, displacement and strength capacity. Since URM wall 1 and the RC wall are flanked by

beams only from one direction (Figure 10b), the axial force at their base changes depending on the loading direction.

Figure 12 represents the force-displacement relation for the reference structure and case study 1 when the longitudinal reinforcement ratio ρ_b of the beams is reduced to 0.20%. This configuration represents the effect of the retrofitting technique when the URM walls develop mainly a rocking behaviour. Since the addition of the RC wall does not particularly change the deformed shape of the structure, there is no significant increase in displacement capacity. In Figure 12, the displacement and strength capacities of the retrofitted configuration change depending on the loading direction since the retrofitted configuration is not plan symmetric (Figure 10a).

Table 4: Increase in drift capacity for the three case studies

	Average drift capacity [%]	Increase in drift capacity [%]
Reference structure	0.24 %	-
Case study 1 - Pos.	0.36 %	+ 50 %
Case study 1 - Neg.	0.36 %	+ 50 %
Case study 2	0.38 %	+ 58 %
Case study 3	0.37 %	+ 54 %

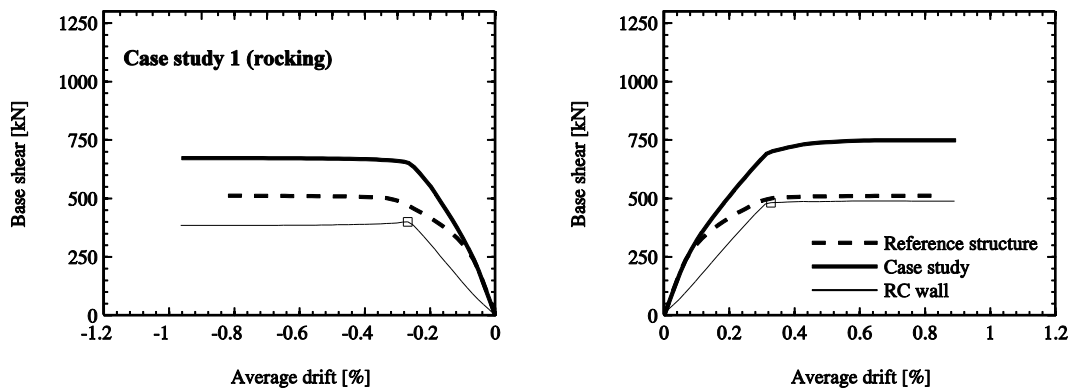


Figure 12: Force-displacement relations: reference structure and case study 1 when the URM walls have a dominant flexural behaviour; squares indicate yielding of the RC walls.

4.2 N2 method

The objective of structural engineers designing a retrofit intervention is that the retrofitted structure can withstand a larger seismic hazard than the original building. In codes the seismic hazard is typically expressed by the peak ground acceleration (PGA), which scales the shape of the design spectrum. Since retrofit interventions affect stiffness, strength and deformation capacity, the resulting increase in maximum peak ground acceleration (PGA_{max}) which the structure can withstand is evaluated by the N2 method. The method evaluates the so called “performance point”, which is found by comparing the capacity curve of the equivalent bi-linear single-degree of freedom (SDOF) system with the seismic demand [Fajfar, 2000]. From the pushover curve of the multi-degree of freedom system (actual MDOF response), the force-displacement response of the SDOF system (actual SDOF response) is computed according to EN 1998-1 [2004], Figure 13a. The bi-linear approximation of the SDOF’s force-displacement response is then constructed using the proposed criteria of Table 5 (see also Figure 13b) and the performance point of the structures is computed according to EN 1998-1 [2004].

Table 5: Definition of the bi-linear envelope of the equivalent SDOF system

Parameters for the bilinear envelope		Proposed criteria
(i)	Total base shear F_b^*	F_b^* is determined so that the energy dissipated by the equivalent SDOF and the actual SDOF systems are equal (Figure 13b)
(ii)	Initial stiffness k_{in}	k_{in} is the secant stiffness at $0.70 V_{max}/I$ (Figure 13b)
(iii)	Ultimate drift δ_u	δ_u corresponds to the displacement Δ_u^* divided the height of the structure

V_{max} : maximum shear force (actual MDOF response);
 F_b^* : maximum shear force (equivalent SDOF system);
 k_{in} : initial stiffness (equivalent SDOF system);
 δ_u : ultimate average drift (equivalent SDOF system);
 $\Delta_u^* = \Delta_{max,top}/I$: ultimate displacement (actual SDOF response);
 $\Delta_{max,top}$: ultimate top displacement (actual MDOF response);
 I : transformation factor calculated according to EN 1998-1 [2004].

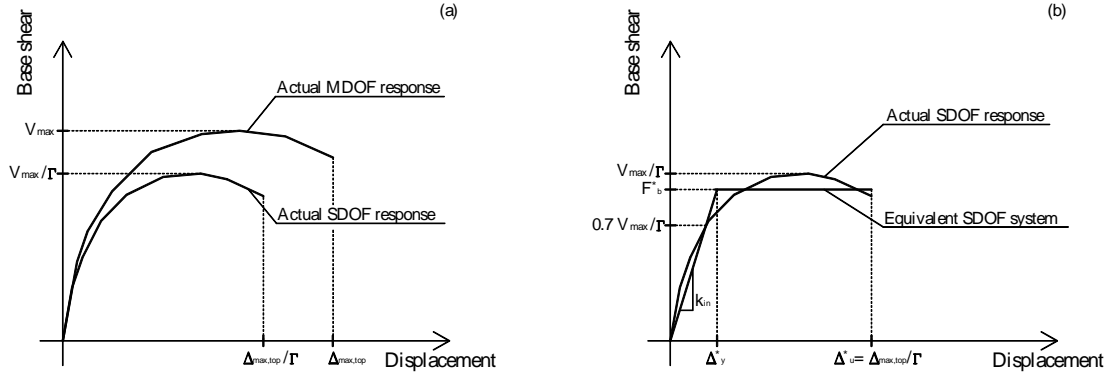


Figure 13: Mixed RC-URM wall structure, force-displacement curve. (a): actual MDOF and SDOF responses; (b): actual SDOF response and equivalent SDOF system.

Besides the comparison of PGA_{max} , the other quantities representing the seismic behaviour of the bilinear approximation of the equivalent SDOF systems (T^* , Δ_y^* , Δ_u^* , μ^* , F_b^*) are summarised in Table 6. In the analyses, the seismic demand is represented by an acceleration design spectrum of soil class C ($T_B = 0.2$ s; $T_C = 0.6$ s and $T_D = 2$ s [EN 1998-1, 2004]). Note that for all the structures the equivalent period T^* (period of the equivalent SDOF system) is lower than T_C , as it is generally the case for URM structures. As for all the configurations $T^* < T_C = 0.6$ s, the performance point of the equivalent SDOF system Δ_u^* is calculated as follows [EN 1998-1, 2004]:

$$\Delta_u^* = \frac{\Delta_{et}^*}{q_u} \left(1 + (q_u - 1) \frac{T_c}{T^*} \right) \geq \Delta_{et}^* \quad (12)$$

where Δ_{et}^* is the performance point of the SDOF system with period T^* and unlimited elastic behaviour:

$$\Delta_{et}^* = S_a(T^*) \left(\frac{T^*}{2\pi} \right)^2 \quad (13)$$

q_u is the ratio between the peak acceleration in the structure with unlimited elastic behaviour and in that with limited strength. $S_a(T^*)$ is the elastic acceleration response spectrum at the equivalent period T^* . Figure 14a shows the used acceleration design spectrum for $PGA =$

1 m/s², whereas Figures 14b to 14f represent the identification of the performance point in the acceleration-displacement response spectra for the maximum PGA that the structures withstand (PGA_{max}).

For the three case studies, the system's yield displacements Δ_y^* are between 1.15 to 1.45 times the one of the reference structure. The ultimate displacements Δ_u^* increase between 1.50 and 1.60 times, mainly because of the change in displacement profile due to the insertion of RC walls. As a result, the ductility of the system μ^* increases between 5% and 30%. The base shear capacity of the equivalent SDOF system (F_b^*) rises for all the case studies. In case study 3 the increase in base shear is larger than for the other configurations due to the larger frame effect developed by the presence of the two RC walls. As a result of the increase displacement and force capacity, the maximum PGA that the structures can sustain (PGA_{max}) rises between 140-170%.

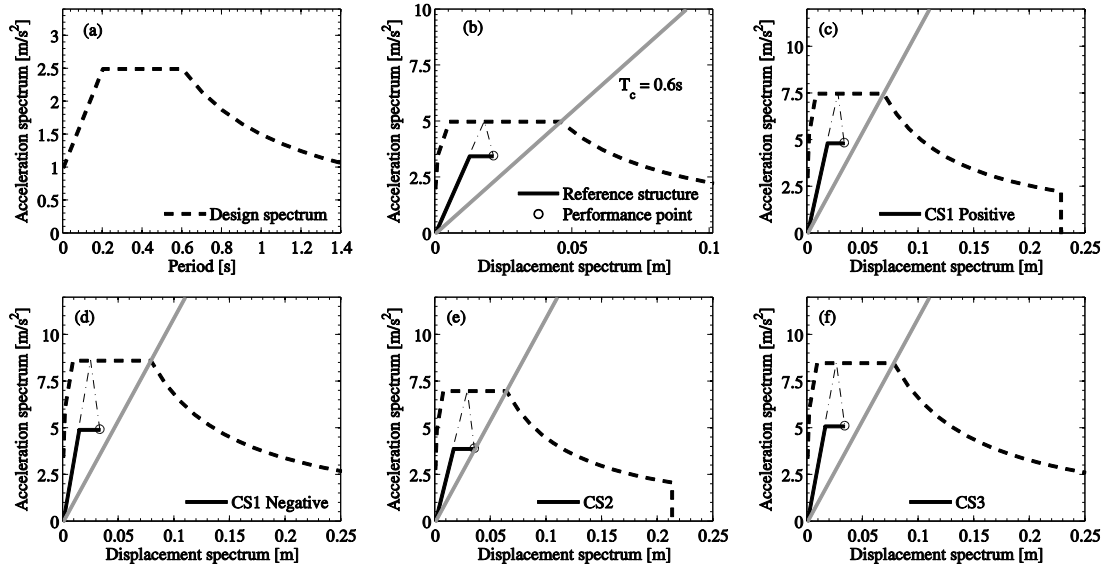


Figure 14: (a) Design acceleration spectrum adopted for the evaluation of the N2 method; (b-f) identification of the performance points in the acceleration-displacement response spectra diagram for the maximum PGA that the structures withstand.

Table 6: Comparison between the reference structure and the three case studies (except for the equivalent period T^* and $PGA_{max,abs}$ values of the reference structure taken as unit)

	Reference structure	Case study 1- Pos.	Case study 1- Neg.	Case study 2	Case study 3
T^*	0.38 s	0.38 s	0.34 s	0.41 s	0.35 s
$PGA_{max,abs}$	2.0 m/s ²	3.0 m/s ²	3.4 m/s ²	2.8 m/s ²	3.4 m/s ²
Δ_y^*	1.00	1.45	1.15	1.31	1.28
Δ_u^*	1.00	1.50	1.50	1.58	1.52
μ^*	1.00	1.04	1.30	1.21	1.19
F_b^*	1.00	1.42	1.45	1.50	2.02
PGA_{max}	1.00	1.50	1.70	1.38	1.68

T^* : equivalent period (equivalent SDOF system);

$PGA_{max,abs}$: absolute maximum PGA the structures can sustain;

Δ_y^* : normalised yield displacement (equivalent SDOF system);

Δ_u^* : normalised ultimate displacement (equivalent SDOF system);

μ^* : normalised system's displacement ductility (equivalent SDOF system);

F_b^* : normalised total base shear (equivalent SDOF system);

PGA_{max} : normalised maximum PGA the structures can sustain.

5 Conclusions and outlook

The article presented a retrofit technique for modern URM buildings connected by RC slabs by adding or replacing RC walls to the original structure. The study targeted structures where the RC members are designed to fail for larger displacement demands than the URM walls. Mixed RC-URM buildings in which the RC members are not capacity-designed were not herein considered. The advantages of this retrofitting technique are related to (i) an increase in strength capacity and (ii) a change of the deformed shape. The latter provides a failure mechanism with larger top displacements for the same level of inter-storey drift at the ground floor (Figure 4).

In order to analyse such structures, two computational strategies were presented, namely a shell-model and a macro-model approach. The results of the two techniques were compared against experimental results and judged satisfactory. The macro-model, although requiring limited computational efforts, was capable of representing all the main features of the seismic behaviour of mixed RC-URM wall structures: (i) distribution of the reaction forces between the walls at peak strength, (ii) evaluation of the inter-storey drift profile over the height of the structure, (iii) evaluation of the ultimate displacement capacity and (iv) damage modes that

occurred in the URM walls. As a consequence a macro-element model, which follows the indications proposed in Section 3.3, is particularly recommended for practically oriented analysis of complete mixed RC-URM wall structures. A shell-model approach, instead, can be adopted for analysing in detail the mechanical behaviour of small substructures where more refined analyses are needed.

The case studies evaluated the benefits in terms of design quantities: the increase in displacement capacity ranged between 50% and 60% and the increase in PGA_{max} was between 40% and 70%. The displacement ductility μ^* increased between 5% and 30%.

The RC wall length, as well as its reinforcement ratio, was kept constant. Further studies will address the effects of varying the RC wall length and its reinforcement ratio with the objective of optimising the efficiency of the retrofitting technique.

6 Acknowledgments

The authors thank Chris Genis for proofreading the manuscript.

7 References

- Beyer, K and Dazio, A. [2012] “Quasi-Static Cyclic Tests on Masonry Spandrels”, *Earthquake spectra*, 28(3), 907-929.
- Beyer, K., Tondelli, M., Petry, S. and Peloso, S. [2014a] “Dynamic testing of a 4-storey building with reinforced concrete and unreinforced masonry walls”, submitted to *Bulletin of Earthquake Engineering*.
- Casoli, D. [2007] “Assessment of existing mixed RC-Masonry structures and strengthening by RC shear walls”, Pavia, Italy.
- Cattari, S. and Lagomarsino, S. [2013] “Seismic design of mixed masonry-reinforced concrete buildings by non-linear static analyses”, *Earthquakes and Structures*, Vol. 4, N°3.
- Červenka, J. and Papanikolaou, V.K. [2008] “Three dimensional combined fracture-plastic material model for concrete”, *International Journal of Plasticity*, 24, 2192-2220.

- Červenka, V., Jendele, L. and Červenka, J. [2010] “Atena - Computer Program for Nonlinear Finite Element Analysis of Reinforced Concrete Structures”, *Theory and User Manual*, Prague, Czech Republic.
- Chen, W. [1970] “Double punch test for tensile strength of concrete”, *ACI Journal*, 67, 993-995.
- EN 1052-1 [1998] *Eurocode 6: Methods of test for masonry – Part 1: Determination of the compressive strength*, CEN, Brussels.
- EN 1052-3 [2002] *Eurocode 6: Methods of test for masonry – Part 3: Determination of the initial shear strength*, CEN, Brussels.
- EN 1992-1-1 [2004] *Eurocode 2: Design of concrete structures – Part 1-1: General rules and rules for buildings*, CEN, Brussels.
- EN 1998-1 [2004] *Eurocode 8: Design of structures for earthquake resistance – Part 1: General rules, seismic actions and rules for buildings*, CEN, Brussels.
- EN 1998-3 [2005] *Eurocode 8: Design of structures for earthquake resistance – Part 3: Assessment and retrofitting of buildings*, CEN, Brussels.
- Fajfar, P. [2000] “A non linear analysis method for performance-based seismic design”, *Earthquake Spectra*, 16(3), 573-591.
- Hannenwald, P. [2013] “Seismic behaviour of poorly detailed RC bridge piers” Ph.D. thesis, EPFL, Lausanne, Switzerland.
- Jurukovski, D., Krstevska, L., Alessi, R., Diotallevi, P.P., Merli, M. and Zarri, F. [1992] “Shaking table tests of three four-storey brick masonry models: original and strengthened by RC core and by RC jackets”, *Proc. of 10th World Conference on Earthquake Engineering*, Madrid, Spain.
- Lagomarsino, S., Penna, A., Galasco, A. and Cattari, S. [2009] “Tremuri User Guide”, Genova, Italy.
- Lagomarsino, S., Penna, A., Galasco, A. and Cattari S. [2013] “TREMURI program: an equivalent frame model for the non-linear seismic analysis of masonry buildings”, *Engineering Structures*, 6, 1787–1799.
- Lang, K. [2002] “Seismic vulnerability of existing buildings”, Ph.D. thesis, ETH Zurich, Zurich, Switzerland.
- Lourenço, P.B. [1996] “Computational Strategies for Masonry Structures”, Ph.D. thesis, Delft University, Delft, The Netherlands.

- Magenes, G. and Calvi, G.M. [1997] “In-plane seismic response of brick masonry walls”, *Earthquake Engineering and Structural Dynamics*, 26, 1091-1112.
- Magenes G. [2006] “Masonry building design in seismic areas: recent experiences and prospects from a European standpoint” Keynote address, *Proc. of 1st European Conference on Earthquake Engineering and Seismology*, Geneva, Switzerland.
- Mander, J.B., Priestley, M.N.J. and Park, R. [1988] “Theoretical stress-strain model for confined concrete” *ASCE Journal of Structural Engineering*, 114(8), 1804-1826.
- Mandirola, M. [2014] “Non-linear macroelement modelling of experimental tests on masonry building specimens with rigid diaphragms”, Pavia, Italy.
- Mann, W. and Müller, H. [1982] “Failure of shear-stressed masonry: an enlarged theory, tests and application to shear walls”, *Proc. of the British Ceramic Society*, 30, 223-235.
- Paparo, A. and Beyer, K. [2012] “Pushover Analyses of Mixed RC-URM wall structures”, *Proc. of 15th World Conference on Earthquake Engineering*, Lisbon, Portugal.
- Paparo, A. and Beyer, K. [2014] “Quasi-static tests of two mixed reinforced concrete – unreinforced masonry wall structures”, *Engineering Structures*, 71, 201-211.
- Paulay, T. and Priestley, M.N.J. [1992] *Seismic design of reinforced concrete and masonry buildings*, John Wiley & Sons, Inc., New York.
- Penna, A., Lagomarsino, S. and Galasco, A. [2013] “A nonlinear macro-element model for the seismic analyses of masonry buildings”, *Earthquake Engineering and Structural Dynamics*, 10.1002/eqe.2335.
- Petry, S and Beyer, K. [2014a] “Cyclic test data of six unreinforced masonry walls with different boundary conditions”, *Earthquake Spectra*.
- Petry, S and Beyer, K. [2014b] “Influence of boundary conditions and size effect on the drift capacity of URM walls”, *Engineering Structures*, 65, 76-88.
- Reyes, E., Casati, M.J. and Galvez, J.C [2008] “Cohesive crack model for mixed mode fracture of brick masonry”, *International Journal of Fracture*, 151, 29-55.
- Priestley, M.J.N., Calvi, G.M. and Kowalsky, M.J. [2007] *Displacement-Based Seismic Design of Structures*, IUSS Press, Pavia, Italy.
- SIA 162/1 [1995] *Building code, Swiss Society of Engineers and Architects (SIA): Ouvrages en béton – Essais des matériaux*, SIA, Zurich.
- SIA 262 [2004] *Building code, Swiss Society of Engineers and Architects (SIA): Concrete Structures*, SIA, Zurich.

- Smith, B.S. and Coull, A. [1991] *Tall building structures: analysis and design*, John Wiley & Sons, Inc., New York.
- Tomaževič, M., Modena, C., Velechovsky, T and Weiss, P. [1990] “The effect of reinforcement on the seismic behaviour of masonry buildings with mixed structural systems: an experimental study”, *Proc. of 9th European Conference on Earthquake Engineering*, Moscow, Russia.

Paper III: Development of a displacement-based design approach for modern mixed RC-URM wall structures

Submitted to *Earthquake and Structures*

Development of a displacement-based design approach for modern mixed RC-URM wall structures

Abstract

The recent re-assessment of the seismic hazard in Europe led for many regions of low to moderate seismicity to an increase in the seismic demand. As a consequence, several modern unreinforced masonry (URM) buildings, constructed with reinforced concrete (RC) slabs that provide an efficient rigid diaphragm action, no longer satisfy the seismic design check and have been retrofitted by adding or replacing URM walls with RC walls. Of late, also several new construction projects have been conceived directly as buildings with both RC and URM walls. Despite the widespread use of such construction technique, very little is known about the seismic behaviour of mixed RC-URM wall structures and codes do not provide adequate support to designers. The aim of the paper is therefore to propose a displacement-based design methodology for the design of mixed RC-URM edifices and the retrofit of URM buildings by replacing or adding selected URM walls with RC ones. The article describes also two tools developed for estimating important quantities relevant for the displacement-based design of structures with both RC and URM walls. The tools are (i) a mechanical model based on the shear-flexure interaction between URM and RC walls and (ii) an elastic model for estimating the contribution of the RC slabs to the overturning moment capacity of the system. In the last part of the article the proposed design method is verified through non-linear dynamic analyses of several case studies. These results show that the proposed design approach has the ability of

controlling the displacement profile of the designed structures, avoiding concentration of deformations in one single storey, a typical feature of URM wall structures.

Keywords: Displacement-based design; Modern mixed reinforced concrete- unreinforced masonry wall structures; Seismic design; Pushover analyses; Inelastic time history analyses.

1 Introduction

In recent years, many modern unreinforced masonry (URM) buildings, which have been constructed with reinforced concrete (RC) slabs, have been retrofitted by adding RC walls to the existing structure or by replacing selected URM walls with RC ones [Magenes, 2006; Cattari and Lagomarsino, 2013]. If the RC members are designed to withstand larger displacement demands than URM walls, experimental and numerical studies have shown that this retrofit technique can substantially increase the displacement capacity of the system [Paparo and Beyer, 2014a; Paparo and Beyer, 2014b]. Of late, also new buildings have been designed directly as mixed RC-URM wall structures since structures with URM walls only would not pass the classical force-based design check.

Mixed RC-URM construction varies significantly from region to region [Magenes, 2006; Cattari and Lagomarsino, 2013] and this paper is limited to modern mixed RC-URM systems representative of residential buildings in Switzerland, whose detailed description is outlined in the introduction of the thesis. Despite the popularity of these constructions, research efforts have been directed only recently towards developing seismic design methodologies for mixed RC-URM wall buildings. As a consequence, codes do not provide guidelines for such mixed structures [Magenes 2006] and design engineers have generally designed them using oversimplified assumptions.

Noting the importance of such buildings and, at same time, the lack of guidelines, the principal objective of this investigation is to develop a displacement-based design (DBD) methodology for the design of mixed RC-URM wall structures and the retrofit of URM buildings by replacing or adding selected URM walls by RC ones. The methodology follows the direct DBD (DDBD) approach by Priestley et al. [2007] and consists of three main phases:

(i) A preliminary DDBD check of the plain URM building.

(ii) If the structure does not satisfy the seismic design requirements and shows a dominant shear behaviour, a mixed structural system with improved behaviour is devised by replacing the critical URM wall or walls with RC ones. If the URM walls show a dominant rocking behaviour, adding RC walls will increase the strength but not the displacement capacity.

(iii) The DDBD design of the mixed RC-URM wall structure is carried out. Several aspects concerning the interaction between RC and URM walls are evaluated by using a mechanical model which represents the URM walls with an equivalent shear beam and the RC walls with an equivalent flexural cantilever. At the end of the procedure, guidelines for the design of the RC members and the out-of-plane check of the URM walls are briefly outlined.

As the mechanical model represents these mixed buildings close to failure (see Section 3), the proposed DDBD approach can be used for the design of systems which are expected to attain, according to [EN 1998-3, 2005], the significant damage (SD) limit state. Furthermore, as the article focuses on the in-plane interaction between RC and URM walls, the possible formation of out-of-plane mechanisms is not examined. Investigations on the out-of-plane behaviour of systems with RC and URM walls have been carried out by Tondelli and Beyer [2014]. In addition, to simplify matters, possible sources of uncertainty are neglected (for instance, uncertainty in the deformation capacity of the URM walls is not accounted for).

Section 2 introduces features of this typology of mixed systems relevant for DDBD and outlines how the displacement capacity of such structures has been evaluated. The section is then followed by a description of the mechanical model that represents the effects of the interaction between RC and URM walls. Sections 4 to 6 introduce the concepts of the DDBD approach and develop its application for mixed RC-URM wall structures. The algorithm is then applied to a set of case studies and validated against results from inelastic time-history analyses (Section 7). The article closes with a summary of the main findings and an appendix with a design example.

2 Features of mixed RC-URM wall structures

In this section, features of mixed RC-URM walls structures relevant for DDBD are introduced with the following objectives:

- (i) To define the design displacement profile that will be adopted in DDBD;
- (ii) To define for which cases the interaction between URM and RC walls may improve the structural behaviour;
- (iii) To set the design drift limits that will be adopted.

Under lateral loading, shear dominated URM wall buildings display concave displacement shapes as illustrated in Figure 1a. On the other hand, the displacement profiles of slender RC wall are convex when struck by an earthquake, Figure 1b. Consequently, as represented in Figure 1c, it seems reasonable to assume a global linear design displacement profile when RC and URM walls are coupled together. Indeed, Section 3 will show that such an assumption can be controlled during the DDBD process by varying the strength and stiffness of the RC walls.

The same behaviour was described by Paulay and Priestley [1992] for dual frame-wall buildings. Slender wall elements, which show mainly flexural deformations, are coupled to frames, whose global behaviour can be approximated by that of a shear beam. As a result, and similarly to mixed RC-URM wall buildings, the deformed shape of dual frame-wall buildings tends to be linear over the height of the building.

If the masonry walls have a dominant rocking response, they will exhibit a linear or slightly convex deformation profile and less benefit is gained by coupling RC walls with URM walls. However, due to the significant out-of-plane stiffness and strength of the RC slabs [Lang 2002] and the resulting moment restraint at each floor level, a shear critical behaviour of the URM walls is very common in such mixed systems.

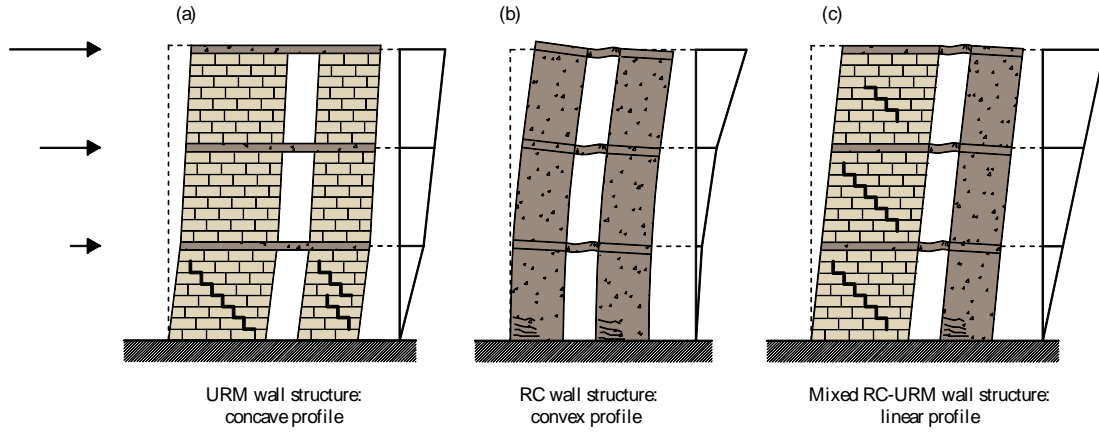


Figure 1: URM (a), RC (b) and mixed RC-URM wall (c) structures: deflected shapes and displacement profiles.

For this typology of modern mixed structures, the RC members are designed to exhibit larger displacement capacities than those relative to URM walls. As a consequence, the SD limit state is always controlled by the URM walls since they attain the limit state before the RC members [Paparo and Beyer, 2014a; Paparo and Beyer, 2014b]. In the following, the SD limit state is considered attained when the first URM wall reaches its inter-storey drift capacity [Paparo and Beyer, 2014b] that is set equal to 0.4% for walls with dominant shear behaviour and $0.8\%H_{CF}/L$ for walls with dominant rocking behaviour [EN1998-3, 2005]. H_{CF} and L are the height of contra-flexure point and the length of the wall, respectively. The inter-storey drift δ is calculated as the relative horizontal displacement between the beams underneath and above the selected storey (Δ_i and Δ_j) divided by the storey height h :

$$\delta = \frac{\Delta_i - \Delta_j}{h} \quad (1)$$

3 Shear-flexure cantilever model

The interaction between shear and flexural dominated systems has been studied over the last 50 years and several methods for analysing dual frame-wall systems have been proposed. One of these is the so-called “shear-flexure cantilever”, which treats walls and frames as flexural and shear cantilevers respectively [e.g., Chiarugi, 1970; Rosman, 1974; Pozzati, 1980;

Smith and Coull, 1991]. Given the similarities of mixed RC-URM wall buildings to dual frame-wall structures, the shear-flexure cantilever model is extended for analysing such structures. The objective is to develop a simple tool able (i) to check the displacement profile of mixed RC-URM wall structures and (ii) to evaluate the height of the contra-flexure point of the RC walls ($H_{CF,RC}$). Both parameters will be used in the DDBD process presented in Section 6.

After the description of the mechanical model (Section 3.1) and the comparison of several results against numerical simulations (Section 3.2), charts which can be directly used during the DDBD procedure are presented (Section 3.3).

3.1 Differential equations of the shear-flexure cantilever model

The interaction between RC and URM walls can be described with a simple mechanical model which consists of a pure bending cantilever, representing the RC walls, and a pure shear cantilever, which describes the URM walls. The two beams are continuously connected over the height by axially rigid links with zero moment capacity, Figure 2.

The differential equations for a shear-flexure cantilever have been first set up and solved by Rosman [1967] and the following work is based on the textbook by Pozzati [1980]. At any cross section at height x , the drift $\theta(x)$ can be calculated as the ratio between the shear carried by the shear cantilever, $V_I(x)$, divided by its shear stiffness GA :

$$\theta(x) = \frac{dv(x)}{dx} = \frac{V_I(x)}{GA} \quad (2)$$

where $v(x)$ is the horizontal displacement of the system. The shear $V_I(x)$ is the derivative of the moment carried by the shear cantilever $M_I(x)$ with respect to x . Its derivative can be written as:

$$\frac{d^2v(x)}{dx^2} = \frac{1}{GA} \frac{d^2M_I(x)}{dx^2} \quad (3)$$

At any height, the ratio $\frac{1}{GA} \frac{d^2 M_1(x)}{dx^2}$ of the shear cantilever has to be equal to the curvature of the flexural beam. Given $OTM(x)$ the overturning moment introduced by the external forces and $M_2(x)$ the moment carried by the flexural beam, it therefore follows:

$$\frac{1}{GA} \frac{d^2 M_1(x)}{dx^2} = -\frac{1}{EI} M_2(x) = -\frac{1}{EI} (OTM(x) - M_1(x)) \quad (4)$$

The general solution of Eq. 4 is:

$$\text{Shear beam:} \quad M_1 = A \cosh\left(\alpha \frac{x}{H}\right) + B \sinh\left(\alpha \frac{x}{H}\right) + M_p(x) \quad (5a)$$

$$\text{Flexure beam:} \quad M_2(x) = OTM(x) - M_1(x) \quad (5b)$$

where α is the stiffness ratio of the shear and flexural beam and is obtained as:

$$\alpha = H \sqrt{\frac{GA}{EI}} \quad (6)$$

where EI is the sum of the flexural stiffnesses of the concrete walls and GA is the sum of the shear stiffnesses of the masonry walls. In Eq. 5a $M_p(x)$ is the particular solution which, for constant horizontal load q , takes the following form:

$$M_p(x) = OTM(x) - q \left(\frac{H}{\alpha}\right)^2 \quad (7)$$

In Section 3.3 the limitations related to the adoption of the constant load pattern will be discussed. The two constants A and B of Eq. 5a are found by assigning two boundary conditions. In literature the shear-flexure cantilever was used to solve the elastic behaviour of dual structures. Hence, the equations were solved for boundary conditions where (i) the moment at the top of the shear cantilever is zero and that (ii) the rotation at the base of the flexure cantilever is zero, which implies that the flexure cantilever is fixed at the bottom. For the mixed RC-URM wall structure at SD limit state the equations need to be solved for different boundary conditions, which will be discussed in the following.

Since the model aims to represent the structure attaining SD limit state, it is expected that the RC walls yield. In order to account for the formation of the plastic hinge at their base, the flexural cantilever is modelled with a pinned base condition. A base moment, corresponding to the total flexural capacity of the RC walls, is then applied as external moment to the hinge in addition to the externally applied horizontal load q . The parameter β_{RC} describes the ratio between the base moment $M_2(x=0)$ provided by the flexural (RC) wall and $OTM(x=0)$:

$$\beta_{RC} = \frac{M_2(x=0)}{OTM(x=0)} \quad (8)$$

The second constant can be derived by setting the moment at the top of the shear beam equal to zero: $M_1(x=H) = 0$. The shears $V_1(x)$ and $V_2(x)$ are found as the derivate of $M_1(x)$ and $M_2(x)$ with respect to x . By analytically integrating the drift $\theta(x)$ between the base ($x=0$) and the height of the floor ($x=h_i$), the horizontal displacement v_i of each storey is calculated:

$$v_i = \int_0^{h_i} \theta(x) dx \quad (9)$$

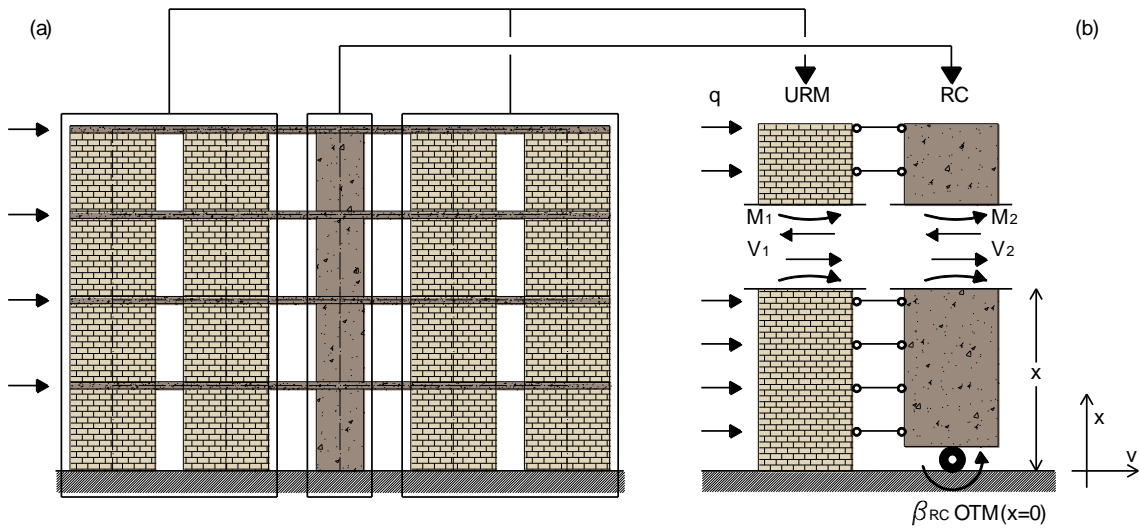


Figure 2: Mechanical model: identification of shear (URM) and flexural (RC) walls (a); definition of the reference system and of the internal forces (b).

3.2 Comparison of the results of the shear-flexure cantilever model against numerical simulations

For several configurations of mixed RC-URM wall structures, the inter-storey drift predicted by the shear-flexure cantilever model is compared to the one obtained by pushover analyses. The objective is to check the influence of four parameters on the displacement profile and on the height of the contra-flexure point of the RC wall. The parameters are: (i) number of storeys, (ii) number of URM walls, (iii) length of URM walls and (iv) longitudinal reinforcement ratio of the RC slabs. Table 1 shows the combination of the four variables.

Figure 3 represents the elevation of the 4-storey layout configurations. The thickness of the walls is always 0.20 m and the clear storey height of the walls is always 2.8 m. The length of the RC walls is fixed to 3.30 m. The moment capacities at the base of the RC walls, $M_2(x = 0)$, are 1600 kNm, 1700 kNm and 1800 kNm for the 3, 4 and 5 storey configurations, resulting in values of β_{RC} within the range of 16% and 34%. The transverse reinforcements of the RC members are designed to prevent shear failure. As two-dimensional analyses are carried out, the slabs are represented by RC beams with a cross section of 0.25x0.60 m. The effective width of 0.60 m corresponds to three times the wall width [Priestley et al., 2007]. The free span of the RC beams is equal to 1.05 m and the area of their longitudinal reinforcement is varied between 500 and 750 mm² ($\rho_{CB} = 0.38\%-0.57\%$). The two reinforcement ratios correspond, approximately, to longitudinal reinforcing bars D10 every 110 mm ($\rho_{CB} = 0.38\%$) and D12 every 90 mm ($\rho_{CB} = 0.57\%$). Finally, the masses, which are constant per storey, are proportional to the length of the walls. It results that the storey masses are equal to 35.7 t for layout 1 and 3 and 21.4 t for layout 2. Sections 3.2.1 and 3.2.2 describe the mechanical and geometrical properties adopted for the shear-flexure cantilever model and the pushover analyses and Section 3.2.3 compares the results obtained from the two different approaches.

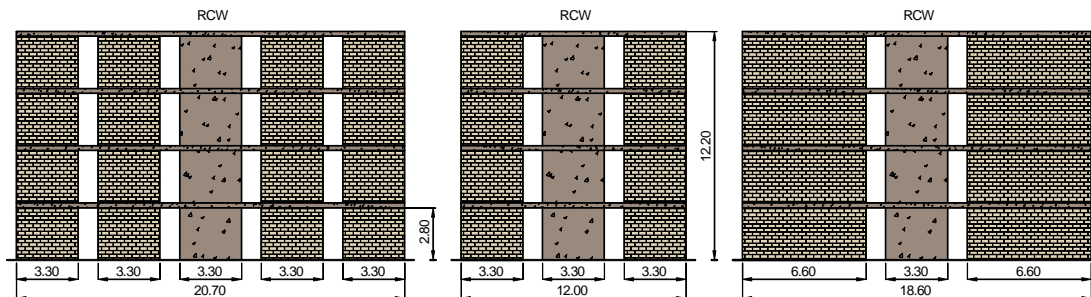


Figure 3: Layouts 1, 2 and 3 (4-storey configurations). All dimensions in m.

Table 1: Parameters investigated to compare the shear-flexure cantilever model against numerical simulations

	Number of storeys [-]	Number of URM walls [-]	Length of URM walls [m]	A_s [mm ²]
Layout 1	3, 4, 5	4	3.30	500 - 750
Layout 2	3, 4, 5	2	3.30	500 - 750
Layout 3	3, 4, 5	2	6.60	500 - 750

A_s : longitudinal reinforcing bars of RC beams

3.2.1 Mechanical and geometrical properties for the shear-flexure cantilever model

The mechanical model aims to represent the interaction between URM and RC walls by means of an ideal shear and an ideal flexure cantilever which have constant stiffnesses GA and EI along their height (Section 3.1). In this section, analogies and differences between the seismic behaviour of mixed RC-URM structures obtained from experimental campaigns [Paparo and Beyer, 2014a; Beyer et al., 2014; Tondelli et al., 2014] and the hypotheses of the mechanical model are discussed. Based on this comparison, recommendations for setting up the shear-flexure cantilever model are formulated.

i) In the experimental campaigns it was observed that in the URM walls the shear cracks are distributed over the height of the building. Hence, the stiffness of the shear beam can be based on the cracked stiffness GA of the masonry walls. According to EN 1998-3 [2005], GA is assumed as half of the uncracked stiffness of the masonry walls.

Table 2: Mechanical and geometrical properties adopted for the shear-flexure cantilever model

	Shear beam (URM walls)		Flexural beam (RC walls)	
	A [m ²]	G [GPa]	I [m ⁴]	E [GPa]
Layout 1	2.20	0.265	0.599	36.0
Layout 2	1.10	0.265	0.599	36.0
Layout 3	2.20	0.265	0.599	36.0

A : sum of the shear areas of the masonry walls

G : cracked shear stiffness of the masonry walls from Paparo and Beyer (2014b)

I : sum of the moment of inertia of the uncracked RC walls

E : elastic modulus of the concrete

ii) The experimental tests have shown that the cracks in the RC walls are concentrated in the first storey, resulting in a stiffness of the first storey which is lower than the stiffness of the upper storeys. In order to find closed form solutions for the mechanical model, the flexure beam has to be assigned a constant stiffness EI over the height of the building. To account for the reduced stiffness of the first storey, the flexure beam is pinned at the base and a moment equal to the yield moment of the wall is applied.

iii) From the dynamic test [Beyer et al., 2014] it was observed that in the top storeys the URM walls feature significant rocking deformations. As the URM walls are only represented by a shear beam, this rocking deformation is not accounted for and the mechanical model overestimates for the top storeys the influence of the shear cantilever on the displacement profile (see also Section 3.2.3). To compensate this effect, the stiffness of the flexural beam EI is based on gross sectional properties, without considering a reduction factor to account for the small construction-joint cracks which develop between RC walls and slabs in the top storeys. Table 2 summarises the mechanical and geometrical properties adopted for the shear-flexure cantilever models.

3.2.2 Mechanical and geometrical properties for the numerical simulations

To validate the results from the shear-flexure cantilever model, numerical simulations are carried out using the software TREMURI [Largomarsino et al., 2013]. The structure is modelled as a 2D equivalent frame where the elements representing URM and RC walls are connected at the storey heights by RC beam elements representing the RC slabs. The macro-element developed by Penna et al. [2013] is used for the masonry walls. Such an element is representative of a storey-high masonry panel and allows, by means of a relation between average stresses and average strains, to represent the two main in-plane failure mechanisms (i.e., shear and bending-rocking). Timoshenko beams with plastic hinges at their extremities, whose hysteretic behaviour is characterised by the Takeda model, represent RC members. For further details of the software, the reader is referred to Penna et al. [2013] and Lagomarsino et al. [2013].

Concerning the adopted material properties and the construction of the equivalent frame, the indications proposed by Paparo and Beyer [2014b] are followed. Table 3 resumes the assumed mechanical properties: c_{eq} and μ_{eq} are the equivalent friction and cohesion parameters

of the macro-element [Penna et al., 2013] resulting from the homogenization technique. They are calculated by assigning half of the shear strength V_{sh} to the friction component V_μ and half of the shear strength to the cohesion component V_c [Paparo and Beyer, 2014b].

According to Penna et al. [2013], V_{sh} can be estimated on the basis of the strength criterion which is representative of the expected failure. In this case, the strength of the masonry walls is calculated according to Mann and Müller [1982]. If the material properties of the URM walls are not known, an alternative for calculating the shear strength V_{sh} of a masonry wall is proposed by Priestley et al. [2007]: given N the axial force on section, V_{sh} can be predicted as:

$$V_{sh} = \mu_m N + c_m A_{eff} \quad (10a)$$

$$V_{sh} \approx 0.46N \quad (10b)$$

In Eq. 10a the parameters μ_m and c_m have the meaning of global strength parameters and A_{eff} is the effective un-cracked section. Eq. 10b is an approximation of Eq. 10a and results from the assumption of $\mu_m = 0.4$ (global friction) and $c_m/f_{cM} = 0.05$ (global cohesion over compressive strength of the masonry wall). A_{eff} is calculated taking into account the wall cracking due to flexure [Priestley et al., 2007].

Differently from the mechanical model, TREMURI can account explicitly for the stiffness variation over the height of the RC walls by assigning different stiffnesses from one storey of the RC walls to another. The first storeys of the RC walls are assigned the effective stiffness EI_e and the storeys above the first one are assigned one half of the gross sectional uncracked stiffness. The 50% of reduction of the gross sectional uncracked stiffness is to account for the small construction-joint cracks that develop between RC walls and slabs [Paparo and Beyer, 2014b] and is considered applicable if the mean longitudinal reinforcement ratio of the RC walls is larger than 0.2%, which is minimum value according to EN 1992-1 [2004]. Additionally, also the RC beams are assigned the effective stiffness EI_e .

The effective stiffness EI_e corresponds to the nominal moment M_N divided by the yield curvature φ_y [Priestley et al., 2007]. M_N is calculated considering the axial force acting at the base of the wall under gravity loads only, and φ_y is the nominal yield curvature, which is equal to $C\varepsilon_y/l_w$. C is a constant that depends on the geometrical properties of the section; for

rectangular RC walls Priestley et al. [2007] recommends $C=2.00$. ε_y is the yield strain of the longitudinal reinforcing bars and l_w is the wall length.

3.2.3 Validation of the shear-flexure cantilever model

In order to gauge the ability of the shear-flexure cantilever model to predict the displacement profile of a mixed RC-URM wall structure, the inter-storey drift profiles calculated by the shear-flexure cantilever model (“mechanical model”) are compared with drift profiles obtained from the TREMURI pushover analyses (“TREMURI”, Figure 4). The mechanical model aims at representing the structure with its properties at the SD limit state (see Sections 3.1 and 3.2.1). Hence, the drift profiles computed with the mechanical model are benchmarked against the TREMURI profiles for which an inter-storey drift demand of 0.4% is first attained (SD limit state for URM walls failing in shear, see Section 2). For the comparison of the two approaches, the drift profiles are normalised to the maximum inter-storey drift attained over the height of the systems, as the mechanical model does not provide information on the magnitude of the inter-storey drifts but just on the shape of the profiles.

Table 3: Mechanical properties adopted for the numerical simulations in TREMURI

Members	Material properties		Macro-model
URM members	μ_{eq}	[-]	0.19
	c_{eq}	[MPa]	0.06 (three storeys)
			0.08 (four storeys)
			0.10 (five storeys)
	f_{cM}	[MPa]	6.30
	E_{mx}	[GPa]	5.10
	G_m	[GPa]	0.53
	Gc_t	[-]	1.00
RC members	β	[-]	0.10
	E_c	[GPa]	E_e (1 st storey walls & beams)
			18.00 (above storey walls)
	G_c	[GPa]	$E_e/2.40$ (1 st storey walls & beams)
			7.50 (above storey walls)
	f_y	[MPa]	550

μ_{eq} and c_{eq} : equivalent friction and cohesion coefficients

f_{cM} : masonry compressive strength

E_{mx} : E- modulus of masonry panels subjected to compression orthogonal to bed-joints

G_m : masonry shear modulus

G_c : parameter for the non-linear plastic deformation in the pre-peak response (shear-damage behaviour of the URM walls)

β : parameter for the non-linear plastic deformation in the post-peak response (shear-damage behaviour of the URM walls)

E_c and G_c : RC member's Young's and shear modulus

f_y : reinforcing bar yield strength adopted in RC members

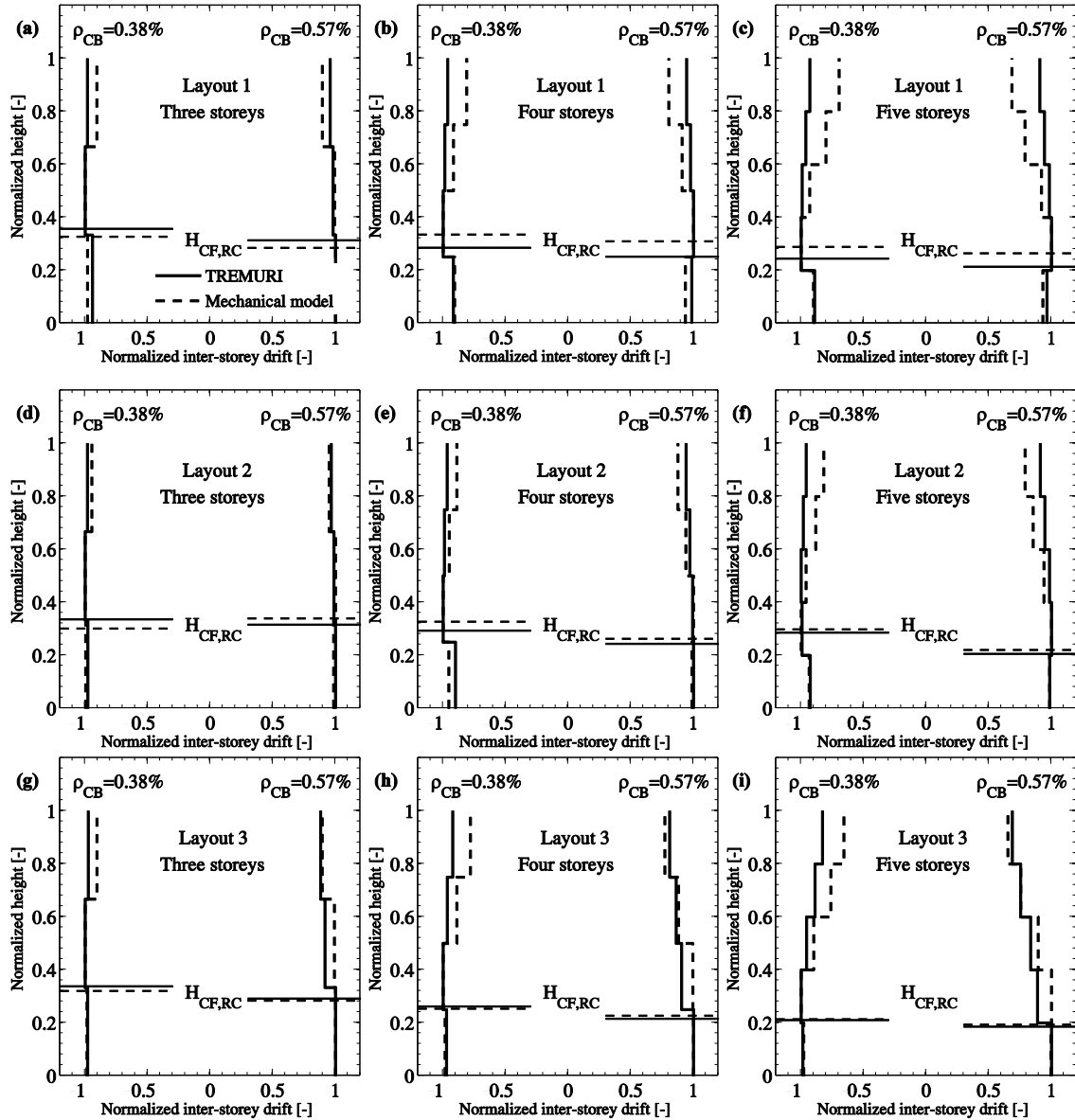


Figure 4: Normalized inter-storey drifts and normalized height of contra-flexure points in the RC walls $H_{CF,RC}$.

Figure 4 shows that the mechanical model estimates the inter-storey drift profile obtained from the TREMURI analyses rather well. For the two lowest storeys, the difference between the two predictions is generally small, while for the upper storeys the discrepancy increases. As outlined in Section 3.2.1, the mechanical model does not account for the rocking behaviour of the URM walls, which is likely to take place in the upper storeys because of the low axial force acting on the URM walls. As a result, the mechanical model overestimates the restraining action provided by the URM walls in the upper levels and therefore underestimates the drifts in the upper storeys.

In addition, the mechanical model leads to a good estimation of the height of contra-flexure point of the RC walls $H_{CF,RC}$ (Figure 4, horizontal lines). Using the mechanical model, $H_{CF,RC}$ can be calculated by setting in Eq. 5b $M_2(x)$ equal to zero and solving for x . For the pushover analyses, $H_{CF,RC}$ is computed as the ratio between the base moment and the base shear carried by the RC wall.

3.3 Application of the shear-flexure cantilever model

This section presents charts (Figure 5) that will be used in the DDBD process to check if the displacement profile of the mixed structure can be assumed as linear. The charts summarise the results of a parametric study, carried out with the shear-flexure cantilever model, in which three parameters are investigated: (i) the number of storeys n ; (ii) the mechanical (E and G) and geometrical (H , I and A) characteristics of the URM and RC walls, which are combined in the stiffness ratio α ; (iii) the strength repartition between the different structural systems, which are expressed by the RC wall strength ratio β_{RC} .

The solid lines in Figure 5 show, for different values of n , α and β_{RC} , the ratio $R_\delta = \delta_1/\delta_2$ that is obtained from the mechanical model, where δ_1 and δ_2 are the inter-storey drifts of the first and second storey. The inter-storey drifts of the upper storeys are not explicitly considered for the following reasons: (i) δ_1 and δ_2 are particularly well predicted by the mechanical model (Figure 4); (ii) the pushover analyses carried out in Section 3.2.3 showed that the displacement profile is approximately linear over the entire height of the building if R_δ is close to one (Figure 4).

It is proposed that the assumption of a linear displacement profile can be considered valid, if the ratio R_δ of first to second storey drifts that is predicted by the mechanical model takes a value between 0.80 and 1.25:

$$R_\delta = \frac{\delta_1}{\delta_2} \in [0.80 - 1.25] \quad (11)$$

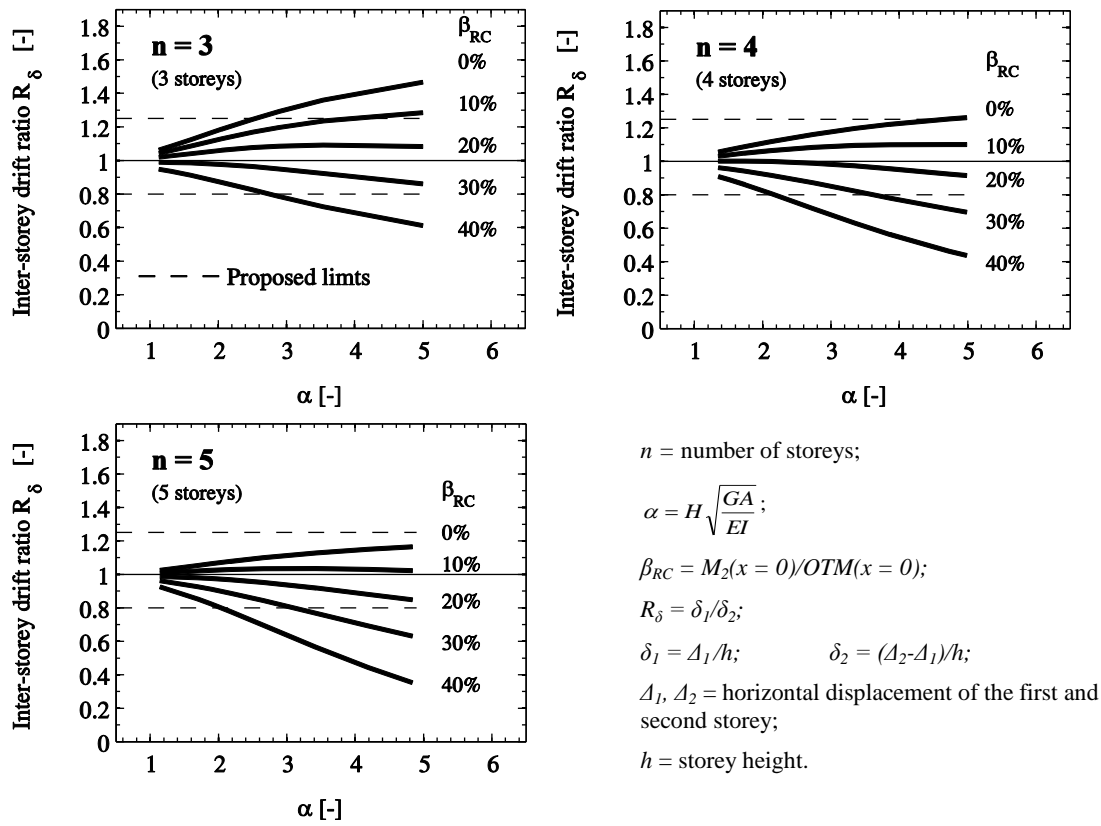


Figure 5: Influence of the parameters n , α and β_{RC} on the inter-storey drift ratio R_δ . Proposed limits for considering a linear displacement profile of the structure.

The charts in Figure 5 are derived by assuming a horizontal load q , which is constant over the height of the shear-flexure cantilever (Section 3.1). Provided that the masses are constant over the height of the building, the mechanical model therefore assumes that the structure is subjected to an acceleration profile that is also constant over the height. In order to check the

actual acceleration profile, dynamic analyses are carried out with TREMURI. The results, plotted in Figure 6, show that:

(i) The most appropriate acceleration profile would be bi-linear (i.e., constant over the two bottom storeys and linearly increasing over the storeys above—see grey lines in Figure 6).

(ii) The constant and inverted triangular acceleration profiles, represented in Figure 6 with solid and dashed black lines, are bounds of the actual acceleration profile.

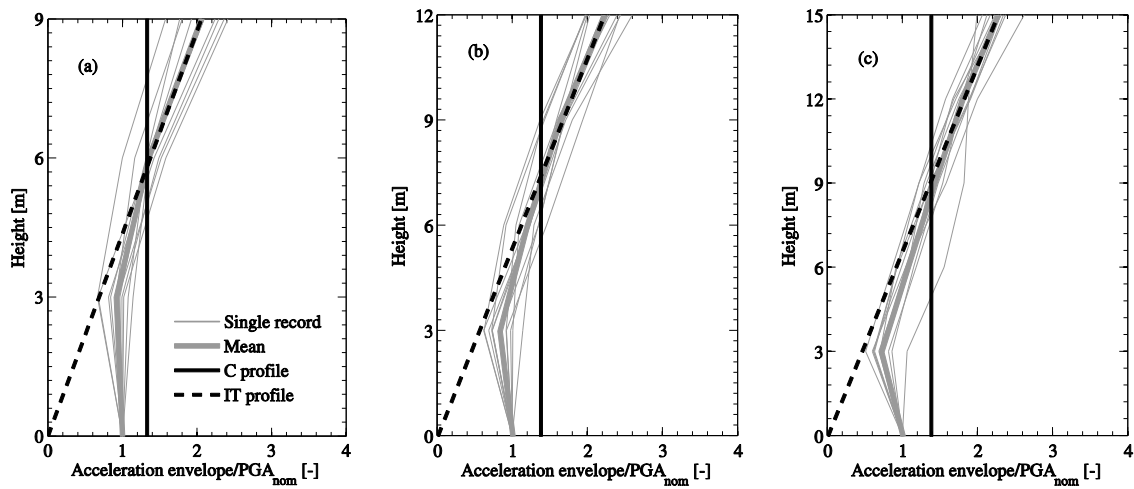


Figure 6: Acceleration profiles for three mixed buildings (L1S3, L2S4 and L1S5, see Section 7 for the description of the three structures) and comparison with the constant (C) and inverted triangular (IT) acceleration profiles.

As a consequence, there is a theoretical inconsistency between the adoption of the uniformly distributed load and the actual lateral forces obtained from dynamic analyses. In order to check if the inconsistency might strongly affect the results, pushover analyses of mixed buildings are carried out with TREMURI. The analyses are performed with an inverted triangular and a constant load distribution and the resulting displacement profiles are compared at an average drift of 0.4%. The results show that the displacement profile of mixed RC-URM buildings is not strongly affected by the assumed horizontal load pattern (Figure 7). As a consequence, from an engineering point of view, the adoption of a constant load pattern for the evaluation of the displacement profiles at SD limit state is acceptable.

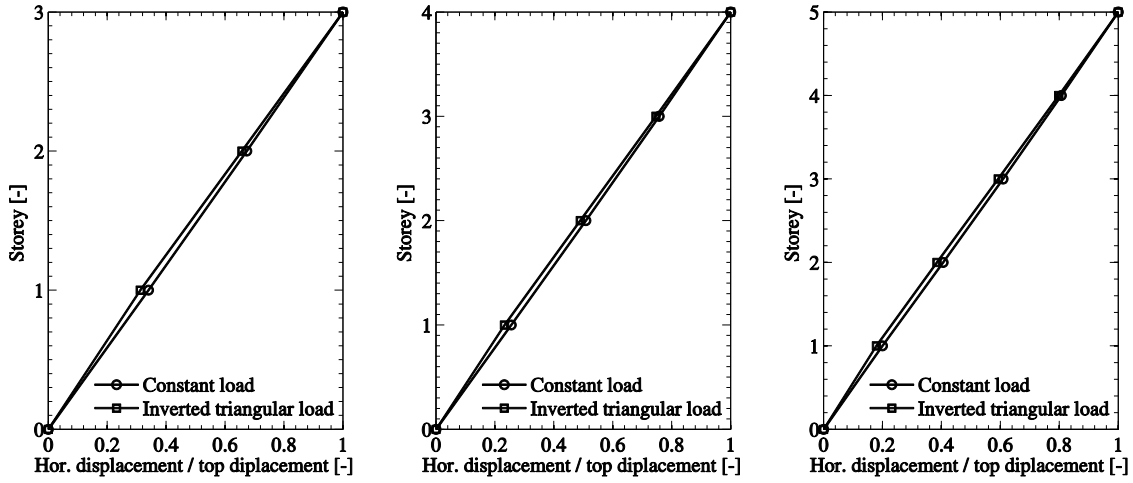


Figure 7: Normalised displacement profiles for three case studies (3, 4 and 5 storeys): comparison between the displacement profiles obtained with the constant and inverted triangular load patterns.

Using a simple constant load pattern rather than a more complicated bilinear pattern is supported further by the following two findings reported in the literature:

(i) Shake table tests on a four-storey building composed of RC and URM walls [Beyer et al., 2014] have shown that, when the structure is close to failure, the acceleration profile is rather constant over the height (Figure 8).

(ii) Mandirola [2014] simulated the test by Beyer et al. [2014] in TREMURI and compared the TREMURI acceleration profiles to those measured in the test. They observed that TREMURI tends to overestimate the acceleration amplification in the upper floors when the structure is close to failure.

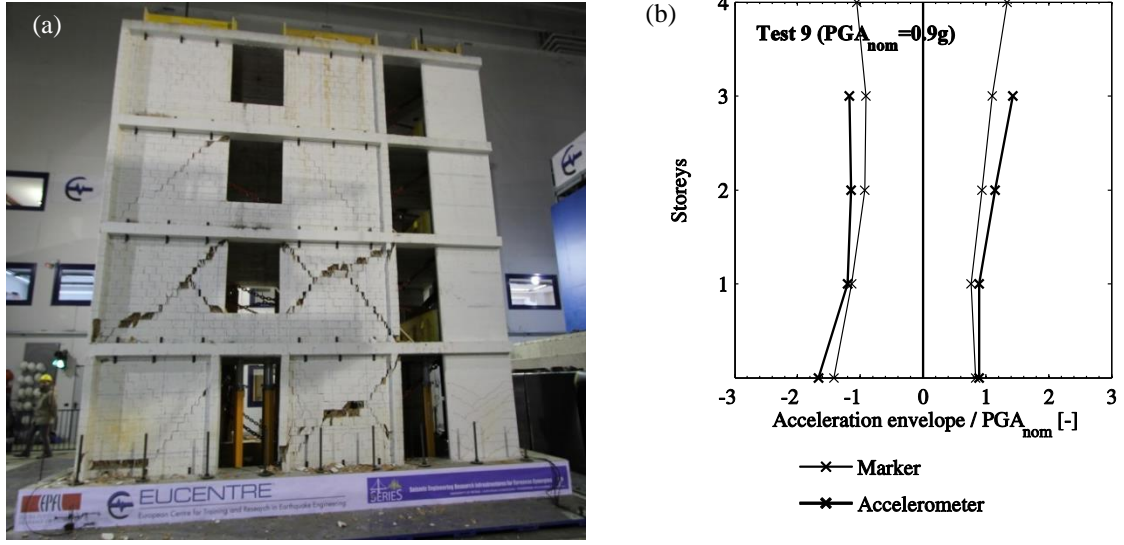


Figure 8: Four-storey mixed RC-URM wall building (a). Normalised acceleration envelope for the last test (b), from Beyer et al. [2014].

4 General direct displacement-based design procedure

Direct displacement-based design is a procedure developed over the last 20 years [e.g., Priestley, 1993; Priestley, 1998; Priestley et al., 2007; Cardone et al., 2009; Pennucci et al., 2009; Pennucci et al., 2011; Sullivan et al., 2012] with the objective of mitigating weaknesses in the current force-based design approach. DDBD fundamentals are illustrated in Figure 9: a multi-degree-of-freedom (MDOF) structure is converted into a single-degree-of-freedom (SDOF) system, Figure 9a. Given m_i and Δ_i the floor masses and design displacements and H_i the storey height, the design displacement Δ_d , effective mass m_e and effective height h_e are calculated as:

$$\Delta_d = \frac{\sum m_i \Delta_i^2}{\sum m_i \Delta_i} \quad (12)$$

$$m_e = \frac{\sum m_i \Delta_i}{\Delta_d} \quad (13)$$

$$h_e = \frac{\sum m_i \Delta_i H_i}{\sum m_i \Delta_i} \quad (14)$$

In addition to Δ_d , the bilinear envelope of the SDOF system is characterised by defining the yield displacement Δ_y from which the displacement ductility demand μ_d is found, Figure 9b. μ_d is then used to determine the equivalent viscous damping ratio ξ_e , representing the combined elastic damping and the hysteretic energy absorbed by the structure during inelastic deformations, Figure 9c. Once the equivalent viscous damping ratio ξ_e is known, from the damping reduction factor η_ξ

$$\eta_\xi = \left(\frac{0.07}{0.02 + \xi_e} \right)^{0.5} \quad (15)$$

the over-damped displacement spectrum is calculated and used to find the effective period of the structure, T_e , which corresponds to the period associated with the design displacement Δ_d (Figure 9d). From T_e the effective stiffness of the structure and the design base shear force V_{base} are derived:

$$K_e = \frac{4\pi^2 m_e}{T_e^2} \quad (16)$$

$$V_{base} = K_e \Delta_d \quad (17)$$

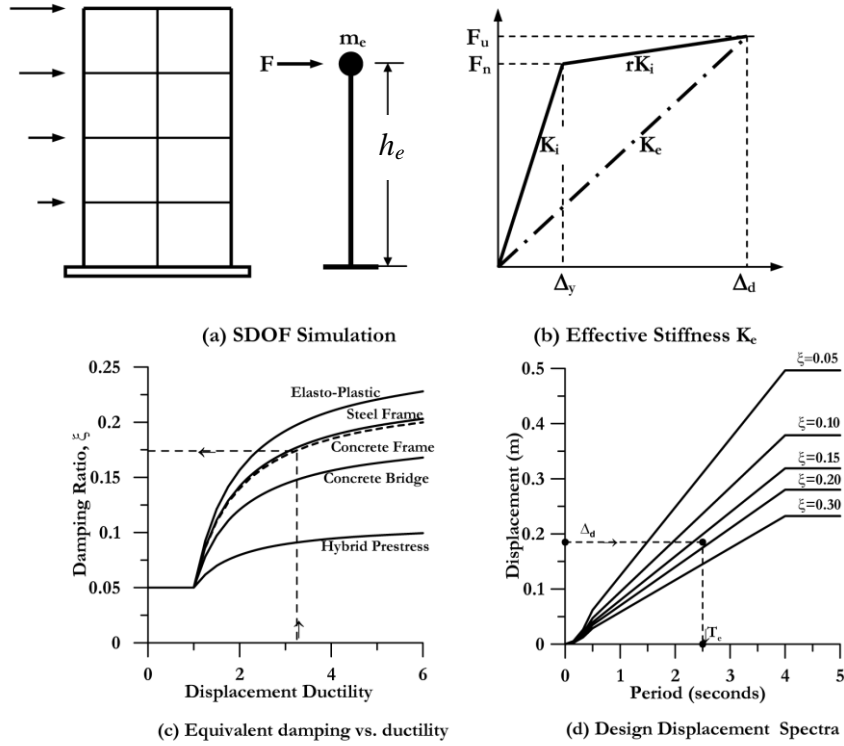


Figure 9: Fundamentals of direct displacement-based design [Priestley 1998].

5 Evaluation of the equivalent viscous damping

As presented in Section 4, DDBD requires the definition of an equivalent viscous damping ξ_e . Priestley et al. [2007] propose equations for calculating the equivalent viscous damping for different structural types and materials. For instance, for reinforced concrete walls the following equation is proposed:

$$\xi_e = 0.05 + 0.444 \left(\frac{\mu_\Delta - 1}{\mu_\Delta \pi} \right) \quad (18)$$

For URM walls, however, equations for the equivalent viscous damping ξ_e are still preliminary [Sullivan et al., 2012]. In particular, values of ξ_e for the investigated URM walls (i.e., modern hollow clay brick masonry walls typically used in central Europe) were not found in literature. Therefore the objective of this section is to determine ξ_e for the analysed typology of URM walls with dominant shear behaviour (ξ_e for URM walls with dominant flexural

behaviour is not evaluated as the analysed URM walls are expected to exhibit a dominant shear behaviour). In the following, Section 5.1 outlines remarks related to the use of the equivalent viscous damping in DDBD and Section 5.2 describes how the equivalent viscous damping values for the studied URM walls (ξ_{URM}) have been calculated.

5.1 Remarks with regard to the use of the equivalent viscous damping approach in DDBD

As previously discussed, in DDBD [Priestley et al., 2007] the over-damped displacement spectrum is derived by multiplying the spectrum for 5% damping with the damping reduction factor η_ξ (Eq. 15), which is a function of the equivalent viscous damping ξ_e . Recently Pennucci et al. [2011] argued that the expressions of the equivalent viscous damping ξ_e are sensitive to the spectral shape of the earthquake and proposed an alternative method based on the displacement reduction factor η_{in} , defined as the ratio of the maximum inelastic displacement to the elastic displacement at the effective period. This method does not require the definition of an equivalent viscous damping and is not significantly affected by ground motions characteristics.

In addition, Pennucci et al. [2011] observed that the ξ_e is sensitive to the relative position of the spectral displacements at initial (T_i) and effective (T_e) periods with respect to T_C and T_D . This effect, which might be particularly large for short period structures like mixed RC-URM buildings, might also explain the period dependency of the ξ_e for short period structures [Priestley et al., 2007]. To overcome this problem, Pennucci et al. [2011] suggest relating the inelastic demand to the demand slope factor ρ , which is a function of the relative position of initial and effective periods.

However, the demand slope factor approach is not yet implemented in the DDBD procedure and Pennucci et al. [2011] note the need for further research before it can be readily incorporated. As a consequence, this research builds on the equivalent viscous damping approach for evaluating the effective period of the structure. In order to account for the period dependency of ξ_e , a correction factor [Priestley et al., 2007] is applied. Note that Graziotti [2013] propose displacement reduction factors η_{in} for solid clay brick masonry walls accounting for the likely failure mechanism. However, as the period dependency is not taken into account, these results are not used herein.

5.2 Evaluation of the equivalent viscous damping

To evaluate the inelastic response of the URM walls studied herein, time history analyses on inelastic SDOF systems have been carried out. The ground motion set used in this study is composed of 12 non-stationary accelerograms [see also Michel et al., 2014] compatible with soil class C ($T_C = 0.6$ s). The displacement spectra of these records have corner periods T_D of about 2 s and all records are scaled to peak ground accelerations (PGA) of 2.5 m/s^2 , (Figure 10).

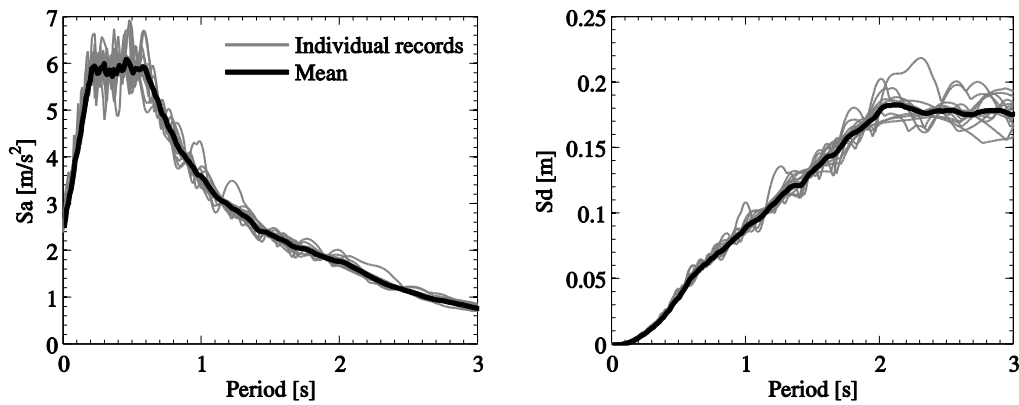


Figure 10: Acceleration and displacement response spectra ($\zeta = 5\%$).

The equivalent viscous damping ζ_{URM} for URM walls failing in shear is determined in two steps: first, the damping ζ_{URM} is evaluated for structures with an initial period T_i longer than 0.6 s and effective period T_e shorter than 2 s. For these systems the damping ζ_{URM} is assumed to be independent of T_e . Most URM and mixed URM-RC buildings will be, however, rather stiff and have initial periods shorter than 0.6 s. In this period range the displacement spectrum does not vary linearly with T but depends on T^3 or T^2 . The influence of the spectral shape on the damping ζ_{URM} is accounted for in a second step, where URM walls with $T_i > 0.1$ s and $T_e < 2$ s are investigated.

As a first step, in order to avoid the influence of the spectral shape on the evaluation of ζ_{URM} and since the mean displacement spectrum is almost linear for $T_C = 0.6 \text{ s} < T < 2 \text{ s} = T_D$ (Figure 10), SDOF systems with the following properties are investigated:

- The minimum considered initial period (T_i) is equal to 0.6 s;
- The maximum considered effective period (T_e) is equal to 2 s;

- The inelastic SDOF systems are modelled with the macro-element developed by Penna et al. [2013] and the dynamic analyses are carried out with TREMURI [Lagomarsino et al., 2013].
- Priestley et al. [2007] recommend performing the inelastic time-history analyses with 5% tangent stiffness proportional damping. As tangent stiffness proportional damping is not available in TREMURI, all analyses are carried out with initial stiffness proportional viscous damping. For this case Priestley et al. [2007] propose to adopt an artificially low damping coefficient ξ^* :

$$\xi^* = 5\% \frac{1 - 0.1(\mu - 1)(1 - r)}{\sqrt{\frac{\mu}{1 + r\mu - r}}} \quad (19)$$

where μ is the ductility of the system and r is the post yield stiffness ratio, herein assumed equal to zero. Since the analysed SDOF systems exhibited ductilities between 2 and 6 (Figure 11a), the artificially low damping coefficient ξ^* obtained from the mean of these two ductilities corresponds to around 2%, value which was used for all analyses.

The following procedure is adopted to find the equivalent viscous damping ξ_{URM} that should be used for the DDBD of URM wall structures failing in shear:

- i)* An inelastic SDOF system representing a URM wall failing in shear is subjected to a selected ground motion.
- ii)* The maximum displacement, the base shear at maximum displacement and the maximum ductility of the SDOF system are recorded. The effective period T_e is therefore calculated as $T_e = 2\pi\sqrt{m_e / K_e}$. The effective stiffness K_e is computed from the maximum displacement and the base shear at maximum displacement recorded in step (i); the effective mass is the mass of the SDOF system.
- iii)* The equivalent viscous damping ξ_{URM} is calculated as the damping value that yields, for an elastic SDOF system with period T_e , the same maximum displacement as the inelastic SDOF system.

Figure 11a shows that the equivalent viscous damping ξ_{URM} increases with displacement ductility μ . In addition, for values of μ larger than 3, ξ_{URM} is rather constant and its median value

is 31%. Since in the buildings analysed in this article the URM walls displayed always a displacement ductility higher than 3 and exhibited a dominant shear behaviour, ξ_{URM} is assumed equal to 31%. For systems that remain elastic the damping is 5% and between $\mu = 1$ and $\mu = 3$ a linear increase in damping from 5% to 31% can be assumed (Figure 11a).

Since mixed RC-URM buildings are generally rather stiff structures, it is likely that their initial period is lower than 0.6 s. In order to check the period dependency of ξ_{URM} , a second set of analyses has been carried out. The new set comprised SDOF systems with initial periods (T_i) longer than 0.1 s, effective periods (T_e) shorter than 2 s and displacement ductilities between 3 and 6 (the minimum ductility is set equal to 3 to avoid the ductility dependency of ξ_{URM}).

The results of the analyses are plotted in Figure 11b, where the hysteretic component of ξ_{URM} is normalised to its mean value obtained for T_e between 1 s and 2 s (for $1 \text{ s} < T_e < 2 \text{ s}$ ξ_{URM} is assumed to be independent of T_e) and plotted versus the effective period T_e . The results show that ξ_{URM} is rather constant for T_e between 1 s and 2 s and increases for T_e smaller than 1 s (Figure 11b, dashed line). In fact, for systems with $T_e < 1 \text{ s}$ and $\mu > 3$, the initial periods are smaller than 0.6 s. For $T < 0.6 \text{ s}$, the displacement spectrum increases parabolically rather than linearly, which is reflected in higher values of ξ_{URM} .

To account for the period pendance of ξ_{URM} , a period dependent correction factor CF is applied on the hysteretic component of the equivalent viscous damping (ξ_{hys}). The hysteretic model of the TREMURI macro-element failing in shear is the Takeda Thin (TT) rule and therefore the period dependency of the TT model proposed by Priestley et al. [2007] is adopted:

$$\xi_{hys} = a \left(1 - \frac{1}{\mu^b} \right) \left(1 + \frac{1}{(T_e + c)^d} \right) \quad (20)$$

where a , b , c and d are equal to 0.215, 0.642, 0.824 and 6.444 [Priestley et al., 2007]. The correction factor CF is calculated as the ratio between ξ_{hys} and ξ_{hys} estimated at $T_e = 4 \text{ s}$ ($\xi_{hys,4s}$):

$$CF = \frac{\xi_{hys}}{\xi_{hys,4s}} \quad (21)$$

CF is represented in Figure 11b by the solid black line. Note that accounting for the effect of the spectral shape through a period dependent correction factor is rather crude and seems to

underestimate the period dependency of ξ_{URM} for effective periods smaller than 0.8 s. Once more advanced approaches are available, they can be used instead.

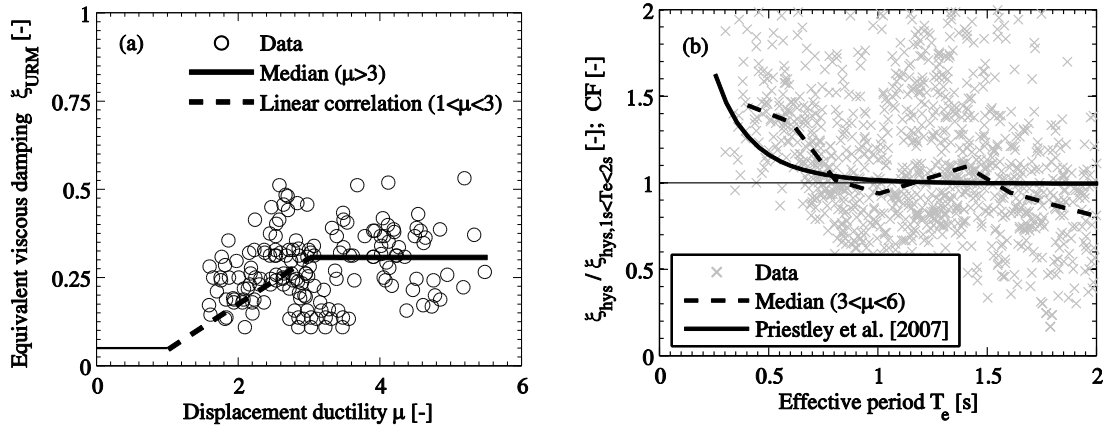


Figure 11: (a): Displacement ductility versus ξ_{URM} for the inelastic SDOF systems with $T_i > 0.6$ s and $T_{eff} < 2$ s. Data, linear relation for $1 < \mu < 3$ and median value for $\mu > 3$. (b): Correction factor CF to account for the period dependency of the hysteretic component of ξ_e from Priestley et al. [2007] and data obtained from the second set of time history analyses.

6 Proposed methodology for mixed RC-URM wall structures

The various steps of the displacement-based design methodology developed for structures with both RC and URM walls are presented in this section. To calculate the yield displacement of the RC walls, the technique follows the DDBD approach for designing regular RC frame-wall buildings [Sullivan et al., 2005; Sullivan et al., 2006], as the structural behaviour of both mixed systems is similar (Section 2). For mixed RC-URM wall structures the conversion of the MDOF system to the SDOF (Eqs. 12 to 17) assumes a linear displacement profile over the height of the structure. This hypothesis will be checked at the end of the design. In the following, the DDBD process is broken down into a step-by-step procedure and summarised in the flowchart of Figure 14.

Step 1 – Preliminary design check of the plain URM wall building according to the DDBD approach

The procedure starts with the DDBD check of a plain URM wall edifice both for the design of new buildings and the retrofit of existing URM buildings. The objective is to verify

that the masonry walls display a dominant shear behaviour and that the structure does not satisfy the seismic design check [Priestley et al., 2007]. If it is the case, replacing one or more URM walls by RC ones is a promising strategy to develop a design or retrofit solution that can sustain the seismic demand.

Step 2 – Replacement of RC walls and estimation of the overturning demand (OTM_{dem}) and the effective period (T_e)

The designer chooses the URM walls to be replaced by RC ones. Even if the choice is arbitrary, it is suggested to (i) conceive the RC walls as external walls to avoid a significant variation of axial force in the URM walls due to the shear forces transmitted by the slabs and to (ii) select symmetric layouts to obtain the same response whether the structure is pushed towards one direction or another.

From the SDOF simulation (Eqs. 12 to 17) the effective period T_e and the base shear V_b are calculated. Consequently, the overturning moment demand (OTM_{dem}) can be estimated as, Figures 12(a) and 12(b):

$$OTM_{dem} = V_{base} h_e \quad (22)$$

The equivalent viscous damping of the mixed system is not known at this stage but is assumed as 20% (the design examples have shown that the equivalent viscous damping of these systems varies between 15 and 25%). In Step 9 it will be recalculated considering the effective energy dissipated by the RC and URM walls.

Step 3 – Estimation of the moment capacity of the mixed structure (OTM_{cap})

The overturning moment capacity of the structure (OTM_{cap}) is the sum of the contributions from the RC and URM walls (M_{RC} , M_{URM}) and the RC slabs (M_S):

$$OTM_{cap} = M_{RC} + M_{URM} + M_S \quad (23)$$

The three contributions are represented in Figures 12(c) and 12(d). In steps 4 and 5, M_{URM} and M_S will be computed while M_{RC} is yet unknown and is calculated as the required strength of the RC walls ($M_{RC,req}$).

Step 4 – Contribution to the overturning capacity of the URM walls (M_{URM})

As the URM walls are expected to fail in shear, their moment capacity is estimated as a function of their shear strength (V_{sh}). For a single wall m , $M_{URM,m}$ results as:

$$M_{URM,m} = V_{sh,m} H_{CF,URM,m} \quad (24)$$

$V_{sh,m}$ is the shear strength of the URM wall m and can be estimated, for instance, according to Mann and Müller [1982], if material tests are available. If not, Eq. 10b can be used for estimating the shear strength of the wall. $H_{CF,URM,m}$ is the height of the contra-flexure point of the URM wall. Its lower bound value corresponds to half of the storey height (h_{st}). Two empirical parameters are added for the calculation of $H_{CF,URM}$. The first one, γ , accounts for the fact that $H_{CF,URM}$ increases with the number of storeys (n):

$$\gamma = 1 + n / 10 \quad (25)$$

The second parameter, ψ , takes into account the aspect ratio of the single URM wall. If $h_{st} > l_{URM}$ (l_{URM} is the length of the URM wall), $H_{CF,URM}$ increases proportionally to ψ , otherwise it is equal to 1:

$$\text{If } h_{st} > l_{URM} \quad \psi = h_{st} / l_{URM} \quad (26a)$$

$$\text{If } h_{st} \leq l_{URM} \quad \psi = 1 \quad (26b)$$

The total contribution of the URM walls to the overturning capacity (M_{URM}) is the sum of the base moments of the individual URM walls ($M_{URM,m}$):

$$M_{URM} = \sum_m M_{URM,m} \quad (27a)$$

$$M_{URM,m} = V_{sh} H_{CF,URM} = V_{sh} \left(\frac{h_{st}}{2} \gamma \psi \right) \quad (27b)$$

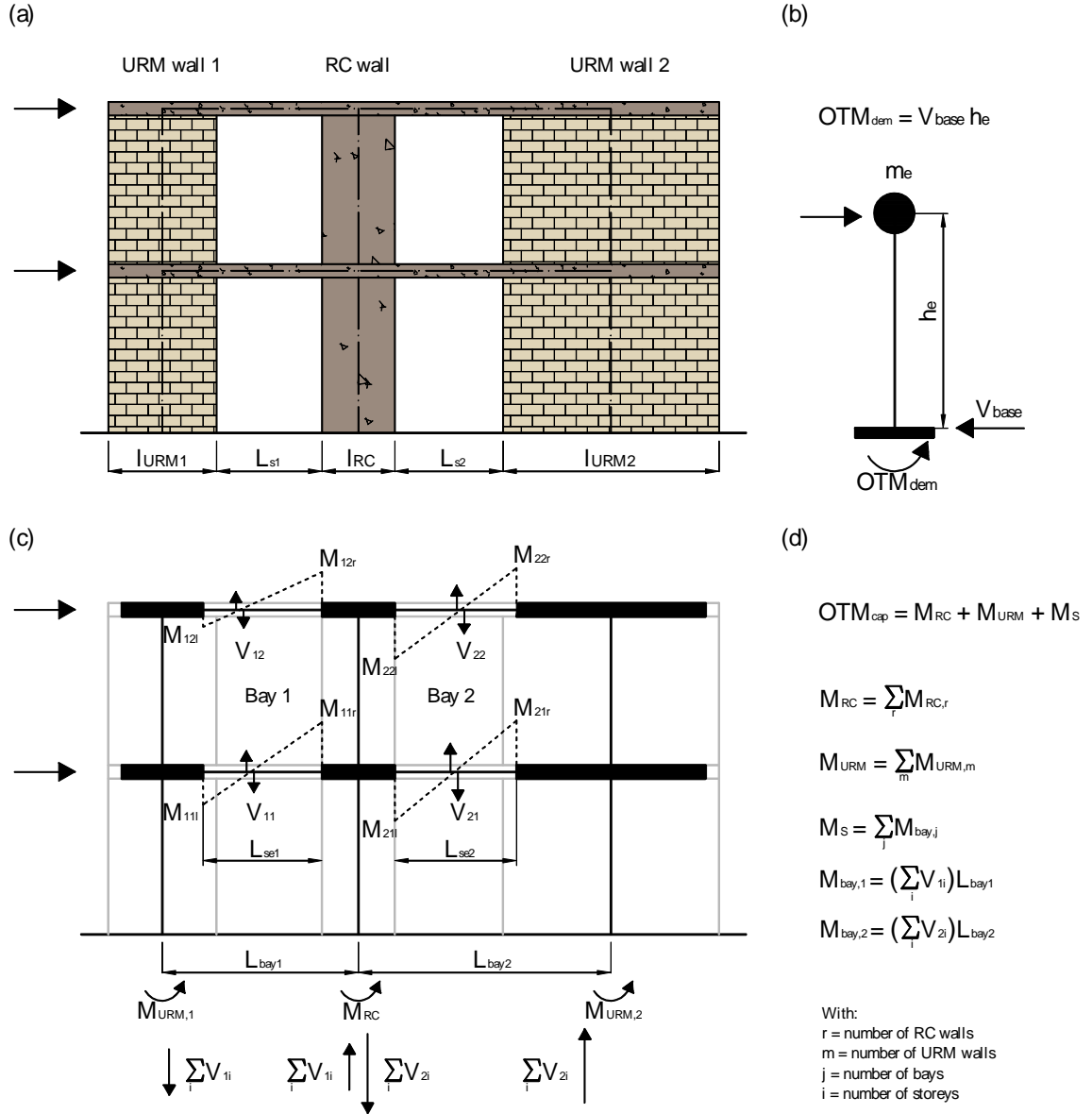


Figure 12: Seismic response of a RC-URM structure. SDOF simulation and estimation of the OTM_{dem} (a)-(b); seismic contribution of the different structural systems and evaluation of the OTM_{cap} (c)-(d).

Step 5 – Contribution of the RC slabs to the overturning capacity (M_S)

The contribution of the RC slabs to the overturning capacity (M_S) is estimated by following the procedure developed for irregular RC frames [Priestley et al. 2007], in which the contribution of each bay is accounted for separately. In the following, the technique for calculating M_S is broken down into five sub-steps:

Step 5a: The overturning moment resisted by the slabs is calculated by separating the contributions of the different bays ($M_{bay,j}$). Given j the number of bays, M_S results as follows:

$$M_S = \sum_j M_{bay,j} \quad (28)$$

Step 5b: Each $M_{bay,j}$ is calculated as the sum of the shear forces transmitted by the RC slabs (ΣV_{ji}) of the considered bay j , multiplied by its length ($L_{bay,j}$), Figures 12(c) and 12(d). Given i the number of storeys $M_{bay,j}$ results as:

$$M_{bay,j} = \left(\sum_i V_{ji} \right) L_{bay,j} \quad (29)$$

Step 5c: Unlike capacity designed RC frames, in URM and mixed RC-URM buildings the connections between URM walls and RC slabs form in general a weak column-strong beam mechanism. This implies that the RC slabs remain largely elastic and the shear forces transmitted by the slabs cannot be estimated from their moment capacity.

Back-analysis of tests has shown that in URM and mixed RC-URM buildings, in order to correctly estimate the shear forces transmitted by the slabs (ΣV_{ji}), the uplift of the RC slabs from the URM walls needs to be captured by the model. To calculate ΣV_{ji} , the RC slabs of each storey are then represented by “elastic continuous beams” which are mono dimensional elements characterised by their length only. The elastic continuous beams are sustained by vertical supports representing the URM walls. The supports work only in compression to take into account the possible uplift of the slabs from the masonry walls, Figure 13b. The connections between the elastic continuous beams and the RC walls are represented by pins through which the moment transmitted to the RC walls ($M_{s,w}$) is applied. The pins can, instead, also transmit tension forces.

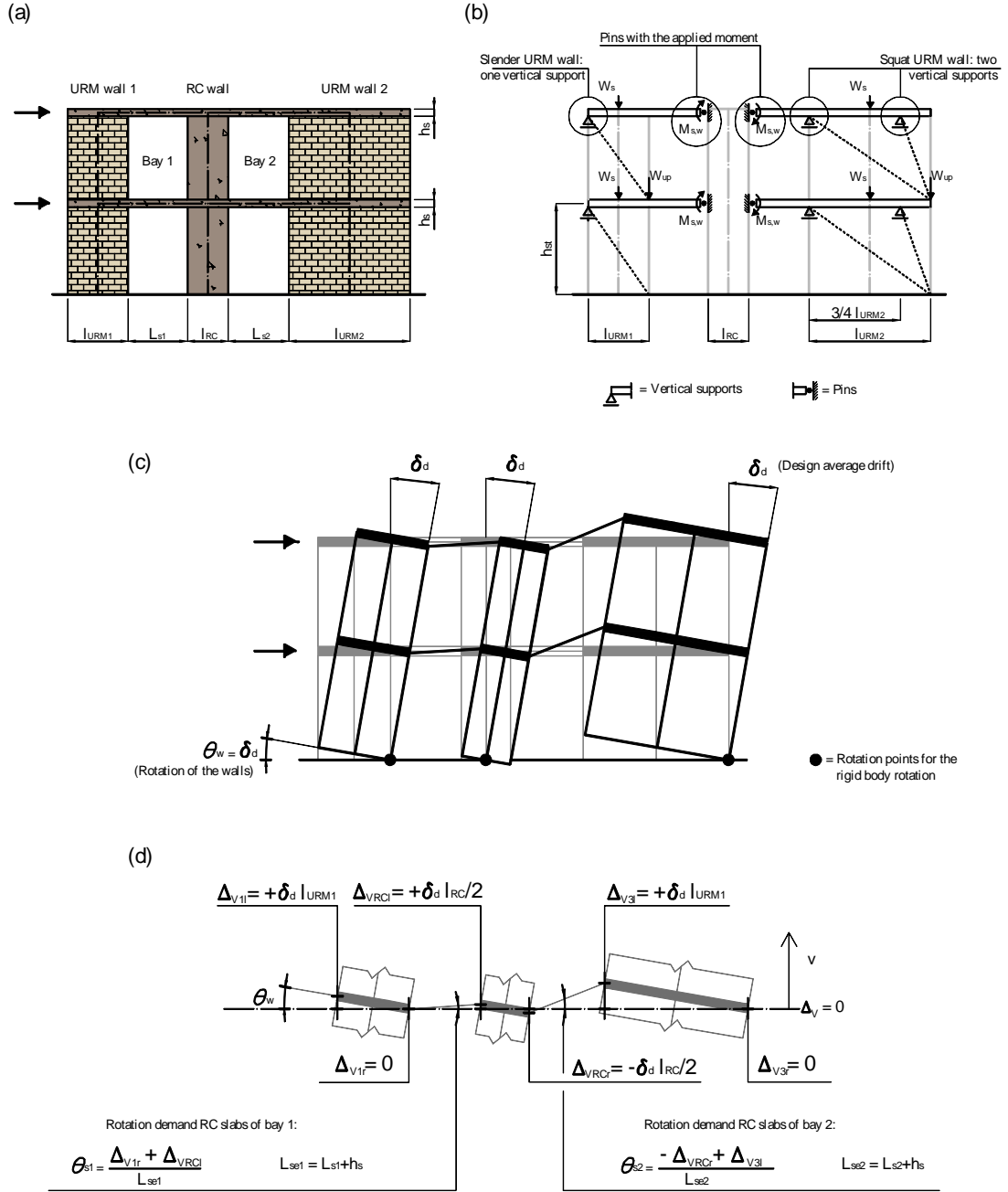


Figure 13: Mixed RC-URM wall structure (a). Construction of the elastic continuous beams (b). Wall and RC beam mechanisms for calculating the rotation demand θ_{b1} and θ_{b2} (c, d).

Step 5d: As input, the geometry of the walls is required. Since at the beginning of the design the dimensions of the RC walls are unknown, a trial length, which will be adjusted

during the design procedure, has to be assumed. For the construction of the elastic continuous beam models, four additional aspects have to be examined:

(i) *Position and number of the supports (for each masonry wall)*: The supports represent the position of the resulting forces where the slabs transmit the forces to the URM walls below. For squat URM walls, i.e., when $l_{URM}/h_{st} > 1$, two supports, as shown in Figures 13(a) and 13(b), are introduced. For slender walls ($l_{URM}/h_{st} < 1$), just one support is required, Figures 13(a) and 13(b).

(ii) *Position of the tributary weight of the slabs (W_s)*: The tributary weight of the slabs W_s is modelled as a concentrated force applied at the centreline of each URM wall, Figure 13b.

(iii) *Magnitude and position of the forces representing the weight transmitted by the walls above the considered storey (W_{up})*: For each wall, the weights transmitted by the walls above the considered storey (W_{up}) are (i) calculated as the sum of the tributary reaction forces of the above slab (Figure 13b, dotted lines) and (ii) applied as shown in Figure 13b.

(iv) *Bending moment applied to the pins connecting the slabs to the RC walls ($M_{s,w}$)*: Firstly, the yield rotation (θ_{ys}) and the rotation demand (θ_s) of the slabs are calculated. The former can be computed according to Priestley et al. [2007]:

$$\theta_{ys} = 0.35\epsilon_y \frac{L_{se}}{h_s} \quad (30)$$

The deformable part of the RC slabs (L_{se}) is the free span of the slab (L_s) increased by its section depth (h_s) on either side where it frames into URM walls [Priestley et al., 2007; Paparo and Beyer, 2014b]. From geometrical considerations, the rotation demand θ_s on the slab is related to the design drift δ_d . To simplify matters, the rotation demand is estimated assuming that URM and RC walls undergo only rigid body deformations. For the URM walls a rigid body rotation around the base corner in compression is assumed; for the RC walls a rigid body rotation around its centreline, Figures 13(c) and 13(d). As rigid body rotations are assumed, the rotation of the walls (θ_w) is equal to the design average drift (δ_d). More advanced kinematic models are of course feasible but might not be necessary at this stage of the design. The flexural moment capacity of the slab ($M_{ys,w}$) can be calculated by considering an effective slab width equal to three times the wall thickness [Priestley et al., 2007], allowing to compute the bending moment $M_{s,w}$ as:

$$\text{If } \theta_s > \theta_{ys} \quad M_{s,w} = M_{ys,w} \quad (31a)$$

$$\text{If } \theta_s < \theta_{ys} \quad M_{s,w} = \frac{\theta_s}{\theta_{ys}} M_{ys,w} \quad (31b)$$

Step 5e: The procedure to determine the shear transmitted by the RC slabs starts from the top storey and progresses downwards floor by floor. At the top floor the force W_{up} is equal to zero, W_s and $M_{s,w}$ are known and the reaction forces of the supports can be calculated. By summing up the tributary reaction forces from the slabs above (Figure 13b, dotted lines), the forces W_{up} applied to the walls of the storey below are determined. The procedure continues down to the first floor.

Step 6 – Choice of the ductility of the RC walls (μ_{ARC})

The designer chooses the level of ductility which the RC walls will undergo. The quasi-static and dynamic tests on mixed RC-URM wall structures [Paparo and Beyer, 2014a; Beyer et al., 2014; Tondelli et al., 2014] have shown that the RC walls experience very small inelastic deformations when the URM walls failed. Hence, regarding the design at the SD limit state, it is pertinent to choose that the RC walls will exhibit a displacement ductility μ_{ARC} within the range of 1 and 2.

Step 7 – Calculation of the height of the contra-flexure point of the RC walls ($H_{CF,RC}$)

From Eq. 5b the height of the contra-flexure point of the RC walls $H_{CF,RC}$ is estimated by setting $M_2(x)$ equal to zero and solving for x . The parameter β_{RC} is calculated as the ratio M_{RC} over OTM_{dem} .

Step 8 – Calculation of the length of the RC walls (l_{RC})

From Step 6 the target yield displacement of the RC walls at the effective height is known ($\Delta_{yRC} = \Delta_d / \mu_{ARC}$). With Eqs. 32a and 32b the yield curvature of the RC walls (ϕ_{yRC}) can be estimated [Sullivan et al., 2005]:

$$\text{For } h_e < H_{CF,RC} \quad \phi_{yRC} = \Delta_{yRC} \left(\frac{h_e^2}{2} - \frac{h_e^3}{6H_{CF,RC}} \right)^{-1} \quad (32a)$$

$$\text{For } h_e > H_{CF,RC} \quad \phi_{yRC} = \Delta_{yRC} \left(\frac{H_{CF,RC} h_e}{2} - \frac{H_{CF,RC}^2}{6} \right)^{-1} \quad (32b)$$

The equations are based on a linear moment profile up to $H_{CF,RC}$ and zero moment between $H_{CF,RC}$ and the top of the wall. From the yield curvature, the required wall length l_{RC} can be found:

$$l_{RC} = \frac{2\varepsilon_y}{\phi_{yRC}} \quad (33)$$

Step 9 – Calculation of the equivalent viscous damping ξ_{sys} and the damping reduction factor η_ξ

The equivalent viscous damping of the system ξ_{sys} is obtained from a weighted average proportional to the base shear carried by URM and RC walls:

$$\xi_{sys} = \frac{V_{URM} \xi_{URM} + V_{RC} \xi_{RC}}{V_{base}} \quad (34)$$

ξ_{RC} is the damping associated with the RC walls and can be calculated according to Eq. 35, as the displacement ductility of the RC walls is known:

$$\xi_{RC} = 0.05 + 0.444 \left(\frac{\mu_{\Delta RC} - 1}{\mu_{\Delta RC} \pi} \right) \quad (35)$$

As pointed out in Section 5, the damping associated with the URM walls, ξ_{URM} , can be assumed equal to 31%. This value can be used only if the URM walls fail in shear and if they feature displacement ductilities larger than 3. These requirements are generally fulfilled for the design of such structures for the SD limit state. The hysteretic components of the equivalent viscous damping ξ_{sys} is then corrected according to the correction factor CF (Eq. 21, Section 5.2) in order to account for their period dependency. The damping reduction factor η_ξ , used to compute the spectrum for the desired ξ_{sys} , is then calculated according to Eq. 15.

Step 10 – Re-evaluation of the overturning moment demand (OTM_{dem}) and calculation of the required strength of the RC walls (M_{RCreq})

The new effective period T_e is found by entering the reduced displacement spectrum with the design displacement Δ_d . The effective stiffness K_e and the base shear V_{base} are consequently determined according to Eqs. 16 to 17. The overturning moment demand OTM_{dem} , approximated in step 2 by assuming an equivalent viscous damping of 20%, is now re-calculated by multiplying the base shear V_{base} to the effective height h_e (Eq. 22). The required moment capacity of the RC walls (M_{RCreq}) is then obtained as:

$$M_{RCreq} = OTM_{dem} - M_S - M_{URM} \quad (36)$$

Step 11 – Iterations to find a stable solution

Steps 3 to 10 are iterated until a stable solution is found. The change in required strength of the RC walls (M_{RCreq}) is used as convergence criterion. It is suggested that, if the strength varies less than 5% from one step to the other, the solution can be considered as stable.

Step 12 – Ascertain the displacement profile of the structure

The DDBD procedure assumes a linear displacement profile over the height of the structure. To check this hypothesis, Eq. 11 is used. It is postulated that the profile can be considered as linear if R_δ is between 0.80 and 1.25 (Section 3.3). If this requirement is not fulfilled, the designer has two options: (i) to choose a different number of URM walls to be replaced by RC ones and re-check the procedure from Step 2 or (ii) to change the level of displacement ductility (μ_{ARC}) of the RC walls (Step 6).

Step 13 – Design of RC members

Due to the low displacement ductility that the RC members will be subjected to, spalling of the cover concrete is often unlikely and detailing requirements for the confinement reinforcement can be relaxed. The design procedure does not check the displacement capacity of the RC members as, in the herein examined typology of mixed buildings, the RC members are always designed to develop a flexure mechanism with displacement capacities exceeding those of URM walls. In fact, the RC walls need to reach only displacement ductilities of $\mu_{ARC} = 1 - 2$, values which can be easily reached by RC walls [e.g., Hannewald, 2013]. Additionally,

experimental evidence [Paparo and Beyer, 2014a; Beyer et al., 2014] has clearly shown that the URM walls are the critical elements in this typology of mixed structures.

In the vicinity of the URM walls, the RC slabs do in general not yield because they uplift from the URM walls. The slabs might yield where they frame into the RC walls. However, the rotation ductility demand generally does not exceeds 2.5, also for the slabs with short spans. Additionally, very short spans (say, less than 0.75 m) are rather unlikely in modern residential buildings. Also the dynamic analyses presented in the following section demonstrate that the RC members are not critical and there is no need for their displacement capacity check.

Step 14 –Out-of-plane check of the URM walls

The out-of-plane check of URM walls can be carried out in accordance with EN 1998-1 [2004] where the thickness and the slenderness of the masonry walls have to fulfil the following criteria:

$$\begin{array}{ll} \text{Low seismicity:} & \begin{array}{l} t_{ef} \geq 17 \text{ cm} \\ h_{ef}/t_{ef} \leq 15 [-] \end{array} \end{array} \quad (37a)$$

$$\begin{array}{ll} \text{High seismicity:} & \begin{array}{l} t_{ef} \geq 24 \text{ cm} \\ h_{ef}/t_{ef} \leq 12 [-] \end{array} \end{array} \quad (37b)$$

t_{ef} and h_{ef} are the effective thickness and height of the URM wall calculated according to EN1998-1 [2004].

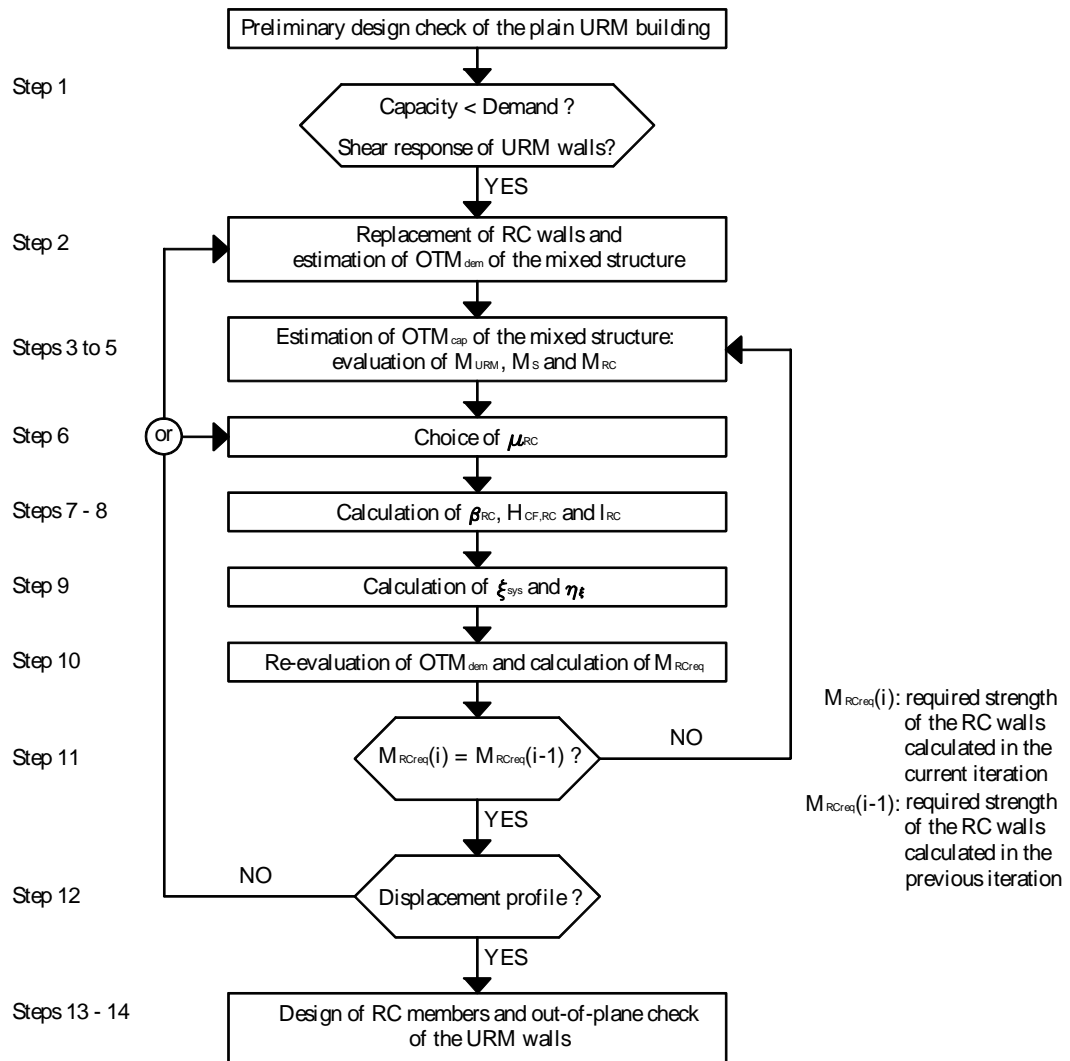


Figure 14: Flowchart of the DDBD methodology for RC-URM wall structures.

7 Case studies

In order to verify the accuracy of the displacement-based design procedure in terms of meeting the assumed performance level, several mixed RC-URM wall structures are designed according to the proposed method (Section 7.1). The buildings are conceived for the design level earthquake to reach the SD limits state. The limit state is controlled by the URM walls to which a drift capacity equal to 0.4% is assigned [EN1998-3, 2005]. Assuming further a constant

inter-storey drift over the height of the structure, the SD limit state is therefore reached if the average drift corresponds to 0.4%.

Based on the DDBD outputs, two-dimensional non-linear models are set up and subjected to one set of ground motions which are compatible with the design spectrum (Section 7.2). The performances of the structures are then gauged comparing design quantities, such as displacement profiles and reaction forces at the base of the walls, to the results from the simulations (Section 7.3).

7.1 Description of the case studies

Several configurations of 3, 4 and 5 storey modern RC-URM wall structures are designed using the new methodology. At the beginning of the procedure, the DDBD check of plain URM wall structures is carried out to check that the masonry walls display a dominant shear behaviour and that the structure does not satisfy the seismic design requirement. The objective is to ascertain that replacing one or more URM walls by RC ones will increase not only the strength but also the displacement capacity of the mixed system in comparison to the plain URM buildings. Figure 15 represents the elevation of the 4-storey buildings with the position of the RC walls replacing the masonry. The RC walls are drawn with dotted lines to stress that their length is not an input parameter.

Concerning the geometry of the structures, the thickness of all walls in these case studies is always 0.30 m. As two-dimensional simulations are carried out, RC beams with a cross section of 0.25x0.90 m represent the slabs. Again, the width of the RC beams is set equal to three times that of the walls according to Priestley et al. [2007]. The area of the longitudinal reinforcements of the RC beams is always equal to 1000 mm^2 ($\rho_{CB} = 0.51\%$) and their free span is 1.00 m. The axial stress ratios σ_o/f_m at the base of the URM walls are around 5.3%, 7.1% and 8.8% for the 3, 4 and 5 storey configurations. The transverse reinforcements of all RC members are designed to avoid shear failure and develop a stable flexural response with a larger deformation capacity than that of the URM walls. The structures are located in an area of moderate seismicity and the seismic demand is represented by an acceleration design spectrum of soil class C ($T_B = 0.2 \text{ s}$; $T_C = 0.6 \text{ s}$ and $T_D = 2 \text{ s}$ [EN 1998-1, 2004]) with PGA equal to 0.25g (Figure 16). Table 4 summarises the main characteristics of the structures and the key DDBD

outputs. Note that the increase of ξ_{hys} due to its period dependency [Priestley et al., 2007] ranged between 4% (5 storeys structures) and 12% (3 storeys structures).

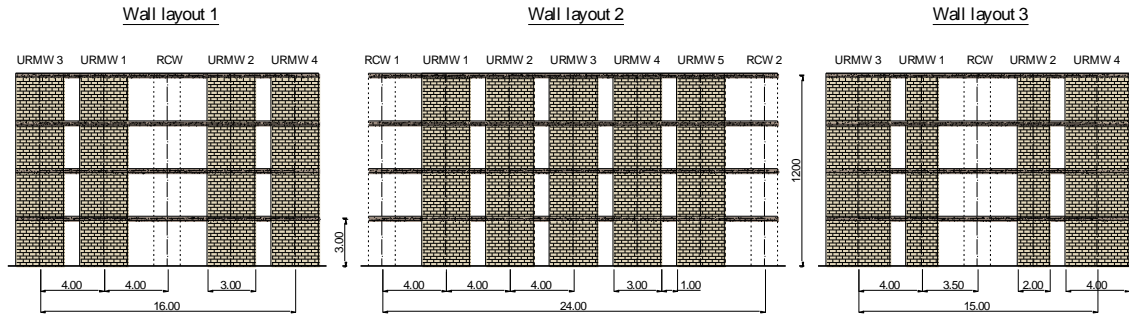


Figure 15: Elevation of the 4 storey buildings. All dimensions in m.

Table 4: Characteristics of the RC-URM wall structures and key design outputs from DDBD approach

Characteristics of the mixed structures				DDBD key outputs					
	<i>Name</i> *	<i>H</i> [m]	<i>M</i> [t]	μ_{ARC} [-]	T_1 [s]	T_e [s]	M_{RC} [kNm]	l_{RC} [m]	ρ_{mean} [%]
Wall layout 1	L1S3	9	306	1.8	0.26	0.57	1720	2.81	0.20
	L1S4	12	408	1.6	0.34	0.69	2280	3.09	0.22
	L1S5	15	510	1.2	0.47	0.84	2250	2.66	0.28
Wall layout 2	L2S3	9	428	1.8	0.27	0.56	1530	2.60	0.21
	L2S4	12	571	1.6	0.37	0.67	1930	2.70	0.24
	L2S5	15	714	1.2	0.50	0.82	1720	2.17	0.31
Wall layout 3	L3S3	9	306	1.8	0.25	0.57	1360	2.44	0.21
	L3S4	12	408	1.6	0.35	0.70	1410	2.33	0.22
	L3S5	15	510	1.2	0.46	0.86	1400	2.15	0.24

H: total height

M: total mass

μ_{ARC} : design ductility of the RC wall(s)

T_1 : first modal period

T_e : effective period

M_{RC} : design strength of the RC wall(s)

l_{RC} : length of the RC wall(s)

ρ_{mean} : mean longitudinal reinforcement ratio of the RC wall(s)

* The name stands for "Layout X Storeys X"

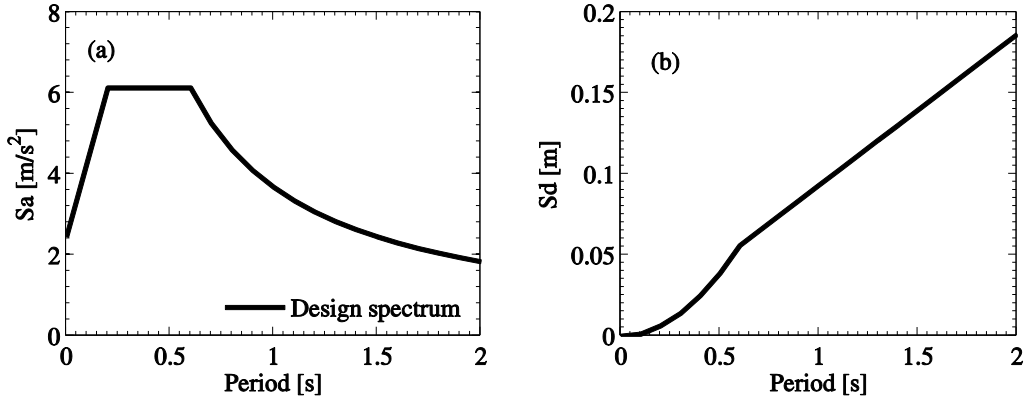


Figure 16: Acceleration and displacement design spectra.

7.2 Modelling and analyses

To assess the designs, the case studies are modelled and analysed through inelastic time history analyses (ITHA) using the TREMURI software [Penna et al., 2013; Largomarsino et al., 2013]. The mechanical properties adopted are those presented in Section 3.2.2 (Table 3) except the equivalent cohesion c_{eq} since the axial stress ratios at the base of the URM walls (σ_0/f_m) are different to the previous case studies (Section 3.2). c_{eq} results equal to 0.063, 0.084 and 0.106 MPa for the 3, 4 and 5 storey configurations.

The structures are subjected to the set of accelerograms outlined in Section 5.2. In the spectra the position of the corner period T_D (equal to 2 s) does not influence the results since the structures do not exhibit periods larger than 2 s (see Table 4). The accelerograms are scaled to a PGA equal to 0.25 g to match the design displacement spectrum adopted in the design procedure (Figure 16). Damping is modelled using initial stiffness proportional viscous damping ratio ζ^* . The value of ζ^* is the lowered damping coefficient computed according to Priestley et al. [2007] (Eq. 19) as tangent stiffness proportional damping is replaced with initial stiffness proportional damping since only the latter is available in TREMURI. The ductility of the system μ is approximated as $(T_e/T_i)^2$, see Table 4.

7.3 Results of time-history analyses

To validate the design method, this section compares the design assumptions to the responses obtained from ITHA for the design level earthquake ($PGA = 0.25\text{ g}$). Figures 17 and 18 present the maximum displacement profiles, their median and the target design values associated with 0.4% average drift. Review of the results indicates that the procedure has performed well in limiting concentration of deformations in one single storey and in providing a linear displacement profile. On the other hand, for the three storey configurations, the maximum displacements obtained from ITHA are rather smaller than the corresponding design value. This difference is most likely caused by the approximate manner in which the period dependency of ξ_{URM} has been accounted for. In fact, it seems that the correction factor CF (Eq. 21, Section 5.2) underestimates the period dependency of ξ_{URM} for effective periods shorter than 0.8 s (Figure 11b). For configurations with longer effective periods (i.e., the four and five storey structures), the difference between the maximum displacements obtained from ITHA and the design displacements decreases.

For Layouts 1 and 2 the design of the six storey structures has been carried out with the objective to check the performance of the design approach for structures in which ξ_{URM} is not affected by the period dependency (i.e., both initial and effective periods are in the linear branch of the displacement spectrum as $T_i \approx 0.6\text{ s}$ and $T_e \approx 1.0\text{ s}$). Figure 19 confirms that, for the six storey configurations, the maximum displacement is rather well estimated by the design approach.

For wall layouts 1 (L1), the hysteretic behaviour obtained from one of the stationary accelerograms (record 12) is plotted, Figure 17b. The objective is to show the global hysteretic behaviour of the systems and the distribution of the base shear among RC and URM walls. The maximum base shear carried by the URM walls appears to be rather well estimated. At the same time, the design procedure overestimates the base shear carried by the RC walls up to 20%. The hysteretic response of the URM walls confirms that the URM walls develop a dominant shear behaviour and that the values of ξ_{sys} obtained from design approach (i.e., between 15% and 25%) are consistent with the results from the ITHA analyses.

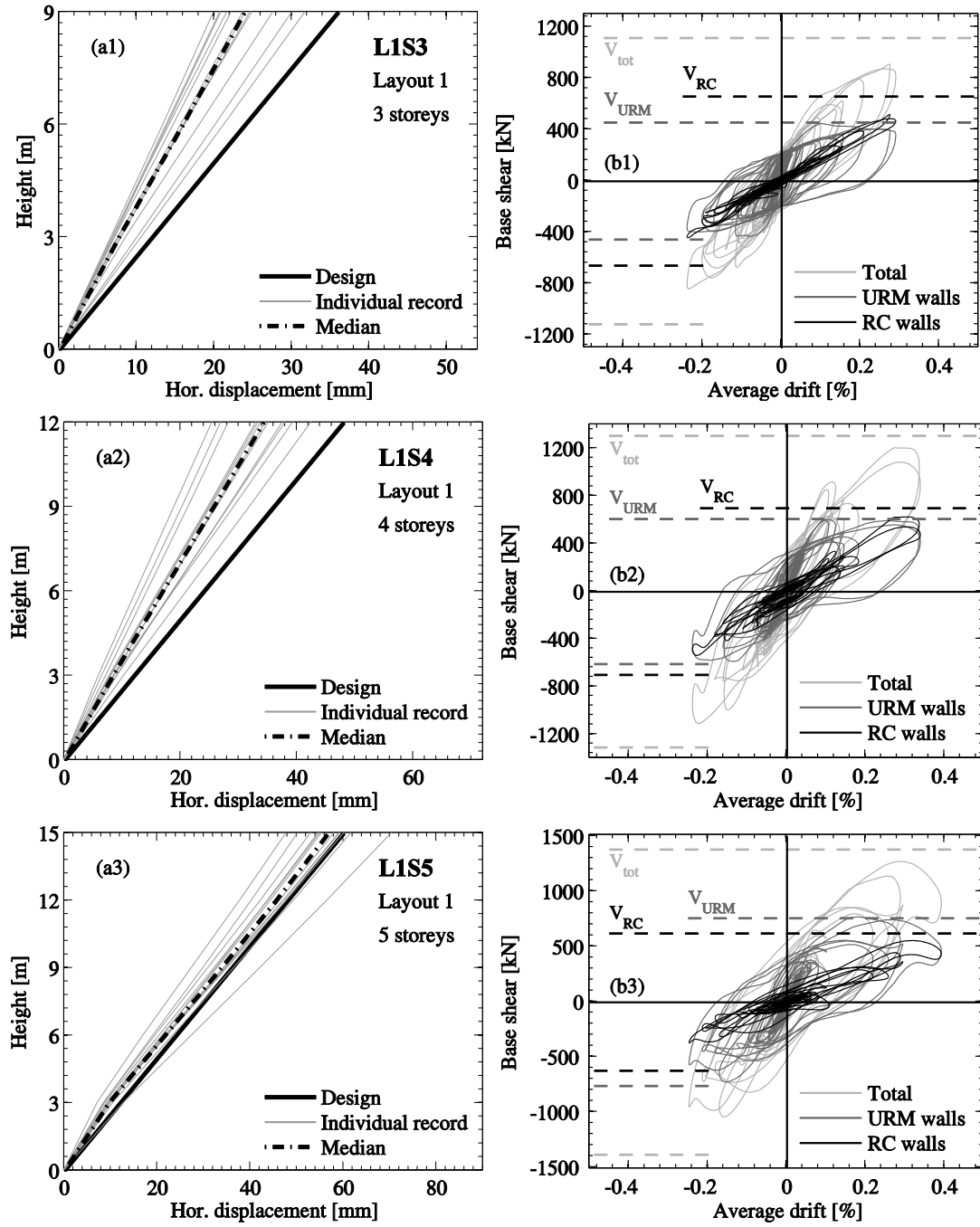


Figure 17: Time-history response for wall layout 1 structures. Displacement profiles (a). Hysteretic behaviour of the structures subjected to record 4 and comparison against design values. V_{RC} , V_{URM} , V_{tot} : design shear forces for RC and URM walls and total design shear force (b).

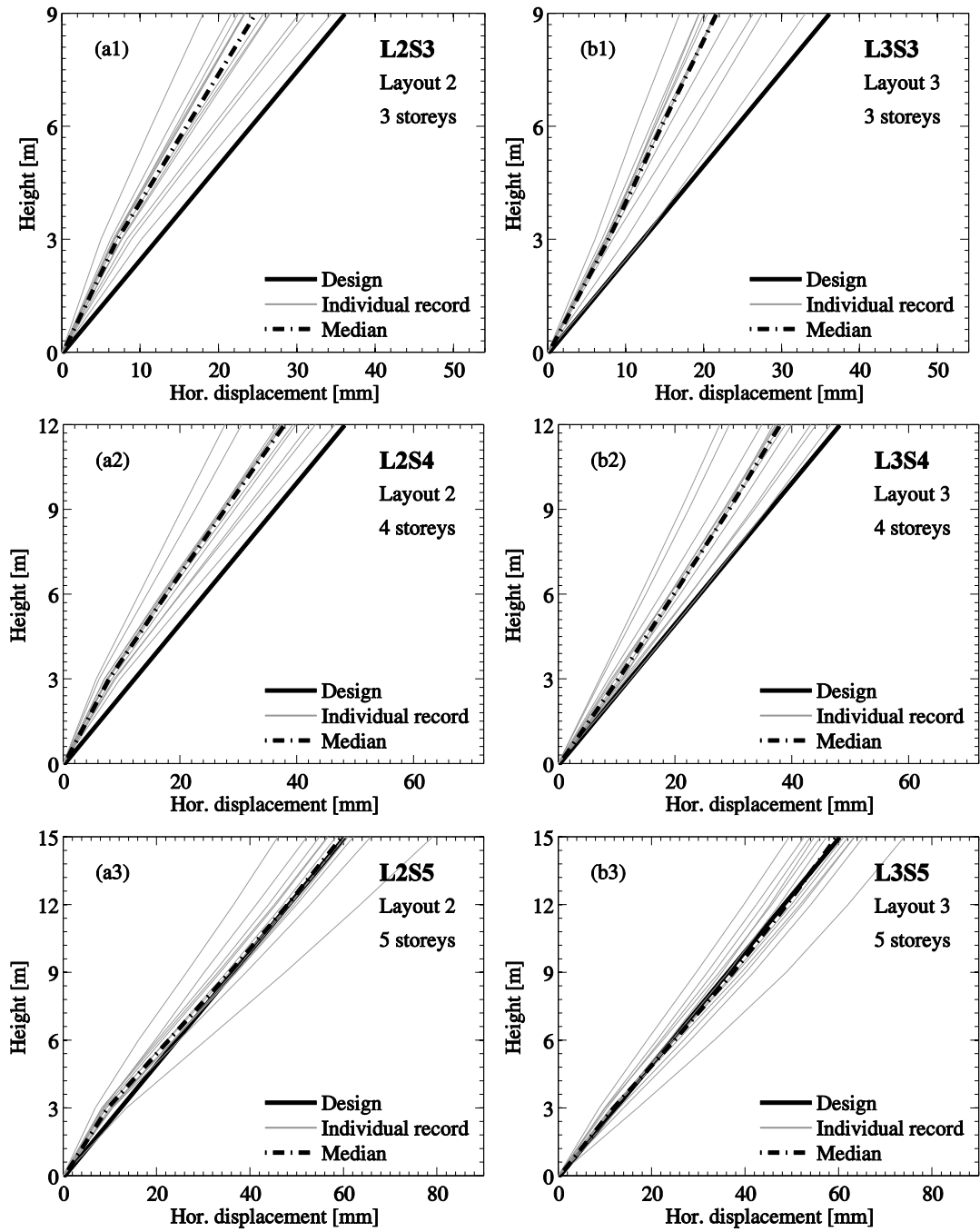


Figure 18: Time-history response for wall layout 2 (a) and wall layout 3 structures (b). Displacement profiles.

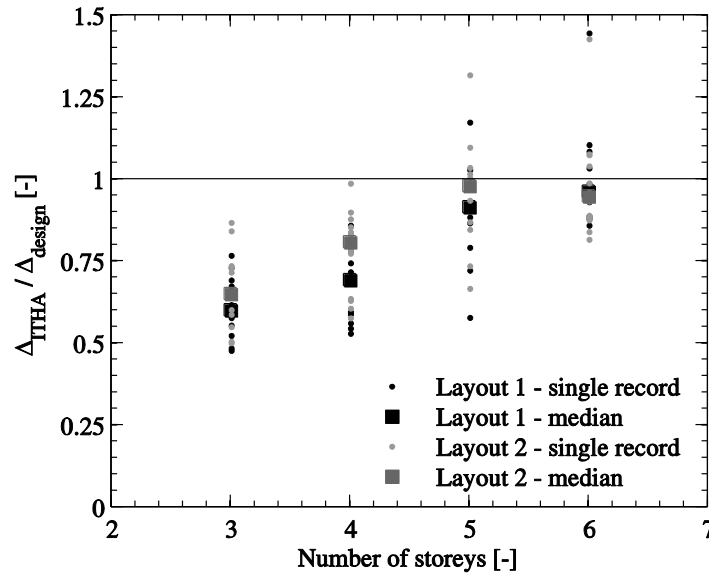


Figure 19: Normalised top displacement recorded from ITHA with respect to the design top displacement $\Delta_{ITHA}/\Delta_{design}$. Influence of the number of storeys.

8 Conclusions

Re-examining the seismic hazard in Europe led, in particular for regions of low to moderate seismicity, to an increase in the seismic demand. As a result, in Switzerland many new residential buildings have been constructed using both RC and URM walls coupled together by RC slabs. Of late, also existing modern URM wall constructions with RC slabs, which no longer meet the requirements of the seismic design check, have been retrofitted by adding or replacing URM walls with concrete ones. Although this technique is rather common, codes do not provide guidelines for the design and assessment of such mixed structures.

The aim of this paper was therefore to propose a displacement-based design methodology for the seismic design of buildings in which the lateral bracing system consists of both RC and URM walls. The methodology follows the direct displacement-based design by Priestley et al. [2007]. The design consists of three main phases: (i) A preliminary DDBD check of the plain URM building. (ii) If the structure does not satisfy the seismic design check and has a dominant shear behaviour, retrofitting the structure by replacing some URM walls by RC ones is a viable solution. (iii) In the final phase, the DDBD design of the mixed RC-URM wall structure is carried out.

In the article, two tools for estimating important quantities relevant for the DDBD are proposed. (i) A simple mechanical model based on the shear-flexure wall interaction is implemented and validated. The objective is to provide a tool for estimating the deformed shape of the structure and the height of the contra-flexure point of the RC walls. Such a model was firstly developed to represent the shear-flexure interaction which arises in dual frame-wall buildings [e.g., Pozzati, 1980]. (ii) Furthermore, the contribution of the RC slabs to the overturning moment capacity is evaluated by elastic continuous beams. Connections between the slabs and the masonry walls are represented by vertical supports which work only in compression. The aim is to represent the limited capacity of the URM walls to equilibrate moments and shears transmitted by the RC slabs. Connections between slabs and RC walls are modelled instead by pins that can also transmit tension forces.

The DDBD methodology has been checked by designing several case studies and comparing their structural performance through ITHA. Two sets of accelerograms were used. The design method effectively controlled the horizontal deflection of the structure, being almost linear over its height. Furthermore, it was observed that, particularly for the three storey configurations, the maximum displacement obtained from ITHA was lower than the design value. This difference is explained by the short effective period of the three storey configurations and how the period dependency of ξ_{URM} has been accounted for. A possible solution would be to correlate the inelastic displacement demand to the demand slope factor, which is a function of the elastic spectral displacement demand variation between the initial and the effective periods [Pennucci et al., 2011]. Also the predicted magnitude of the shear forces carried by RC and URM walls was rather similar to the actual values obtained from ITHA.

9 Acknowledgments

The authors thank Chris Genis for proofreading the article.

10 References

- Beyer, K., Tondelli, M., Petry, S. and Peloso, S. [2014] “Dynamic testing of a 4-storey building with reinforced concrete and unreinforced masonry walls”, to be submitted to *Bulletin of Earthquake Engineering*.
- Cardone, D., Dolce, M. and Palermo, G. [2009] “Direct displacement-based design of seismically isolated bridges”, *Bulletin of Earthquake Engineering*, 7, 391-410
- Cattari, S. and Lagomarsino, S. [2013] “Seismic design of mixed masonry-reinforced concrete buildings by non-linear static analyses”, *Earthquakes and Structures*, Vol. 4, N°3.
- Chiarugi, A. [1970] “Indagine sulla ripartizione delle azioni orrizzontali in telai irrigiditi da pareti”, *Giornale del Genio Civile*, 2, 187-203.
- EN 1992-1-1 [2004] *Eurocode 2: Design of concrete structures – Part 1-1: General rules and rules for buildings*, CEN, Brussels.
- EN 1998-1 [2004] *Eurocode 8: Design of structures for earthquake resistance – Part 1: General rules, seismic actions and rules for buildings*, CEN, Brussels.
- EN 1998-3 [2005] *Eurocode 8: Design of structures for earthquake resistance – Part 3: Assessment and retrofitting of buildings*, CEN, Brussels.
- Graziotti, F. [2013] “Contribution towards a displacement-based seismic assessment of masonry structures”, Pavia, Italy.
- Hannenwald, P. [2013] “Seismic behaviour of poorly detailed RC bridge piers” Ph.D. thesis, EPFL, Lausanne, Switzerland.
- Lagomarsino, S., Penna, A., Galasco, A. and Cattari S. [2013] “TREMURI program: an equivalent frame model for the non-linear seismic analysis of masonry buildings”, *Engineering Structures*, 6, 1787–1799.
- Lang, K. [2002] “Seismic vulnerability of existing buildings”, Ph.D. thesis, ETH Zurich, Zurich, Switzerland.
- Magenes G. [2006] “Masonry building design in seismic areas: recent experiences and prospects form and european standpoint” Keynote address, *Proc. of 1st European Conference on Earthquake Engineering and Seismology*, Geneva, Switzerland.
- Mandirola, M. [2014] “Non-linear macroelement modelling of experimental tests on masonry building specimens with rigid diaphragms”, Pavia, Italy.
- Mann, W. and Müller, H. [1982] “Failure of shear-stressed masonry: an enlarged theory, tests and application to shear walls“, *Proc. of the British Ceramic Society*, 30, 223-235.

- Michel, C., Lestuzzi, P. and Lacave, C. [2014] “Simplified non-linear seismic displacement demand prediction for low period structures”, *Bulletin of Earthquake Engineering*, 12, 1972-1998.
- Paparo, A. and Beyer, K. [2014a] “Quasi-static tests of two mixed reinforced concrete – unreinforced masonry wall structures”, *Engineering Structures*, 71, 201-211.
- Paparo, A. and Beyer, K. [2014b] “Modelling the seismic response of modern URM buildings retrofitted by adding RC walls”, submitted to *Journal of Earthquake Engineering*.
- Paulay, T. and Priestley, M.N.J. [1992] *Seismic design of reinforced concrete and masonry buildings*, John Wiley & Sons, Inc., New York.
- Penna, A., Lagomarsino, S. and Galasco, A. [2013] “A nonlinear macro-element model for the seismic analyses of masonry buildings”, *Earthquake Engineering and Structural Dynamics*, 10.1002/eqe.2335.
- Pennuci, D., Calvi, G.M. and Sullivan, T.J. [2009] “Displacement-based design of pre-cast walls with additional dampers”, *Journal of Earthquake Engineering*, 13, S1.
- Pennucci, D., Sullivan, T.J. and Calvi, G.M. [2011] “Displacement reduction factors for the design of medium and long period structures”, *Journal of Earthquake Engineering*, 13(S1), 1-29.
- Pozzati, P. [1980] *Teoria e tecnica delle strutture*, UTET, Torino.
- Priestley, M.J.N. [1993] “Myths and fallacies in earthquake engineering – conflict between design and reality”, *Bulletin, NZ National Society for Earthquake Engineering*, 26(3), 329-341.
- Priestley, M.J.N. [1998] “Direct displacement-based design of buildings”, *Proc. of 11th European Conference on Earthquake Engineering*, Paris, France.
- Priestley, M.J.N., Calvi, G.M. and Kowalsky, M.J. [2007] *Displacement-Based Seismic Design of Structures*, IUSS Press, Pavia, Italy.
- Rosman, R. [1967] “Laterally loaded systems consisting of walls and frames”, *Tall Buildings*, 291-320.
- Rosman, R. [1974] “Stability and dynamics of shear-wall frame structures”, *Building Science*, 9, 55-63.
- SIA 262 [2004] *Building code, Swiss Society of Engineers and Architects (SIA): Concrete Structures*, SIA, Zurich.

- Smith, B.S. and Coull, A. [1991] *Tall building structures: analysis and design*, John Wiley & Sons, Inc., New York.
- Sullivan, T.J., Priestley M.J.N. and Calvi, G.M. [2005] “Development of an innovative seismic design procedure for frame-wall structures”, *Journal of Earthquake Engineering*, 10 (Special Issue 1), 91-124.
- Sullivan, T.J., Priestley M.J.N. and Calvi, G.M. [2006] “Direct displacement-based design of frame-wall structures”, *Journal of Earthquake Engineering*, 9 (Special Issue 2), 279-307.
- Sullivan, T.J., Priestley M.J.N. and Calvi, G.M. [2012] *A Model Code for the Displacement-Based Seismic Design of Structures*, IUSS Press, Pavia, Italy.
- Tondelli, M., Beyer, K., M., Petry, S. and Peloso, S. [2014] “Data set of a shake-table test on a four-storey structure with reinforced concrete and unreinforced masonry walls”, to be submitted to *Bulletin of Earthquake Engineering*.

10 Appendix: Design example

In order to illustrate the procedure, the DDBD of L1S5 (wall layout 1, 5 storeys) is presented. The methodology is iterative and stops when the variation of the required strength of the RC wall (M_{RCreq}) between two steps is smaller than 5%. The structure is located in a moderate seismicity area and the seismic demand is represented by an acceleration design spectrum of soil class C ($T_B = 0.2$ s; $T_C = 0.6$ s and $T_D = 2$ s [EN 1998-1, 2004]) with PGA equal to 0.25g (Figure 16). The design drift δ_d , associated with the SD limit state for URM walls failing in shear, is set equal to 0.4% [EN 1998-3, 2005]. Assuming further a constant inter-storey drift over the height of the structure, the SD limit state is therefore reached if the average drift corresponds to 0.4%.

The RC wall is designed to exhibit a displacement ductility μ_{ARC} equal to 1.2. The axial force acting at the base of each wall is 500 kN and corresponds to an axial stress ratio at the base of the masonry walls (σ_o/f_m) of 8.8%. The mass whose weight is carried by walls in the direction of excitation ($m_{||}$) is equally distributed between RC and URM walls, resulting in masses of 10.2 t applied at the top of the centrelines of each wall. An additional mass (m_{\perp}) equal to $m_{||}$ is added with a flexible frame and simulates the weight carried by the walls perpendicular to the direction of excitation (Figure 20). It results that the total inertial mass ($m_{tot} = m_{||} + m_{\perp}$) is

510 t while the gravity load carried by the walls in the direction of excitation ($m_{||}$) is 255 t. Additional information on the structure is provided in Section 7.1.

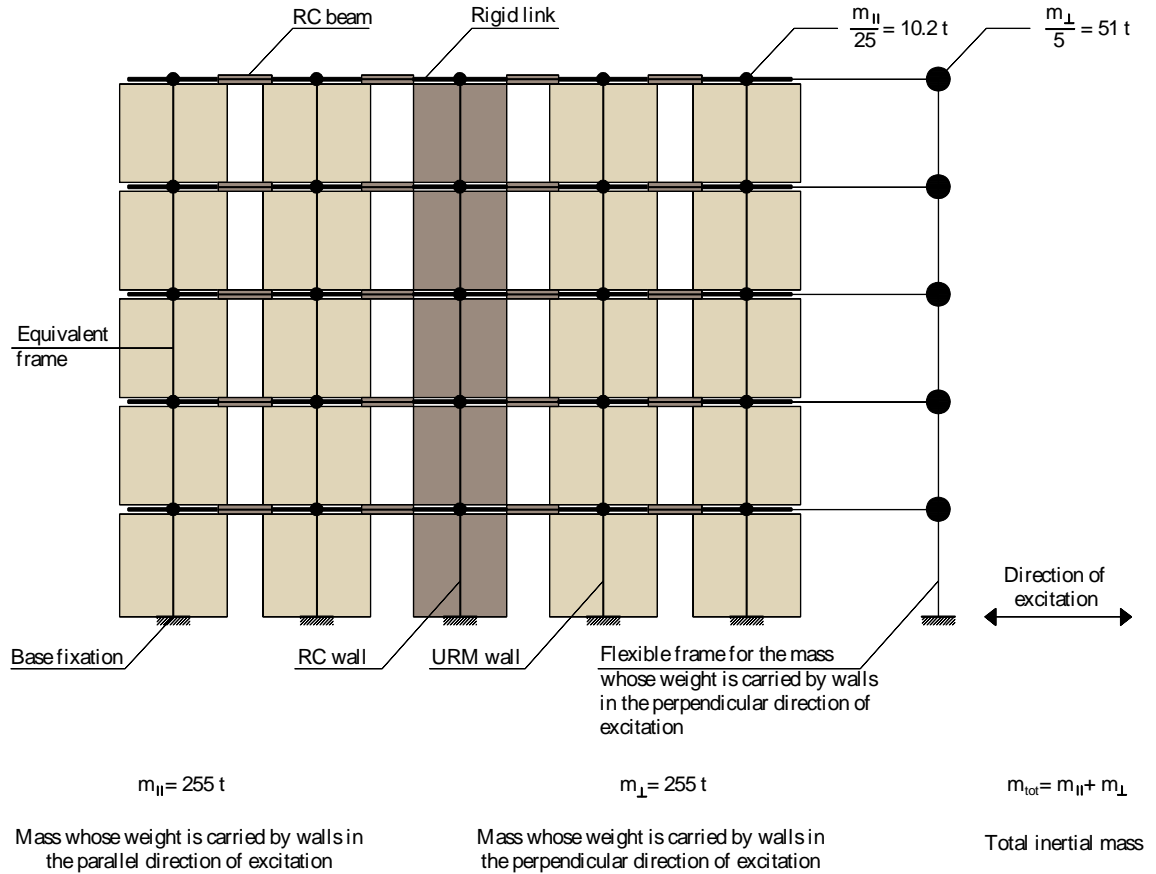


Figure 20: TREMURI model used for ITHA.

A – Preliminary design check of the plain URM wall building

The design starts by checking the plain URM wall structure with RC slabs. Firstly, it has to be verified that the displacement capacity of the URM building (Δ_{cap}) is smaller than the displacement demand (Δ_{dem}). This check is carried out by following the displacement-based assessment approach proposed by Priestley et al. [2007]. The procedure requires the knowledge of the displacement capacity (Δ_{cap}) and the effective mass (m_e) of the structure. The displacement capacity (Δ_{cap}), which corresponds to the design displacement (Δ_d), and the effective mass (m_e) are calculated by assuming a design deformed shape that concentrates the

deformations in the lowest storey (Table 5 and Figure 21a). From Eqs. 12 to 14 results as follows:

$$\Delta_{cap} = \Delta_d = \frac{\sum m_i \Delta_i^2}{\sum m_i \Delta_i} = \frac{0.073}{6.11} = 0.012m$$

$$m_e = \frac{\sum m_i \Delta_i}{\Delta_d} = \frac{6.11}{0.012} = 510t$$

Table 5: Single degree of freedom simulation of the pain URM wall structure

Storey	H_i	m_i	δ_d	$\Delta_i = \delta_d H_i$	Δ_i^2	$H_i \Delta_i$	$m_i \Delta_i$	$m_i \Delta_i^2$	$m_i \Delta_i H_i$
[-]	[m]	[t]	[%]	[m]	[m ²]	[m ²]	[tm]	[tm ²]	[tm ²]
1	3	102	0.40	0.012	0.00014	0.036	1.224	0.015	3.67
2	6	102	0.00	0.012	0.00014	0.072	1.224	0.015	7.34
3	9	102	0.00	0.012	0.00014	0.108	1.224	0.015	11.02
4	12	102	0.00	0.012	0.00014	0.144	1.224	0.015	14.69
5	15	102	0.00	0.012	0.00014	0.180	1.224	0.015	18.36
Sum	-	510		0.060	0.00072	0.540	6.120	0.073	55.08

H_i = storey height

m_i = total storey mass

δ_d = design drift

Δ_i = horizontal storey displacement

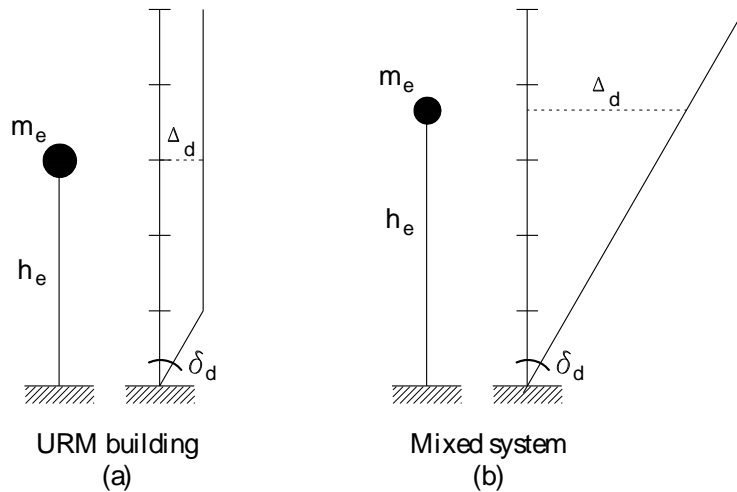


Figure 21: Assumed displacement profile and SDOF simulations for the URM building and the mixed system.

The procedure is iterative and continues by guessing the displacement demand (Δ_{dem}), whose value is revised in the iterations. Furthermore, the knowledge of the equivalent viscous damping (here assumed equal to 0.31) and the shear strength capacity of the building (V_{tot}) are required. The latter is calculated according to Mann and Müller [1982]:

$$V_{tot} = 0.38N_{URM} = 0.38x(5x500) = 950kN$$

At each iteration, the effective stiffness K_e and the effective period T_e are calculated. From T_e the new displacement demand is determined from the over-damped spectra. Table 6 summarises the main outputs of each iteration. The procedure is stopped when the displacement demand varies less than 5% from one step to the other. From the calculations the structure does not satisfy the design check as the displacement demand is higher than the displacement capacity: $\Delta_{dem} > \Delta_{cap}$.

Table 6: Iterative displacement-based assessment procedure of the plain URM building

Iteration	Δ_{dem}	K_e	T_e
[-]	[m]	[kN/m]	[s]
0	<u>0.018</u>	53000	0.61
1	0.027	35200	0.76
2	0.033	28800	0.83
3	0.036	26400	0.87
4	0.038	25000	0.89
5	0.039	-	-

Δ_{dem} = displacement demand

K_e = effective stiffness ($K_e = V_{tot}/\Delta_{dem}$)

T_e = effective period ($T_e = 2\pi\sqrt{m_e / K_e}$)

The starting, guessed, value of the displacement demand is underlined

Additionally, it has to be verified that the URM walls are developing a shear rather than a flexural mechanism: $M_{URM,sh} < M_{URM,fl}$. To simplify matters, no variation of axial force at the base of the masonry walls due to coupling of the slabs is assumed. $M_{URM,sh}$ can be computed (Eqs. 24 to 26):

$$M_{URM,sh} = V_{sh} H_{CF,URM} = (0.38xN) \left(\frac{h_{st}}{2} \gamma \psi \right) = (0.38x500) \left(\frac{3.0}{2} x 1.5 x 1 \right) = 430kNm$$

N is the total axial force at the base of the considered URM wall. $M_{URM,fl}$ can be computed according to EN 1998-3 [2005]:

$$M_{URM,fl} = \frac{N l_{URM}}{2} \left(1 - 1.15 \frac{N}{l_{URM} t f_m} \right) = \frac{500x3}{2} \left(1 - 1.15 \frac{0.50}{3x0.3x6.3} \right) = 675kNm$$

With l_{URM} and t_{URM} the length and thickness of the wall and f_m the masonry compressive strength. As $M_{URM,sh} > M_{URM,fl}$, the masonry building has a dominant shear rather than flexural behaviour.

As the structure (i) does not satisfy the design requirement ($\Delta_{cap} < \Delta_{dem}$) and (ii) has a dominant shear behaviour ($M_{URM,sh} < M_{URM,fl}$), replacing a URM wall by a RC wall is a viable retrofit solution. It is decided to replace the central masonry pier with one RC wall, Figure 23b.

B – Design displacement and SDOF simulation of the mixed RC-URM wall structure

For the SDOF simulation of the mixed RC-URM wall structure, the assumed design deformed shape is linear (Table 7 and Figure 21b). From Eqs. 12 to 14 Δ_d , m_e and h_e are obtained:

$$\Delta_d = \frac{\sum m_i \Delta_i^2}{\sum m_i \Delta_i} = \frac{0.808}{18.36} = 0.044m$$

$$m_e = \frac{\sum m_i \Delta_i}{\Delta_d} = \frac{18.36}{0.044} = 417t$$

$$h_e = \frac{\sum m_i \Delta_i H_i}{\sum m_i \Delta_i} = \frac{202}{18.36} = 11m$$

Table 7: Single degree of freedom simulation of the mixed RC-URM wall structure

Storey [-]	H_i [m]	m_i [t]	δ_d [%]	$\Delta_i = \delta_d H_i$ [m]	Δ_i^2 [m ²]	$H_i \Delta_i$ [m ²]	$m_i \Delta_i$ [tm]	$m_i \Delta_i^2$ [tm ²]	$m_i \Delta_i H_i$ [tm ²]
1	3	102	0.40	0.012	0.0001	0.036	1.224	0.015	3.67
2	6	102	0.40	0.024	0.0006	0.144	2.448	0.059	14.69
3	9	102	0.40	0.036	0.0013	0.324	3.672	0.132	33.05
4	12	102	0.40	0.048	0.0023	0.576	4.896	0.235	58.75
5	15	102	0.40	0.060	0.0036	0.900	6.120	0.367	91.80
Sum	-	510		0.180	0.0079	1.980	18.36	0.808	201.96

H_i = storey height

m_i = total storey mass

δ_d = design drift

Δ_i = horizontal storey displacement

C – Contribution to the overturning moment provided by the URM walls (M_{URM})

The strength capacity of the URM walls (V_{sh}) is calculated according to Mann and Müller [1982] and M_{URM} is estimated from Eqs. 24 to 27 as follows:

$$V_{sh} = 0.38N_{URM} = 0.38x(4x500) = 760kN$$

$$\gamma = 1 + n/10 = 1 + 5/10 = 1.5$$

$$\psi = h_{st} / l_{URM} = 1$$

$$M_{URM} = V_{sh} H_{CF,URM} = V_{sh} \left(\frac{h_{st}}{2} \gamma \psi \right) = 760 \left(\frac{3}{2} x 1.5 x 1 \right) = 1710kNm$$

D – Iterative procedure to find the required strength and the length of the RC wall

Iteration 0 (starting values)

Initially, to calculate the damping reduction factor η_ξ (Eq. 15) and the overturning moment demand (Eqs. 16, 17, 22), the equivalent viscous damping is assumed equal to 20%:

$$\xi_{sys} = 20\% \rightarrow \eta_\xi = \left(\frac{0.07}{0.02 + \xi_{sys}} \right)^{0.5} = 0.564$$

$$K_e = \frac{4\pi^2 m_e}{T_e^2} = \frac{4 \times 3.14^2 \times 417}{0.82^2} = 24400 \text{ kN/m}$$

$$V_{base} = K_e \Delta_d = 24400 \times 0.044 = 1070 \text{ kN}$$

$$OTM_{dem} = V_{base} h_e = 1070 \times 11 = 11820 \text{ kNm}$$

The yield rotation of the RC slabs flanking the RC walls, θ_{ys} , is calculated according to Eq. 30. As the dimensions of the RC walls are unknown, a trial length of 3.0 m is assumed:

$$l_{RC} = 3.0 \rightarrow L_{se} = L_s + h_s = 1.00 + 0.25 = 1.25 \text{ m} \rightarrow \theta_{ys} = 0.35 \varepsilon_y \frac{L_s}{h_s} = 0.48\%$$

ε_y , the yield strain of the longitudinal bars of the RC wall, is calculated from the yield stress and the E-modulus of the reinforcing bars:

$$\varepsilon_y = \frac{f_y}{E} = \frac{550}{200000} = 0.00275$$

The rotation demand is found by assuming for the URM walls rigid body rotations around the base corner in compression and for the RC wall a rigid body rotation around its centreline (Figure 22):

$$\Delta_{V2r} = 0 \text{ mm}$$

$$\Delta_{VRCI} = \delta_d \frac{L_{RC}}{2} = 0.4\% \frac{3.0}{2} = +6 \text{ mm}$$

$$\Delta_{VRCr} = -\Delta_{VRCI} = -6 \text{ mm}$$

$$\Delta_{V3I} = \delta_d L_{URM3} = 0.4\% \times 3.0 = +12 \text{ mm}$$

$$\theta_{s2} = \frac{\Delta_{V2r} + \Delta_{VRCr}}{L_{se}} = \frac{0 + 6}{1000} = 0.6\%$$

$$\theta_{s3} = \frac{-\Delta_{VRCI} + \Delta_{V3I}}{L_{se}} = \frac{6 + 12}{1000} = 1.8\%$$

As the structure is symmetric, the mean rotation demand $\theta_s = (\theta_{s2} + \theta_{s3})/2 = 1.2\%$ is used for calculating the bending moment applied to the pins connecting the slabs to the RC walls ($M_{s,w}$).

As $\theta_s > \theta_{ys}$, $M_{s,w} = M_{ys,w} = 110 \text{ kNm}$, Eq. 31a. The contribution to the overturning moment from the RC slabs, M_s , is then calculated by using elastic continuous beams. According to Eq. 28, M_s is the sum of the contributions of the different bays ($M_{bay,j}$):

$$M_s = M_{bay1} + M_{bay2} + M_{bay3} + M_{bay4} = 7970 \text{ kNm}$$

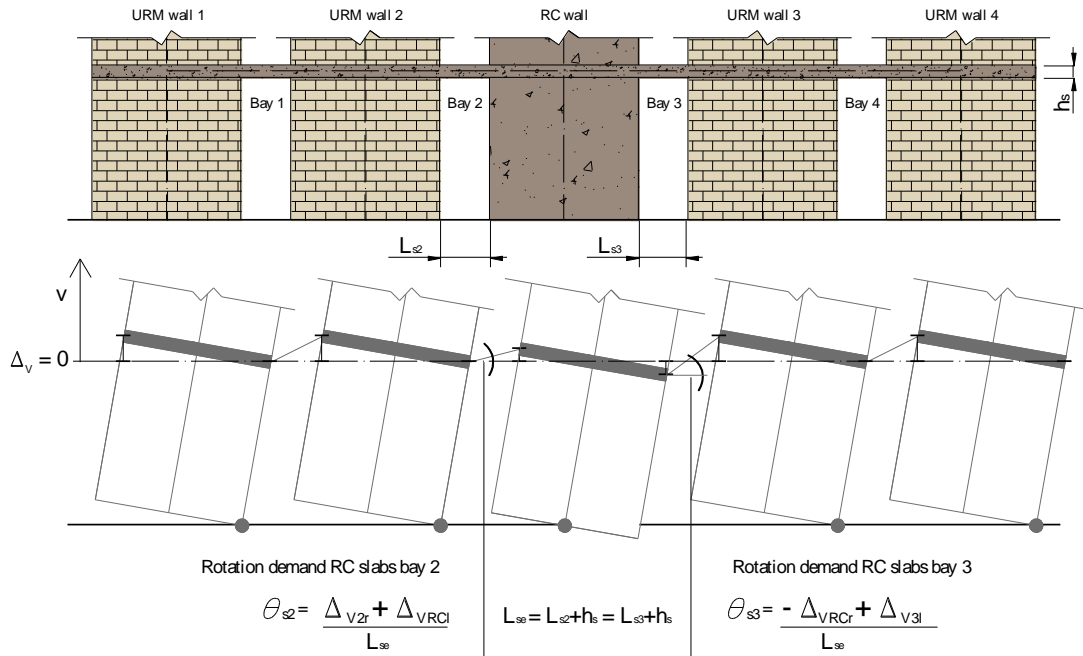


Figure 22: Mechanism for calculating the rotation demands θ_{b2} and θ_{b3} .

The reaction forces of supports and pins of the elastic continuous beams are represented in Figure 24. Note that the vertical supports between URM walls and slabs are all working in compression while some pins connecting RC walls and slabs transmit tension forces.

It is then possible to calculate the required strength of the RC wall (Eq. 36):

$$M_{RCreq} = OTM_{dem} - M_S - M_{URM} = 11820 - 7970 - 1710 = 2140 \text{ kNm}$$

Iterations 1 to 4

The iterations continue until the variation of the strength of the RC wall M_{RCreq} between two steps is smaller than 5%. Table 8 summarises the main DDBD outputs of each iteration.

Table 8: Iterative procedure

Iteration	l_{RC}	ξ_{sys}	OTM_{dem}	M_S	M_{RCreq}	V_{RCreq}	β_{RC}	α
[-]	[m]	[%]	[kNm]	[kNm]	[kNm]	[kN]	[%]	[-]
0	<u>3.00</u>	<u>20.0</u>	11820	7970	2140	630	18	3.5
1	2.53	21.0	11310	7180	2420	640	21	3.1
2	2.75	20.8	11410	7530	2170	630	19	3.4
3	2.60	21.1	11260	7285	2264	620	20	3.3
4	2.66	-	-	-	-	-	-	-

l_{RC} = length of the RC wall

ξ_{sys} = equivalent viscous damping of the system

OTM_{dem} = overturning demand

M_S = contribution to the overturning moment from the slabs

M_{RCreq} = required moment of the RC wall

V_{RCreq} = required shear of the RC wall

β_{RC} = ratio of the contribution of the overturning moment from the RC wall

$\alpha = (GA/EI)^{0.5}$

Starting values are underlined

E – Ascertain the displacement profile of the structure

Once length and strength of the RC wall are defined, the displacement profile of the structure is checked. With the design outputs $n = 5$, $\beta_{RC} = 20\%$ and $\alpha = 3.3$, the drift ratio R_δ is equal to around 0.9, Figure 23a. As the assumption of the linear displacement profile is satisfied, the RC elements are designed, the out-of-plane requirements checked and the procedure is completed. If Eq. 11 is not respected, the designer has two options: (i) to choose a different number of URM walls to be replaced by the RC ones or (ii) to change the level of ductility of the RC wall. Figure 23b represents the final structural configuration.

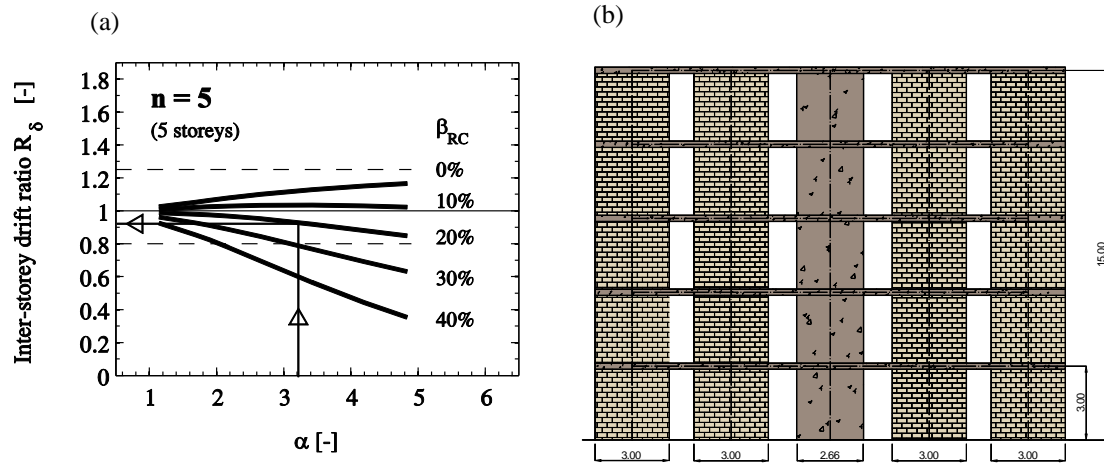


Figure 23: Verification of the displacement profile of the structure (a). Final configuration of the mixed RC-URM wall structure. All dimensions in m (b).

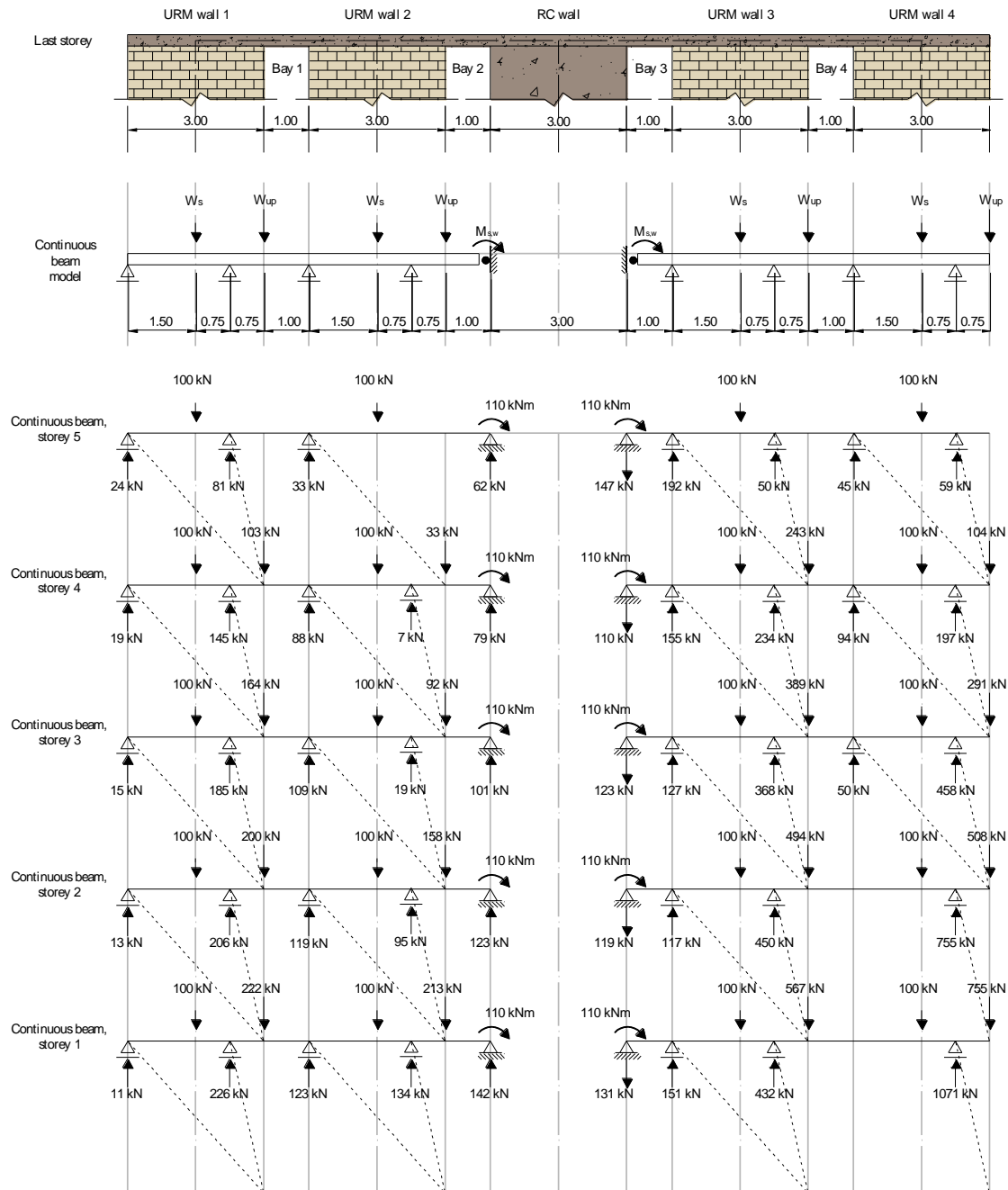


Figure 24: Elastic continuous beams used for calculating M_s . All dimensions in m.

Conclusions

Conclusions

1 Outline

The recent re-examination of the seismic hazard in Europe [Share project, 2013] led for many regions of low to moderate seismicity to an increase in the seismic demand. As a consequence, several modern unreinforced masonry (URM) buildings with reinforced concrete (RC) slabs that no longer satisfy the seismic design check have been retrofitted by adding or replacing URM walls with RC walls. Of late, also several new construction projects have been designed directly as mixed RC-URM wall systems.

This thesis presented a study on the in-plane seismic behaviour of typical Swiss mixed buildings composed of RC and URM walls. The analysed systems are modern buildings of three to five storeys with masses evenly distributed over the height. Both RC and URM walls are continuous over the height and connected at each floor by 20 to 30 cm thick RC slabs, which provide a rigid diaphragm action. The length of the RC walls varies between 2 and 5 m. The RC walls are 20 to 30 cm thick and are designed according to modern codes to develop a stable flexural behaviour with displacement capacities larger than those of URM walls. The URM walls have lengths up to 7 m and always outnumber the RC ones. They are built with hollow clay bricks, which are 20 to 30 cm thick, in combination with standard cement mortar. Since the RC slabs introduce an important framing effect [Lang, 2002], the URM walls, generally, exhibit a dominant shear behaviour.

Although in countries of low to moderate seismicity (e.g., Switzerland) this construction technique is rather common, codes do not provide clear guidance regarding the design of such structures. As a result, these mixed buildings are often designed on the basis of oversimplified

assumptions, such as neglecting the contribution of URM walls to the lateral strength of the building and assigning all the horizontal forces to the RC walls. The objectives of this thesis were therefore (i) to understand better the seismic behaviour of these mixed structures through experimental and numerical investigations; (ii) to formulate practical recommendations for setting up numerical models; (iii) to develop a mechanical model that represents the shear-flexure interaction which arises between masonry and concrete walls; and (iv) to propose a seismic design methodology.

On the basis of these objectives, this concluding chapter summarises the main contributions of the research. Section 2 outlines the main evidence gathered from the experimental campaign. Section 3 compares the two modelling approaches adopted to represent the global behaviour of mixed RC-URM wall structures. Recommendations on the use of the two techniques and a practical example on the behaviour of a mixed system, in comparison with a URM structure, are given. Section 4 follows with a brief description of the mechanical model proposed for estimating the interaction between RC and URM walls. Section 5 outlines the main features of the proposed design approach. Finally, Section 6 concludes the work indicating possible future research areas.

2 Contributions derived from the experimental campaign

Although these mixed buildings are rather common in countries of low to moderate seismicity like Switzerland, their inelastic behaviour was scarcely examined in the past. The lack in design guidelines for structures with both RC and URM walls results partly from the small set of experimental data on such structures [Magenes, 2006; Cattari and Lagomarsino, 2013]. The aim of this part of the thesis was therefore to provide experimental evidence on the in-plane seismic behaviour of these mixed systems. Bearing this scope in mind, two RC-URM substructures, representing the most critical parts of a typical four storey Swiss mixed edifice, were built at two-third scale and tested under quasi-static cyclic loading. Each of the two specimens consisted of a two-storey RC wall coupled to a two-storey URM wall by two RC beams.

The quasi-static tests on the two sub-structures with both RC and URM walls have highlighted several features, typical of such mixed buildings (Paper I):

i) For both loading directions, the displacement capacity of the test units was limited by the failure of the URM walls. At failure, in fact, the RC walls were still in their pre-peak response and they did not exploit their total displacement capacity as they were designed for a fully ductile response.

ii) The interaction between shear (URM) and flexure (RC) dominated walls modified the global deflected shape of the structure, providing a rather linear displacement profile over the height (Figure 1). As a consequence, unlike URM structures where the damage is concentrated in the bottom storey, adding RC walls led to a better distribution of the damage over the height of the building (Figure 2a). Due to the addition of the RC walls, in fact, the two storeys were subjected to similar drift demands and damage patterns. This had also been observed in dynamic tests on four-storey mixed buildings [Beyer et al., 2014; Jurukovsky et al., 1992].

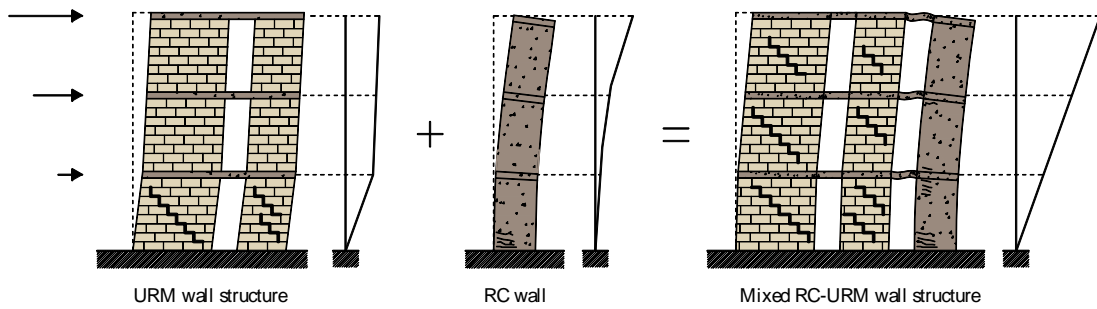


Figure 1: Effect of the interaction between URM and RC walls on the global deflected shape of a mixed system.

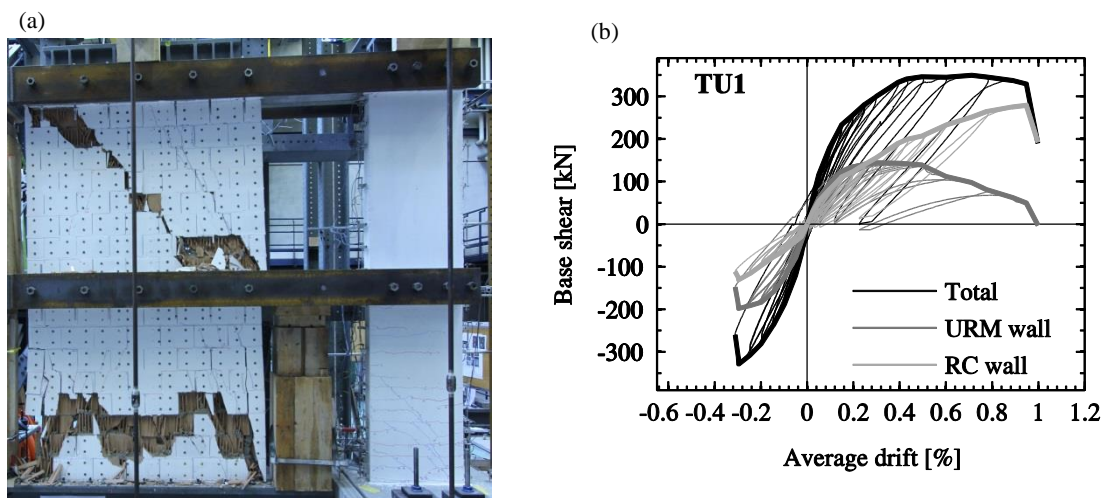


Figure 2: TU1: crack pattern after failure (a) and base shear- average drift relation (b).

iii) In mixed structures the RC walls are often situated at the perimeter of the building as they accommodate lift shafts or staircases. In addition, when the RC walls are added as a retrofit intervention rather than during the original design, an even plan distribution of the walls is difficult to achieve. The two test units simulated such a plan asymmetry and showed that the global force-displacement response is affected by the loading direction. In particular, a factor of three between the displacement capacity associated with the positive and negative loading directions was found (Figure 2b). The critical loading direction was that for which the axial force at the base of the URM wall increased, since an increase in axial stress reduces the deformation capacity of the URM walls [Petry and Beyer, 2014].

3 Contributions derived from the numerical simulations

The evaluation of the seismic response of buildings with both RC and URM walls can be carried out by shell-element models or macro-modelling approaches. The latter are commonly used in engineering practice because of the reasonable compromise between accuracy of results and computational effort [Penna et al., 2013].

Results of numerical simulations, regardless of the modelling approach (shell-element or macro-model) and the analysed structural system (RC, URM or mixed buildings), are sensitive to the modelling assumptions and material properties. For buildings with both RC and URM walls, the parameters which most influence their structural behaviour are those affecting the strength and stiffness of the elements [Casoli, 2007; Paparo and Beyer, 2012]. For instance, when the RC members are modelled as bilinear, the assumed stiffness of the RC walls influences not only the distribution of the reaction forces among the walls, but also the global displacement profile of the system [Paparo and Beyer, 2012].

So far, numerical models could not be directly validated against experimental results of these mixed structures as experimental data were missing. In this part of the thesis, the collected data from the experimental campaign were used to validate two modelling approaches: a shell-element and a macro-model approach. The comparison between the numerical models and the experiments has been performed by checking *(i)* the failure modes, *(ii)* the displacement capacity of the system, *(iii)* the distribution of the reaction forces among the walls, and *(iv)* the global deformed shape.

It was found that both techniques were able to represent all the main features of the seismic behaviour of such mixed structures, except for the shell-model, which was not able to capture the ultimate displacement capacity. The reason stands in the occurrence of numerical issues for high levels of displacement demand. In addition, as mixed RC-URM wall buildings require the analysis of the complete structure to capture the interaction between shear and flexural dominated elements, computational time for shell-models can be too long. As a consequence, a macro-element approach, which follows the indications proposed in Paper II, seems the most suitable means for practically oriented analyses of complete mixed structures like those analysed in this thesis, since accurate results, with respect to a limited computational time, were obtained. A shell-model approach, instead, can be adopted for detailed studies of the mechanical behaviour of small substructures or when the irregular distribution of the openings does not allow the definition of the equivalent frame in the macro-model approach.

Paper II concludes with the analyses of some structural configurations of modern masonry buildings that have been retrofitted by adding or replacing reinforced concrete walls. The analyses, carried out with the macro-modelling approach, confirmed the beneficial effects of adding RC walls to URM buildings in terms of increased strength and displacement capacity (Figure 3).

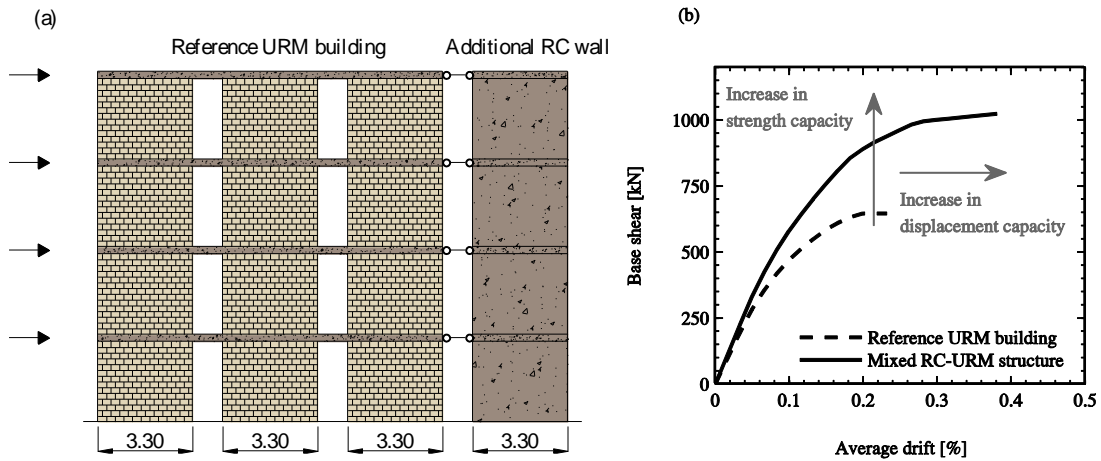


Figure 3: Base shear-average drift relation for a reference URM building and a mixed RC-URM structure. The mixed system features larger strength and displacement capacities, if compared to the reference URM building.

4 Contributions derived from the elaboration of the mechanical model

Over the last 50 years, a considerable amount of research work on the planar interaction between shear and flexural dominated systems has been carried out and simplified methods for analysing dual frame-wall systems have been proposed. One of these is the so-called “shear-flexure cantilever model”. This method assumes walls and frames as pure flexure and shear cantilevers which are continuously coupled together over the height by axially rigid links with zero moment capacity [e.g., Chiarugi, 1970; Rosman, 1974; Pozzati, 1980; Smith and Coull, 1991].

Given the similarities of mixed RC-URM buildings to dual frame-wall structures, the shear-flexure cantilever method was extended for analysing structures with both RC and URM walls. As the model represents structures attaining moderate to extensive damage, (SD limit state), the RC walls are expected to yield. In order to account for the formation of the plastic hinge at their base, the standard boundary condition, which assumes the flexure beam as fixed at the base (e.g., Pozzati [1980]), has been modified. The flexural cantilever, in fact, is modelled with a pinned-base connection to which an external moment, corresponding to the total flexural capacity of the RC walls, is applied (Figure 4a).

The proposed shear-flexure cantilever model was compared to several case studies analysed through non-linear analyses. It was found that the model predicts, with a reasonable degree of accuracy:

- i) The displacement profile over the height of the structure.
- ii) The height of the contra-flexure point of the RC walls $H_{CF,RC}$.

It was observed that three parameters are of particular importance for setting up the model: (i) α , which takes into account the mechanical (E and G) and geometrical (H , I and A) characteristics of the structure. (ii) β_{RC} , which describes the contribution of the RC walls to the overturning moment. (iii) n , the number of storeys. The same parameters are also strongly involved in the design process.

A parametric study, in which the effect of the three aforementioned parameters (α , β_{RC} , n) on the global displacement profile of such mixed systems, was then carried out. The results from this study were summarised in charts which can be used for the evaluation of the displacement profile of these mixed structures (Figure 4b).

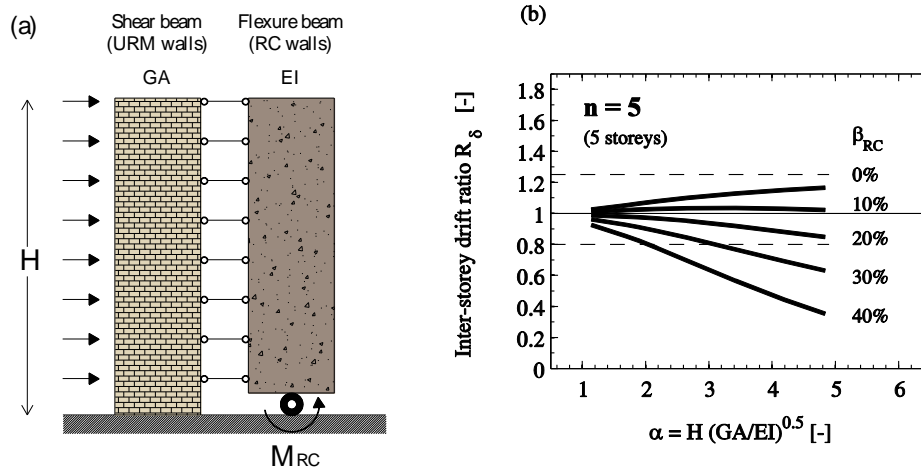


Figure 4: (a) definition of the mechanical model; (b) results, summarising the parametric study carried out with the mechanical model, which are used to estimate the displacement profile mixed buildings.

5 Contributions derived from the development of the design approach

Displacement-based design is a procedure aimed to determine the required strength of different structural systems to ensure that, under a specific level of seismic intensity, a selected performance state is achieved. One of such procedures, the direct displacement-based design approach, has been developed over the last 20 years [Priestley, 1993; Priestley, 1998; Priestley et al., 2007; Pennucci et al., 2011; Sullivan et al., 2012] with the objective of eliminating the weaknesses of the force-based design approach.

Even though in countries of low to moderate seismicity like Switzerland constructions which combine RC and URM walls are rather common, codes do not provide clear guidelines for their design. The objective of this part of the thesis was therefore to extend the DDBD for designing mixed RC-URM wall structures. A displacement-based rather than a force-based methodology was chosen as design approach since it provides a better representation of the real seismic behaviour of the investigated structure and allows the designer to exploit the structural capacities of the building.

In order to calculate the yield curvature of the RC walls, the methodology follows the DDBD approach developed for dual RC frame-wall buildings [Sullivan et al., 2005; 2006], as the structural behaviour of both mixed systems is similar. The methodology assumes that the

presence of concrete walls provides a linear displacement profile over the height. Such a hypothesis is checked at the end of the design with the shear-flexure cantilever model. The proposed procedure can be used to design structures reaching the SD limit state, design for operational limit states is not considered within this research.

Several case studies were analysed and the design outputs used to set up non-linear numerical models subjected to ground motions compatible with the design spectrum. The responses obtained from the inelastic time-history analyses (ITHA) were then compared to the design assumptions to gauge the proposed methodology:

i) Concerning the global displacement profile, the results from the simulations confirmed that the global displacement profiles were almost linear. Indeed, the insertion of the RC walls avoided concentrations of deformations in the bottom storey (Figure 5a), a typical feature of URM wall structures.

ii) It was observed that, particularly for the three storey configurations, the maximum displacement obtained from ITHA was somewhat lower than the design value (between 60% and 70% the design value). This is probably due to how the period dependency of the equivalent viscous damping of the URM walls is accounted for.

iii) From the revision of the hysteretic response, it was possible to see that the URM walls showed a dominant shear behaviour and dissipated a large amount of energy (Figure 5b). This confirms that the values of ξ_{sys} found from the design approach between 15% and 25%, are consistent with the results obtained from ITHA. Also the distribution of the reaction forces among URM and RC walls resulted rather satisfactory.

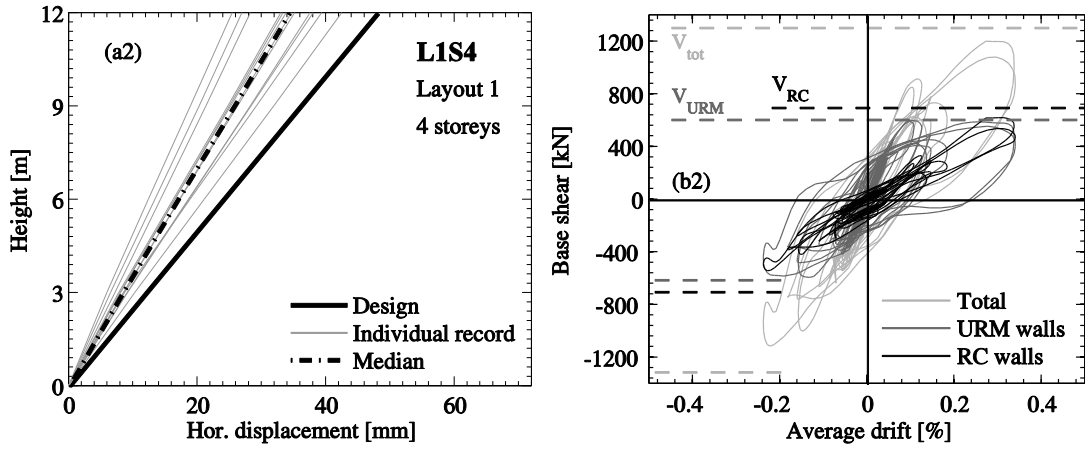


Figure 5: Time-history response for one case study. Displacement profile (a). Hysteretic behaviour of the mixed structure subjected to one single record and comparison against design values (b).

6 Outlook

On the basis of this study, several topics on which further research is needed can be defined. The following are possible areas of interest:

i) Inelastic displacement demand for short period structures: Comparisons between the responses obtained from ITHA and the design values have shown that the proposed DDBD procedure overestimates the maximum displacement for the configurations with the smallest effective periods ($T_e \approx 0.6s$). This overestimation is, most likely, due to the approximated evaluation of the period dependency of ξ_e and can be solved, for example, by relating the inelastic seismic demand to the demand slope factor [Pennucci et al., 2011].

ii) Extension of the procedure to three-dimensional buildings: The design procedure can be easily extended to three-dimensional buildings, if the plan configuration is regular enough to neglect any torsional effect. If it is not the case, the torsional effects can be taken into account with a two-step procedure. (i) The increased drift demand of the walls due to the twist is evaluated following the indications proposed by Priestley et al. [2007] for the design of URM buildings. (ii) The design displacement of the centre of mass is reduced to keep the drift demand of the URM walls within the design drift limit δ_d .

iii) Force-based approach for the design of mixed RC-URM wall structures: In this thesis the seismic design was limited to the displacement-based approach. However, the development of a force-based methodology is also needed. This will require investigations to gain insight into the definition of the q -factor for mixed RC-URM wall structures. In addition, concerning elastic code-based analyses, examinations of the distribution of the reaction forces between the structural systems must be carried out.

iv) Effects of deformable foundations: The DDBD applied for mixed RC-URM wall buildings is sensitive to the ratio of the base moment provided by the RC walls (β_{RC}) as it influences the required length of the RC walls (l_{RC}). As studies carried out on dual RC frame-wall structures have shown that foundation compliance may affect their response [Paulay and Priestley, 1992], it would be interesting to investigate this effect on mixed RC-URM wall structures and its consequences in the design.

v) Effect of URM spandrels: The effect of masonry spandrels should be investigated. Attention ought to be focused when they flank the RC walls as this could decrease the bending mode of the RC walls, leading to a more shear critical behaviour. Furthermore, the accuracy of the shear-flexure cantilever model for estimating $H_{CF,RC}$ when masonry spandrels flank the RC walls should be verified.

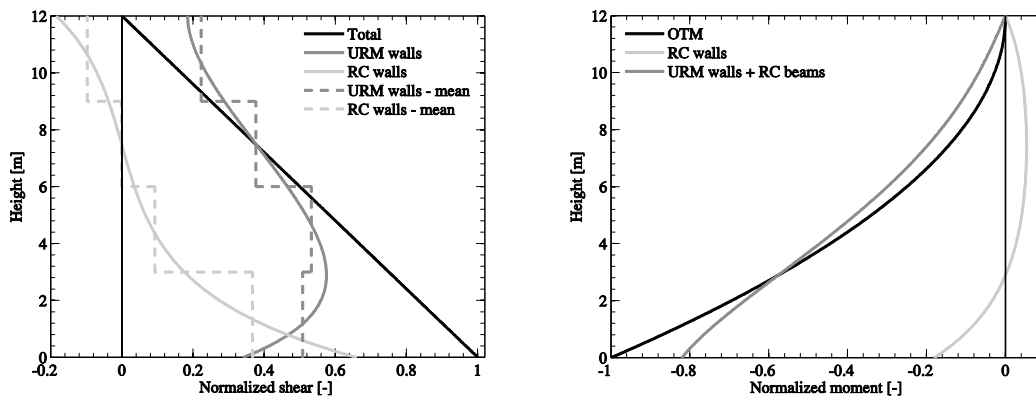


Figure 6: Distribution over the height of the shear force and moment (estimation with the mechanical model).

vi) Shear-flexure cantilever model: Further comparisons between the mechanical model and non-linear analyses could be carried out to validate the force distribution over the height between RC and URM walls (e.g., Figure 6). In addition, the shear-flexure cantilever model can be used in the design of other mixed systems where flexural and shear dominated members are coupled.

vii) Additional tests: On the basis of the aforementioned areas of interest, additional tests could be carried out. For example the influence of masonry spandrels flanking the RC walls can be experimentally investigated. Figure 7 shows a set-up for testing half-scale mixed RC-URM structures in which the main parameter under study is the effect of the masonry spandrels. The test units could be designed according to the proposed DDBD procedure to check also experimentally the design approach.

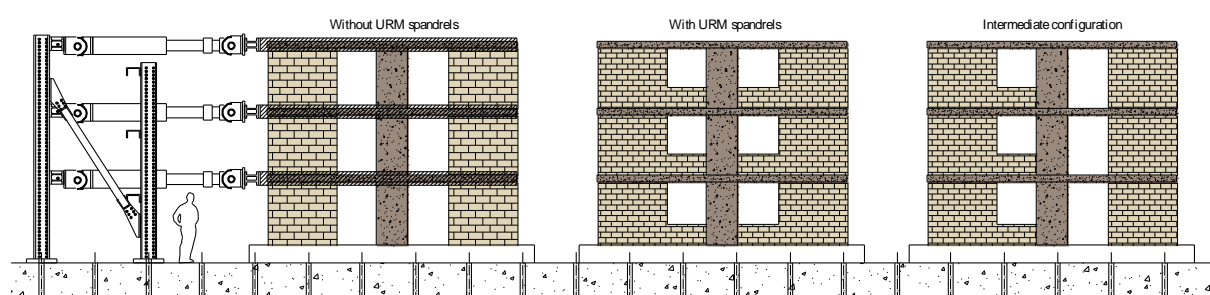


Figure 7: Envisaged test set-up and test units for quasi-static cyclic tests on 3-storey mixed RC-URM wall buildings.

7 References

- Beyer, K., Tondelli, M., Petry, S. and Peloso, S. [2014] “Dynamic testing of a 4-storey building with reinforced concrete and unreinforced masonry walls”, to be submitted to *Bulletin of Earthquake Engineering*.
- Casoli, D. [2007] “Assessment of existing mixed RC-Masonry structures and strengthening by RC shear walls”, Pavia, Italy.
- Cattari, S. and Lagomarsino, S. [2013] “Seismic design of mixed masonry-reinforced concrete buildings by non-linear static analyses”, *Earthquakes and Structures*, Vol. 4, N°3.
- Chiarugi, A. [1970] “Indagine sulla ripartizione delle azioni orrizzontali in telai irrigiditi da pareti”, *Giornale del Genio Civile*, 2, 187-203.

- Jurukovski, D., Krstevska, L., Alessi, R., Diotallevi, P.P., Merli, M. and Zarri, F. [1992] “Shaking table tests of three four-storey brick masonry models: original and strengthened by RC core and by RC jackets”, *Proc. of 10th World Conference on Earthquake Engineering*, Madrid, Spain.
- Lang, K. [2002] “Seismic vulnerability of existing buildings”, Ph.D. thesis, ETH Zurich, Zurich, Switzerland.
- Magenes G. [2006] “Masonry building design in seismic areas: recent experiences and prospects from a European standpoint” Keynote address, *Proc. of 1st European Conference on Earthquake Engineering and Seismology*, Geneva, Switzerland.
- Paparo, A. and Beyer, K. [2012] “Pushover analyses of mixed RC-URM wall structures”, *Proc. of 15th World Conference on Earthquake Engineering*, Lisbon, Portugal.
- Paulay, T. and Priestley, M.N.J. [1992] *Seismic design of reinforced concrete and masonry buildings*, John Wiley & Sons, Inc., New York.
- Penna, A., Lagomarsino, S. and Galasco, A. [2013] “A nonlinear macro-element model for the seismic analyses of masonry buildings”, *Earthquake Engineering and Structural Dynamics*, 10.1002/eqe.2335.
- Pennucci, D., Sullivan, T.J. and Calvi, G.M. [2011] “Displacement reduction factors for the design of medium and long period structures”, *Journal of Earthquake Engineering*, 13(S1), 1-29.
- Petry, S. and Beyer, K. [2014] “Influence of boundary conditions and size effect on the drift capacity of URM walls”, *Engineering Structures*, 65, 76-88.
- Pozzati, P. [1980] *Teoria e tecnica delle strutture*, UTET, Torino.
- Priestley, M.J.N. [1993] “Myths and fallacies in earthquake engineering – conflict between design and reality”, *Bulletin, NZ National Society for Earthquake Engineering*, 26(3), 329-341.
- Priestley, M.J.N. [1998] “Direct displacement-based design of buildings”, *Proc. of 11th European Conference on Earthquake Engineering*, Paris, France.
- Priestley, M.J.N., Calvi, G.M. and Kowalsky, M.J. [2007] *Displacement-Based Seismic Design of Structures*, IUSS Press, Pavia, Italy.
- Rosman, R. [1974] “Stability and dynamics of shear-wall frame structures”, *Building Science*, 9, 55-63.
- Share Project [2013] <http://www.share-project.org/>.

- Smith, B.S. and Coull, A. [1991] *Tall building structures: analysis and design*, John Wiley & Sons, Inc., New York.
- Sullivan, T.J., Priestley M.J.N. and Calvi, G.M. [2005] “Development of an innovative seismic design procedure for frame-wall structures”, *Journal of Earthquake Engineering*, 10 (Special Issue 1), 91-124.
- Sullivan, T.J., Priestley M.J.N. and Calvi, G.M. [2006] “Direct displacement-based design of frame-wall structures”, *Journal of Earthquake Engineering*, 9 (Special Issue 2), 279-307.
- Sullivan, T.J., Priestley M.J.N. and Calvi, G.M. [2012] *A Model Code for the Displacement-Based Seismic Design of Structures*, IUSS Press, Pavia, Italy.

Appendix

Appendix

1 Introduction

This appendix provides additional information on the two quasi-static cyclic tests carried out at EPFL on two mixed reinforced concrete-unreinforced masonry (RC-URM) wall structures. The first part of the appendix outlines the test objectives and the organisation of the data, which are available to the public. In the second part of the appendix, additional photos of the two specimens, showing the evolution of the crack patterns, are provided.

2 Test objectives

The test campaign focuses on the seismic behaviour of mixed RC-URM wall structures representative of residential buildings in Switzerland (their detailed description is presented in the introduction of the thesis). Although such mixed systems are rather common in countries of low to moderate seismicity, current seismic design codes do not address such mixed structures. It is believed that the development of guidelines has been hindered by the lack of experimental evidence, against which numerical and mechanical models could be validated.

To improve the understanding of such mixed systems, a research programme was started at EPFL. Within this programme, two quasi-static cyclic tests on two-third scale models (TU1 and TU2) representing a prototype structure have been carried out. The two storey specimens are composed of one RC wall coupled to a one URM wall by two RC beams (Figures 1 and 2). For a detailed description of the specimens and the test set-up, the reader is referred to Paper I. The objectives of this test campaign were (*i*) to measure the distribution of the reaction forces

3 Organisation of the test data

This part of the appendix presents the experimental data gathered from the two tests. Section 3.1 specifies the instruments used during the tests to monitor global and local quantities. Section 3.2 follows with a description of the organisation of the folders containing photos and data.

3.1 Instrumentation

The two specimens (TU1 and TU2) were instrumented with a series of conventional measurement devices (i.e., load cells, LVDTs, strain gauges and omega gauges). Figure 3 shows the instrumentation used for calculating the global quantities (i.e., the reaction forces at the base of the walls, the storey displacements and the foundation displacements). Next to global quantities, elongations and shear deformations of the RC walls were measured with LVDTs (Figures 4a and 4b). Positive values from the LVDTs correspond to a shortening of the base length of the measurement. Concerning the measurement of the shear deformations of the RC walls, the positions of Diag3, Diag4, Diag7 and Diag8 were slightly changed from TU1 to TU2. Figure 4b represents the instrumentation layout of TU1 with solid lines and the instrumentation layout modified for TU2 with dashed lines. In TU2, the sliding of the RC wall base with respect to the RC foundation was also measured (Figure 4a). A series of strain gauges measured the strain in the central longitudinal reinforcing bars of the RC beams (Figure 5). Positive values from the gauges correspond to tensile strains. Before testing, the strain gauges were checked and, in the positions where the strain gauges were not working, additional omega gauges were installed as presented in Figure 5 (two omega gauges were installed in TU1 and one in TU2). Positive values from the gauges correspond to a shortening of the base length of the measurement.

The deformation pattern of the URM walls was recorded by using the LED-based optical measurement device “Optotrack” from NDI [NDI, 2009]. The system worked with two position sensors. Each of them consists of three digital cameras that record the 3D-coordinates of the LEDs. The LEDs were glued onto the URM wall following a regular 150 mm x 100 mm grid (Figure 6a), except for the LEDs close to the rod and the C-section beams, for which the grid was slightly altered. In Figure 6a, the standard dimensions of the grid are represented only in the bottom-north corner of the URM wall. The figure also shows the dimensions of the altered part

of the grid. Additional LEDs were glued onto the steel foundation under the URM wall, the C-section beams and the RC beams (Figures 6a and 6b).

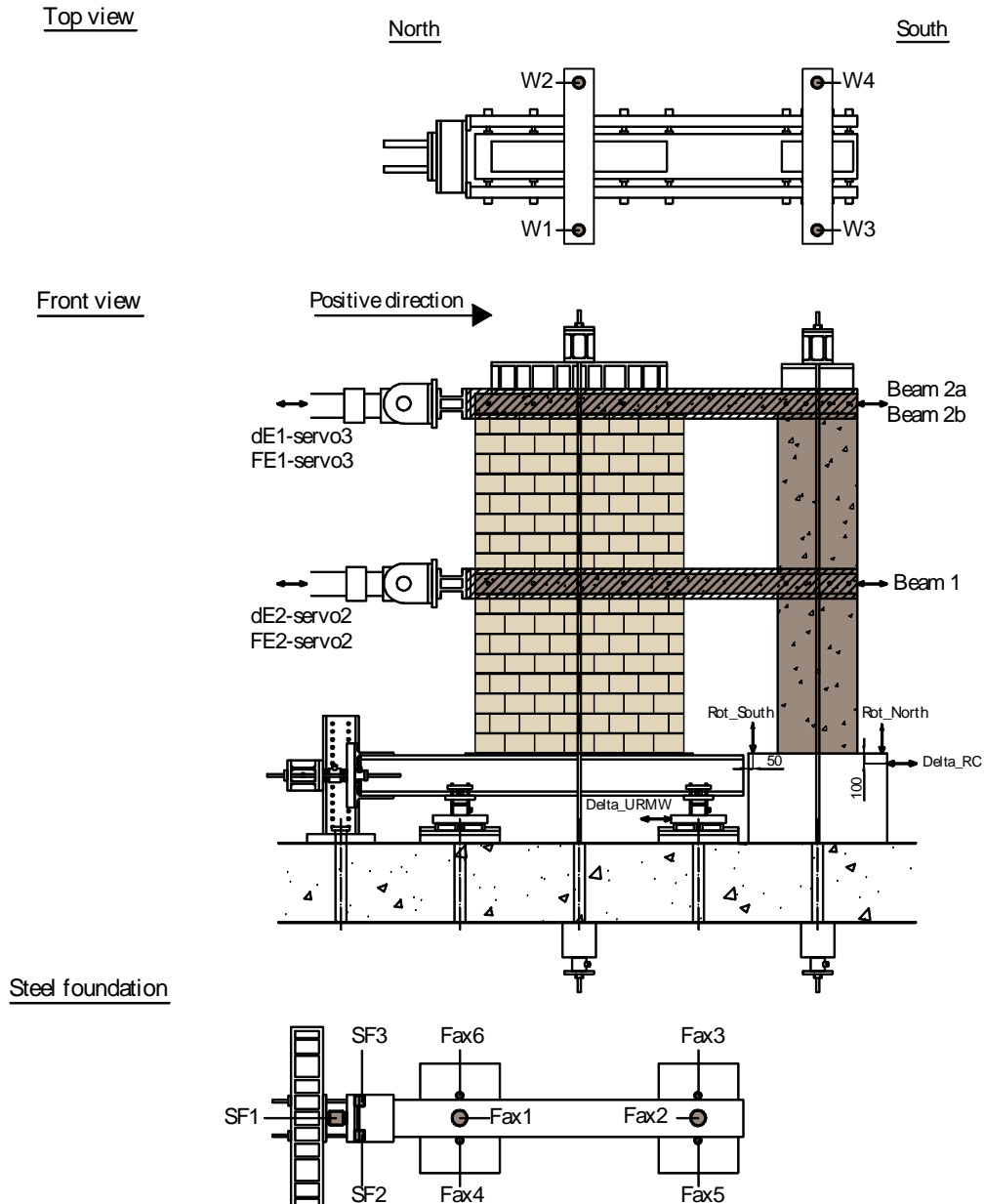


Figure 3: Test set-up with the devices to measure the global response of the specimens and the displacements of the foundations.

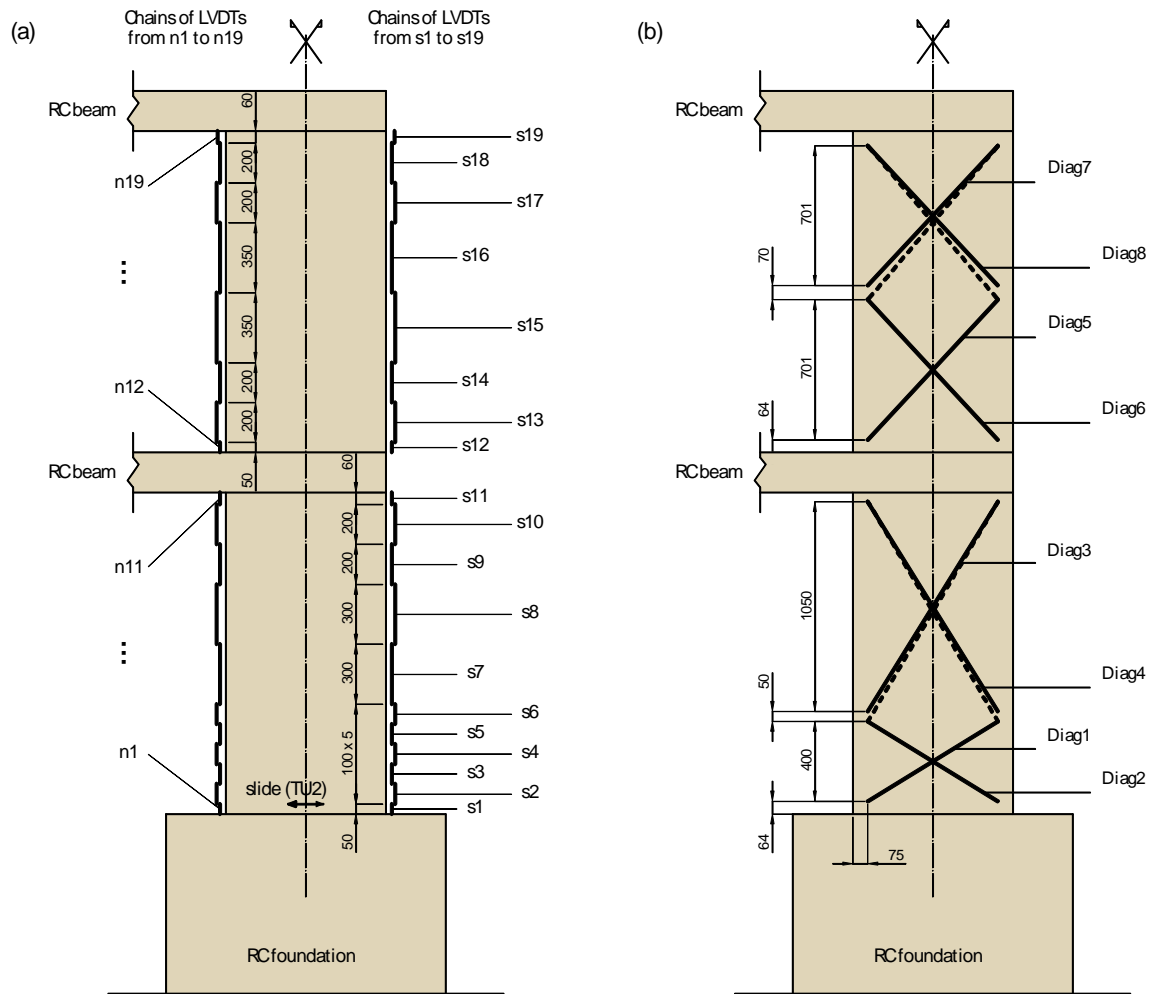


Figure 4: (a) location of the LVDTs to measure the elongation of the edges of the RC wall and the sliding displacement at the RC wall base (TU2 only); (b) LVDTs to measure the shear displacement of the RC wall.

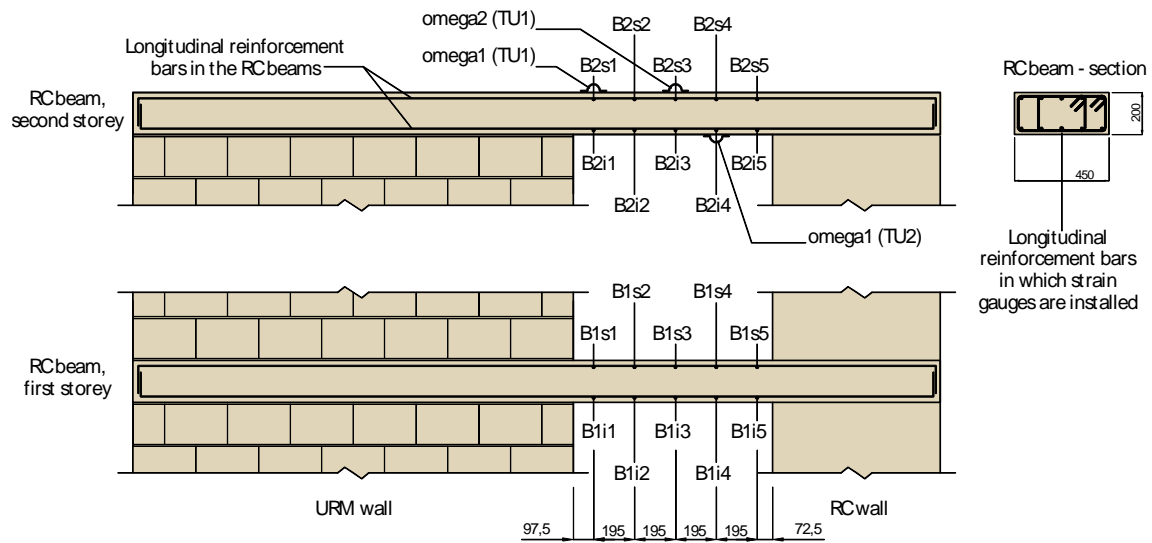


Figure 5: Strain gauges on the reinforcing bars of the RC beams. Omega gauges replacing the strain gauges that were not working in TU1 and TU2.

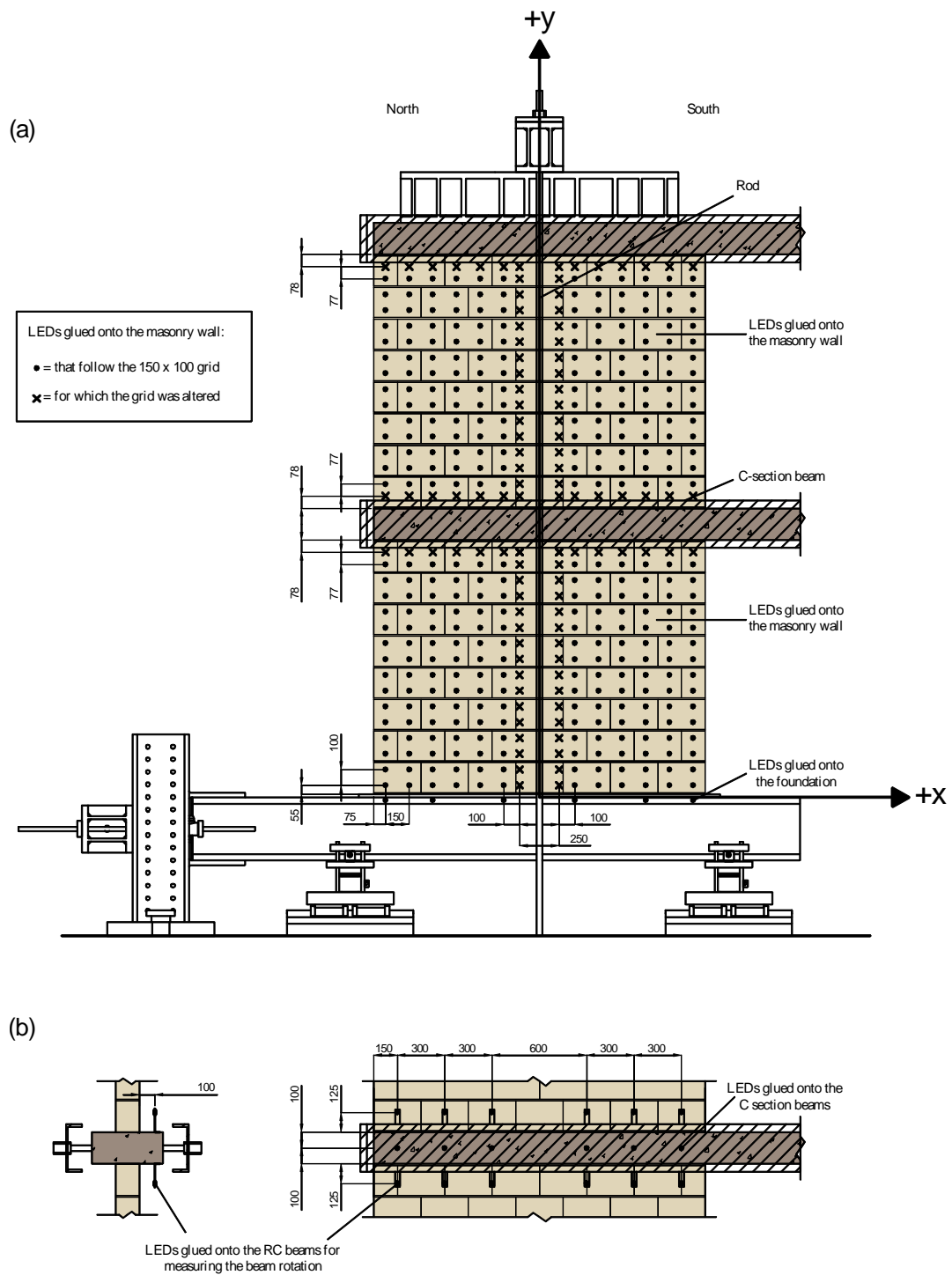


Figure 6: Optical measurement system. (a) LEDs glued onto the URM walls and the steel foundation and sign convention; (b) LEDs glued onto the C-section beams and the RC beams.

3.2 Test data

3.2.1 Data organisation

The data can be downloaded as one zip file from http://eesd.epfl.ch/data_sets. Upon unzipping, the folder structure unfolds as follows (Figure 7). Firstly, the data are organised by specimen (TU1, TU2). For each test unit, there are three folders containing “photos”, “unprocessed_data” and “processed_data”. In addition, each specimen folder contains one file “metadata_conventional_channels.xlsx” that contains information on the instruments used.

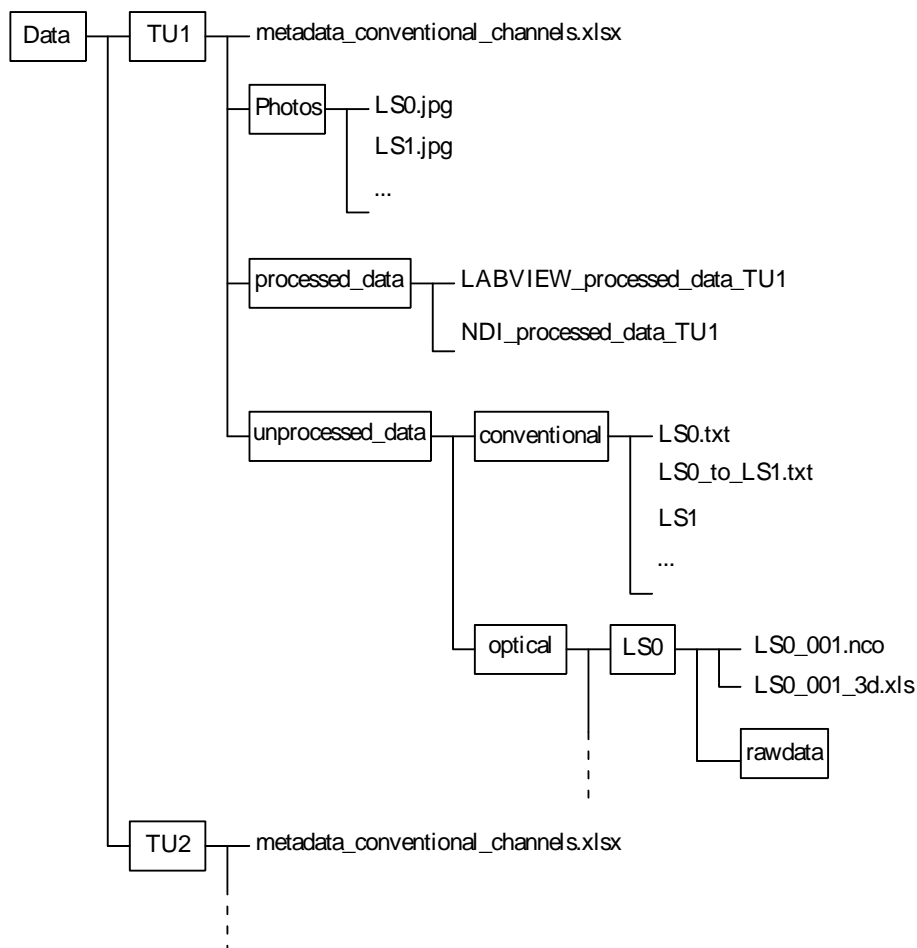


Figure 7: Organisation of the data for TU1 and TU2.

3.2.2 Photos

In addition to the conventional and optical measurements, photos were taken during the test to document the crack pattern of the specimens. Photos are taken at each load step, that is at peak horizontal displacement, and are labelled as “LSxx.JPG”, where xx stands for the load step. At each load step, the cracks were marked with blue and red pens to make them visible in the photos. Cracks that were noticed for the first time at load steps in the positive direction of loading (LS2, LS4, etc.) were marked with blue pens, whereas cracks noticed for the first time at load steps in the negative direction of loading (LS3, LS5, etc.) were marked with red pens. Before the application of the vertical load for TU1, the crane of the laboratory was accidentally hooked up to one C-section beams and uplifted the specimen. This resulted in a horizontal crack running through the top mortar layer of the first storey of the URM wall. This crack was marked in black. However, with the application of the vertical load, this horizontal crack closed and had no influence on the global behaviour of the specimen.

3.2.3 Unprocessed conventional measurement data

The conventional measurements were recorded by using the software LabVIEW (<http://www.ni.com/labview/>). The files, containing the unmodified outputs of the system, are comprised of the following:

- The measurements of forces and displacements of the two horizontal actuators (FE1-servo3, FE2-servo2, dE1-servo3, dE2-servo2);
- The measurements of axial loads applied at the top of the walls (W1, W2, W3, W4);
- The measurements of the load cells at the base of the URM walls (SF1, SF2, SF3, Fax1, Fax2, Fax3, Fax4, Fax5, Fax6);
- The measurements of the LVDSs (Beam1, Beam2a, Beam2b, n1 to n19, s1 to s19, Diag1 to Diag8, Slide, Rot_North, Rot_South, Delta_RC, Delta_URM);
- The measurements of the strain gauges (B1i1 to B2s5) and of the omega gauges (omega1, omega2);
- The voltage channel “NDI”, which was exported from the NDI system to indicate when the optical measurement system was recording. The conventional measurement system was always started before and stopped after the NDI system.

Before the first horizontal load failure (LS27 for TU1 and LS33 for TU2), the measurements are labelled as follows: “LSxx_to_LSxx+1” to indicate the measurement during loading and “LSxx” to indicate the measurement while holding the position at one load step. When the loading is interrupted during the night, the files are labelled as “LSxx_to_0” and “0_to_LSxx+1” and contain the corresponding half load steps with the unloading and the re-loading part.

After the first horizontal failure, the applied horizontal force was held at the maximum value for around one minute and then reduced to zero to avoid the vertical load failure of the specimen during the visual inspection of the unit. As a consequence, the measurements were carried out from zero horizontal force to zero horizontal force (i.e., zero horizontal force → nominal drift → zero horizontal force). Different labelling for TU1 and TU2 was used, and Figure 8 resumes the names of each measurement with respect to the nominal drift.

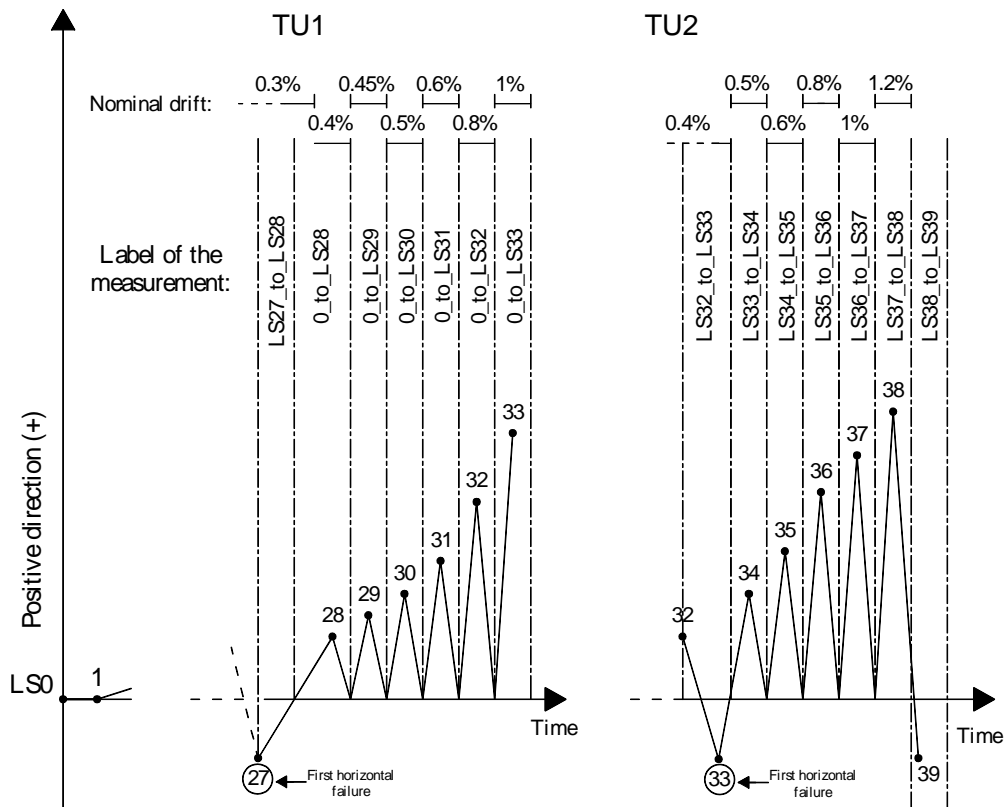


Figure 8: Labels of the measurements for TU1 and TU2 after the first horizontal failure (LS27 and LS33).

3.2.4 Unprocessed optical measurement data

The folder “optical” contains the data measurements from the NDI system. For each recording sequence, the system created a separate folder that contains the data in the specific NDI-format and the measurement data exported to Excel. The folder names are organised as the conventional measurements (e.g., LSxx_to_LSxx+1).

In each Excel-file, the first three lines indicate the included number of frames, the recorder frequency in Hz and the units for the coordinate measurements. After one blank line, the data are organised into columns. The first one contains an index starting from 1. The second and following columns store the x-, y- and z- coordinate for each marker. The labels of these columns are for LED number_1 (Marker_1x, Marker_1y and Marker_1z). At this stage the LED numbers are random. When the LED coordinates of one marker were not visible to the position sensors, the corresponding columns are blank.

3.2.5 Processed conventional measurement data

The channels measuring the local deformations (n1 to n19, s1 to s19, Diag1 to Diag8, B1s1 to B2i5) were shifted to zero in such a way that the displacement at LS0 corresponds to zero. Furthermore, the conventional data were processed to remove any bias or data that are not linked to the actual behaviour of the test data (e.g., offsets because conventional instruments were moved during testing).

In addition to the recorded channels, a set of computed channels was added to the processed data. The objective of these channels is to allow the user to quickly plot fundamental graphs, such as the base shear-average drift. Table 1 defines the computed channels.

Beam2 is the average horizontal top displacement and SF_{urm} is the shear force at the base of the URM wall. F_e is the total force applied by the two horizontal actuators and SF_{rc} is the shear force at the base of the RC wall. $N1$ and $N2$ are the vertical forces measured at the base of the URM wall (Figure 9b) and W is the total axial load applied at the top of the URM and RC wall by the four hollow core jacks.

Table 1: Computed channels

Channel number	Channel name	Unit	Formulae / Explanation	Sign convention
114	<i>index</i>	-	<i>Counter of the row</i>	-
115	<i>Beam2</i>	mm	$\frac{Beam2a + Beam2b}{2}$	+ = towards south
116	SF_{urm}	kN	$SF1 + SF2 + SF3$	+ = for positive loading direction (Figure 12)
117	F_e	kN	$FE1 + FE2$	
118	SF_{rc}	kN	$F_e - SF_{urm}$	
119	$N1$	kN	$Fax1 - Fax4 - Fax6$	+ = pushing to bottom
120	$N2$	kN	$Fax2 - Fax3 - Fax5$	
121	W	kN	$W1 + W2 + W3 + W4$	
122	$M3$	kNm	$\frac{0.05 \cdot d_m}{2} SF1$	+ = for positive loading direction
123	$N3$	kN	$\frac{2 \cdot N3}{l_h}$	- = pushing to top
124	ΔN	kN	$N1 + N2 - N3$	+ = pushing to bottom
125	N_{urm}	kN	$W1 + W2 + \Delta N + 60kN$	
126	N_{rc}	kN	$W3 + W4 - \Delta N + 25kN$	
127	M_{urm}	kNm	$(-N1 + N2) \cdot a + N3 \cdot b + SF_{rc} \cdot c$	+ = for positive loading direction
128	OTM	kNm	$FE1 \cdot d_2 + FE2 \cdot d_1$	
129	Tl	kNm	$\Delta N \cdot l_{aw}$	
130	M_{rc}	kNm	$Tl - OTM - M_{urm}$	+ = towards south
131	<i>Drift</i>	%	$\frac{Beam2}{H_{top}} \cdot 100$	

$M3$ is the moment that the rotational hinges (GX45F), part of the system to measure the horizontal reaction force, transmit. The equation, provided by the hinge producer (SKF, <http://www.skf.com>), assumes friction equal to 0.05 [-] and d_m (diameter of the hinge) equal to 89.2 mm. $N3$ is the parasitic force generated by the two rotational hinges and l_h is the distance between the two hinges that is equal to 174 mm (Figure 9a).

ΔN is the variation in axial force at the base of the walls due to the applied horizontal force ($\Delta N_{rc} = -\Delta N_{urm}$). N_{urm} and N_{rc} are the axial forces at the base of the two walls and are calculated by adding to the variation of the axial force ΔN the vertical forces applied by the hollow core jacks plus the self-weight of the test unit and parts of the test set-up supported by the walls.

M_{urm} is the moment at the base of the URM wall. a , b and c are the lever arms of the reaction forces with respect to the centre of the URM wall (point A, Figure 9b) and are equal to 1200 mm, 2445 mm and 220 mm, respectively. OTM is the total overturning moment and d_1 and d_2 correspond to the height of the two actuators and are equal to 3520 mm and 1710 mm. Tl is the contribution of the RC beams to OTM and l_{aw} is the distance between the two wall axes, which is equal to 2400 mm. M_{rc} is the moment at the base of the RC wall.

Drift is the average drift of the specimen (H_{top} is equal to 3520 mm). Channels 115 to 118, 124 and 127 to 131 were shifted to zero in such a way that the measurements at the beginning of LS1 correspond to zero (*index* = 601 for TU1; *index* = 2501 for TU2).

The processed conventional data are saved in a txt file. The first two lines of the file assign the name of the channel and the unit. When channels are empty, the numerical values are replaced with “NaN”.

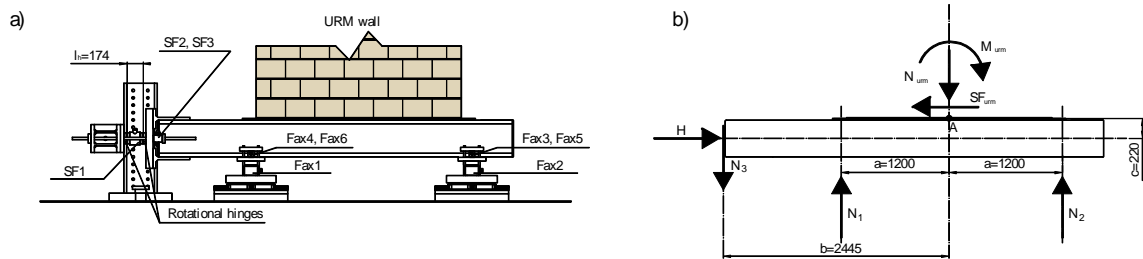


Figure 9: Steel beam with the system to measure the horizontal and vertical forces at the base of the URM wall (a); free body diagram of the steel beam with reaction forces (b). All dimensions in mm.

3.2.6 Processed optical measurement data

The data acquired from the two position sensors were merged together and the coordinate system was rotated and shifted to align the axes with the x- and y-axes as indicated in Figure 6. The LEDs glued onto the URM walls were then re-numbered from 1 to 448 from the bottom-north corner of the first storey (Marker_1) to the top-south corner of the second storey (Marker_448). These markers are then followed in the numeration by the markers glued onto the steel foundation, the RC beams and the C-section beams. The optical measurement data at each load step were averaged and condensed to one measurement point. The processed optical

data are saved in a txt file. The first two lines of the file assign the name and the coordinate measurement of each LED and the following lines store the -x, -y and -z coordinates at each load step starting from LS0.

4 Additional photos describing the progressive damage in the test units

This section provides photos describing the damage evolution of the two specimens for several limit states associated with the nominal drifts summarised in Table 2.

Table 2: Limit states and corresponding nominal drifts

Limit state	TU1	TU2
No significant stiffness degradation of the URM walls	+0.1%	+0.1%
Horizontal load failure of the test units for the negative loading direction	-0.3%	-0.4%
URM wall heavily damaged (*) for the positive loading direction	+0.6%	+0.6%
Onset of horizontal load failure of the units for the positive loading direction	+0.95%	+1.12%

(*): strength of TU1's URM wall dropped by ~20%; crack pattern of TU2's URM wall mainly developed

4.1 TU1

4.1.1 No significant stiffness degradation of the URM wall ($\delta = +0.1\%$)

At an average drift δ equal to +0.1%, very small shear cracks following the joints started forming in the URM wall (Figure 10a). In the RC wall, small flexure cracks in the first storey were detected (Figure 10b).

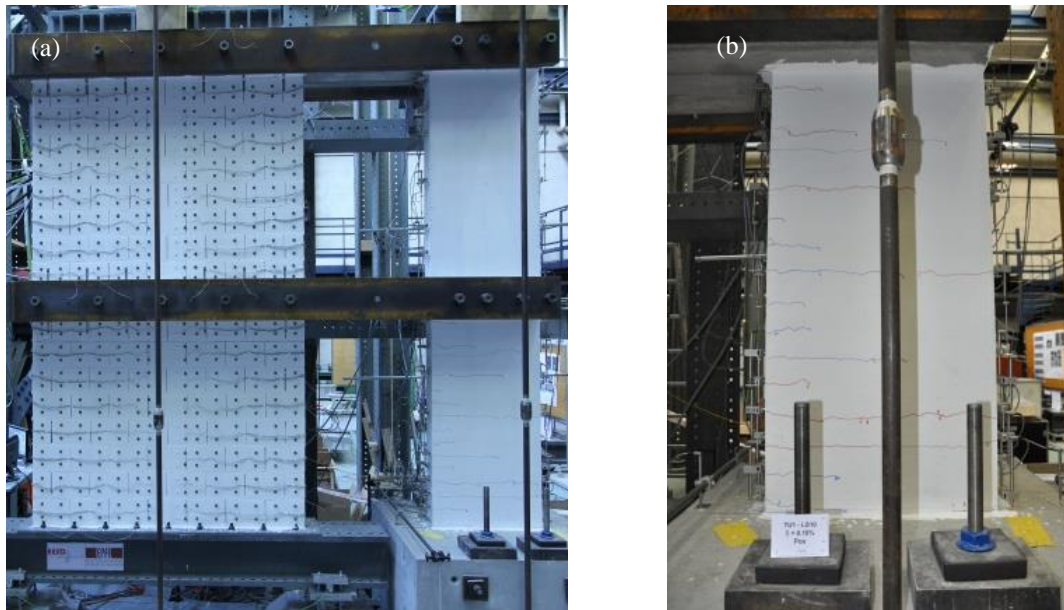


Figure 10: Crack pattern at LS10, $\delta = +0.1\%$. (a) specimen; (b) RC wall, first storey.

4.1.2 Horizontal load failure of the unit for the negative loading direction ($\delta = -0.3\%$)

At LS27, when the target average drift of $\delta = -0.3\%$ was reached, the horizontal load was stopped, photos were taken and cracks were marked. In the first storey of the URM wall, inclined shear cracks and the onset of toe-crushing were observed. In the second storey of the URM wall, only thin inclined shear cracks appeared (Figures 11a, 12a and 12b). During the crack marking, a relaxation in the URM wall occurred: the number of cracks in the compressed corner grew, the shear strength of the URM wall rapidly decreased and the specimen attained horizontal load failure. In order to avoid axial load failure of the URM wall, the horizontal load was reduced to zero. Figures 11b, 12c and 12d show the specimen crack pattern after the strength degradation of the URM wall.

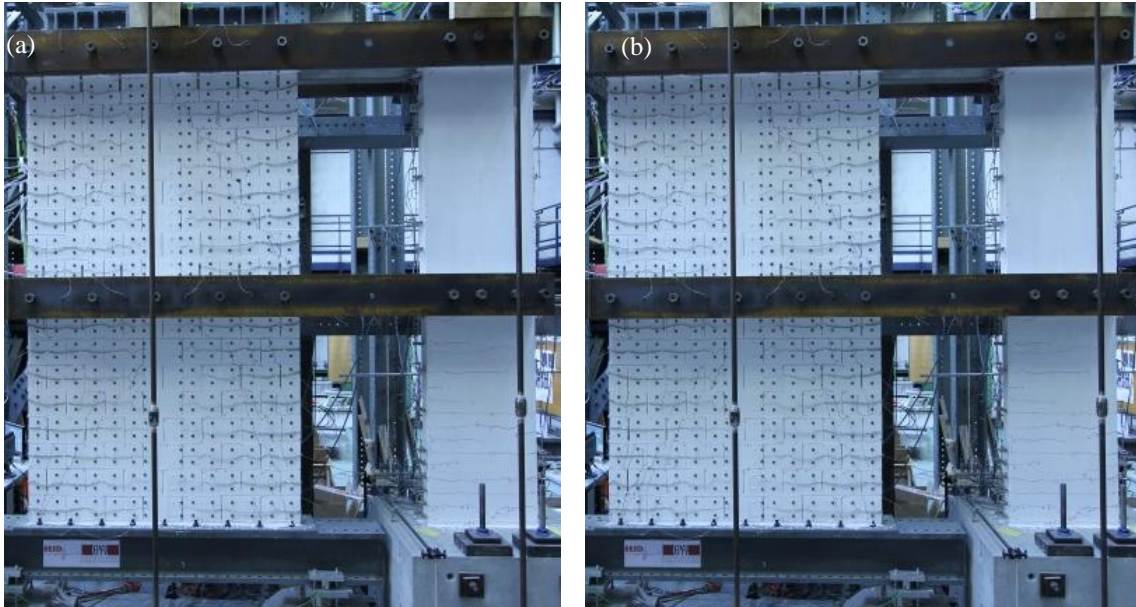


Figure 11: Specimen crack pattern at LS27, $\delta = -0.3\%$. Before (a) and after (b) the horizontal load failure.

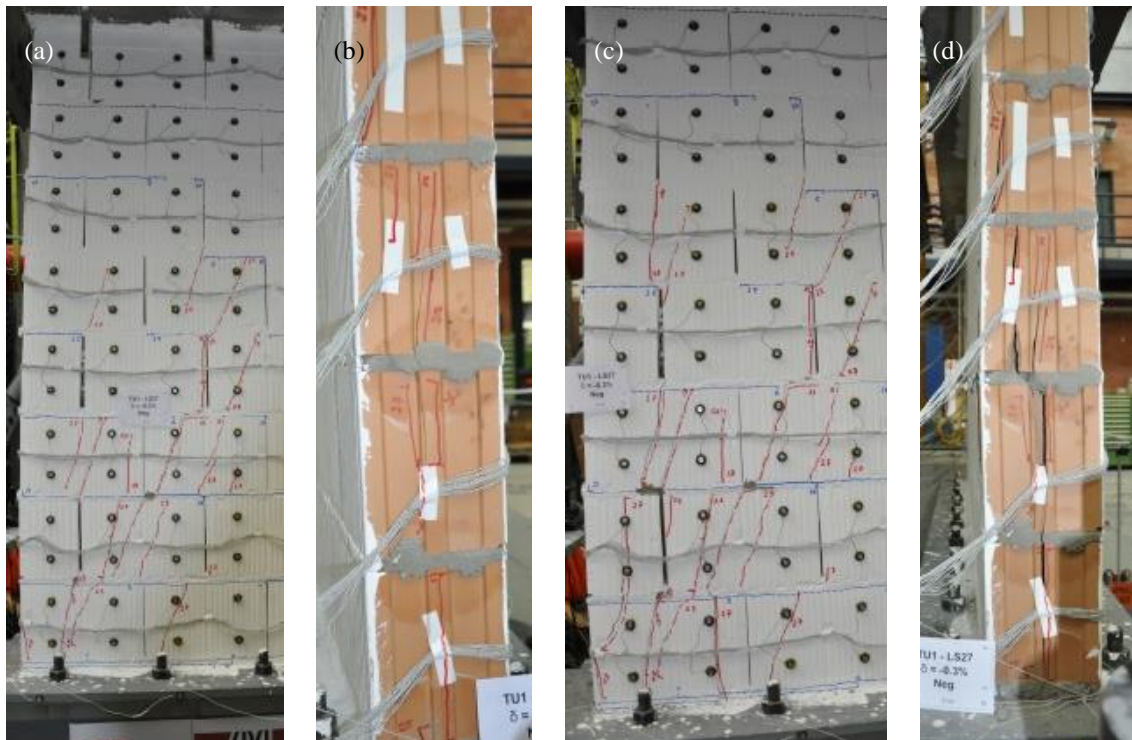


Figure 12: Crack pattern at LS27 ($\delta = -0.3\%$) of the compressed corner of the first storey of the URM wall. Before (a, b) and after (c, d) the horizontal load failure.

4.1.3 URM wall heavily damaged for the positive loading direction ($\delta = +0.6\%$)

At LS31, the URM wall was heavily damaged: steeply inclined shear cracks passing mainly through bricks were detected in both storeys of the URM wall (Figures 13a, 13c and 13d). At this load step, the strength of the URM wall dropped by around 20%. Figure 13b shows that the extent of the curvature penetration of the first storey RC beam into the URM wall was around 60 cm.

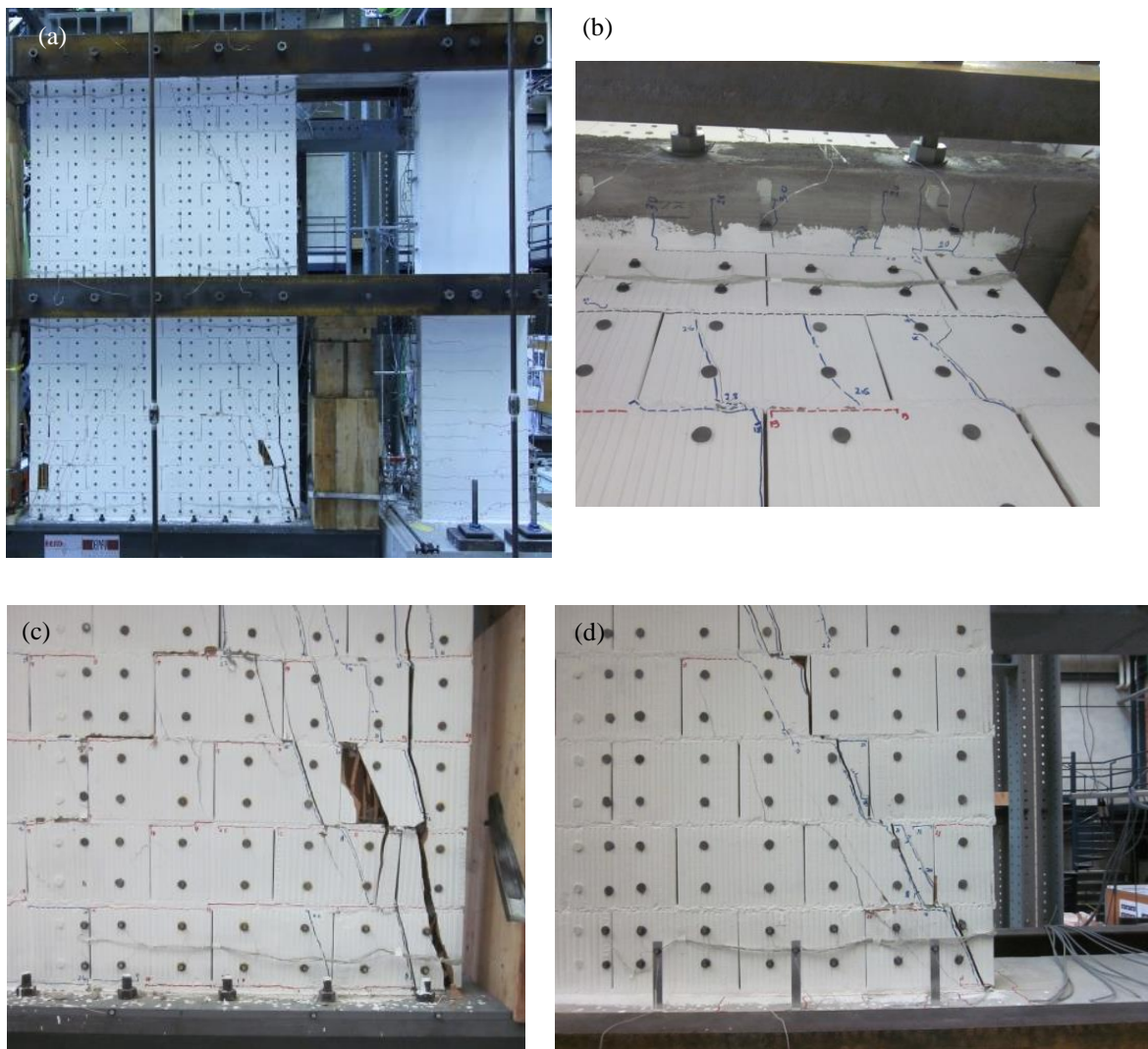


Figure 13: Crack pattern at LS31, $\delta = +0.6\%$. (a) specimen; (b) RC first storey beam, curvature penetration into the URM wall; (c, d): compressed corner of the first and second storey of the URM wall.

4.1.4 Horizontal load failure of the unit for the positive loading direction ($\delta = +0.95\%$)

Horizontal load failure of TU1 occurred during the half cycle with $\delta = +0.95\%$ (LS33), i.e., at a drift demand around three times the drift capacity for loading in the negative direction ($\delta = -0.3\%$). The axial load failure of the first storey of the URM wall, due to the crushing of the compressed toe, was quickly followed by the horizontal load failure. Figure 14a shows that in the URM wall the cracks were not concentrated in the bottom storey, as is typical for URM walls, but they also spread up to the second storey because of the presence of the RC wall that changed the global deformed shape of the system. At the same load step (LS33), the RC wall was still in the pre-peak response and only some of the longitudinal reinforcing bars at the north edge had yielded. The crack pattern of the first storey of the RC wall consisted of horizontal flexure cracks plus some shear-flexure cracks that started developing in the previous cycle (LS32, $\delta = +0.8\%$), as seen in Figure 14b. The second storey of the RC wall exhibited only small cracks in the construction joints. Figures 14c and 14d show the detail of the crack pattern after the failure of the first and second storey of the URM wall.



Figure 14: Crack pattern at LS33, $\delta = +0.95\%$. (a) specimen; (b) RC wall, first storey; (c, d) close-ups of the first and second storey of the URM wall.

4.2 TU2

4.2.1 No significant stiffness degradation of the URM wall ($\delta = +0.1\%$)

At an average drift δ equal to $+0.1\%$, the URM wall displayed only small horizontal cracks (Figure 15a). In the first storey of the RC wall, only small flexure cracks were observed (Figure 15b).

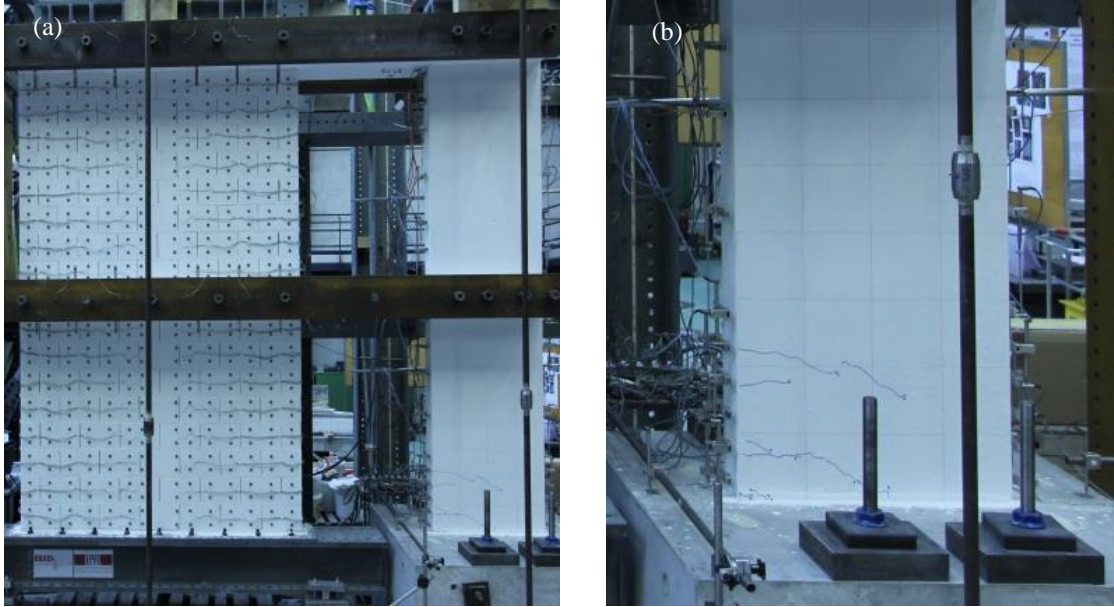


Figure 15: Crack pattern at LS10, $\delta = +0.1\%$. (a) specimen; (b) RC wall, first storey.

4.2.2 Horizontal load failure of the unit for the negative loading direction ($\delta = -0.4\%$)

At LS33, when the target average drift of $\delta = -0.4\%$ was reached, the shear strength of the URM wall dropped by 10% and the horizontal force was immediately reduced to zero to avoid the axial load failure of the URM wall. The crack pattern in the URM wall comprised diagonal cracks in the first storey pointing towards the compressed corner (Figures 16a and 16c): the onset of the toe-crushing was also observed (Figure 16d). The second storey of the URM wall was crossed by just one thin shear crack in addition to a horizontal crack at the base of the second storey. In the first storey of the RC wall, shear-flexure cracks were observed (Figure 16b).

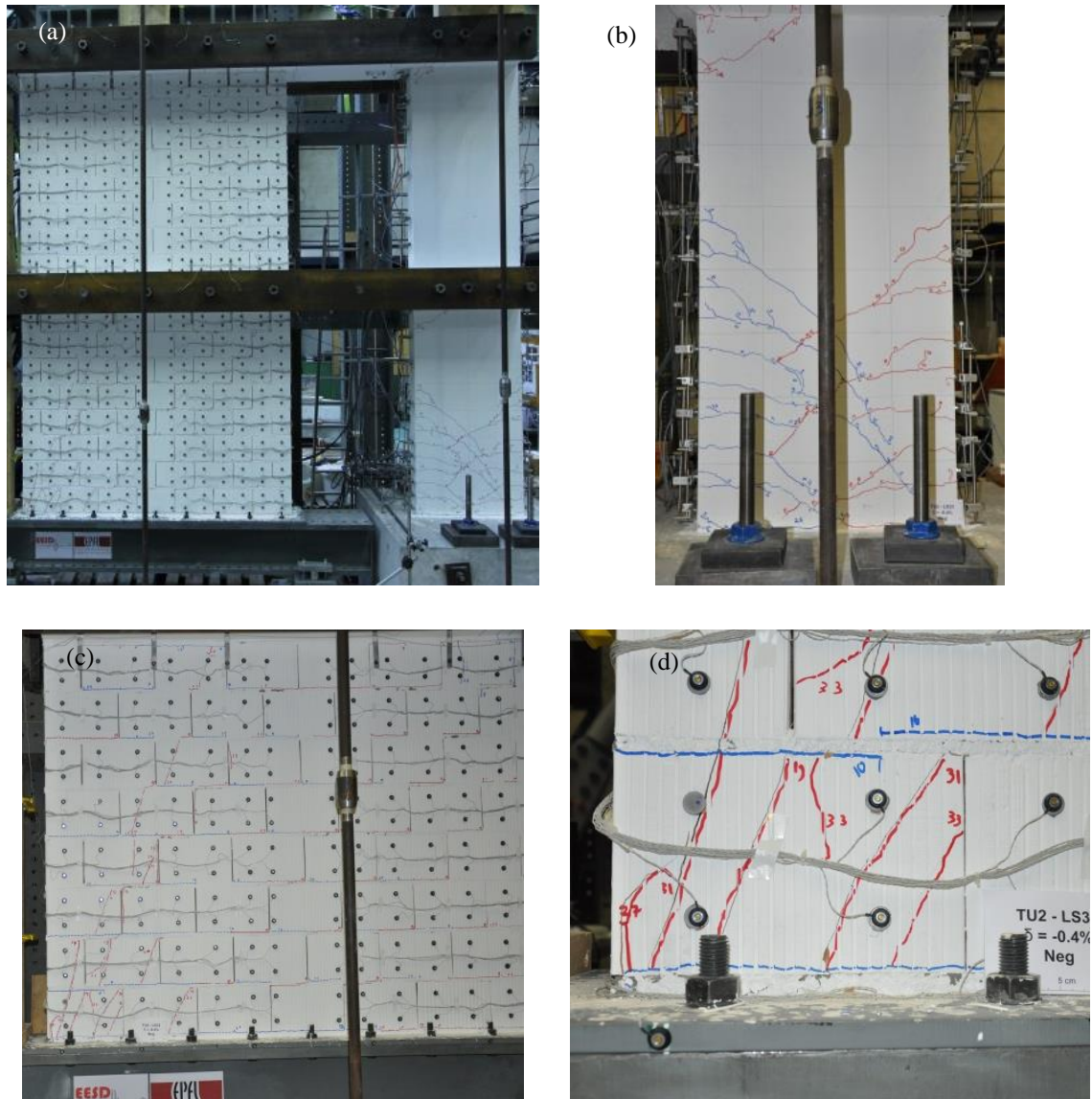


Figure 16: Crack pattern at LS33, $\delta = -0.4\%$. (a) specimen; (b, c) crack pattern at the bottom storey of the RC and URM wall; (d) compressed corner of the first storey of the URM wall.

4.2.3 URM wall heavily damaged for the positive loading direction ($\delta = +0.6\%$)

At LS35, the crack pattern was mainly developed in the URM wall (Figure 17a). In the bottom storey of the URM wall, steeply inclined shear cracks were detected. In addition, vertical splitting cracks due to the rocking motion appeared at the toe of the wall (Figure 17c). In the second storey of the URM wall, a stair-stepped crack passing through the mortar joints

formed and splitting cracks in the compressed corner were observed (Figure 17d). Figure 17b shows that the extent of the cracked part of the RC beam penetrating into the URM wall was around 60 cm.

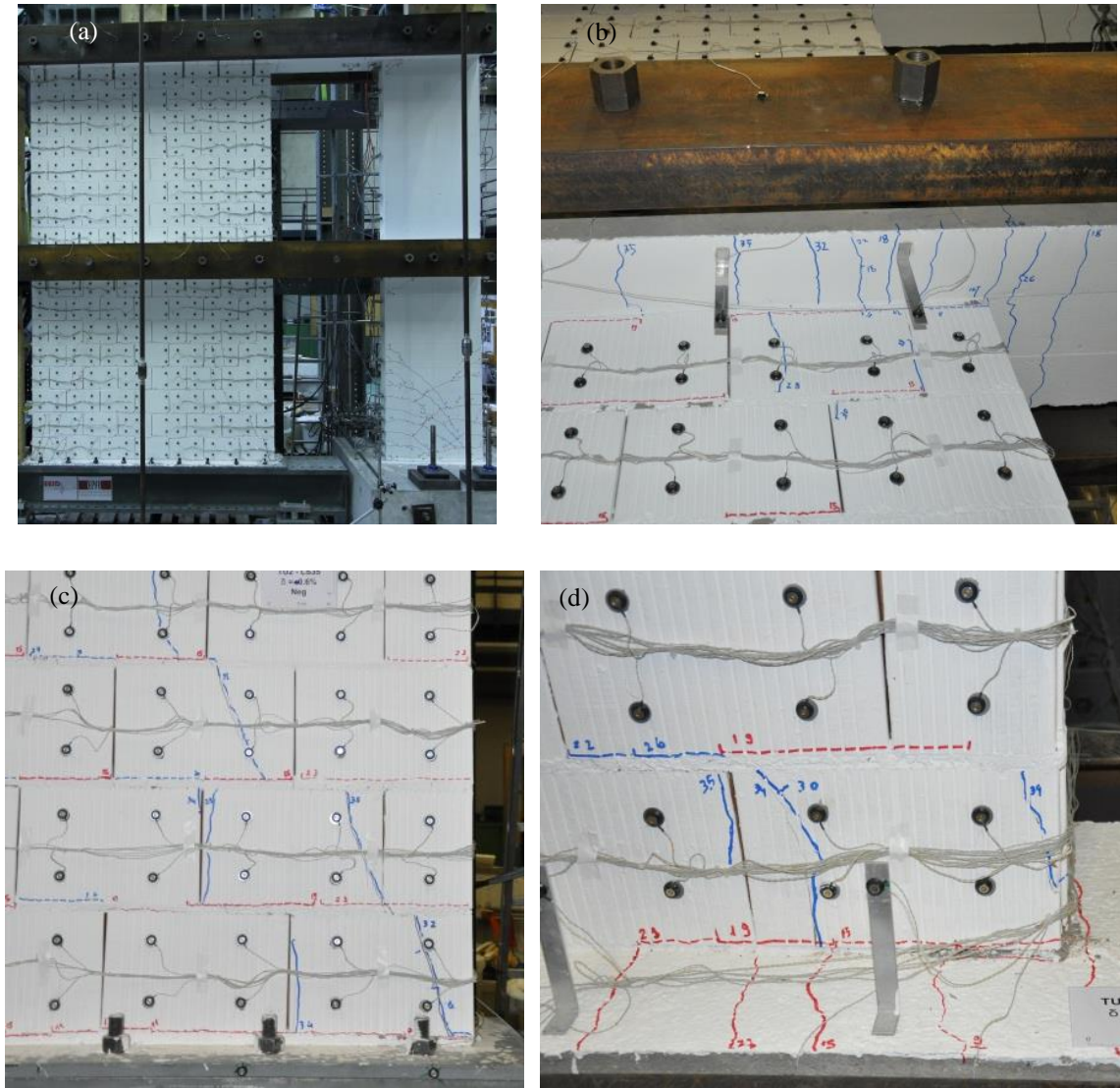


Figure 17: Crack pattern at LS35, $\delta = +0.6\%$. (a): specimen; (b) RC first storey beam, curvature penetration into the URM wall; (c, d): compressed corner of the first and second storey of the URM wall.

4.2.4 Onset of horizontal load failure of the unit for the positive loading direction ($\delta = +1.12\%$)

Horizontal load failure of TU2 occurred during the half cycle with $\delta = +1.12\%$ (LS38), i.e., at a drift demand around three times the drift capacity for loading in the negative direction ($\delta = -0.4\%$). Figure 18a shows that, similarly to TU1, in the URM wall the cracks were not concentrated in the bottom storey, but they also spread up to the second storey because of the presence of the RC wall that changed the global deformed shape of the system. Figure 18b shows that the RC wall was far from failure and only shear-flexure cracks in the first storey were observed. As for TU1, the second storey of the RC wall exhibited only small cracks in the construction joints.

Steeply inclined shear cracks passing mainly through bricks were detected in the bottom storey of the URM wall (Figure 18c). Toe-crushing of the compressed corner was also observed. In the second storey of the URM wall, the plastic deformations were mainly concentrated in one single stair-stepped crack that crossed the wall (Figure 18d). Toe-crushing of the compressed corner was also observed in the second storey.

Curriculum vitae

Personal

Name	Alessandro
First name	Paparo
Date of birth	January 16, 1984
Nationality	Italian
E-mails	alessandro.paparo@epfl.ch; alessandro.paparo@yahoo.it

Education

2010 to present: PhD student at École Polytechnique Fédérale de Lausanne (EPFL), Lausanne, Switzerland. Earthquake Engineering and Structural Dynamics Laboratory (EESD).

2010: Licenced to practice civil engineering in Italy (“Esame di stato di Ingegnere sezione A”).

2003-2009: MS and BS in Building Engineering / Architecture, University of Bologna, Bologna, Italy.

1998- 2003: Liceo Classico Dante Alighieri, Ravenna, Italy.

Teaching experience

2012: Teaching Assistant for the Bachelor level course Algèbre Linéaire.

2011: Teaching Assistant for the Master level course Earthquake Engineering.

Professional experience

2008: Two-month internship as structural engineer, GiaProject, Bologna, Italy.

Professional affiliations

Swiss Society for Earthquake Engineering and Structural Dynamics, SGEB.

Languages

Italian: native language

English: full professional proficiency

French: full professional proficiency

Journal articles

- Paparo, A. and Beyer, K. [2015] “Development of a displacement-based design approach for modern mixed RC-URM wall structures”, submitted to *Earthquake and Structures*.
- Paparo, A. and Beyer, K. [2015] “Modelling the seismic response of modern URM buildings retrofitted by adding RC walls”, submitted to *Journal of Earthquake Engineering*.
- Beyer, K., Petry, S., Tondelli, M. and Paparo, A. [2014] “Towards displacement-based seismic design of modern unreinforced masonry structures”, *Perspectives on European Earthquake Engineering and Engineering Seismology*, 1, 401-428.
- Paparo, A. and Beyer, K. [2014] “Quasi-static tests of two mixed reinforced concrete – unreinforced masonry wall structures”, *Engineering Structures*, 71, 201-211.
- Wenk, T, Baur, M., Duvernay, B. and Paparo, A. [2012] “Die Erdbebenserie in der Emilia-Romagna im Mai 2012: Schäden an Industriehallen und geotechnische Aspekte” (The earthquake sequence in Emilia-Romagna in May 2012: Damage to industrial buildings and geotechnical aspects), *Der Bauingenieur*, 87, S2-S7.
- Paparo, A., Landi, L. and Diotallevi, P.P. [2012] “Extension of Direct Displacement-Based Design to Plan-Asymmetric RC Frame Buildings”, *Journal of Civil Engineering and Architecture*, 10, 1280-1291.

International conference papers

- Paparo, A. and Beyer, K. [2014] “Performance-based approach for the retrofit of URM wall structures by RC walls”, 2nd *European Conference on Earthquake Engineering and Seismology*, Istanbul, Turkey.
- Paparo, A. and Beyer, K. [2013] “Seismic behaviour of mixed RC-URM wall structures: comparison between numerical results and experimental evidence”. *Vienna Congress on Recent Advances in Earthquake Engineering and Structural Dynamics*, Vienna, Austria.
- Paparo, A. and Beyer, K. [2013] “Quasi-static cyclic tests of mixed RC-URM wall structures”, 12th *Canadian Masonry Symposium*, Vancouver, Canada
- Paparo, A. and Beyer, K. [2012] “Pushover analyses of mixed RC-URM wall structures”, 15th *World Conference on Earthquake Engineering*, Lisbon, Portugal.
- Paparo, A., Diotallevi, P.P. and Landi, L. [2011] “Application of Direct Displacement-Based Design for plan-asymmetric RC frames”, XIV Convegno Nazionale L'Ingegneria Sismica in Italia, ANIDIS, Bari, Italy.
- Paparo, A., Diotallevi, P.P. and Landi, L. [2010] “Displacement-based seismic design and analysis of plan-asymmetric RC frames”, 14th *European Conference on Earthquake Engineering*, Ohrid, Macedonia.